UNIVERSITY OF Southampton

University of Southampton Research Repository
ePrints Soton

Copyright © and Moral Rights for this thesis are retained by the author and/or other copyright owners. A copy can be downloaded for personal non-commercial research or study, without prior permission or charge. This thesis cannot be reproduced or quoted extensively from without first obtaining permission in writing from the copyright holder/s. The content must not be changed in any way or sold commercially in any format or medium without the formal permission of the copyright holders.

When referring to this work, full bibliographic details including the author, title, awarding institution and date of the thesis must be given e.g.

AUTHOR (year of submission) "Full thesis title", University of Southampton, name of the University School or Department, PhD Thesis, pagination

http://eprints.soton.ac.uk

University of Southampton

Faculty of Physical and Applied Sciences

Simulating the Colour of Port Wine Stain Skin

by

Tom Lister

Thesis for the degree of Doctor of Philosophy

February 2013

UNIVERSITY OF SOUTHAMPTON

ABSTRACT

FACULTY OF PHYSICAL AND APPLIED SCIENCES

Electronics and Computer Science

Doctor of Philosophy

SIMULATING THE COLOUR OF PORT WINE STAIN SKIN

by Thomas Stephen Lister

Currently, laser treatments for Port Wine Stain (PWS) lesions are considered the choice therapy, but response is poor or treatments are ineffective for around half of patients. It is proposed in this thesis that improvements to the effectiveness of laser treatment can be achieved through the acquisition of estimated PWS vessel number density, depths and diameters for each individual lesion.

Information regarding PWS vessel architecture is found to be contained within the colour of the lesion. Presented in this thesis is a method of extracting this information through colour measurements and the inverse application of a skin model.

Colour measurements are performed on 14 participants using a Konica-Minolta CM2600d spectrophotometer employing a xenon flashlamp illumination source and an integrating sphere. Light transport is simulated through an 8 layer mathematical skin model inclusive of horizontal, pseudo-cylindrical PWS blood vessels using a new Monte Carlo programme. Within the programme, model parameters were adjusted in an iterative process and skin colour was reproduced with a mean discrepancy of 1.9% reflection for clinically normal skin (24 datasets) and 2.4% for PWS skin (25 datasets).

The programme estimated anatomical properties of the measured regions of skin, yielding epidermal melanin volume fractions from 0.4% to 3.3% and mean melanosome diameters from 41 nm to 384 nm across the participant group. The response to laser treatment was assessed for 10 participants through colour measurements taken immediately before and at least 6 weeks after treatment and

through expert analysis of photographs for 9 participants taken at these times. Treatment response was not found to correlate directly with the pre-treatment melanin parameters estimated by the programme.

Mean depths, diameters and number densities of PWS vessels were also estimated by the programme before and after treatment. These parameters were compared to data obtained from Optical Coherence Tomography (OCT) images for 5 participants. Number densities and diameters predicted by the simulation varied by no more than 10% from the values determined by OCT for 4 and 5 out of 7 regions respectively. Mean depths predicted by the simulation did not correspond with those determined by OCT however. This may be a result of the limited contribution of deeper vessels to the colour of PWS skin.

Predicted PWS parameters were compared to treatment response assessed by colour measurement for 10 participants and by photographic analysis for 9 of these. Predicted vessel number densities were not found to correspond with treatment response. Vessel diameters predicted by the simulation correlated with treatment response when compared with the pulse lengths selected for treatment. Optical coefficients derived from the skin model were used to estimate appropriate laser treatment radiant exposures at the predicted mean vessel depths and these radiant exposures corresponded strongly with the treatment response.

Suggestions for improvements in the predictions of melanosome diameters through changes in the adjacent skin minimisation procedure within the programme are discussed. The apparent underestimation of PWS blood vessel number densities and mean depths (compared to biopsy studies) may be a result of the reduced influence of deeper PWS vessels upon skin colour. Further investigation, including modifications to the PWS vessel minimisation procedure within the programme, would be necessary to determine whether improvements in these predictions may be achievable.

The results of the study show that the new Monte Carlo programme is capable of extracting, from measurements of skin colour, realistic estimates of PWS skin characteristics which can be used to predict treatment response and therefore inform treatment parameters on an individual PWS.

List of Terms

Chromophore	A pigment which provides a significant contribution to the colour of skin or to the absorption of light during laser therapy
Haemoglobin	Red pigment in blood. Haemoglobin is responsible for the difference in colour between normal and PWS skin. The target chromophore for PDL therapy.
Implicit Capture	A statistical approximation which considers a large number of photons travelling along the same path at once, intended to save time (computational cost) in Monte Carlo simulations
Melanin	Brown pigment found in the epidermis and in hair, considered a competing chromophore to haemoglobin in PDL therapy
PDL	Flashlamp-pumped Pulsed Dye Laser, the treatment of choice for PWS
Pulse length/ Pulse Length	The length in time of a single laser pulse
PWS	Port Wine Stain: a congenital vascular malformation usually presenting as a red lesion on the skin
Spectrophotometer	A device used for measuring light within the visible region
WSLC	Wessex Specialist Laser Centre, Salisbury District Hospital, UK. This is a specialist skin laser centre in an NHS hospital
RTT	Radiative Transfer Theory, a mathematical technique of modelling energy transfer in straight lines (rays or beams)

Table of Contents

Acknowledgements

I have to admit that I enjoyed almost every bit of work that has gone into this thesis and I leave it still with enthusiasm. This could not have been the case without the unerring support and wisdom that I have received from those around me.

Dr Philip Wright has been my guide, my mentor and my friend, as well as sharing an office with me. He has endured the brunt of my questions and has always been pleased to discuss them. Thus, it is he who takes the majorty blame for my continued enthusiasm and whom I can never thank enough.

Dr Paul Chappell has had the luxury of spending most of his time 20 miles from me, but has always been at most a quick phone call or email away. Always reassuring, interested and with a healthy understanding of the processes involved in creating a PhD, Paul ensured a smooth ride.

Syenna, my wife (by some massive fortune on my behalf) gave me the confidence to undertake this PhD and to continue asking questions throughout. My two eldest sons undermined this slightly by stumping me with questions of their own, such as 'Daddy, what is light?' and 'Could you build a laser? Could you build one out of wood? Lets go and build one now' (Charlie) and 'What is that supposed to be a picture of?' (Hugo, smirking, in reference to beam trajectories). Rupert is just as capable of putting things into perspective, usually leaving the room as soon as I begin talking about my PhD. But it is perspective, and love, that my family have always provided and which makes such a small achievement as a PhD seem all the more possible.

Lastly, I would like to thank my examiners, Profs James Wilkinson and Martin van Gemert. For deciding that my work was good enough, but also for a genuinely helpful discussion and perhaps the final chance to have a good long chat about my work.

1. Introduction

1.1 Motivation

Port Wine Stains (PWS) are the most common of all congenital vascular malformations. They are caused by a permanent swelling of blood vessels within the dermis and present as a red lesion on the skin. PWS often constitute a significant disfigurement and can result in major psychological problems. Thus, many people who suffer with PWS seek treatment.

Laser treatment is currently considered the therapy of choice for PWS. The object of treatment is to selectively heat the swollen blood vessels which constitute the lesion, resulting in irreversible damage and subsequent removal of these vessels. Selectivity may be achieved through careful selection of treatment parameters including wavelength, pulse length and energy per pulse to match the depths, diameters and number density of vessels within a lesion.

Approximately half of patients who undergo laser treatment for PWS respond poorly or not at all. One reason for this poor response is that the laser parameters used are virtually identical for all PWS patients despite the availability of laser systems with user specific settings [1, 2]. In order to optimise laser settings for each individual patient, the practitioner must be provided with information regarding the vascular architecture from each patient, such as the depths, diameters and number density of PWS vessels.

Historically, such information has been made available from some patients through punch biopsies. However, such a technique is subject to distortion in the sample and is likely to result in a scar, which would contribute further to the disfigurement of the lesion. Imaging methods designed to provide 'virtual biopsies', such as ultrasound imaging or Optical Coherence Tomography may one day provide a non-invasive alternative but, due to the need for high resolution and imaging depths of 3-4 mm, the devices currently available to the practitioner are not able to provide adequate information.

In this thesis, it is proposed that colour measurement is a practical method for the clinic which may be able to provide the practitioner with information regarding the

depths, diameters and numbers of vessels in an individual PWS lesion using technology currently available.

1.2 Contributions

An expansive survey of the literature has been carried out covering the following topics:

- Anatomy of PWS skin
- Colour measurement of PWS
- Mathematical modelling of PWS skin colour

Further to this, a Monte Carlo simulation of light transport through PWS skin has been created and verified as part of the thesis. The principle original contributions which have emanated from this work are:

- The use of two separate layers with the living epidermis of the skin model to accommodate variations in melanin properties across the epidermis
- The consideration of mean melanosome sizes in the skin model and their contributions to light scatter
- A minimisation procedure which adjusts the melanin volume fractions and mean melanosome sizes in the skin model in order to reproduce the spectral reflectance of clinically normal skin
- A minimisation procedure which introduces horizontal, pseudo-cylindrical blood vessels with random orientation into the skin model and adjusts their depths, diameters and numbers in order to reproduce the spectral reflectance of PWS skin.
- The contribution of PWS blood vessels walls to the absorption and scatter of light within the skin model.

The work from this thesis has also been presented in the following publications:

Journal Papers

Lister TS, Wright PA, and Chappell PH, *Spectrophotometers for the Clinical Assessment of Port Wine Stain Skin Lesions: A Review*. Lasers in Medical Science, 2010. **25**(3): p. 449.

Lister TS, Wright PA, and Chappell PH, *The Optical Properties of Human Skin.* Journal of Biomedical Optics, 2012. **17**(9): p. 90901-1.

Lister TS, Wright PA, and Chappell PH, *Simulating Light Transport through Skin for Color Prediction of Port Wine Stain Lesions: A Review.* Journal of Biomedical Optics, 2012. **17**(11): p. 110901.

Oral Presentations

Lister TS, Wright PA, and Chappell PH, *Why use Spectrophotometry to Asses Port Wine Stains?* 27th Annual Conference of the British Medical Laser Association, Salisbury, UK, May 2009.

Lister TS, Wright PA, and Chappell PH, *Light Transport Through Skin.* 29th Annual Conference of the British Medical Laser Association, Woburn, UK, May 2011.

Lister TS, Wright PA, and Chappell PH, *A New Monte Carlo Simulation.* Annual Conference of the European Laser Association, London, UK, May 2012.

1.3 Organisation

This thesis aims to answer the question: Can the information contained within the colour of an individual PWS lesion be used to estimate the characteristics of its constituent vessels (such as depth diameter and number density) and therefore predict the likely efficacy of laser treatment? If this is possible, the ability to predict the effectiveness of laser treatment may be applied inversely to determine whether one combination of treatment settings would be likely to provide a better result than another combination, thus informing the most appropriate settings for an individual laser treatment.

Chapter 2 contains an introduction into the background of the topic, including a brief overview of skin anatomy focussing on the features which contribute towards its colour. A survey of the literature regarding PWS skin and the features which constitute its colour is also presented. This is followed by a description of laser treatments for PWS skin.

Chapter 3 comprises a literature survey regarding colour measurements of PWS skin and determines the appropriate tools required for carrying out such measurements. Chapters 4 and 5 include further reviews of the scientific literature with the aim of determining an appropriate mathematical approach to interpreting skin colour measurements as well as appropriate skin optical coefficients.

The methods of data collection are described in Chapter 6 as well as a description of the Monte Carlo programme developed for this thesis. The performance of these methods, including reproducibility of colour measurements and appropriateness of skin optical coefficients are then verified in Chapter 7.

The main results from the thesis are presented in Chapter 8 and analysed in detail in Chapter 9. A summary of the findings and potential directions of future work are presented in Chapter 10.

2. Background

2.1 The Colour of Skin

This section contains a brief overview of the main features of human skin which give rise to its colour, and the variations in these which may be expected in both normal and Port Wine Stain (PWS) skin. For a more general discussion of current opinions regarding general human skin anatomy, the reader is directed towards some excellent textbooks [3, 4].

Skin Features

It is convenient to describe the structure of skin as a series of layers. These are not always entirely distinct but can be classified by their structure and content [4]. The colour of skin is almost entirely derived from the two outermost layers, the epidermis and dermis (Figure 1), as light penetrating beyond these is unlikely to return to the surface.

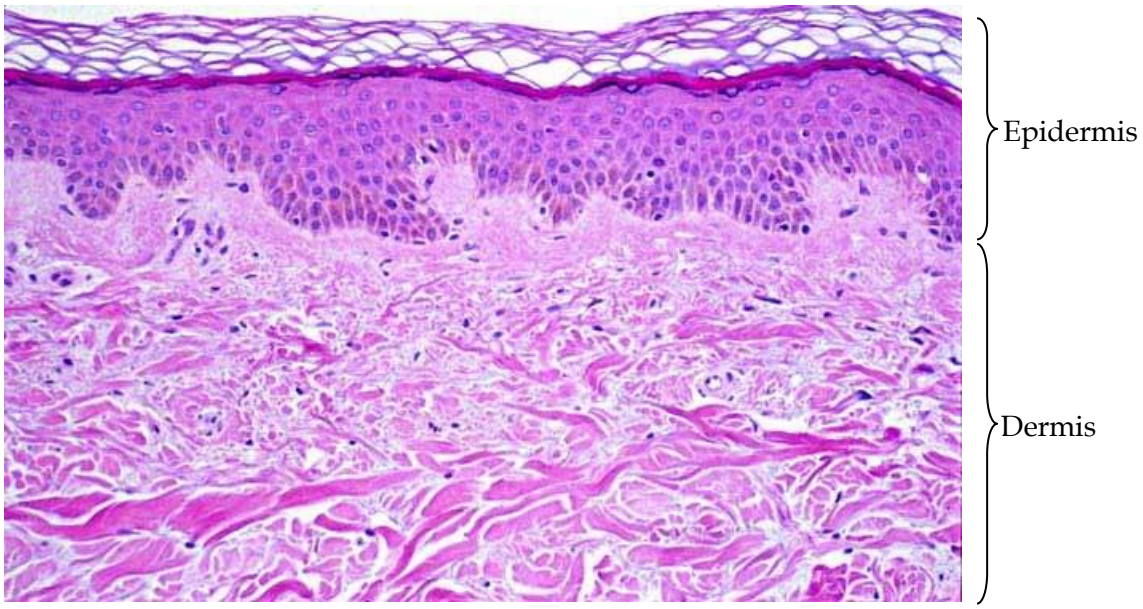

Figure 1: Histological vertical section of clinically normal skin demonstrating clear differences in structural components between layers on H&E staining. Courtesy of Dr. I Cook, Consultant Histopathologist, Salisbury District Hospital.

Epidermis

The epidermis is the outermost layer of skin and serves to protect the underlying dermis. It consists primarily of keratinocytes. These cells proliferate in the deepest (basal) layer of the epidermis as polygonal cells containing keratin filament bundles and large nuclei (Figure 2). Keratin filaments form this layer's major constituent [3] and are the primary contributors to light scatter within the epidermis [5].

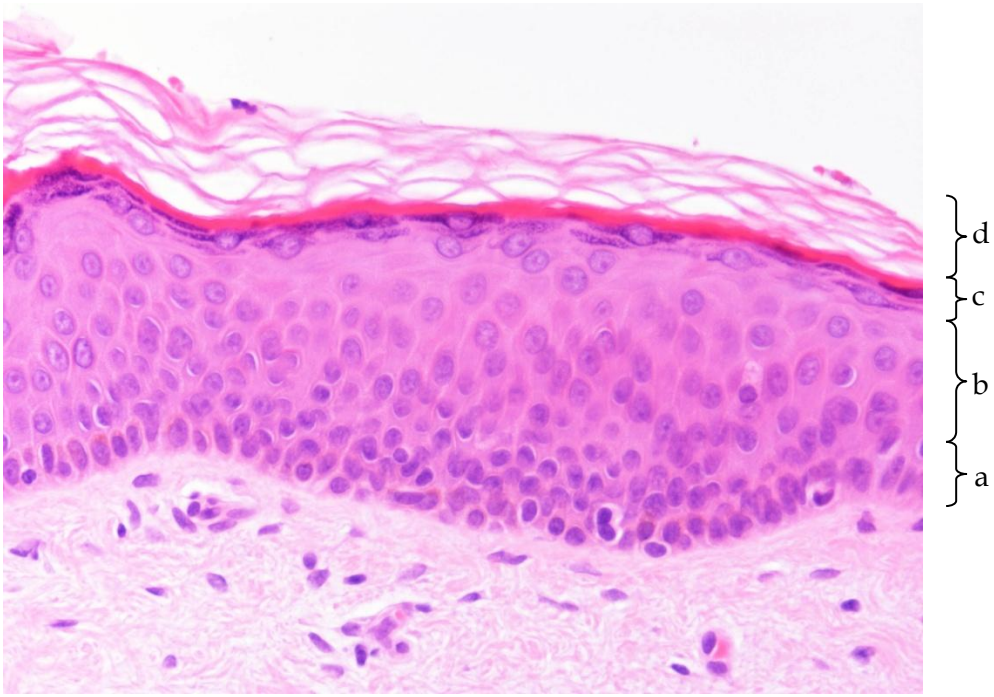

Figure 2: Histological vertical section of clinically normal epidermis showing the graduation of keratinocytes as they progress towards the surface. Basal layer (a), prickle cell layer (b), granular layer (c) and cornified layer (d) are identified. Courtesy of Dr. I Cook, Consultant Histopathologist, Salisbury District Hospital.

As they progress towards the outer surface of the skin, keratinocytes are thought to form a series of columns, with a central basal stem cell surrounded by six to eight amplifying proliferative cells over which a column of progeny cells extends through the superficial layers. The keratinocytes undergo a progressive change in shape and content during this migration (a process known as cornification [4]). The keratin bundles contained within the cell become more prominent as they progress into the prickle cell layer and then become more compact as the cells become flatter in the granular layer. The nuclei and other organelles degrade during cornification, and are no longer present by the time the keratinocytes reach the outermost (cornified) layer. The cornified layer may be only a few cells deep, and these cells appear flat, consisting almost entirely of a dense array of keratin filaments [4]. Thus, light scattering may vary with depth across the epidermis.

Melanin pigments are the primary absorbers of visible light in the epidermis. They are high molecular weight polymers known as eumelanins (brown-black in colour) and phaeomelanins (red-yellow), which attach to a structural protein and form large, complex molecules. Melanin producing cells are known as melanocytes and are

situated in the basal layer of the epidermis. Here, melanin is packaged within organelles called melanosomes, which travel along the dendrites of melanocytes to be engulfed and internalised by adjacent keratinocytes. The quantity of melanosomes produced is influenced by ethnic background and sun exposure, with sun exposed dark African and Indian skin types demonstrating a mean epidermal melanosome volume fraction of up to 10%, compared to a typical 1.2%-3% for type 2-3 European skin or as low as 1% for light European skin types where minimal sun exposure has occurred [6-11]. Melanosome diameter also varies across these groups. Melanosomes have been shown to accumulate in a crescent shaped cap over the distal part of the nucleus in basal keratinocytes and degrade during cornification as they migrate towards the surface of the skin, to form dust like remnants in cornified keratinocytes [4, 10]. This process results in a variation in melanin concentration, and therefore light absorption, across the epidermis, with a maximum concentrations and melanosome sizes in the basal layer [10]. Sun-exposed and darker African skin types have been found to contain the largest melanosomes, up to 400 nm in diameter. Paler, sun-protected European skin types have the smallest, with diameters between 30 nm and 200 nm across the living epidermis [7, 8, 12, 13]. This variation in melanin quantity and distribution between individuals and across the epidermis further contributes to variations in the absorption and scattering of light.

Lipids are arranged in a lamellar pattern through the epidermis, with phospholipids and glycolipids accumulating just above the basal layer and cholesterol and its esters (fatty acids, ceramides) accumulating towards the surface. These lipids play a function in absorbing light [14], as do other constituents of the epidermis such as urocanic acid, which is present in sweat and is thought to act as a sunscreen to protect the skin from UV light [14, 15]. The proportion of visible light absorbed by these constituents is negligible when compared to melanin. However, such oils have been reported to enhance optical coupling between air and the superficial layers of the skin, improving the transmission of light [16].

Dermis

The epidermal-dermal junction is convoluted, forming papillae or ridges which are most apparent in the thick skin of the palm and sole, and fewer and smaller in so-called thin skin (which covers the rest of the body), especially at regions of low

mechanical stress and minimal sensitivity. Each dermal papilla contains a capillary loop which provides metabolic support to the epidermis [17] along with densely interwoven fine bundles of collagen fibres (approx 2 μm in diameter [18]). Collagen fibres are the main structures responsible for light scattering in the dermis and are present throughout the dermis, increasing in thickness towards the deeper reticular layer (up to 15 μm in diameter [18]). The thickness and number density of these fibres also vary with anatomical region, age and sex, occupying approximately 18-30% of the volume of the dermis on average [3].

The blood supply to the dermis also has a substantial effect on light absorption and scattering. Blood normally occupies around 0.2%-0.6% of the physical volume of the dermis [19-24] depending upon anatomical location. It is commonly described as being contained within horizontal networks of interconnected blood vessels [17]. At the deepest part of the dermis is the deep dermal plexus. This does not significantly affect the apparent colour of most skin [25]. The deep dermal plexus gives rise to vertical branches whose calibers reduce from approximately 26 μm to 15 μm in diameter, with wall thicknesses of 1.0-3.5 μm, as they extend into the dermis [17]. These may divide further at the mid-dermal plexus but go on to supply the most superficial network of vessels, the subpapillary plexus. Within the subpapillary plexus, these vessels (now categorised as arterioles) are around 17-26 μm in diameter with wall thicknesses of 1.0-3.5 μm [26]. Subpapillary arterioles give rise to capillary loops (10-12 μm in outside diameter and wall thicknesses of 2-3 μm [26]), which are directed towards the epidermal/dermal junction and may branch before undergoing u-turns in the dermal papillae. These capillary loops drain into postcapillary venules which are approximately 18-23 μm in outside diameter with wall thicknesses of 3.5-5.0 μm and are the predominant vessel in the papillary dermis [17]. These in turn pass to the mid-dermal plexus, a primarily venous layer consisting of venules up to 30 μm in outside diameter [4, 20], and eventually to the deep-dermal plexus [4].

Port Wine Stain Skin

PWS are the most common of all congenital vascular malformations, affecting around 250,000 people in the UK and approximately 25 million people worldwide [27-30]. They are characterised by a clearly visible red-to-purple lesion on the skin (Figure 3). Two thirds of PWS are thought to occur on the face, with further disfigurement

resulting from hypertrophy of underlying bone and soft tissue in many cases [31]. This constitutes a significant cosmetic problem and can result in major psychological problems, in part due to the negative reactions of other people [2, 28].

PWS are typically present at birth and do not resolve spontaneously but usually progress from a lighter pink to a darker purple colour with age. The abnormal colour of PWS skin is derived from an increase in the dermal blood content, with blood composing around 2%-8% by volume of the average PWS dermis [19, 20, 32-34] compared to approximately 0.2%-0.6% in normal skin [19-24].

Figure 3: Examples of individuals with PWS to the face, showing variations in coverage

and colour.

PWS are thought to involve the subpapillary plexus in all cases, with most extending down into the deeper dermal layers [32, 35-38] . However, inconsistencies exist in the literature around the type of blood vessels involved in PWS skin. For example, Braverman *et al* [39] found that dilation was confined to the post capillary venules, but others have stated involvement of dermal capillaries [28, 38, 40, 41]. This confusion may have arisen from the change in vessel structure caused by long term ectasia, resulting in a thickening of vessel walls [37, 38]. Furthermore, differentiation between normal and diseased vessels may not always be clear [42]. Thus, rather than specifying the type of vessel affected, many authors have chosen to use more general terminology, stating that PWS skin consists of *dilated blood vessels in the dermis* [20, 36, 42-48].

Although PWS is a vascular lesion, observations have been made in the literature regarding changes in the intervascular dermis of PWS skin. Schneider *et al* [38] reported inconsistent and variable intervascular alterations in their histological and electron microscopy study of 12 PWS patients. Notably, they reported oedema (deposition of fluid outside of the vessels) resulting in an eventual splitting up of collagen bundles. In support of tissue oedema, Nagore *et al* [44] found a general trend to thicker skin in PWS lesions when using high-resolution ultrasound imaging to investigate 21 children with facial PWS. Schneider *et al* also found lesions with an accumulation of loosely arranged or densely packed collagen fibrils of small diameter and some with a reduction in the total collagen proximal to dilated vessels. Such changes in the fibrous make-up of dermal tissues may cause a change in its light scattering properties, although, to date, this has not been investigated directly.

The Colour of PWS Skin

The colour of PWS skin has long been used as a clinical identifier and much work has been carried out to determine the factors which influence PWS skin colour. As well as the differences between patients and body sites associated with normal variations of skin colour, it is the quantity and distribution of dermal blood which contributes most to the variations in PWS skin colour.

A comprehensive study of PWS anatomy was carried out by Barsky *et al* on 100 facial PWS lesions [32]. They took a 3 mm punch biopsy from a representative area of each

lesion and the "best oriented and prepared" section was chosen subjectively from this. Barsky *et al* recorded a mean ectatic vessel depth of 460 ± 170 μm in PWS skin, but observed that the depth of PWS lesion correlated poorly with colour using a visual comparison of the skin against a Pantone colour chart. Instead, the mean vessel area and total vascular area within each section of PWS skin was found by Barsky *et al* to correlate strongly with colour. Thus, Barsky's results suggest than skin colour is derived from the quantity of blood in PWS skin, independent its distribution through the dermis.

Fiskerstrand *et al* [42] recorded a more superficial mean ectatic vessel depth of 240 ± 80 μm, using the same method of 3 mm punch biopsies on 30 patients. A significant factor in this difference may have resulted from Fiskerstrand *et al*'s technique excluding vessels below 800 μm, whereas Barsky *et al* reported an average biopsy depth of 1800 μm. However, Fiskerstrand *et al* found that "pink and purple lesions were significantly deeper located than were the red lesions" using the same method as Barsky of comparing skin colour against a Pantone colour chart. Fiskerstrand *et al* also concluded that larger diameter vessels corresponded with a darkening of PWS colour, from pink to purple [37, 42].

Nishidate *et al* performed colour measurements on a physical skin model consisting 3 vessels filled with stationary de-oxygenated horse blood [49]. The vessels were 0.45 mm, 0.92 mm and 1.3 mm in diameter and were embedded in a 10% solution of intralipid. The appearance of the vessels at the surface of the model was reported to correspond subjectively with the appearance of similar diameter vessels within skin. Using a CIExyz analysis of spectral data measured obtained using a fibre setup, Nishidate *et al* found that the larger diameter vessels appeared more blue and that an increase in depth changed the measured colour from 'blue' to 'bluish-green'. They also found that oxygenating the blood gave a more red appearance. Although there are clear differences between flowing blood in human skin and the physical model used in Nishidate *et al*'s study, these results appear to be consistent with the aforementioned *in vivo* studies.

Theoretical work has also suggested a correlation between the depth of ectatic vessels and the colour of PWS skin. Svaasand *et al* [50] modelled the colour of PWS skin using a simple diffusion theory technique. They concluded that "shallow, thin PWS lesions...

have a more well-defined red colour than thick lesions; the additional reduction in backscattered red light in thicker lesions will result in a more dark red/blackish colour". Verkruysse *et al* [23] used a Monte Carlo simulation of five different skin models, involving an approximation of the paths of light beams through a simple computer model of human skin. They predicted that PWS with larger diameter vessels and the same blood volume fraction would appear 'less red'. Also, Findlay [51] described the changes of perceived colour with depth of melanin pigmentation within the skin. Without melanin, the epidermis was described as grey in appearance, due to forward scatter and absorption which is nearly uniform across the visible spectrum. When studying the dermis, Findlay commented that blue light is backscattered from a thin layer of dermis and red, from a thick layer. Thus, melanin in the epidermis appears brown due to its absorption across the entire visible spectrum, which increases moderately with decreasing wavelength. When situated in the dermis, red to green light is still absorbed, but blue light is backscattered before reaching the melanin, giving the Nevus of Ota (a condition where melanin is deposited in the dermis) a blue appearance. If these findings are instead applied to regions of high blood concentration, the normal absorption of blue and green light by red blood cells will be less influential with increasing depth in the dermis, as will the absorption of green light, causing a change in lesion colour from red in the superficial papillary loops to a more purple colour deeper within the dermis.

Barsky *et al* found the mean vessel wall thickness in the affected vessels of PWS skin to be between 4 μm and 6 μm [32]. This is in agreement with Fiskerstrand *et al*'s observations [42] and suggests little change from vessel wall thicknesses in normal skin [17]. However, Schneider *et al* observed an increase in vessel wall thickness up to 13.5 μm when investigating the lesions of 12 patients using an electron microscope [38]. Barsky *et al* were not able to determine a correlation between vessel wall thickness and lesion colour [32].

Summary

Skin can be conveniently described as a series of layers. Its colour is primarily determined from the absorbing pigments melanin and haemoglobin and the scattering properties of filamentous proteins.

Variation in dermal blood volume fraction is the primary contributor to differences in PWS skin colour. The literature shows significant correlations between vessel size and lesion colour, although vessel wall thickness has not been shown to contribute to this variation in colour. Despite Barsky *et al*'s conclusions, it is also likely that the depth of ectatic vessels in PWS skin has a significant effect on the perceived colour, with deeper lesions being less red and more purple or pink.

Reducing the number or mean diameter of PWS blood vessels, and therefore the quantity of dermal blood, will act to reduce the perceptibility of PWS skin. This is the primary mechanism employed for the treatment of PWS.

2.2 Laser Treatments for Port Wine Stains

Laser therapy is well established for the treatment of PWS skin [52-56] and is widely considered the treatment of choice [57-68]. The objective of laser therapy is to reduce the colour difference between PWS and clinically normal adjacent skin by selective damage of ectatic vessels. This is achieved through selective absorption of light by haemoglobin [69]. The absorbed light causes heating of the haemoglobin which is subsequently transmitted to the vessel wall by thermal conduction [70, 71]. If the vessel wall is raised to a sufficient temperature, then irreversible damage is incurred. If the temperature of the blood within the vessel increases fast enough to cause rapid expansion, then vessel rupture occurs. In each case, if irreversible damage is inflicted over a large enough proportion of the vessel wall, it is thought that normal repair mechanisms result in the removal of the ectatic vessel [70, 72] and thus a reduction in the redness of PWS skin (Figure 4).

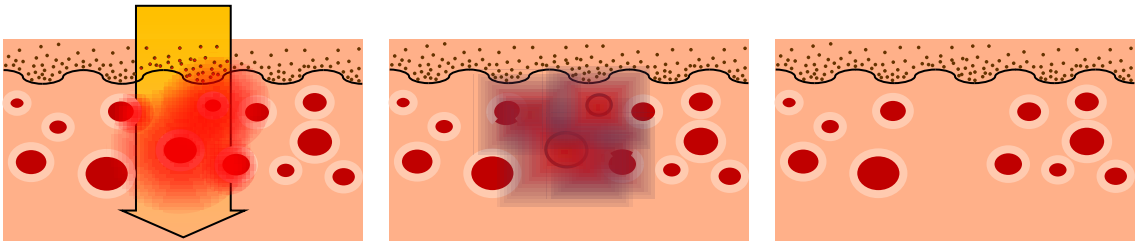

a b c

Figure 4: Diagrams illustrating the effects of laser treatment during irradiation (a) where heating of vessels and indirect heating of surrounding tissue occurs; immediately after irradiation (b) where vessel wall necrosis and hemorrhaging have taken place and long term (c), where PWS vessels have been eradicated.

Treatments are routinely carried out over multiple sessions, each involving short (0.45-10 ms) pulses of laser light fired onto the surface of the skin. A single pulse covers a circular target area approximately 1 cm in diameter. Thus, treatments may consist of tens or hundreds of laser shots per session, delivered at a repetition rate of around 1-2 Hz, to cover the entire treatment area (often the entire lesion).

Along with their ease of use, non-invasive delivery and localised targeting of PWS lesions, lasers are considered the preferential form of treatment due to their capability of selective damage to ectatic PWS vessels and therefore their ability to spare the remaining skin. This is achieved through careful selection of wavelength, pulse length (the length in time of a single pulse) and energy per pulse.

Wavelength Selection

Both the degree of light absorption by chromophores within the skin and the degree of scattering are highly dependent upon the wavelength of light. Within the visible and infrared regions of the electromagnetic spectrum, scattering is greater at shorter wavelengths, limiting the penetration depth (and therefore the effectiveness of laser treatment for deeper vessels) of blue wavelengths relative to red and infrared wavelengths (Figure 5).

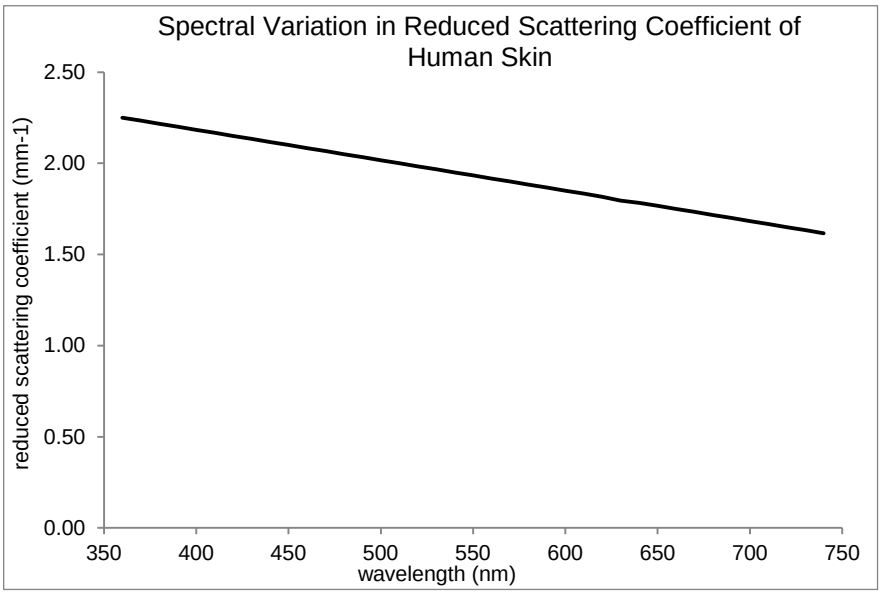

Figure 5: Variation in reduced scattering coefficient (a representation of the mean distance between isotropic scattering events) over the visible wavelength range, data from [73].

Blood is not a strong scatterer of visible light [74, 75], and so scattering within blood vessels is not routinely considered when selecting appropriate wavelengths for the treatment of PWS skin.

Absorption of light within the epidermis is dominated by melanin. This acts as a shield to the underlying PWS vessels, preventing much of the light from reaching them. Absorption by melanin is greatest towards the blue end of the visible spectrum and decreases uniformly with increasing wavelength, with around five times as much light absorbed at 360 nm compared to 720 nm. Thus, to maximise efficient transmission of light to the PWS vessels and also minimise collateral damage secondary to absorption of light within the epidermis, longer wavelengths are preferred.

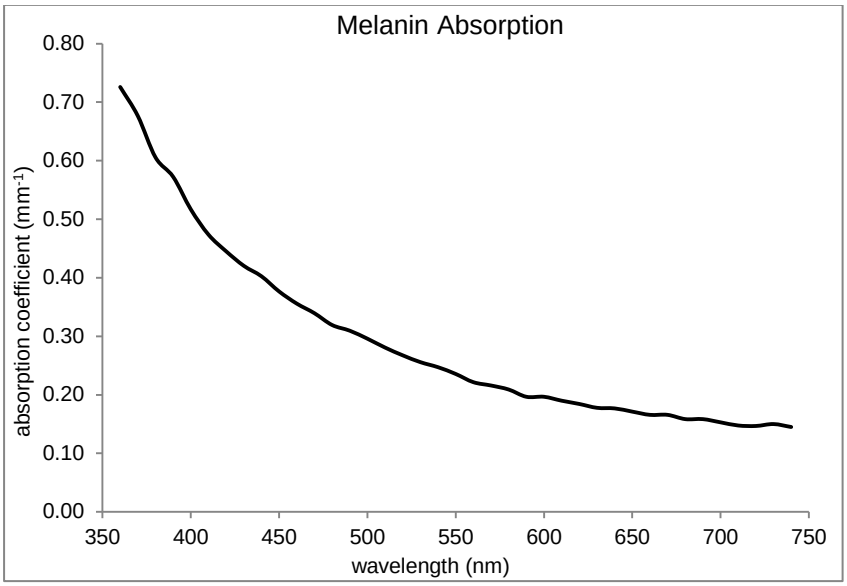

Figure 6: Variation of melanin absorption coefficient with wavelength, from [7].

Haemoglobin is the target structure for PWS laser therapy and is contained both within normal vessels of the dermis and within enlarged PWS vessels. Haemoglobin, in its various ligand states, has a more complex absorption spectrum, showing absorption peaks in the blue and green regions.

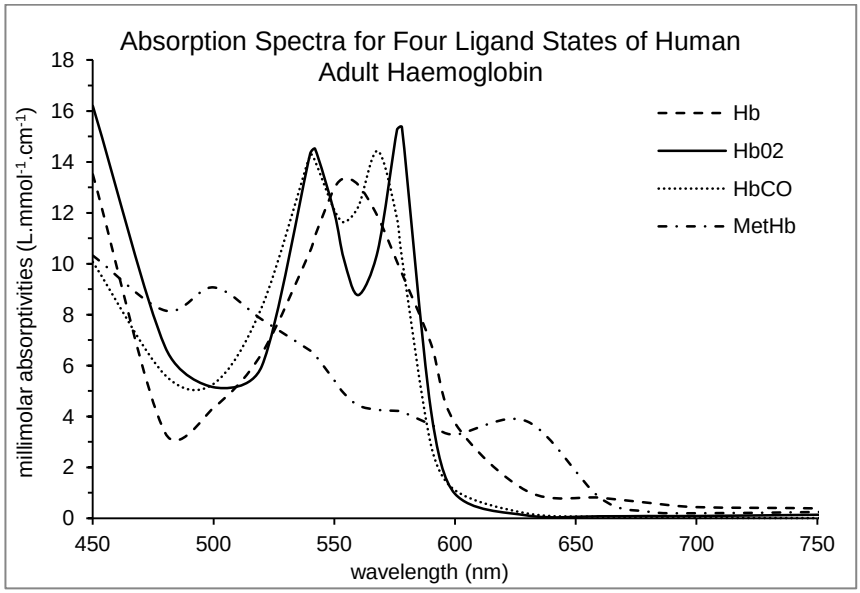

Figure 7: Absorption spectra of deoxyhaemoglobin (Hb), oxyhaemoglobin (HbO_2), carboxyhaemoglobin (HbCO) and methaemoglobin (MetHb) in the visible region, from [76].

A wavelength which is highly absorbed by blood is preferable to ensure efficient targeting of PWS blood vessels whilst minimising absorption by other structures in the skin. However, if absorption by haemoglobin is too efficient, light is not able to penetrate beyond overlying vessels (such as the capillary loops at the dermal

epidermal junction) or sufficiently through an enlarged PWS vessel to cause damage to the lower parts of the vessel wall. Accordingly, as damage around the majority of a vessel wall is thought to be necessary to ensure subsequent clearance of that vessel [50, 72, 77-79], minimal reduction in vasculature (and therefore colour) is likely to be inflicted.

A wavelength of 595 nm is currently considered the preferred choice for the selective damage of blood vessels for skin types I to III [67, 80, 81]. For skin types IV-VI, which contain more melanin in the epidermis, 1064 nm is the preferred choice in clinical practice, where absorption by melanin is approximately 10 times less than at 595 nm.

Pulsewidth Selection

A further means by which lasers selectively damage target tissues is by careful selection of pulse length, the theory of which is described as *selective photothermolysis* [56]. Selective photothermolysis considers the cooling rate for structures within the skin. The theory is characterised by the calculated thermal relaxation time τ, described as "the time required for the central temperature of a Gaussian temperature distribution with a width equal to the target's diameter to decrease by 50 percent" [56]. Equation 1 has been used to describe the thermal relaxation time of a blood vessel with radius R and thermal diffusivity χ [53, 56]:

$$\tau \cong \frac{R^2}{4\chi} \qquad \text{Equation 1}$$

Anderson and Parrish [56] proposed that selective damage is achieved when the entire pulse of laser light is delivered within the time, τ. To target ectatic PWS vessels, pulse lengths need to be long enough to minimise damage to melanosomes, which are very small structures (average diameters ranging from approximately 40-80 nm [8] and thermal relaxation times from around 250 ns [15]) and normal blood vessels (diameters ranging from 6-30 μm [20]) whilst being short enough to heat the PWS vessels sufficiently (diameters ranging from 25-280 μm [20]) (see Table 1).

Table 1: Summary of thermal relaxation times for various vessel sizes, calculated from Equation 1[56] using a fixed value of thermal diffusivity $X = 1.39 \times 10^{-7}$ m^2s^{-1}[72].

Vessel Diameter (um)	Thermal Relaxation Time (ms)
25	0.3
50	1.1
100	4.5
200	18
300	41

In practice, vascular laser treatments are usually performed between 0.45 ms and 1.5 ms [82]. Longer pulsewidths are available, although these comprise multiple 'pulselets' rather than a single pulse. For example, the Cynosure Cynergy PDL is capable of producing nominal pulse lengths between 0.5 ms and 40 ms. However, a study carried out by the author using a simple photodiode detector placed adjacent to the laser beam to measure indirect illumination produced by the laser (unpublished) demonstrated that such pulses contain between 3 and 6 pulselets of varying characteristics spaced out over the nominal pulse length (Figure 8).

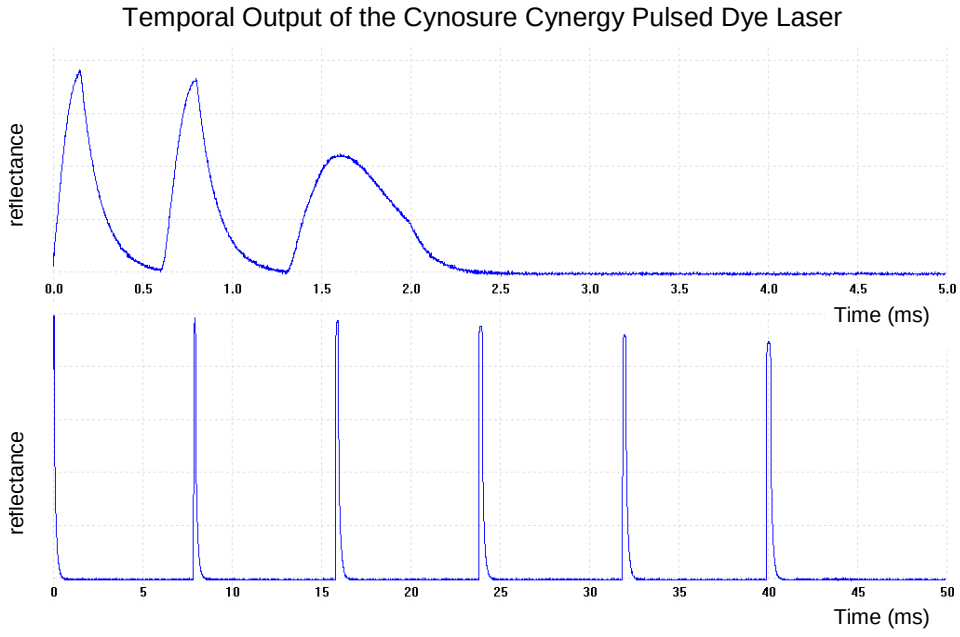

Figure 8: Temporal profile from a nominal 2 ms pulse (top) and 40 ms pulse (bottom) of the Cynosure Cynergy Pulsed Dye Laser determined from diffuse reflectance, measured using a photodiode.

As shown in Figure 8, the length in time and proportionate ditrubution of energy across the pulselets varies for each nominal pulse width. An approximation of these

parameters in provided in Table 2. More details of the methodology used can be found in Appendix G.

Table 2: Estimated pulselet train characteritics derived from the work described in Appendix G.

Nominal pulse length (ms)	Number of pulselets	Pulselet pulse lengths (ms)	Proportional distribution of energy
0.5	1	0.84	n/a
2	3	0.57, 0.62, 0.99	0.28, 0.29, 0.42
6	3	0.63, 0.63, 110	0.20, 0.22, 0.58
10	4	0.77, 0.77, 0.83, 1.3	0.14, 0.17, 0.20, 0.49
20	6	0.68, 0.78, 0.89, 0.89, 0.89, 0.89	0.12, 0.15, 0.18, 0.19, 0.18, 0.18
40	6	0.78, 1.15, 1.15, 1.15, 1.15, 1.15	0.10, 0.14, 0.17, 0.19, 0.18, 0.21

These pulse trains are delivered at intervals of 0.75 or 1.0 seconds as the laser handpiece is moved the cover the entire treatment area. The effects of such a pulselet train relative to an ideal 'top hat' temporal energy distribution are complex, but are likely to result in poorer responses from large blood vessels. This is partcularly apparent for the longest nominal pulse lengths, where the interval between individual pulselets is greatest, probably allowing for substantial cooling of the target vessels between pulselets.

Although work has been carried out elsewhere to describe in detail the effects of a pulselet distribution [80], due to the uncertainty in size distribution of vessels within an individual PWS, such work is not routinely applied in the clinical setting.

Pulse Energy

The quantity of energy (i.e. dose) delivered per pulse of laser light is of great importance when selecting treatment parameters. A dose per pulse which is too low will result in little or no treatment effect, as temperatures within the vessel lumina cannot be raised to a sufficient temperature for a sufficient time to cause irreversible damage to the vessel walls. At the WSLC, purpura (bruising resulting from haemorrhaging of blood from the targeted vessels and occurring immediately) is

currently considered a normal (and expected) response to laser therapy of PWS lesions. Higher energies per pulse can result in:

- blistering and/or scabbing.
- hyperpigmentation: brown staining caused by darkening of melanin. This is a transient effect, although it may last several months.
- hypopigmentation: localised skin lightening caused by damage to melanocytes. Such damage leaves the melanocytes unable to produce further melanin. This may be transient but is often permanent.
- scarring: excessive energies or poor wavelength/pulse length selection can result in significant damage to the dermis whereby the body is no longer able to replenish damaged tissue, resulting in scar formation.

The choice of energy per pulse has historically been established using empirical techniques. Laser manufacturers test their devices at a range of settings and sell the model of laser along with recommended optimal dose per pulse values for a range of indications. Upon receipt, clinical centres collate information from the manufacturer, case studies in the scientific literature and advice from other centres. Further to this, adjustments may be made on an individual patient basis, in response to adverse effects (overtreatment) or inadequate fading (undertreatment), either immediately following their first few laser pulses or when returning for their next treatment.

The author was not able to find any recommendations regarding typical energy per pulse values at 595 nm derived from theoretical studies. This may be because the radiant exposure value depends very much on the wavelength and pulse length selected, as well as individual patient and laser characteristics, some of which are not routinely available to the clinician. For reference, typical nominal PDL (595 nm) radiant exposures used at the WSLC range from 7 Jcm^{-2} to 12 Jcm^{-2} for 0.5 ms pulse lengths, and 13 Jcm^{-2} to 20 Jcm^{-2} for 6.0 ms pulse lengths.

Summary

Laser therapy is the treatment of choice for PWS skin. Reduction in PWS colour is achieved by selective heating of ectatic vessels, which in turn causes damage to the vessel walls.

Selection of ectatic PWS vessels, and sparing of the remaining skin, can be achieved through careful selection of wavelength, pulse length and energy per pulse. Longer wavelengths generally penetrate deeper into the skin and are less well absorbed by melanin within the epidermis. Optimal absorption by PWS vessels is thought to be at around 595 nm. This allows adequate penetration of light through the blood vessels to induce damage around the entire vessel walls whilst providing sufficient absorption to produce the required localised heating.

Pulse length selection is usually based upon a simple mathematical relationship which considers both the thermal diffusivity and size of structures within the skin. Optimal values of pulse length for ectatic PWS vessels vary from approximately 0.3 ms to 10 ms. This reflects the variation in vessel diameters expected from PWS skin.

Careful selection of energy per pulse is important to achieve adequate heating of PWS vessels whilst minimising collateral damage, however the choice of this parameter is highly dependent upon wavelength, pulse length and the individual characteristics of the patient.

Although general assumptions can be made of PWS characteristics, effective selection of laser parameters for the treatment of PWS skin requires individual information regarding the depth and size of ectatic vessels, along with estimates of the scattering properties of surrounding skin and the quantity of melanin in the epidermis. Although a number of techniques have been used to perform such estimates, visual observation is the only method which is currently used in widespread clinical practice. This involves an estimate of PWS colour and henceforth an inference of the structure of ectatic vessels within the PWS. There are a number of drawbacks associated with such a method, many of which may be overcome with an objective measurement of skin colour. This is the topic of the next chapter.

3. The Objective Measurement of Port Wine Stain Skin Colour

3.1 Spectrophotometry for the Measurement of Port Wine Stain Skin Colour

Based upon the published work by Lister et al [27]

Introduction

The clinical presentation of a PWS lesion is principally determined from its colour. This colour is representative of the size and depth of abnormal vessels within the lesion and of the overlying epidermis. These, in turn, are indicative of the response of the lesion to laser therapy. Thus, a considerable portion of research into PWS skin involves the assessment of colour for the prediction of its response to laser therapy.

The earliest and most commonly performed assessment of PWS colour is visual assessment, sometimes called clinical assessment, involving a direct viewing of the lesion by clinical staff or members of the research team. This is a subjective method which is made unreliable by a number of influencing factors, including the ambient lighting conditions, colours surrounding the subject, eye adaptation prior to viewing and viewing geometry [30, 83]. Even if these factors are accounted for, the sensitivity to light of the human eye is variable, with around 10% of the population not considered as "colour normal" observers [25]. Furthermore, the communication of perceived colour is difficult, with no universal cut-off between pink, red and purple, the three colours used almost exclusively to describe PWS lesions across the literature, so that even when an identical colour is perceived by two observers, discrepancies may occur. Such discrepancies are further confounded when using photographs. Viewing geometries and ambient lighting during image acquisition and subsequent viewing, quality of the print-out or visual display of the image, magnification and camera sensitivity are amongst those factors which contribute further to the uncertainty in photographic assessments [84].

Both direct and photographic assessments do however appear to be inexpensive methods of assessing PWS lesions. But, when considering the cost of extended treatment programmes resulting from a lack of ability to accurately judge and communicate the level of improvement and therefore the point at which the treatment has stopped working, coupled with the clinical risk of undergoing general anaesthetic

where this is used in young children, the overall costs may be considered high [30]. Furthermore, perhaps due to the uncertainty in individual PWS anatomy, the laser parameters used are virtually identical for all PWS patients despite the commercial availability of laser systems with user specific settings, suggesting that sub-optimal parameters are applied in many cases [1, 2].

In order that laser treatment may be optimised on an individual basis, objective methods of assessment are required which are practical in the clinical setting: *i.e.* non-invasive, fast and simple to perform. Such methods could be used to track the progress of treatments [67, 85, 86], predict treatment outcome [30, 35, 86-88], recommend a required number of treatments [88] and even select appropriate treatment strategies for the individual patient [2, 89].

The literature contains a wide variety of non-invasive diagnostic techniques used in assessing PWS, including videomicroscopy and other Charge-Coupled Device (CCD) based imaging techniques [84, 86, 90], perfusion imaging techniques such as laser Doppler flowmetry [30, 58] and optical coherence tomography [2, 91, 92], pulsed photothermal radiometry [93, 94], photoacoustic imaging [95-98] and infrared tomography [2, 30]. However, reflectance spectrophotometry is the most established and widely used technique for the objective assessment of PWS skin [30, 65, 99] and has developed significantly since its introduction into dermatological applications nearly a century ago [100].

Spectrophotometry

A spectrophotometer is a specific type of spectrometer, designed to measure light over the visible and near visible portion of the electromagnetic spectrum. At its most basic level, a reflectance spectrophotometer consists of a diffuse light source to illuminate the skin, a means of collecting the reflected and/or backscattered light from the surface, a spectral analyser and a means of measuring light intensity [101] (Figure 9). From this, the quantity of reflected light can be determined at specific wavelengths. The visual appearance of skin is derived almost entirely from diffuse, backscattered light from within the tissue. Therefore, when measuring skin colour, it is preferable to avoid detecting surface spectral reflectance and instead measure the quantity of diffuse photon flux of reflected light. This can be achieved by occluding the surface of

the skin from the primary light source, leaving the irradiance* at the skin consisting entirely of diffuse photons.

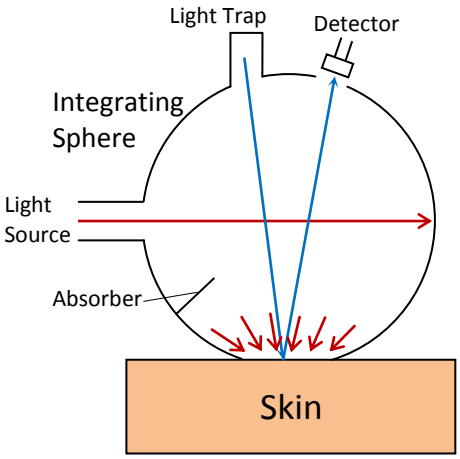

Figure 9: Schematic diagram showing a basic spectrophotometer setup. The integrating sphere acts both as a means of producing a diffuse light source, and for collection of light from the patient surface.

The proportions of different chromophores in the skin may be approximated from knowledge of their distinctive optical absorption characteristics, taking into account the scattering effects of tissue [21]. Such approximations are usually based upon relatively simple models of skin structure, typically consisting of optically homogeneous layers. The chosen model is then applied inversely, such that optical properties of the given layers are adjusted until the calculated reflectance spectrum matches the measured spectrum [102]. From these optical properties, concentrations of specific chromophores in each layer, such as haemoglobin, may be estimated.

In general, spectrophotometers can be divided into three categories: scanning, narrow band and tristimulus [27].

Scanning Spectrophotometry

Scanning reflectance spectrophotometry is the most established quantitative method of measuring skin colour [100], although it was not until the early 1980's that the method was first applied to PWS skin [55, 89]. At this time, work carried out by authors such as Ohmori and Huang [55] and Tang *et al* [89] highlighted the potential for accurately predicting individual treatment response to laser therapy of PWS

* The power of light incident on the surface of the skin per unit area. Units Wcm^{-2}

lesions. As previously mentioned, such a diagnostic method could be used to select appropriate treatment strategies on an individual patient basis.

Figure 10: An example of a modern scanning spectrophotometer, the Konica-Minolta CM2600-d.

Modern devices (such as those produced commercially by Spectral Research, Minolta and Zeiss) are contained completely within a hand held unit and can calculate absorbance spectra within seconds (Figure 10). For example, Sheehan-Dare and Coterill [103] used a scanning spectrophotometer (Spectral Research, UK) on 43 Caucasian patients to determine a statistically significant improvement in skin blanching achieved using the conventional PDL compared to the newly proposed Copper Vapour Laser (578 nm). Their method involved the comparison of an index calculated from the logarithm of the inverse reflectance (for a detailed explanation, see Appendix B). Although this index limited the ability to identify individual contributions from haemoglobin, melanin and other skin chromophores, it did allow for a simple and objective comparison of overall light absorbance.

Tomson *et al* [67] reported a statistically significant increase in skin blanching for 2-week intervals between PDL treatment sessions when compared to 6-week intervals, assessed using an overall reflectance measurement. The results were taken from a selection of only 13 PWS patients however, and no follow up study has been performed on a larger set of patients to the author's knowledge.

In order to provide a more detailed analysis of spectral reflectance data, a technique involving the inverse application of skin reflectance models is employed. Usually, these estimations involve either a solution to the diffusion approximation or Monte Carlo simulations.

The diffusion approximation is by far the most widely used approximation in biomedical optics, with Farrell *et al*'s method [104] accumulating over 400 citations alone [105]. This is due to its relative simplicity and low demand on computing power. Studies by Verkruysse *et al* [106], Zhang *et al* [107] and Lakmaker *et al* [25] show that the diffusion approximation is capable of producing fast results but may overestimate values of blood volume fraction, oxygenation levels and melanin concentration in PWS skin.

Monte Carlo methods are widely regarded as the most accurate simulations [107] and have become increasingly popular in recent times due to advances in computing power. Kienle and Hibst [81] are amongst those who used Monte Carlo simulations to estimate the optimal laser wavelength for achieving selective photothermolysis, based upon their reflectance measurements. Verkruysse *et al* [23] also chose to use a Monte Carlo simulation when analysing the influence of skin anatomy on perceived PWS skin colour, claiming superior accuracy to the diffusion approximation in the blue region, below 450 nm†.

Irrespective of the simulation used, the choice of skin model employed can greatly affect the overall accuracy of data interpretation. For instance, layers containing homogeneous distributions of blood and melanin are often approximated. There is strong evidence, however, that vessel diameter influences the perceived colour of the lesion and therefore the spectral reflectance characteristics [23, 40, 107] and the effectiveness of laser therapy [36, 42, 86]. Also the presence of melanin in the skin causes significant changes in the quantity of absorbed and reflected light over the entire visible spectrum. An increase in melanin will reduce the radiant exposure‡ at the epidermal/dermal junction and therefore the effectiveness of laser therapy. This may also increase the estimated dermal blood content if care is not taken to account for this when constructing the skin model. Despite these challenges, simulations have proven a powerful tool in the assessment of PWS lesions.

---

† Further investigations involving the Monte Carlo technique are discussed from page 60.
‡ The quantity of light incident upon a given area. Units Jcm^{-2}.

In summary, scanning spectrophotometers have been used successfully to determine favourable treatment regimes and to predict accurately treatment outcome on an individual patient basis. Further work is required in refining a skin model that can relate accurately and repeatably the spectral properties of PWS skin to anatomical properties which may be used in the diagnosis of PWS lesions.

Narrow Band Spectrophotometry

In the mid 1990s, portable optoelectronic devices designed specifically for measurements of the skin pigments melanin and haemoglobin became available. These relatively simple devices only necessitate measurements over two or more specifically selected wavelengths and so could be contained within a single hand-held unit, allowing for greater convenience in clinical measurements, at a lower cost than competing devices.

Narrow band spectrophotometers use a model based upon the work of Diffey *et al* [108] which illustrates that the sum of absorbencies from the skin's constituent pigments can be approximated from the decimal logarithm of the inverse reflectance from the skin (see Appendix). From this, an Erythema Index (EI), relating to the dermal blood content, has been constructed:

$$EI = log_{10}\left({}^{I_R}/_{I_G}\right) \qquad \text{Equation 2}$$

where I_R is the intensity of the red component of backscattered light (660-690 nm) and I_G is the intensity of the green component of backscattered light (530-560 nm).

Lanigan and Cotterill [43] used narrow band spectrophotometry alongside laser Doppler to objectively evaluate the response of PWS skin to a vasodilator cream, supporting the theory of reduced neural control in the pathogenesis of PWS. A comparison between three spectrophotometers by Clarys *et al* [109] included the Mexameter (Courage-Khazaka Electronic, Köln, Germany), a device which emits light at 568 nm, 660 nm and 880 nm using a circular arrangement of 16 LEDs. They reported good repeatability of measurements both *in vivo* and *in vitro* but found that the sensitivity of the device was inferior to that of a more popular unit, the DermaSpect (Cortex Technology, Hadsund, Denmark). The DermaSpect is the most widely used narrow band spectrophotometer for the assessment of PWS skin and emits light at 568 nm (green) and 655 nm (red) using LEDs. Troilius and Ljunggren

[57] investigated the possible use of the DermaSpect as a tool to predict and monitor PDL treatment of PWS on sixty six patients of Scandinavian descent. To take into account variation in normal skin (such as seasonal, temperature or other changes), they used ΔEI values, where:

$$\Delta EI = EI_{PWS\ skin} - EI_{normal\ skin} \qquad \text{Equation 3}$$

The results were simple to interpret, based on a scale of 0 – 100% where 0% represented no blanching and 100%, total blanching of PWS skin relative to normal skin. Results clinically assigned to the "fair" category may have had blanching between 0 and 80% whereas those from the "good" category may have had blanching anywhere between 20 and 100%, showing a noticeable overlap. However, there was a good correlation (r = 0.844) between ΔEI results and clinical assessment. Troilius and Ljunggren commented that this method could be used diagnostically, to predict outcomes of therapy by the time of the second treatment.

In most cases, the quality of information available from narrow band spectrophotometry is bound to the definition of EI used. However, the SIAscope (Astron Clinica, Cambridge) matches information over 8 wavebands of light against a model of spectral properties of chromophores in the skin over a 2 dimensional array of points [110]. The result is a series of two-dimensional maps named SIAgraphs, detailing the distribution of collagen, melanin and haemoglobin over the interrogated volume of skin. Laube *et al* [61] used this device alongside another narrow band device (Dermatronics, Cardiff) in the evaluation of a long pulse-duration PDL treatment for resistant PWS lesions. They described "considerable variations" between sets of three measurements in a single session when using both instruments. Furthermore, their methods resulted in disagreements between clinical assessments and SIAscope indications. However, the SIAgraph demonstrated subjectively a change in vessel diameter between treatments, information that is not available from the "point" measurement of other spectrophotometers.

When compared to spectral devices, narrow band spectrophotometers provide less detailed information and are thus limited in their applications. Furthermore, the value of EI has been found to increase with skin pigmentation due to the absorption of green light by melanin, resulting in an overestimation of the dermal blood content [111]. However, the recorded data is considerably easier to handle and devices are much

cheaper. These factors have helped maintain their popularity in dermatological studies. In the future, it is likely that other narrow band devices like the SIAscope will continue to emerge alongside the development of sophisticated PWS skin models used in scanning spectroscopic methods.

Tristimulus Colourimetry

Tristimulus colourimetry is widely used in chemistry and in dermatology, and provides an easy to operate and portable method for use in assessing PWS lesions. In general, a Tristimulus device illuminates the skin with a xenon arc lamp, which provides almost continuous bands across the visible spectrum. Reflected light is filtered and subsequently analysed using high sensitivity photodetectors. Results are commonly displayed using the CIEL*a*b* colour convention (see Appendix C) but often a number of output options are available.

The Minolta Chroma-Meter CR-200 and the newer CR-300 version (Osaka, Japan) are considered as standard instruments for CIEL*a*b* data acquisition in dermatology due to their proven reliability, accuracy and sensitivity [109]. Excellent inter- and intra-user repeatability has been reported for skin measurements using both the CR-200 and CR-300 [112, 113], and when compared to the DermaSpect narrow band spectrophotometer, the a* value was found to have a strong linear correlation with EI [30, 111], meaning that CIEL*a*b* may be meaningful in the context of dermal blood content. Koster *et al* [88] used the CR-300 to obtain ΔE and Δa^* values (colour differences between PWS and normal, adjacent skin; defined in Appendix) from facial PWS lesions on 70 Caucasian patients. These were used to determine retrospectively an exponential fit to PWS clearance over a series of treatments. They suggested that such a fit could be used to predict the best possible clearance and the required number of treatment sessions for an individual patient by obtaining information over two or three treatments. The use of ΔE and Δa^* takes into account differences in skin melanin content, based on the assumption that such differences are equivalent for both PWS and normal adjacent skin [114]. The methods used by Koster *et al* however did not relate skin melanin content to the predicted treatment outcome. They also ignored the association between anatomical location of the lesion and its clinical response to laser therapy [65]. This study does nevertheless highlight the potential for predicting prospectively the progress of a specific treatment.

When compared to Doppler flowmetry, Serup and Agner [115] found that the CR-200 and the Dr Lange Micro Color (Dr Bruno Lange GmbH, Dusseldorf, Germany) tristimulus spectrophotometers had superior technical reproducibility and were both better suited to the busy laboratory environment. This must hold true for the busy clinical environment too. Kim *et al* [116] also found that the CR-200 was better suited to clinical assessments of PWS skin when compared to a cross-polarised CCD based imaging system.

Many tristimulus devices are produced for the manufacturing industry and are thus designed to perform surface measurements. Therefore, errors pertaining from lateral diffusion and specular surface reflection within the skin are often not accounted for, resulting in a measurement which is greyer than the perceived colour of the skin [51]. Spectral surface reflection consists approximately 4-7% of the incident beam [15, 117] and can be effectively reduced by the design of the integrating sphere setup. The introduction of a light trap to avoid the detection of spectral surface reflection and an absorber to avoid direct illuminance from the light source are methods which are commonly employed (for example, see Figure 9).

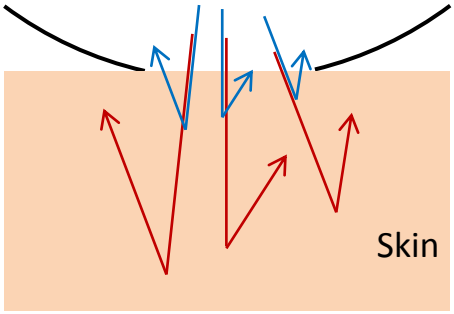

Figure 11: Illustration of lateral diffusion error. Backscattered red light is more likely to escape the aperture of the spectrophotometer due to a greater mean distance between scattering events.

Lateral diffusion error arises from the variation in scattering lengths of light with wavelength. As demonstrated in Figure 11, this results in a greater loss of red light *vs.* blue light for example. Takiwaki *et al* [118] demonstrated the influence of lateral diffusion error by measuring skin colour with two equivalent devices, each with a different sized aperture. They found that a statistically significant difference in measured skin colour between the two devices, with the larger aperture device producing a brighter, redder (in a red-green scale) and more yellow (in a yellow-blue scale) measurement of colour. This is in agreement with the lateral diffusion error

hypothesis, although other differences between the two devices cannot be completely ruled out without further investigation.

There have been a number of investigations comparing the performance of tristimulus spectrophotometers to the DermaSpect narrow band device. Both Takiwaki *et al* [111] and Clarys *et al* [109] commented that tristimulus measurements provide more direct information on overall skin colour rather than estimates of erythema provided by narrow band devices. Thus, tristimulus measurements may be considered of greater relevance to the cosmetic significance of a given lesion, although the interpretation of these data may be more complex. Furthermore, Clarys *et al* [109] found that a* was more sensitive to induced changes in redness of the skin when comparing maximum relative changes in value, a conclusion also supported by Shriver and Parra's observations [119].

Tristimulus devices offer reliable and repeatable information regarding relative changes in dermal blood content, which can be understood more readily than spectral data. This has led to promising results in the treatment planning of PWS patients. However, the potential of determining complex effects of diverse skin chromophores, including different types of melanin, is limited in both tristimulus and narrow band devices when compared to scanning spectrophotometers. Thus, further understanding of the effects of chromophores other than haemoglobin on tristimulus a* and L* values must be obtained to allow for a detailed diagnosis of PWS lesions on an individual basis.

When compared to both tristimulus and narrow band devices, scanning spectrophotometers boast greater versatility as they measure data from which CIEL*a*b* and EI, along with many other colour notations, can be calculated and will provide more detailed information over the entire visible and near visible spectrum. However, the greater cost of such devices (currently 2-3 times that of both tristimulus and narrow band [120]) continue to limit their popularity in dermatological research.

Conclusions

There are currently a range of spectrophotometric devices that are specifically designed for, and well established in, dermatology and in the study of PWS lesions. Scanning devices are the most substantial and versatile, and consequently the most expensive spectrophotometers used in dermatology. They are able to provide data which may be used to determine the complex effects of various skin chromophores on the overall perceived colour of both normal and PWS skin and have been used in the detailed analysis of PWS anatomy and subsequent treatment implications. However, unlike narrow band and tristimulus spectrophotometers, considerable expertise is required to interpret the complete data set. Narrow band devices are the most simple to use and interpret, but provide limited information that does not account for the complex effects of melanin and other chromophores. This is also true for tristimulus devices, although they are more sensitive to changes in redness and have the advantage of presenting results related directly to human visual perception. Tristimulus spectrophotometers produce a more direct measurement of skin colour, although interpretation of this may be limited due to errors incurred by lateral diffusion, spectral surface reflection and the effects of skin chromophores other than haemoglobin, not accounted for with the devices currently used.

Overall, scanning spectrophotometers are the most diverse spectrophotometers available and provide a more thorough interpretation of skin colour, making them the preferred choice for the majority of investigators. However, other devices offer cheaper, simpler and quicker results, which have proven reliability. They have been adequate for use in a number of clinical investigations and may better suit the needs of some research projects. For this particular project, the Minolta CM-2600d scanning spectrophotometer has been selected as the most appropriate tool for the objective assessment of PWS skin (see Figure 10). This is a commercially available device and so has the potential for immediate introduction as a routine clinical assessment tool. It was chosen above other devices due to the quality of the white light source and the additional options of selecting aperture size (which may be used to approximate lateral diffusion error) and estimating the proportion of specular reflectance (by using 2 separate light sources, see Appendix D).

The following chapter discusses in detail the techniques and methods by which colour measurements can be used to infer information regarding the composition of PWS vessels on an individual basis.

4. The Optical Properties of Human Skin

Based upon the published work by Lister et al [5]

Introduction

The colour of human skin has long been used as a subjective adjunct to the detection and diagnosis of disease. More recently, the introduction of skin colour measurements has extended this to include the potential for objective determination of skin features [27], including melanin and haemoglobin concentrations [21, 23, 121-123], the depth and diameter of blood vessels [124-126], the depth of pigmented skin lesions [127, 128], the maturity and depth of bruises [127-130] and keratin fibre arrangements [131].

Such advances have proved invaluable for the advancement of skin laser treatments [2] and photodynamic therapy [132-134], and have contributed to further advances in the diagnosis of cancerous and non-cancerous skin lesions [128, 135-137].

However, the success of these methods depends entirely upon adequate knowledge of the behavior of light as it impinges upon, and travels through the skin. A description of the major interactions of visible light with skin and the principal skin features which contribute to these is presented. This is followed by an analysis of published optical coefficients used in simulations of light transport through skin.

Background

Absorption

Absorption describes a reduction in light energy. Within the visible region, there are two substances are generally considered to dominate the absorption of light in skin: haemoglobin and melanin.

Haemoglobin is the dominant absorber of light in the dermis. Normal adult haemoglobin (Hb A) is a protein consisting four polypeptide chains, each of which is bound to a heme [138]. The heme in Hb A is named iron-photoporphyrin IX [139, 140] and is responsible for the majority of light absorption in blood. The free-electron molecular-orbital model describes this absorption as an excitation of loosely bound 'unsaturation electrons' or 'π-electrons' of the heme [141]. Within the visible region, Hb A contains 3 distinctive peaks. The dominant peak is in the blue region of the spectrum and is thus referred to as the Soret peak or Soret band. Two further peaks can be distinguished in the green-yellow region, between 500 nm and 600 nm which, in combination with the Soret band, cause Hb A to appear red. These are known as the α and β bands, or collectively as the Q-band, and have intensities of around 1-2% of the Soret band [142]. The excitation levels of π-electrons vary, and therefore the positions and intensities of these bands vary with the ligand state of the heme (Figure 7).

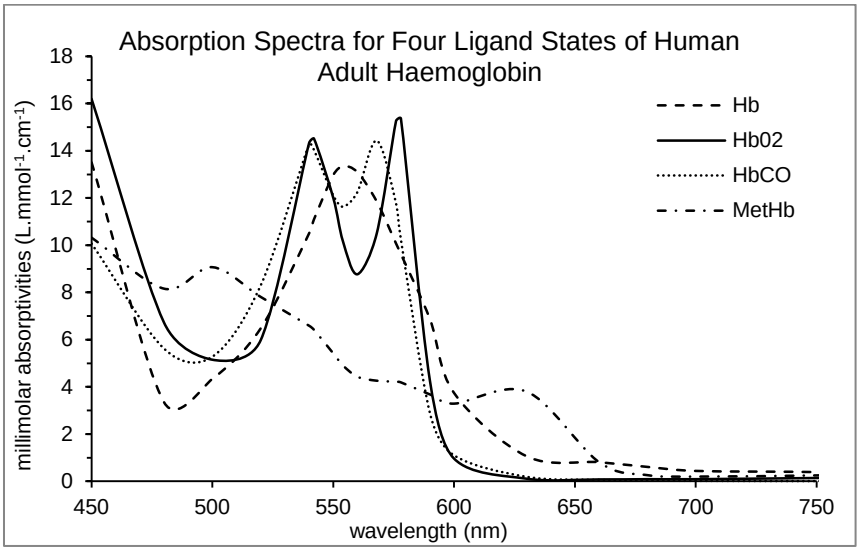

Figure 7: Absorption spectra of deoxyhaemoglobin (Hb), oxyhaemoglobin (HbO_2), carboxyhaemoglobin (HbCO) and methaemoglobin (MetHb) in the visible region, from [76].

Melanins are ordinarily contained within the epidermis and produce an absorption spectrum which gradually decreases from the UV to the IR regions. In contrast to haemoglobin, the variation and complexity of melanins means that their detailed structures are not yet fully understood, despite intense research over the last 5 decades, and this broadband absorbance spectrum is still a topic of scientific debate [143-145]. At present, the scientific consensus appears to gravitate towards a 'chemical disorder model' [13, 123, 143-147]. This model proposes that melanins consist of a collection of oligomers or polymers in various forms arranged in a disordered manner. This results in a number of absorption peaks which combine to create a broadband absorbance effect [144, 146] (Figure 13).

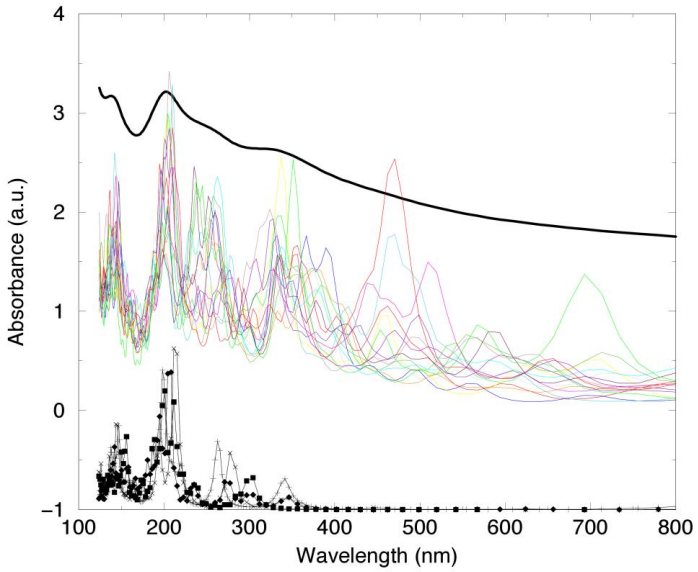

Figure 12: Coloured lines show individual absorption spectra of tetramer subunits within melanin extracted from human epidermis. The average absorption spectrum of these is shown by thick black line, shifted up 1.5 units for clarity. Thin black lines shifted down by 1 unit represent absorption spectra from monomer subunits. a.u. = arbitrary units. Reprinted figure with permission from [146].

Further absorption of light may be attributed to chromophores such as bilirubin and carotene [148], lipids [149] and other structures, including cell nuclei and filamentous proteins [101, 150]. Although the individual contributions from these secondary chromophores may be considered separately [130, 151, 152], most simulations group them into a single overarching value [33, 106].

Despite its abundance in all tissues, water is not a significant absorber of light in the visible region, although its contribution has been considered when simulating skin colour [153].

Scattering

As well as absorption, scattering contributes significantly to the appearance of skin. Scattering describes a change in the direction, polarisation or phase of light and is commonly portrayed as either a surface effect (such as reflection or refraction) or as an interaction with a small region whose optical properties differ from its surroundings (particulate scatter).

It has been estimated that 4-7% of visible light is reflected from the surface of the skin, independent of wavelength and skin colour [15, 117]. The remaining light is refracted as it passes from air into the skin.

The primary sources of particulate scatter within the skin are filamentous proteins. Keratins are the filamentous proteins of the epidermis and form this layer's major constituent, whereas collagen is the principal filamentous protein of the dermis and occupies approximately 18-30% of its volume [3]. Further scatter is attributed to melanosomes in the epidermis, cell nuclei, cell walls and many other structures in the skin which occur in smaller numbers [154].

Scatter from filamentous proteins has been approximated using a Mie solution to Maxwell's equations applied to data from *in vitro* skin samples [155, 156]. This approach provides an increase in simulated scattering probability with increasing fibre diameter and also with decreasing wavelength. The dependence of scatter on fibre diameter suggests that the protein structures of the dermis, which may be 10 times as large as those in the epidermis [3, 10] possess a greater scattering cross-section. This in part compensates for the lower number densities of filamentous proteins in the dermis. The scattering events which occur are mainly in the forward direction, meaning that, on average, light which returns to the surface will have undergone a large number of scattering events [157]. One implication of the wavelength dependence of scatter is that blue and green light which has returned to the surface of the skin will have, on average, travelled less deeply than red light. This is considered the primary reason why blood vessels and pigmented nevi which are situated deeper within the skin are only able to absorb light from the red end of the spectrum and therefore appear bluer than their superficial equivalents [51, 158].

The volume fraction of melanosomes in the epidermis varies typically from 1% in pale skin to 5% in darker skin [6], although one group has suggested greater values [22, 159]. However, despite their low numbers relative to keratins, melanosomes are approximately ten times the diameter of the largest keratin structures in the epidermis [160] and possess a greater refractive index [161] (and therefore a greater difference in refractive index at their interface with skin). Melanin has been shown to contribute significantly to the degree of scatter within the epidermis [7, 136]. As well as the volume fraction, the distribution and size of melanin structures in the epidermis also vary with skin type. Thus, the total amount of scatter which occurs as a result of melanin in the epidermis can vary substantially between individuals [162, 163], although this is not always taken into account when simulating the effects of varying melanin concentration on skin colour [153, 164], or when simulating laser treatments [2, 77] for example.

Blood normally occupies around 0.2%-0.6% of the physical volume of the dermis [19-24] depending upon anatomical location. The vessel walls surrounding this blood, in addition to the walls of vessels which remain vacant, may occupy a similar volume. Dermal vessels vary in thickness and structure from capillaries of around 10-12 μm diameter at the epidermal junction to terminal arterioles and post-capillary venules (approximately 25 μm in diameter) in the papillary dermis and venules (approximately 30 μm) in the mid-dermis [17]. Furthermore, blood vessels occur in higher densities at particular depths, giving rise to so-called blood vessel plexi [17]. The contribution to light scatter by these structures, inclusive of refraction effects, may be significant[4] [165-167] and varies with location and depth, as well as between individuals. Larger, deeper vessels may also contribute to the colour of skin.

Scattering from the remaining structures of the skin, including cell walls, nuclei and organelles [150], hairs and glands, is rarely of central interest to a study of skin optics. As a result, the contributions from these structures to the total measured scattering coefficients are not routinely considered separately [168].

---

[4] Assuming a reduced scattering coefficient of 0.5 mm^{-1} for blood and 3 mm^{-1} for vessel walls at 633 nm [210], a 0.5% volume fraction of each contributes approximately 0.02 mm^{-1} to the dermal reduced scattering coefficient, measured at around 1-5 mm^{-1} (See page 58). The contribution will be larger within blood vessel plexi.

Simulating Light Transport through Skin

Optical simulations involving mathematical models of healthy human skin generally approximate the surface as perfectly smooth, although some computer graphics models have applied calculations of directional reflectance from rough surfaces [169]. Surface scattering effects (reflection and refraction) can be calculated for smooth surfaces using Fresnel's equations and Snell's law respectively:

$$R = \frac{1}{2}\frac{(a-c)^2}{(a+c)^2}\left\{1+\frac{[c(a+c)-1]^2}{[c(a-c)+1]^2}\right\} \qquad \text{Equation 4}$$

Fresnel reflection (R) of unpolarised light from air to skin, where $c = cos(\vartheta_i)$, ϑ_i is the angle of incidence, $a = n^2 + c^2 - 1$ and n is the refractive index of skin.

$$\theta_t = \arcsin\left(\frac{1}{n}\sin\theta_i\right) \qquad \text{Equation 5}$$

Angle of refraction (ϑ_t) at the skin's surface calculated using Snell's law.

Within the skin, both absorption and scatter must be considered simultaneously. These may be described in the classical approach by Maxwell's equations, which consider the interactions between the electric and magnetic fields of light with matter. However, an exact solution to Maxwell's equations requires precise knowledge of each structure within the medium and becomes prohibitively complex for the case of human skin.

The most commonly used approximation to Maxwell's equations in the field of skin optics is Radiative Transfer Theory (RTT) [170]. This considers the transport of light in straight lines (beams). Absorption is simulated as a reduction in the radiance of a beam and is dependent upon the absorption coefficient (μ_a). The degree of scattering is described by the scattering coefficient (μ_s), which considers both a loss of radiance in the direction of the beam and a gain from beams in other directions, and the phase function (p), the probability that an individual beam will scatter in any particular direction. The reduced scattering coefficient (μ_s') combines these variables, i.e. $\mu_s' = \mu_s(1 - g)$, where g is the anisotropy factor, the average cosine of the scattering angle θ:

$$g = \int_{4\pi} p(\cos\theta)\cos\theta d\omega \qquad \text{Equation 6}$$

where $d\omega$ is a differential solid angle.

In order for RTT to be valid, it must be assumed that any cause for increasing or decreasing the radiance of a beam other than that described by the absorption and scattering coefficients, including inelastic scatter (fluorescence or phosphorescence) and interactions between beams (interference), is negligible. The skin model must also consist of volumes which are homogeneous with regards to μ_s, μ_a and p, and which do not change over time.

Optical Coefficients of Skin

A considerable amount of work has been carried out to determine appropriate values of the RTT coefficients. Cheong *et al* [171] described both direct (*in vitro*) and indirect (*in vivo*) methods of measuring absorption and scatter. A comprehensive analysis of the literature involving each method is presented here.

Absorption Coefficients

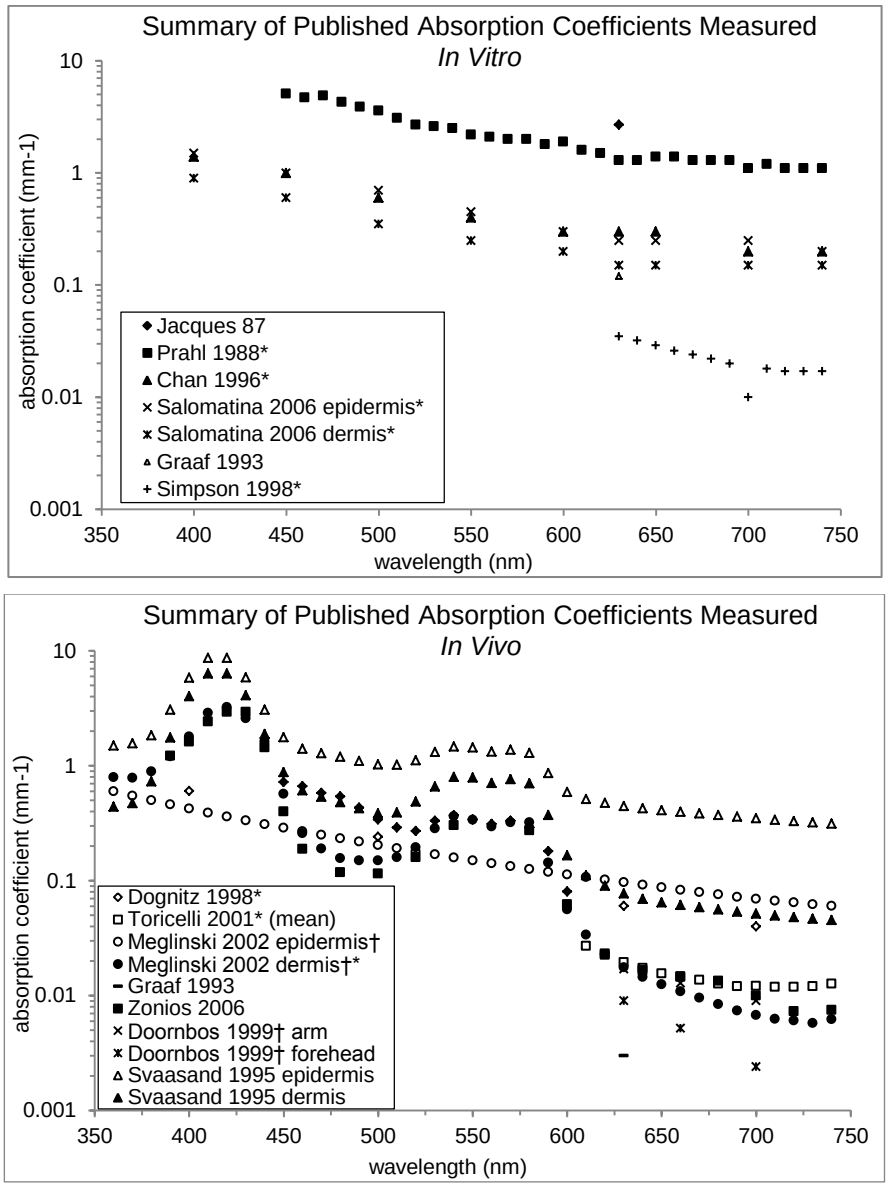

Figure 13: Summary of absorption coefficients available in the literature. *In vitro* data represents absorption coefficients from exsanguinated skin whereas dermal *in vivo* data is inclusive of blood absorption. *data obtained from graphical presentation. †data presented was not complete and required input of haemoglobin or water optical properties obtained from [149]. The raw data is provided in Appendix E (Table 17).

In Vitro

Direct measurements have the potential to produce repeat measurements of a predetermined volume or section of skin and, unlike *in vivo* measurements, can include transmission data. However, the processes necessary to extract and prepare a skin sample cannot be carried out without altering its optical properties.

The *in vitro* studies presented in Figure 14 vary significantly in tissue processing methodologies, measurement setup and the interpretation of data. For example, Jacques *et al*'s work [172] included three methods of tissue preparation. The epidermis was separated from the dermis using a microcryotome for one set of skin samples, after mild thermal treatment in a water bath in another set, and was not separated in a third set. The same mild thermal treatment was used to separate the dermis and epidermis in Prahl's work [159] and a microcryotome was also applied in Salomatina *et al*'s study [136]. No separation of the epidermis was reported by Chan *et al* [173] or Simpson *et al* [174]. Although Salomatina's work shows greater absorption from the *in vitro* epidermis when compared to the dermis, the studies analysed here do not demonstrate a clear distinction in absorption coefficients reported between the methods of separation described, nor between those which separated the epidermis and those which did not.

The level of hydration is likely to have varied considerably between the studies analysed. Prahl [159] and Jacques *et al* [172] soaked samples in saline for at least 30 minutes before carrying out measurements, during which the samples were placed in a tank of saline. Salomatina *et al* [136] also soaked their skin samples prior to measurement and sealed them between glass slides to maintain hydration. Chan *et al* [173] and Simpson *et al* [174] did not soak their samples prior to or during measurement. Jacques *et al* reported that soaking the sample increases backscattered reflectance, although the effects on the calculated absorption are not described. Chan *et al* commented that dehydration may elevate the measured absorption coefficient. However, the greatest reported absorption coefficients are those from rehydrated tissue samples. From the information available, the effect of tissue hydration on the measured absorption coefficients is not clear.

Data was interpreted using Monte Carlo simulations by Salomatina *et al* [136], Simpson *et al* [174] and Graaf *et al* [175], an adding-doubling technique by Prahl *et al* [159], and by direct interpretation in Chan *et al*'s [173] and Jacques *et al*'s [172] studies.

Both the methods described in the Monte Carlo simulations and Prahl's adding-doubling technique are based upon assumptions of optically homogeneous tissue layers, uniform illumination and no time dependence, and both are essentially discrete solutions to the radiative transport equation. The methods described contrast in their approach to internal reflection for beams exiting the skin model and the adding-doubling method relies upon accurate representation of the angular distribution of beams exiting the thin layer upon which the model is built. It is not directly clear if, or how, these differences may have contributed to the higher absorption coefficients reported by Prahl *et al*.

It is also of interest that Prahl *et al*'s [159], Chan *et al*'s [173] and Salomatina *et al*'s [136] studies, whose samples varied in thickness between 60 and 780 μm, did not demonstrate a clear correlation between sample thickness and published absorption coefficients but Simpson *et al*'s published absorption coefficients, which are an order of magnitude smaller than the other values analysed here, involved much thicker samples (1,500 to 2000 μm thick). Thus, differences between the published absorption coefficients across these studies may have resulted from variations in the regions of skin investigated or the ability of the simulations to correctly account for boundary effects at the lower boundary.

In Vivo

Indirect measurements do not suffer from such changes in the properties of the interrogated skin volume, although care must be taken to consider variations in blood perfusion for example, which may result from sudden changes in ambient temperature, the use of some drugs and even contact between the skin and the measurement device [176].

In general, absorption coefficients measured *in vivo* may be expected to be higher than *in vitro* values where the highly absorbing pigments from blood are removed from the samples. This is particularly true in the blue-green regions of the visible spectrum. Assuming a value of 0.5% blood volume in the dermis, this would contribute approximately 8 cm^{-1} at 410 nm (Soret band), 0.6 cm^{-1} at 500 nm and 1.4 cm^{-1} at 560 nm (Q-band), but only around 0.05 cm^{-1} at 700 nm (values calculated from [149]). This contribution is not reflected in the literature. Absorption coefficients obtained from *in*

vivo work show greater variation, but are not consistently higher than those obtained from *in vitro* work (Figure 14).

Absorption coefficients from Svaasand *et al* [177], Zonios *et al* [73] and Meglinski and Matcher [153] clearly demonstrate the effect of blood on the measured absorption coefficients. Each study shows an absorption peak between 400 and 450 nm corresponding to the Soret band and a double peak at approximately 540 nm and 575 nm corresponding to the α and β bands of oxyhaemoglobin (see Figure 7). There are, however, notable differences between the absorption coefficients produced from the three studies. Meglinski and Matcher and Svaasand *et al* considered epidermal absorption coefficients separately to dermal values. The reported values from Svaasand *et al* are greater, and show a different spectral curve to those from Meglinski and Matcher. This is a direct result of Svaasand *et al*'s inclusion of 0.2% blood by volume in the calculation of epidermal absorption coefficients, representing blood infiltrating the modelled epidermal layer from the papillae. Compared to Meglinski and Matcher's dermal values and Zonios *et al*'s absorption coefficients for their skin model consisting a single layer, both of which also included the influence of blood, Svaasand *et al*'s reported dermal absorption coefficients were consistently high. This is despite using a dermal blood volume fraction of 2%, compared to an average of 4.6% from Meglinski and Matcher's study and a value of 2.6% in Zonios *et al*'s work. The cause of this discrepancy is the variation in magnitude of the blood absorption coefficients applied across the three studies (Figure 112, Appendix E). Bosschaart *et al* [178] employed a diffusion approximation technique to their data collected from neonates, effectively applying a single value of absorption across the skin volume. Their data is in close agreement to Meglinski and Matcher's dermal absorption coefficients in the 530-600 nm range, but the contribution of melanin produces a relative increase in Bosschaart *et al*'s values at shorter wavelengths.

Data selected for analysis in this work involved 'Caucasian' skin types only. Where stated, these studies involved skin types described as Northern European. Where not stated, it was assumed that such skin types were used except for the studies carried out by Zonios *et al* [73] and Torricelli *et al* [179] which were conducted in Southern Europe. The latter two studies did not however report higher absorption coefficients, as may be expected from measurements on darker skin types. In Zonios *et al*'s work, this is primarily a result of the low values of blood absorption coefficient applied.

Torricelli *et al* [179] was the only group to apply time-resolved reflectance spectroscopy. This involves a prediction of the temporal spread of a laser pulse using a diffusion model. The values presented can only be as good as the diffusion model, and rely upon a wavelength dependence determined from phantom measurements [180].

The absorption coefficients from both Graaf *et al*'s [175] and Doornbos *et al*'s [181] studies were lower than those from the remaining studies. Graaf *et al*'s and Doornbos *et al*'s studies involved an integrating sphere and multifibre probe respectively, as did the higher values from Svaasand *et al* [33] and Meglinski and Matcher [153]. Graaf *et al* and Doornbos *et al* applied a Monte Carlo Simulation and diffusion approximation respectively, as did Meglinski and Matcher and Svaasand *et al*. The multiple layered mathematical skin models which Svaasand *et al* and Meglinski and Matcher applied when considering separately the effects of the epidermis and dermis may be a more accurate approach than the single homogeneous layer used in Graaf *et al*'s and Doornbos *et al*'s work. Although the cause of lower values is not clear, Graaf *et al* commented that their absorption coefficient at 633 nm was 'much smaller than expected from *in vivo*' results. Doornbos *et al* did not comment directly on the cause of their low values, but mentioned that their 'results resemble those of Graaf *et al*'.

Scattering Coefficients

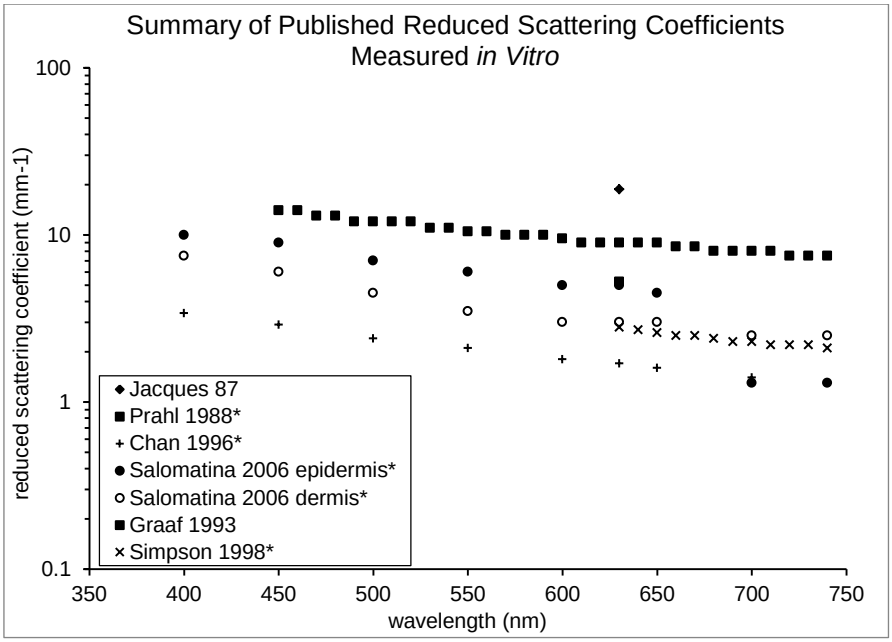

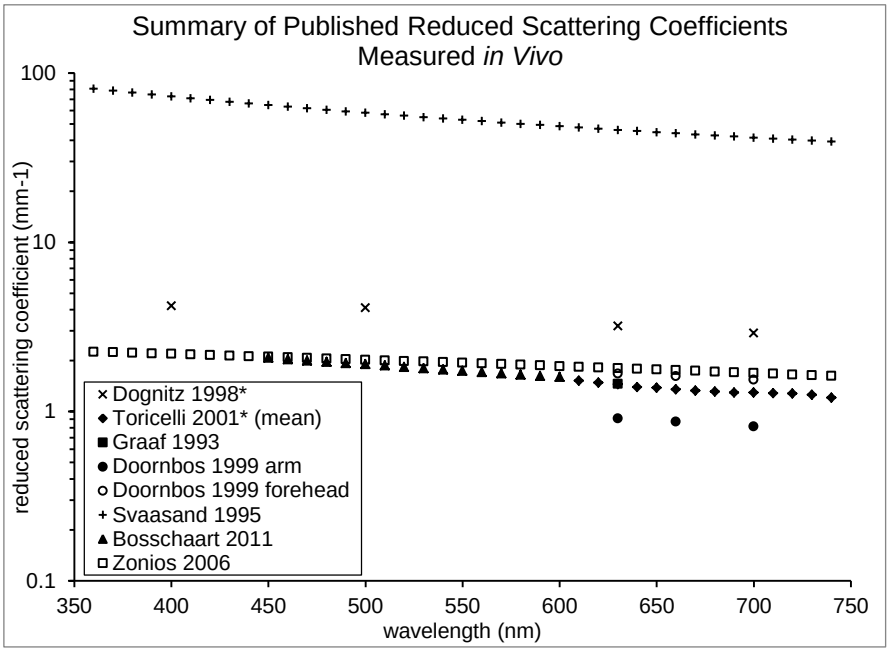

Figure 14: Summary of reduced scattering coefficients available in the literature. *In vitro* data represents absorption coefficients from exsanguinated skin whereas dermal *in vivo* data is inclusive of blood absorption. *data obtained from graphical presentation. †data presented was not complete and required input of haemoglobin or water optical properties obtained from [149]. Raw data is provided in Appendix E (Table 18).

In Vitro Studies

Of the studies analysed here, both Prahl's [159] and Jacques *et al*'s [172] studies describe a number of processes between tissue extraction and measurement which are likely to have had an effect on the measured reduced scattering coefficient, including: exposure to a 55˚C water bath for 2 minutes to aid with separating the epidermis from the dermis; freezing, cutting and stacking of 20 μm thick slices of the dermis; and

soaking in saline to rehydrate and wash away any blood. The bloodless samples were then held between glass slides in a saline filled tank and illuminated using a 633 nm laser. Freezing and drying, heating to remove the epidermis and deformation of skin samples have all been reported to change the measured values of scattering and absorption coefficients [172, 174, 175]. In particular, experimental work by Pickering *et al* [182] suggested that heating tissue to 55 degrees may increase the value of μ_s'. Also, Jacques *et al* [172] commented that soaking the dermis (in saline) will increase the backscattered reflectance, and thus may increase the calculated scattering coefficient. In contrast, Chan *et al* [173] and Simpson *et al* [174], whose reduced scattering coefficients were substantially lower, reported minimal tissue processing (although Chan *et al*'s specimens had previously been frozen).

A further source of disparity between *in vivo* data from earlier studies [159, 172, 175], which involved more tissue processing than the more recent *in vivo* data presented in Figure 15 [136, 173, 174], may have arisen from the choice of measurement setup. For example, Graaf *et al* [175] reported that discrepancies may arise when internal reflectance is not taken into consideration. Due to a larger difference in refractive indices, this will have a greater effect for samples in air compared to samples in water or saline solution. All samples were placed between glass slides. However, only the earlier studies analysed here, those which produced higher values of reduced scattering coefficient, submerged the sample in water or saline [159, 172].

Salomatina *et al*'s study [136] determined separately the reduced scattering coefficients of the epidermis and dermis. Their data show that the epidermal reduced scattering coefficient was consistently 2-3 mm^{-1} higher than the dermal reduced scattering coefficient over the visible spectrum. This suggests that studies which excluded the epidermis, such Chan *et al*'s [173] and Simpson *et al* 's [174], should provide lower values of reduced scattering coefficient than data obtained from studies in which the epidermis remained, such as Graaf *et al*'s [175] and Prahl's [159]. However, most probably due to a prevailing effect from the aforementioned influences, this is not the case.

In Vivo Studies

In addition to their interpretation of Prahl's *in vitro* data [159], Graaf *et al* [175] performed measurements of reflection on 5 male subjects with 'white' skin at 660 nm using an LED source. Despite using a similar wavelength light source to Prahl's 633 nm, reduced scattering coefficients from Graaf *et al*'s *in vivo* measurements were appreciably lower than their interpretation of *in vitro* data (Figure 15). This is likely to be a result of the posthumous tissue processing performed in Prahl's study as previously described. However, this effect is not reflected across the literature as, in general, reduced scattering coefficients from *in vivo* studies were not substantially lower than those evaluated from *in vitro* studies, nor did they demonstrate an appreciable difference when considering the variation in reduced scattering coefficients across the visible spectrum.

Any solution involving two independent variables (such as μ_s' and μ_a) can suffer from non-uniqueness, where equivalent results can be obtained from two or more sets of input values (local minima). When applying RTT to skin, a simulated increase or reduction in reflection can be attributed to a change in either μ_a or μ_s'. The reduced scattering coefficients from Svaasand *et al*'s study [33] were considerably higher than any of the other *in vivo* studies assessed. This is in addition to their high values of absorption coefficient discussed in the previous section. The paper stated that 'the fact that the calculated [skin reflectance] values tend to be higher than the measured ones might indicate that the used values for the epidermal and dermal [reduced] scattering coefficients are somewhat too high'. The reduced scattering coefficient from Svaasand *et al*'s work was derived from a single data point at 577 nm measured by Wan *et al* [183] fitted to a simple $\mu_s' \propto \text{wavelength}^{-1}$ relationship and therefore may not be as reliable as data derived from a series of direct measurements. It should also be noted that the remaining studies which produced the highest reduced scattering coefficients analysed here also provided the highest absorption coefficients, including both *in vivo* and *in vitro* data. Similarly, those studies presenting the lowest reduced scattering coefficients produced the lowest absorption coefficients (Figure 14). Furthermore, when applying high values of dermal scattering to a minimisation procedure, Verkruysse *et al* demonstrated the effect of non-uniqueness errors on derived skin properties, resulting in a clear overestimation of dermal blood volume fractions [106].

Dognitz *et al* [184] used a spatial frequency domain reflectometry (SFDR) method alongside a simulation constructed using the Wang and Jacques Monte Carlo programme [102] to calculate reduced scattering coefficients from the forearms of 6 subjects with Caucasian skin. Dognitz *et al* commented that due to the differences in measurement techniques their method interrogates a more superficial region of tissue than reflectance spectroscopy (as used in the work by Graaf *et al* [175], Svaasand *et al* [33] and Doornbos *et al* [181]) as there is no separation between source and detector. Salomatina *et al*'s *in vitro* results demonstrate epidermal reduced scattering coefficients which are greater than dermal values [136], suggesting that studies involving SFDR may expect an increase in measured reduced scattering coefficients compared to studies involving reflectance spectroscopy. Dognitz *et al* further commented that discrepancies due to surface reflection may cause their method to overestimate the reduced scattering coefficient. These comments are supported elsewhere in the literature [185] and by the remaining datasets which (with the exception of Svaasand *et al*'s work) demonstrate good agreement.

Other techniques used to assess reduced scattering coefficients include Torricelli *et al*'s time-resolved reflectance spectroscopy [179], Bosschaart *et al*'s diffusion approximation technique [178] and a Mie theory calculation by Zonios *et al* which included spherical scatterers with Gaussian distribution in size [73, 186]. The results from these studies are consistent with the majority of *in vivo* studies and with those *in vitro* studies which reported minimal tissue processing.

Further Causes of Discrepancy in the Absorption and Scattering Coefficients

It may be the case that the primary cause of discrepancy between the studies analysed here is a result of true differences between the skin samples selected. The degree to which such differences influence the measured coefficients is difficult to extract as, to the authors' knowledge, there are no studies which involve the measurement of optical properties from large numbers of skin samples, and none which determines the expected variation between samples with any one method of data acquisition or interpretation. Of the studies reviewed, the largest datasets involving a single measurement technique involved 6 subjects (one involved a range of skin types [33], the other used 3 male and 3 female subjects [184]). Only the former study commented

on the variation between individuals, with darker skin types demonstrating greater absorption across the visible spectrum. However, measurements were carried out on only one or two subjects from each skin type and the difference in epidermal scattering due to variations in melanin content was not considered.

Further variations between published absorption and scattering coefficients may have been caused by differences in the interpretation of data. Perhaps the most widely referenced set of absorption and scattering data for human skin is that published by Jacques *et al* [172]. Interpretation of the acquired data was carried out using the diffusion approximation. Prahl, who was an author of this paper, presented an almost identical process for determining the optical properties of abdominal skin samples in his PhD thesis [159] but applied a technique described as an 'adding-doubling' method. This is a 1 dimensional iterative technique that uses RTT to estimate the transport of light through skin from the reflection and transmission of two or more mathematical 'slabs' [159, 187]. Graaf *et al* [175] provided a further analysis of Prahl's data [159] using a Monte Carlo technique. The absorption coefficients calculated across these studies varied from 0.12 to 0.27 mm^{-1} and the reduced scattering coefficients from 5.3 to 18.7 mm^{-1} at 633 nm. This demonstrates that an alternative analysis of the same data can lead to a wide range in estimates of optical coefficients.

Van Gemert *et al* [188] used a diffusion theory model to compare absorption and scattering coefficients from a compilation of *in vitro* measurements including Jacques *et al*'s study [172] and papers published elsewhere [157, 183, 189]. Despite applying the same method of interpretation for each dataset, dermal absorption and scattering coefficients varied at 633 nm by a factor of nearly 2.5 (approximately 0.18 - 0.43 mm^{-1} and 1.8 - 4.1 mm^{-1} respectively). Hence, not only do alternative analyses provide noticeable differences in reported coefficients, but the same analysis of data from similar studies shows that there is a considerable difference in calculated coefficients across the published data.

Phase Functions

By far the most widely used approximation to the phase function of human skin is that first used by Henyey and Greenstein when trying to model diffuse radiation in the Milky Way galaxy [190]. The principal benefit of applying the Henyey-Greenstein (HG) phase function is that it can be described using only a single parameter, the modified anisotropy factor, g_{HG}.

$$p(\cos\theta) = \frac{1 - g_{HG}^2}{2\left(1 + g_{HG}^2 - 2g_{HG}\cos\theta\right)^{3/2}}, \qquad \text{Equation 7}$$

A number of investigations have been conducted to determine the validity of the HG phase function when applied to human skin. For example, Mourant *et al* [154] used a goniometer setup to measure the phase function of cell suspensions *in vitro* and Dunn and Richards-Kortum [191] simulated scattering from an individual cell using a finite difference time domain simulation[5]. Both studies found that the HG function was a poor approximation to the scattering from individual cells as it underestimates scattering at large angles, although Mourant *et al* commented that the HG phase function reproduces the experimentally measured phase function "reasonably well for angles less than 75°". This is in agreement with other work [192-195].

In order to compensate for the weaknesses in non-forward scattering, Jacques *et al* [172] introduced an additional empirical term representing the proportion of isotropic scattering. They performed goniometric measurement of scattered light through tissue samples and fitted the data to the modified HG function (Equation 8).

$$p(\cos\theta) = \frac{1}{2}\left[b + (1-b)\frac{1 - g_{\text{mod}}^2}{2\left(1 + g_{\text{mod}}^2 - 2g_{\text{mod}}\cos\theta\right)^{3/2}} \right] \qquad \text{Equation 8}$$

where $g_{\text{mod}} = \int_{4\pi} p(\cos\theta)\cos\theta d\omega'$ and where b is the proportion of isotropic scattering. Applying a value of b = 0.1, they calculated g_{mod} = 0.82 at 633 nm. Van Gemert *et al* [188] and Sharma and Banerjee [196] supported the use of this modified HG phase function when comparing results to *in vitro* goniometer measurements and Monte Carlo simulations respectively. Furthermore, Graaf *et al* [155] reported that the value of the anisotropy factor used in Jacques *et al*'s study was in agreement with a Mie scattering model of a set of spherical scattering particles with radius of 0.37 μm.

The Henyey-Greenstein expression is purely empirical, however the Mie phase function is derived from a mechanistic theory of light transport and can be used to

[5] a direct solution of Maxwell's equations in the time domain

accurately determine the phase function from a single spherical particle. Several authors have attempted to justify the use of Mie theory calculation for the phase function within specified volumes of a skin model [162, 197, 198]. However, calculations require adequate knowledge of the sizes and refractive indices of scattering particles within the skin and are complex when considering a distribution of these parameters. Although such calculations are possible [199], they have not been shown to offer significant advantages over the conventional HG phase function.

The FDTD method used by Dunn and Richards-Kortum [191] and Mourant [154] was capable of predicting the effects of cell structures on the scattering phase function for a single cell, including nuclei and melanin, but did not offer a comparison with measured skin data. Liu [200] introduced a new phase function in an attempt to improve upon the HG phase function. This study concluded that the new phase function showed better agreement to a Mie calculation when compared to a HG phase function. Again, no direct comparison to measured skin data was presented.

Refractive Indices

The surface of the skin is usually approximated as perfectly smooth and thus simulations of surface scatter depend entirely upon an input of refractive index. Ding *et al* [201] illuminated the skin *in vitro* using a number of light sources ranging in wavelength from 325 nm to 1557 nm. By fitting their data to dispersion schemes used previously on ocular tissues, they predicted values of refractive index ranging from approximately 1.41 to 1.49 in epidermal tissues and 1.36 to 1.41 in dermal tissues over the wavelength range. This is in agreement with other data published using an equivalent technique [202, 203]. However, Tearney *et al*'s study [204] applied Optical Coherence Tomography to measure refractive indices of *in vivo* skin at 1300 nm and determined values from a single participant of 1.52 for the stratum corneum, 1.34 for the living epidermis and 1.41 for the dermis. Considering the aforementioned influence of posthumous tissue processing on measured reduced scattering coefficients, it may also be the case that refractive indices are similarly affected. Comparing Tearney *et al*'s *in vivo* refractive indices to Ding *et al*'s *in vitro* values (1.46 for the combined epidermis and stratum corneum and 1.36 for the dermis at 1300 nm), there is a suggestion that *in vitro* methods may result in an increase in the measured refractive indices.

Blood and Blood Vessels

The optical properties of blood differ from those of other tissues within skin as blood does not contain significant intercellular scatterers. Thus, the optical properties of blood are primarily determined from the concentration and distribution of erythrocytes. Although a number of investigations have been carried out on human blood, many have used agitated vials containing randomly distributed and oriented erythrocytes which are not representative of blood as it appears in the dermis [205, 206]. Changes in erythrocyte organisation, shape and orientation have all been shown to influence the optical properties of blood flowing within vessels [205]. Only two studies were found which have attempted to measure the optical properties of flowing blood [74, 75]. Although the results from these two studies are not in complete agreement, they both suggest that blood exhibits increased absorption and decreased scattering relative to remaining skin, with a reduced scattering coefficient and absorption coefficient of flowing blood of around 2.5 mm^{-1} and 0.5 mm^{-1} respectively at a wavelength of 633 nm.

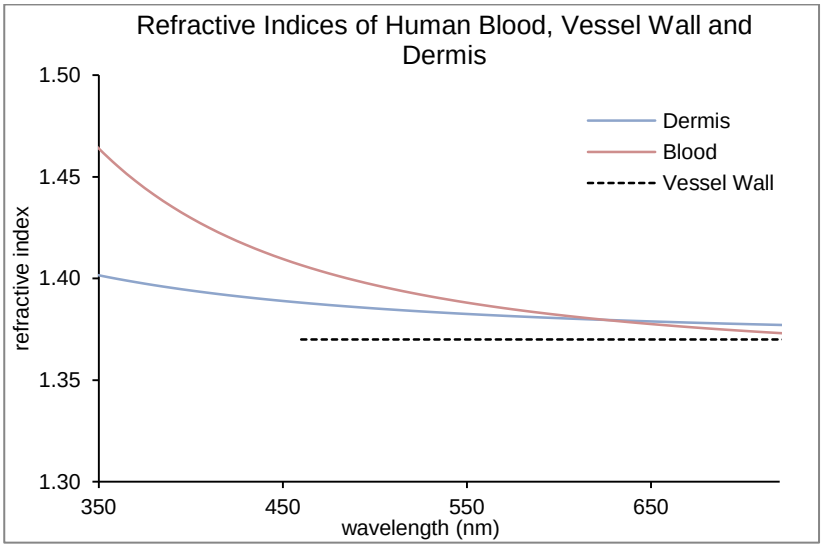

Figure 15: Refractive indices of human blood [207], vessel wall [208, 209] and dermis [201].

To the author's knowledge, the optical properties of dermal blood vessel walls have not been investigated directly. However, studies of scatter from aortic walls suggest a scattering coefficient of around 3 mm^{-1} at 633 nm [210], similar to that of the surrounding dermis (Figure 14, page 58). Surface scattering (as estimated using

refractive indices) is also of particular importance when considering blood vessels in the skin (Figure 16).

It can be seen in Figure 16 that the reported refractive indices of the vessel wall, blood and surrounding dermis are similar in the yellow to red regions (>550 nm) but differ significantly at the blue to violet end. Thus, greater scattering (reflection and refraction) will occur at the vessel wall at shorter wavelengths within the visible spectrum. It may be of interest to note that the scattering effects described here further contribute to the green/blue appearance of larger vessels in the skin.

Although studied, [211, 212] the HG phase function has not been substantially supported for the approximation of *in vivo* blood scattering anisotropy in skin. At present, analytical methods have more success in this case [206, 213].

Conclusions

Light transport through skin is dependent both upon the effects of scattering structures such as filamentous proteins, and upon the quantity and distribution of highly absorbing chromophores such as melanin and haemoglobin. Simulations of these effects are most commonly achieved using RTT.

Orders of magnitude variation were found to exist between RTT absorption and scattering coefficients across the literature. Absorption coefficients were found to be profoundly affected by the presence of blood, as demonstrated when comparing *in vitro* to *in vivo* data, and reduced scattering coefficients demonstrated a clear increase in magnitude resulting from tissue processing of *in vitro* samples. Fewer studies were found which analysed anisotropy factors and refractive indices, or which considered directly the optical properties of dermal blood vessels.

Due to the known effects of tissue processing on reduced scattering coefficients and the unavoidable coupling between absorption and scatter on measurements on *in vivo* skin, *in vitro* scattering coefficients which report minimal tissue processing, such as the study by Chan *et al* [173] should be considered foremost in future studies of skin optics. The effect of blood on the reported absorption coefficients, along with the observed coupling effects between absorption and scatter, suggest lower values of absorption coefficients measured *in vivo*, such as those reported by Meglinski and Matcher [153] or Zonios *et al* [73], appear to be the most reliable choice. The HG phase

function has a proven track record in skin optics, but published values of anisotropy factor and refractive indices are too few to provide a thorough comparison.

The following chapter provides an analysis of simulations which have applied skin optical coefficients to simulate the colour PWS skin.

5. Simulating the Colour of Human Skin

Based upon the published work by Lister et al [214]

Introduction

Port Wine Stains (PWS) are progressive vascular lesions of the dermis affecting around 25 million people worldwide. They often constitute a significant cosmetic problem and, if left untreated, are likely to develop nodular or hypertrophic areas which are prone to spontaneous or trauma-induced bleeding and consecutive infection [215, 216]. The long-term psychological effects of PWS are documented widely but have been shown to be mitigated significantly after treatment [217].

Although flashlamp-pumped pulsed dye laser (PDL) treatments are widely considered the treatment of choice for PWS, fewer than 20% of patients experience complete lightening using this method, whereas 20–30% are considered "poor responders" [28, 30, 218]. It has been proposed that one reason for inadequate clinical results is that the laser parameters used are virtually identical for all PWS patients despite the commercial availability of laser systems with user-specific settings [1, 2]. In order that laser treatment may be optimised on an individual patient basis, the practitioner must be aware of the vascular architecture constituting each lesion, including the number, distribution and sizes of affected vessels [2]. It is these characteristics, as well as the properties of overlying skin (such as epidermal melanin content) which constitute the colour of PWS skin [5].

The simplest method of assessing PWS colour is through visual observation. However, this is both subjective and qualitative. Perceived colour may be influenced by a number of factors such as ambient lighting conditions, colours surrounding the subject, eye adaptation prior to viewing and viewing geometry [30, 83]. Although photographic images have been applied to determine the efficacy of laser treatment for PWS, great care must be taken to minimise the effects of variations in patient positioning, camera sensitivity and lighting during acquisition, and the quality of printing or visual display of the image [84, 219]. To confound this further, communication of perceived colour is difficult as, for example, most PWS skin may correctly be described as 'red' in colour.

Quantitative, reproducible assessments of PWS lesions have been achieved using colour measurements (for a full discussion, see [27]). Colour measurement devices consist of one or more optical fibres or integrating spheres which are placed in contact with the skin and through which incident and reflected light are passed. Data

available from these devices may include spectral reflectance curves covering a broad spectrum (Figure 17), colour co-ordinate values relating to human colour perception or indices representing approximations of blood or melanin content. Once a technique restricted to the laboratory, modern hand-held devices are capable of collecting skin colour data instantaneously. Although care must be taken to avoid blanching during contact and to replicate the positioning of the device between assessments, colour measurements have been shown to produce excellent inter- and intra-user repeatability [84, 113] and have been applied successfully in the determination of laser treatment efficacy in PWS lesions [220].

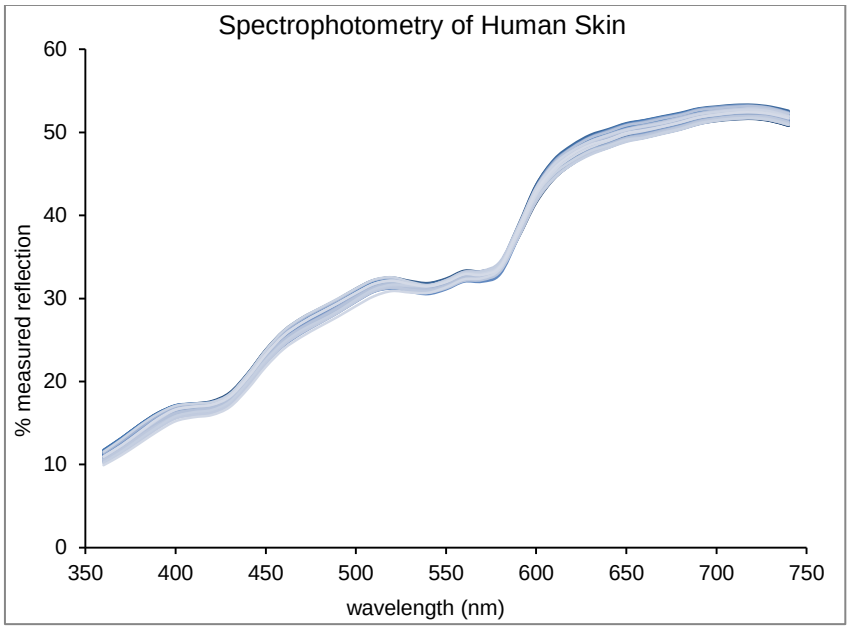

Figure 16: Spectral reflectance of 50 consecutive measurements from the inner forearm of the author obtained using a Konica-Minolta 2600d integrating sphere spectrophotometer.

Clinically relevant, objective information may be determined from skin colour measurements through the inverse application of a skin model. This method begins by creating a mathematical skin model through which light transport is simulated. Specific features of the model are then adjusted until its simulated colour is in adequate agreement with the measured colour of the patient's skin. These adjusted features, such as concentrations and distributions of melanins and haemoglobins, can be used to inform diagnosis or treatment. Simulations of skin colour require an understanding of the optical properties of skin [5] and must consider the prominent interactions of light. A comprehensive review and analysis of the approaches used to simulate light transport through PWS skin is presented, addressing the latter.

Skin Colour

When skin is illuminated with a white light source, its colour is determined by the spectral variation in reflected and backscattered light. The proportion of light reflected from the surface of skin has not been shown to vary substantially with wavelength or between individuals, and does not contribute appreciably to the colour of skin [15, 117]. The remaining light may be absorbed within the skin or scattered back to the surface. The proportion of backscattered light varies considerably with wavelength, pigment content and scattering properties of the skin [5]. Thus, it is this backscattered light which is predominantly responsible for the colour of skin.

With regards to PWS skin, vessel number, mean diameter and depth have been shown to influence the colour of the lesion [32, 37, 42, 49]. It has been suggested that equivalent colours can be obtained through different combinations of these parameters. For example, Barsky *et al* carried out an investigation involving biopsy samples from 100 facial PWS lesions [32]. They observed that the mean vessel area and total vascular area correlated strongly with colour assessed using a visual comparison of the skin against a Pantone colour chart. Thus, Barsky's results suggest than skin colour is derived from the quantity of blood in PWS skin, independent its distribution through the dermis. Fiskerstrand *et al* [42] used the same methods of 3 mm punch biopsies on 30 patients and comparisons against a Pantene colour chart. They also reported that skin colour was dependent upon vascular area, but found that "pink and purple lesions were significantly deeper located than were the red lesions" and larger diameter vessels corresponded with a darkening of PWS colour, from pink to purple [37, 42]. Verkruysse *et al* introduced a correction factor to investigate the effect of vessel diameter on PWS colour through Monte Carlo simulations [23]. They suggested that several small vessels, close to each other, may be optically equivalent to one large vessel over the yellow and blue regions of the visible spectrum. However, their simulated results showed that the proportion of red light reflected from the skin was influenced strongly when varying dermal blood fraction but only minimally when varying vessel diameter (Figure 17).

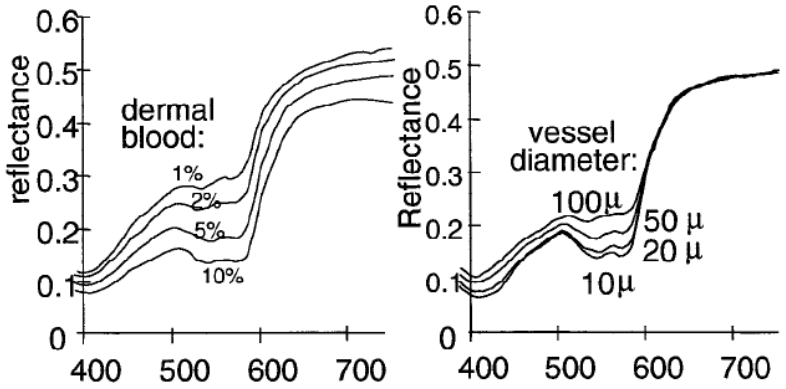

Figure 17: Change in simulated spectral reflection with varying dermal blood concentration (left) and vessel diameter (right). With kind permission from [23].

Simulating PWS Skin Colour

In order to accurately reproduce human skin colour, and variations in colour between individuals or regions, over time or as a result of a medical condition such as PWS, a simulation must account for the prominent interactions of light within skin. These interactions may be described using classical electromagnetics, based upon Maxwell's equations, whereby light is treated as a wave containing an electric component and a magnetic component. When travelling through a medium such as skin, this wave causes elements of electric or magnetic charge (e.g. electrons) to oscillate and, in turn, the oscillating elements radiate electromagnetic waves. The observed transmitted or scattered wave is a result of the summation of each of these secondary waves. The secondary waves may not have the same phase or magnitude as the incident wave and some of the energy will be lost to the charged elements; further energy is lost to the medium through destructive interference of secondary waves.

An exact calculation of the resultant wave is exceedingly complex, as it relies not only on the precise position of each charged element in the medium, but also upon the local electromagnetic environment, which is continually altered by the interaction of the wave with the medium. Instead, specific solutions to Maxwell's equations have been developed for simplified situations.

At the Skin Surface

The effects of surface topology on skin appearance are of considerable interest to the cosmetic [221] and computed animation [165, 222] industries, as well as medicine [59, 223]. These investigations are primarily concerned with differences in appearance as a

result of varying viewpoints or angles of illumination. However, the majority of studies into PWS skin colour consider a simple approach to approximating surface reflection. By modelling the skin surface as a perfectly smooth interface, and by assuming the superficial region of the skin can be assigned a single value of refractive index for the wavelength or wavelength range considered, the Fresnel equation may be used to estimate the relative quantities of reflected (R) and transmitted ($1-R$) light:

$$R = \frac{1}{2}\frac{(a-c)^2}{(a+c)^2}\left\{1+\frac{[c(a+c)-1]^2}{[c(a-c)+1]^2}\right\} \qquad \text{Equation 9}$$

Fresnel reflection (R) of unpolarised light from air (refractive index = 1) to skin, where $c = cos(\theta_i)$, θ_i is the angle of incidence, $a = n^2 + c^2 - 1$ and n is the refractive index of skin.

Refraction occurs as light passes from air to skin, or between regions of the skin whose refractive indices differ. Simulations of skin optics which account for the effects of refraction generally do so through the application of Snell's law:

$$\theta_t = \arcsin\left(\frac{1}{n}\sin\theta_i\right) \qquad \text{Equation 10}$$

Angle of refraction (θ_t) at the skin's surface calculated using Snell's law.

Both Fresnel's equation and Snell's law require knowledge of the refractive indices of skin and the incident angle of light. Angles of incidence and transmission may be calculated simply for a skin model consisting smooth or flat interfaces. Refractive indices are generally obtained from direct measurements [5].

Light Transport through Skin

The behavior of the remaining (transmitted) light is commonly simulated using Radiative Transfer Theory (RTT) [170]. This considers the transport of light in straight lines (beams). Absorption is modelled as a reduction in the radiance of a beam and is dependent upon the absorption coefficient (μ_a). The degree of scattering is described by both the scattering coefficient (μ_s), which considers both a loss of radiance in the direction of the beam and a gain from beams in other directions, and the phase function (p), which describes the distribution of scattering angles.

Due to the complex nature of skin, a general solution to the application of RTT is not available [188]. Thus, a further approximation is required. There are two main approaches to approximating the application of RTT: those which use a deterministic

approach and those which employ a stochastic 'ray tracing' technique. In addition, Prahl described an 'adding-doubling' method in his PhD thesis and associated publications [159, 170, 187]. This is a 1 dimensional iterative technique that uses RTT to estimate the transport of light through skin from the reflection and transmission of two or more mathematical 'slabs'. Although relatively simple in principle, it has not been used greatly outside of Prahl's work.

Beer-Lambert Law

The Beer-Lambert law is a simple deterministic technique which has been applied to estimate the reflectance (R) from a skin model. Although empirically derived [224], this is essentially a solution to the application of RTT to the interaction of light with a static homogeneous absorbing (non-scattering) medium.

The Beer-Lambert law uses an estimate of the attenuation of light (A) obtained by measurements of on-axis transmission through thin samples of skin, and the optical path length (l):

$$R = e^{-Al} \qquad \text{Equation 11}$$

Modified versions of the Beer-Lambert law have been applied to estimate the quantities of melanin and haemoglobin in the skin [121, 133, 225]. These generally involve an additional exponential term to describe loss due to scattering and use an approximation of the mean optical path length $\langle l \rangle$, for example:

$$R_{modified} = e^{-\mu_a \langle l \rangle + A_0} \qquad \text{Equation 12}$$

where μ_a is the absorption coefficient and A_0 is the attenuation caused by scatter. This technique is only applicable in a medium where absorption and scattering are relatively homogeneous [36]. In skin, where areas of high scattering (*e.g.* deep epidermis) and high absorption (such as those found in PWS skin) exist, the Beer-Lambert Law is not appropriate. Furthermore, it is not possible to account for the effects of vascular architecture in PWS skin using this method alone. When compared to an alternative simulation method, Shimada *et al* [121] confirmed that the Beer-Lambert law is not sufficiently accurate for investigating human skin.

The Diffusion Approximation

The Diffusion Approximation to RTT is by far the most widely used deterministic approach in biomedical optics, with Farrell *et al*'s method [104] accumulating over 500 citations alone [38].

The Diffusion Approximation is described in detail elsewhere [170, 171]. In summary, it has a low demand for computing power and thus provides fast convergence for a wide range of applications. For example, it has been applied successfully to real-time light dosimetry during photodynamic therapy (PDT) of superficial skin cancers [226, 227], differentiation between pigmented skin lesions (including malignant melanoma) [137] and to determine blood oxygen saturation levels faster, and over a larger area than existing methods with equivalent reliability [228]. However, it suffers from a number of limitations, in part because it relies upon approximate solutions to an equation that itself represents an approximation to the equation of radiative transfer [229]. For example, there is a requirement that scattering is dominant over absorption. This may be appropriate in clinically normal pale skin types, as the probability of scattering within the skin may be as high as twenty times that of absorption [5, 35]. However, absorption is much greater in the epidermis of darker skin types, the blood vessel plexi of the normal dermis, and within PWS lesions. Thus, the validity of this approximation is limited in such cases [106, 229-232].

These drawbacks have limited the application of the Diffusion Approximation to investigations of PWS skin. For example, Verkruysse et al. [106] reported that data obtained from their 2 layered skin model could be obtained quickly but compared poorly to measured spectra, resulting in an overestimation of blood volume fraction, oxygenation levels and melanin concentration in Port Wine Stain (PWS) skin. Zhang *et al* [107] found similar problems when applying a genetic algorithm minimisation procedure to their Diffusion Approximation results, as did Lakmaker *et al* [25] when investigating a method of predicting the maximal treatment depth response required for complete clearance of PWS lesions. Svaasand *et al* [33] applied a diffusion approximation to their model, predicting the effects on skin colour resulting from changes in the depth and thickness of a PWS lesion. However, simulated spectral reflectance curves compared poorly to their single example of a measured dataset, suggesting that these predictions of skin colour may not be applicable on an individual basis.

The Monte Carlo Method

Monte Carlo simulations used in biomedical optics are simply ray-tracing procedures, where a statistical analysis is used to calculate, step-by-step, the movements of simulated photons or light beams through a mathematical skin model [81] (see Figure 18). This has been described as a discrete version of the radiative transport equation [200]. The Monte Carlo method was first introduced to the field of skin optics by Wilson and Adam in 1983 [233] and was developed further by a number of groups over the next decade [208, 234-237]. Although its use at this time was limited due to high demands in computing power, Monte Carlo methods are widely regarded as the most accurate simulations of light transport through skin [107] and, as a result of recent advances in computing hardware, they are now routinely used for the interpretation of spectral data [27].

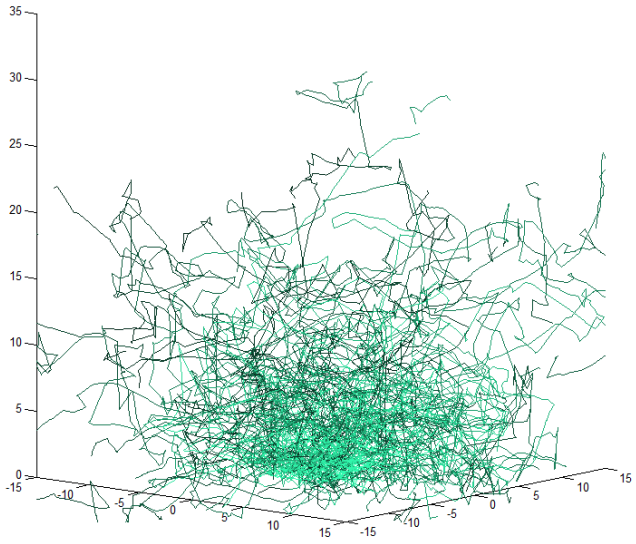

Figure 18: Example of ray traces from 100 beams at a wavelength of 590 nm, simulated using a Monte Carlo programme developed by the first author (T. Lister). Beams are initiated on the x-y plane (bottom of image). Reduction in beam 'weight' along each path is represented as a transition from light to dark green (color online). Dimensions in mm.

In 1989, Keijzer *et al* published their Monte Carlo simulation, analysing the effectiveness of vascular laser treatments [238]. This programme employs a two layer skin model and was developed for investigating PWS skin, in particular for determining the energy deposition within a single vessel during laser treatment. A pencil beam directed perpendicular to the surface of the skin model is initiated at a position randomly allocated within a circular region. The beam propagates through

the skin model, undergoing absorption and scatter at events separated by a distance (s), calculated as follows:

$$s = \frac{-\ln(\varepsilon)}{\mu_a + \mu_s} \qquad \text{Equation 13}$$

where ε is a random number generated from a uniform distribution between 0 and 1, μ_a is the absorption coefficient and μ_s is the scattering coefficient. At the end of each 'step', a reduction in the beam *weight* (W, representing the total beam total energy of the beam) is calculated in accordance with Equation 14:

$$\Delta W = W \frac{\mu_a}{\mu_a + \mu_s} \qquad \text{Equation 14}$$

Keijzer *et al*'s programme has the advantage of easy insertion of a sphere, ellipsoid or cylinder into the skin model, to simulate blood vessels for example, but lacks versatility as it uses a pre-determined set of optical parameters determined from phantom measurements.

Keijzer *et al*'s programme was used by Lucassen *et al* [239] to study the effects of laser wavelength on the response of PWS skin to laser therapy. The simulation calculated the absorbed energy within a single straight blood vessel of varying diameters, a curved blood vessel and multiple straight blood vessels. A 585 nm laser beam was predicted to be more effective than a 577 nm beam. This is in agreement with the results found in clinical practice, as a transition of standard practice between these two wavelengths followed worldwide (prior to the shift from 585 nm to 595 nm), as did the introduction of epidermal cooling during laser therapy, also recommended in Lucassen *et al*'s study. Verkruysse *et al* [23] also used Keijzer *et al*'s simulation to study the influence of PWS anatomy on skin colour. They created five models consisting of varying blood layers containing homogenous distributions of blood, with a correction factor to account for reduced light absorption when blood is contained within vessels. Verkruysse *et al* commented that their simple skin model failed to take into account the effects of high epidermal scattering, even though they were able to model a diffuse irradiance of photons. Predicted changes of skin colour with the removal of superficial vessels did not correspond with the reported clinical response.

In 1992, Wang and Jacques (the latter of which was listed as an author on the previously discussed paper by Keizer *et al*) published a Monte Carlo simulation of steady-state light transport in multi-layered tissue using the ANSI Standard C computing language [102, 237]. This programme is freely available on the internet [237] and allows users to create a two-dimensional skin model by inputting custom values of absorption coefficients, scattering coefficients, refractive indices and (Henyey-Greenstein) anisotropy factors for any number of layers. Like the programme produced by Keijzer *et al*, the simulation begins with an infinitely narrow beam incident normal to the skin surface whose path through the skin is governed by Equation 13 and Equation 14. A convolution algorithm may then be applied retrospectively to simulate a light source of finite size, such as a laser beam. This effectively repeats the results from the infinitely narrow beam over a finite area without performing any further simulations.

Mantis and Zonios [240] developed a two layer mathematical skin model to estimate the thickness and absorption coefficient of a superficial absorbing layer using Wang and Jacques' Monte Carlo programme. They inputted reflectance values obtained from a fibre optic spectrophotometer setup and compared them to the results simulated from an infinitesimally narrow incident laser beam. Nishidate *et al* [126] applied the same programme to a skin model consisting of an epidermis, dermis and local blood region. The depth and thickness of the simulated local blood region was adjusted until the simulated reflectance was in adequate agreement with a measured spectrum, forming an estimate of these parameters in the measured sample. They inputted measurements from a tissue phantom using a diffuse illuminant and a CCD camera setup. Both studies reported absorption and reduced scattering coefficients with errors of around 10% compared to values expected from their skin phantoms. Considering the addition of uncertainty and optical inhomogeniety in a genuine skin sample, these errors are considerable. In fact, the study by Nishidate *et al* [126] used the same method to estimate the depth of *in vivo* human veins. They reported errors of up to 0.6 mm for the depth and 0.2 mm for the thickness of veins when compared to ultrasound measurements. Again, these errors are large when considering normal skin thickness [241].

Other research groups have developed Monte Carlo simulations for use in biomedical optics. Graaf *et al* produced a condensed Monte Carlo simulation based upon the same governing equations (Equation 13 and Equation 14) but utilising the derived relationship between simulated reflectance and albedo. In detail, the same simulated diffuse reflectance may be obtained by increasing the scattering coefficient and simultaneously decreasing the absorption coefficient, maintaining a fixed value of albedo (a dimensionless coefficient defined as the ratio of scattering coefficient to the sum of absorption and scattering coefficients) [242]. To demonstrate the effects of varying absorption and scattering coefficients whilst maintaining a fixed albedo, the following parameters to a simulation of 1 million photon packets were applied using Wang and Jacques' programme [237]. The skin model consisted of a single layer with an effectively infinite depth (1x10^8 cm) (Table 3):

Absorption Coefficient	Scattering Coefficient	Albedo	Calculated Diffuse Reflectance (MCML)
1.0 cm^{-1}	50 cm^{-1}	0.980	18.4%
1.0 cm^{-1}	100 cm^{-1}	0.990	28.7%
0.5 cm^{-1}	50 cm^{-1}	0.990	28.7%

Table 3: Results from a simulation of 1 million photons. Values are presented for a simulation carried out using the Wang and Jacques Monte Carlo programme (MCML) [102] with a simple single layered skin model of 1x10^8 cm depth; values of g=0.9, refractive index =1.3 and pencil beam irradiation were used throughout (simulated by the first author, T. Lister).

This technique vastly improved simulation time for a uniform skin model and was shown to determine skin optical coefficients consistent with other studies [5, 175]. This work was later extended by Wang *et al* [243] who considered the effects of varying the diameter of the source. Wang *et al* also demonstrated superior calculation times whilst maintaining good agreement with a standard Monte Carlo simulation.

Meglinski and Matcher's programme [153, 230] involved a seven layered skin model to simulate the reflectance spectrum of human skin, as measured using a fibre optic probe setup. Path lengths were calculated according to Equation 15 and absorption coefficients applied separately (Equation 16):

$$s = \frac{-\ln(\varepsilon)}{\mu_s} \qquad \text{Equation 15}$$

$$\Delta W = We^{-\mu_a s} \qquad \text{Equation 16}$$

The programme has undergone a number of developmental steps since its first publication in 2001 and is currently available online as an interactive object oriented programme with a multitude of potential outputs [244, 245].

Meglinski and Matcher found good agreement between their calculated reflectance and a single example of measured reflectance between 450 and 600 nm wavelengths, although the skin properties used outside of this wavelength range did not appear to provide a good agreement. This shortcoming may have been as a result of the constant scattering properties applied to the skin model over the entire wavelength range investigated. When applying the coefficients used by Meglinski and Matcher to Wang and Jacques' Monte Carlo programme, Maeda *et al* [246] reported a "rather strange spectral curve that had much worse agreement with measured results than [another set of coefficients]", demonstrating a clear discrepancy between the two programmes.

In summary, Monte Carlo simulations have contributed substantially to the field of skin optics since their introduction in 1983 [233]. Initial development by Keijzer *et al* [238] and later by Wang and Jacques [237] facilitated a number of studies into the colour of PWS skin. More recent work has demonstrated gradual development in Monte Carlo techniques for the simulation of PWS skin colour and with continuing advancements in computing power available to the researcher, and an ever increasing interest in skin optics, such advances are likely to continue into the foreseeable future.

Conclusions

The colour of PWS skin depends primarily upon the number, depth and sizes of affected vessels. Thus, by measuring skin colour, it may be possible to inform a better knowledge of these characteristics for an individual lesion, providing essential information for the optimisation of laser treatment. The most common approach to extracting information from a measurement of skin colour is through the inverse application of a skin model, whereby a simulation of light transport based upon RTT is performed.

Due to its low demand for computing power, the Diffusion Approximation has been applied widely in the field of skin optics. However, its limitations, along with the availability of increased computing power, have resulted in an increase in popularity of Monte Carlo simulations. Keijzer *et al*'s and Wang and Jacques' Monte Carlo programmes employed implicit capture to increase the speed of their simulations. These simulations have contributed significantly to the field of biomedical optics. However, recent developments have improved upon these, to provide more accurate simulations of light transport through skin. As the scope for applying such techniques continues to broaden, with the possibility of introducing such a technique into routine clinical practice and with the continuing increase in computing power available to the researcher, further developments should be investigated to overcome the shortcomings of the studies presented here.

5. Methods

5.1 Data Collection

Recruitment

The degree of fading achieved by laser therapy has been shown to be influenced by the anatomical location of a PWS lesion [47, 65]. Approximately two thirds of PWS lesions are thought to occur on the face [31]. Furthermore, facial PWS are more likely to receive treatment (over the period March 2008 to March 2009, the Wessex Specialist Laser Centre at Salisbury District Hospital, UK (WSLC) treated 127 patients, of which 91 involved treatments to the face). Therefore, it was decided to restrict the study to individuals receiving treatment for facial PWS.

PWS lesions are thought to thicken and darken with age [247]. The WSLC treated 68 new facial PWS patients over the period March 2008 to March 2009, of which 63 were children (less than 18 years old at the start of treatment). Thus, in order to reduce variation in the participant group, ethical approval was initially sought for carrying out assessments on 40 children.

Based on an estimated 85% uptake, it was assumed that 40 participants under the age of 18 could be obtained in approximately 9 months. Patient numbers over the following months unexpectedly declined[6], with a total of 5 new patients (2 of which were under 18 years) over the period 1st July 2010 to 1st December 2010. Neither of these eligible patients were invited to take part in the study.

In order to improve uptake into the study, an amendment was made (and approved by the appropriate committees) to include patients over 18 years of age. As part of this amendment, the way in which the study information was provided to eligible patients was also changed such that the author was able to present the information directly.

Due to a continued lack of patients attending the WSLC for treatment, a second amendment was made and approved by the appropriate committees. This further widened the potential participant group to include current patients who had already

[6] This appears to have been caused by the 2008 global financial crisis, which caused a tightening in NHS spending and changes in funding criteria.

undergone laser treatment at the WSLC. This is supported by previous studies, which show a consistent reduction in PWS colour after each treatment [88, 248].

Exclusion Criteria

- Patients with dark skin types (Fitzpatrick scale IV-VI) as skin laser treatment is known to carry greater risks of adverse effects in this population. This is acknowledged to be a contra−indication to Pulsed Dye Laser treatment at the WSLC.
- Patients with co−morbidity of diabetes or other disease that may impair healing.
- Participants who have previously undergone any alternative treatments on the site of interest (not involving the 595 nm Pulsed Dye Laser that is employed in the department), as the effect of these treatments to the PWS may be unpredictable.
- Patients with medical conditions or injuries (*e.g.* purpura, burns) that affect the perfusion of the skin or other determinants of skin colour in the anatomical regions being investigated were excluded due to the unknown and unreliable effects on measurements of skin colour.
- Cosmetics and topical products affect the measurement of skin colour and were removed at least 10 minutes before the assessment. If this was not possible (*e.g.*in the case of some self tanning products), then the participant was excluded from the study.
- A number of drugs are known to affect skin perfusion and other factors which influence skin colour (40). Exclusion based upon the use of drugs was considered on an individual basis, as listing the possible drugs that may affect the measurement would be an exhaustive task.

Interview and Measurements

Throughout the time of the study, a PWS patient's first appointment at the WSLC involved a "test patch" treatment, a treatment to a small area to determine the effectiveness of the laser settings used and to identify any adverse effects. The first definitive treatment was then carried out at around four months after the test patch appointment and treatments repeated at approximately 4 month intervals.

Each new patient recruited for the study was provided with an information sheet during their test patch appointment. Existing patients were provided with the same information during the first available appointment. Planned assessments were performed immediately before the participants' next two definitive laser treatments.

A short interview was undertaken before each assessment to establish whether the participant continued to meet the study criteria. During this time, participants were allowed to rest and acclimatise to the ambient temperature of the room (for a minimum of 10 minutes). This ensured that perfusion of the skin (and therefore skin colour) could be stabilised [85, 176]. The regions to be assessed remained uncovered and free from cosmetics during this time, as recommended by Pierard *et al* [176].

The temperatures of the rooms in which assessments were carried out were controlled by a heat exchange system. Two of the three rooms were monitored over a 3 month period prior to any assessments using an Omega OM-62 temperature data logger. During this time, the temperature was found to be consistently 22.5 ^{o}C (± 1 ^{o}C) in both rooms. It was assumed that the third room (used for one participant) also retained a stable temperature. Although one study [85] suggests that the colour of PWS skin (as measured by reflectance spectrophotometry) does not change significantly with ambient temperature, room temperature was recorded during acclimatisation as a precaution. This was done using the same Omega OM-62 temperature data logger and uploaded to a PC.

Spectrophotometry

Skin colour was measured using the Minolta CM-2600d spectrophotometer. A suitable site was chosen for the measurement of colour on the PWS lesion. This site was consistent in colour over the measurement area with no blemishes (*e.g.* moles or blebs) and minimal hair. It was also situated on a smoothly contoured area of skin to ensure skin contact over the full aperture and therefore no loss of light. A contralateral site on the normal skin was also chosen, subject to the same criteria. With the participant seated in one of the temperature controlled rooms, 5 measurements were carried out in series on both the PWS and contralateral ('normal skin') sites. To reduce the possible effects on the colour measurement from skin blanching resulting from contact with the spectrophotometer, minimal pressure was applied and the spectrophotometer was removed and replaced between each

measurement. Posture is known to affect the supply of blood to different body areas [176]. For this reason, all participants were asked to remain seated whilst acclimatising and during the colour measurements.

Assessing the Repeatability and Reproducibility of Spectrophotometry Measurements

The repeatability of skin spectrophotometry measurements is primarily dependent upon the inherent properties of the device employed as well as variations in measurement technique. Reproducibility may be further affected by physiological or environmental changes (such as variations in ambient temperature or humidity). Both the repeatability and reproducibility have the potential to influence the colour measurements carried out in this study.

The principle sources of error affecting the repeatability of any spectrophotometric measurement include dark-current (electronic noise within the CCD array and associated components) and variations in the output of the illumination source. Saturation may also be a considerable cause of error when measuring samples with regions of high reflectivity, although this is not usually applicable to human skin samples.

The effect of dark-current from the Konica-Minolta CM2600d was assessed through a set of 50 measurements performed with an open aperture (no sample) in a dark room. The room selected was situated next door to the room in which the majority of participant data was taken, and whose temperature is mediated by the same system. The room was chosen as it contains a blackout blind on the window and so-called fire resistant doors. Combined, these allow very little light to infiltrate the room.

Further sources of error in measured reflectance may result from variations in output of the source. This is corrected automatically during measurement by the CM2600d using a direct measurement of the source output performed simultaneously with spectral reflectance measurements. The consistency of the source output and the performance of this method of correction were assessed separately through 50 consecutive measurements of a fixed sample. The sample selected was a faux wood desk surface, chosen for its convenience and its relative similarity in colour to human skin. This similarity ensured that the assessment was not likely to be biased through saturation effects.

The remaining sources of error corresponding to the repeatability of skin colour measurements result primarily from variations in the measurement technique, although physiological changes such as erythema or blanching caused by gentle but repetitive contact with the skin are also possible. The overall repeatability of skin colour measurements was assessed by performing measurements upon the inner forearm of the author (region overlying the flexor carpi). Repeatability was determined from a single session where 50 consecutive measurements were carried out at approximately the same region of skin.

Melanin content does not only vary over the small region covering consecutive skin colour measurements, but may vary over time, in particular due to sun exposure. This, along with changes in ambient conditions and a combination of other, less significant factors can result in further sources of error when comparing measurement sets taken weeks or months apart. The reproducibility of skin colour measurements was assessed through 2 sets of single measurements carried out at 1 week intervals; one set was taken in winter (19th January-16th February 2009) and another taken in summer (20th July-17th August 2009). A photograph marked with the measured region of skin was used to help reduce repeatability errors.

Optical Coherence Tomography

Optical Coherence Tomography (OCT) is a non-invasive imaging modality which produces cross sectional images analogous to ultrasound b-mode scans. OCT requires a coherent light source, which is split into an object beam and a reference beam. The object beam interrogates the region of interest whilst the reference beam is reflected from a reference mirror. Singularly scattered light returning from the region of interest interferes constructively with the reference beam. The depth of this region of interest can be altered by moving the reference mirror and the lateral position is adjusted by moving the beam, creating an image from regions of varying backscattering strength.

OCT has been used extensively in ophthalmology, where the low scattering within the vitreous region of the eye allows for good penetration depth. Its introduction into skin imaging is more recent [249-251], perhaps due to the challenges associated with the highly forward scattering nature of skin, which limits the signal to noise ratio and the imaging depth which can be achieved. Despite having a penetration depth of

approximately 0.5 mm, work has been carried out elsewhere in applying OCT to PWS skin [91].

During the study, an opportunity arose to trial two separate OCT devices designed for cutaneous applications (for one day each). Two patients were assessed using a Thorlabs OCS1300SS (Thorlabs Imaging Systems, Sterling, VA, USA) and three further patients were assessed using a VivoSight (Michelson Diagnostics Ltd. Maidstone, UK). Both devices employ a broadband swept source with a centre wavelength of 1300 nm. The devices differ primarily in the software used to interpret and display the data.

OCT imaging was performed alongside spectrophotometry. The area scanned using the OCT device was left with a conspicuous (although temporary) ring which clearly demarcated the region for spectrophotometric data to be collected (Figure 20).

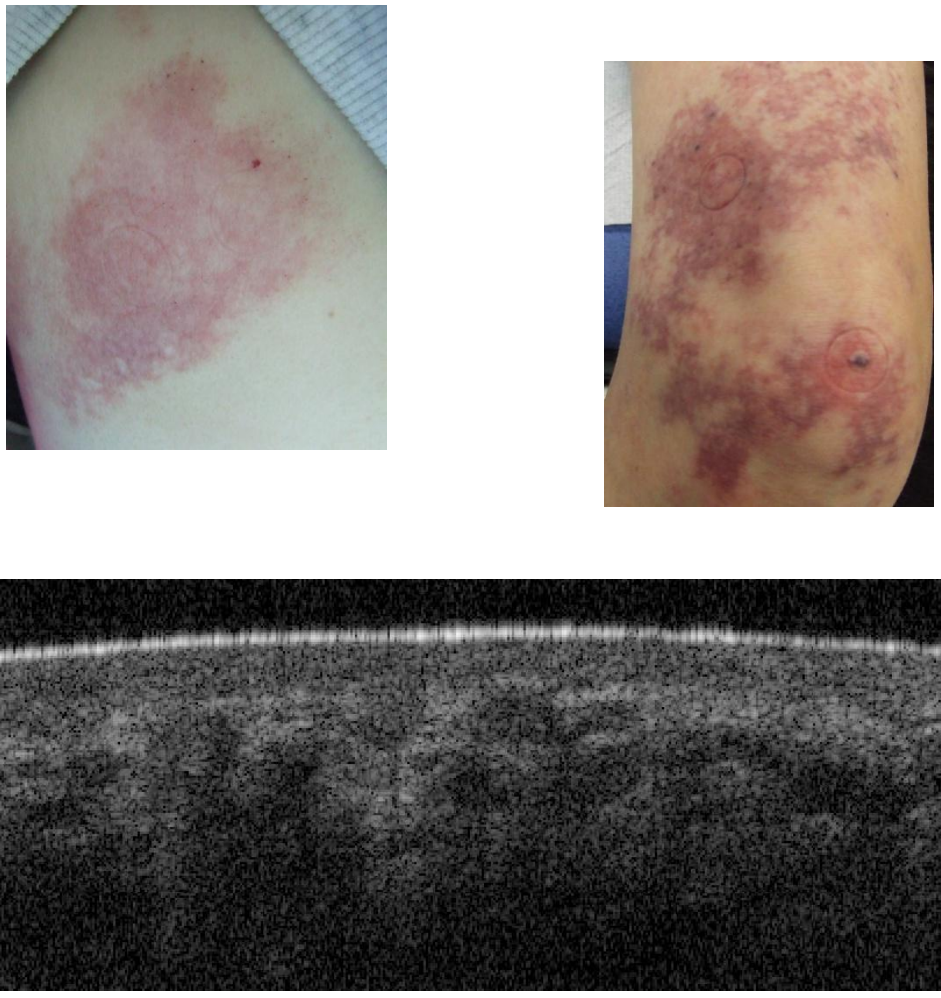

Figure 19: Temporary demarcation of scanned area following OCT image acquisition (top) and an example image from an OCT acquisition (bottom).

A visual analysis of the OCT datasets was performed to obtain estimates of vessel numbers, diameters and a subjective evaluation of PWS depth. This was achieved by looking at 20 tomographic images spread equally throughout the volume acquired. Measurements were performed on each identified vessel to determine its depth and diameter on the image. Vessel depth was measured from the centre of the region of high reflectance at the skin surface (see Figure 20) to the centre of the vessel area, as determined visually. Diameter was simple to measure for those vessels imaged in axial section but was more difficult to determine accurately for vessels, or part vessels, imaged in transverse section or those oriented otherwise with respect to the imaging geometry. In all cases, the measurement of vessel diameter was aided by viewing images obtained from adjacent sections of skin to help determine the orientation of the vessel in question. Where vessels imaged in transverse section were present, measurements from adjacent images were used to establish an estimate of the true diameter of these vessels (using the largest value obtained over the image investigated and the two images adjacent to this).

Photographic Assessment

Photographs of the lesion were taken by the author during each assessment. Assessments of these photographs were carried out individually and remotely on screen by 5 individuals considered experts in PWS lesions. This technique avoided variations in the reproduction of the images caused by producing printed copies, although some variation in the display setups would have been present. However, the use of non-professional photography is likely to have decreased the reproducibility of photographs due to greater relative changes in ambient lighting, geometries and quality.

The before-treatment and after-treatment images were presented simultaneously for each participant. Both the order in which the participants were presented and the left-right arrangement of the before treatment and after treatment photographs were assigned using the MATLAB rand command.

Scores ranging from 1-7 were recorded by hand on printed sheets for the following categories:

- The skin type of the adjacent skin for each photograph. The briefing explained that there were "7 points on the scale, much like the Fitzpatrick scale, with 1 being the fairest skin type and 7 being the darkest." [7]
- The severity of the PWS (a general sense for each image).
- Comparisons between the two images, i.e. the change in the darkness of the PWS skin, and its hue (red, pink and purple).

A copy of the record sheet can be found in Appendix F.

The regions from which colour measurements were taken were marked on the digital copy for reference, to ensure good repeatability of skin colour measurements over the two sessions.

To ensure the best possible repeatability and reproducibility across the study, the same individual (the author) undertook all interviews, photographs, colour measurements and OCT image acquisitions for each participant.

Ethical Issues

Approval for this study, including the subsequent amendments, was given by the Wiltshire NHS Ethics Committee (Ref no: 09/H0104/63), University of Southampton School of Electronics and Computer Science Ethics committee, University of Southampton Research Governance and Salisbury Hospital Research and Development Unit.

One important ethical consideration was the use of participant time. This was kept to a minimum by performing assessments on the days of definitive treatments, avoiding the necessity to arrange separate appointments. Acclimatisation time was also kept to a practical minimum.

[7] A 7 point scale was used to allow for consistency with the other assessments made during the photgraphic analysis. Odd numbered scales are preferred when comparing before and after images to allow for a 'no change' option.

Participant confidentiality was also considered in detail. A digital copy of the clinical photographs was stored on a password protected PC accessible only to Mr. T Lister and the PhD supervisory team. Data from the interview and colour measurements were stored on the PC. All digitally stored data were encrypted on the hard drive of the PC. A copy of the encrypted data (including photographs) was also stored on an external hard drive to insure against possible loss or corruption of the original copy. The external hard drive remained password protected and accessible only to the author. Signed consent forms were stored in a locked drawer.

Consent was obtained from all participants to use the collated data, photographs and quotations from interviews in scientific publications and presentations regarding the pilot study and any resultant work.

Consent was obtained separately for the 5 individuals assessed using OCT.

Summary

This study was approved by the relevant ethical and research governance committees to collect and use colour measurement data and photographic images immediately prior to two consecutive treatments. A number of measures were put in place to ensure the repeatability of the assessments.

Although ethical approval was obtained for 40 participants in the first instance, unforeseeable changes in the numbers of patients available for the study prompted a change in the approach to this project. The primary focus of this work evolved into the creation and development of a Monte Carlo programme for simulating light transport through skin, such that the influence of PWS vessel characteristics upon skin colour and treatment efficacy may be predicted.

5.2 A New Monte Carlo Simulation

Introduction

A new Monte Carlo programme was produced for simulating light transport through clinically normal and PWS skin. The programme consists of an eight layer mathematical skin model constructed from optical coefficients described in the literature. The absorption and scattering coefficients of the epidermis are dependent upon the simulated concentrations and mean diameters of epidermal melanosomes. Pseudo-cylindrical horizontal vessels are added to the skin model to simulate a PWS lesion. A simulation including diffuse illumination at the surface of and subsequent light transport through the model is carried out using a Radiative Transfer Theory (RTT) ray-tracing technique. Total reflectance over 39 wavelength values are scored by the addition of simulated light returning to the surface within a specified region and surface reflections (calculated using Fresnel's equations). These reflectance values are compared to measurements from individual participants and characteristics of the model are adjusted until adequate agreement is produced between simulated and measured skin reflectance curves.

Skin Model

An eight layer skin model was created in 3 dimensional Cartesian space. The dimensions and chromophore concentrations of the model layers were based upon the work of Meglinski and Matcher [153] whose parameters are in agreement with experimental studies (see page 53 and [9, 17, 252] for example). The overal mean dermal blood volume fraction used in Meglinski and Mather's work (4.6%) is greater than used in other studies. This is thought to be a result of the difference in blood absorption coefficients used (see page 56), but may also be a result of the difference in distribution of blood through the dermis.

The layer representing the living epidermis in Meglinski and Matcher's work was divided into two layers here, to facilitate differences in melanin properties (Table 4).

Table 4: Summary of layer dimensions and initial chromophore content; values derived from *[153] and +[10].

Layer	Thickness (µm)*	Melanin Volume Fraction (%)+	Mean Melanin Granule Diameter (nm)+	Blood Volume Fraction (%)*
Stratum Corneum	20	0.1	10	0
Superficial Epidermis	30	1.0	50	0
Deep Epidermis	50	2.0	100	0
Papillary Dermis	150	0	n/a	4
Upper Vascular Plexus	80	0	n/a	30
Reticular Dermis	1500	0	n/a	4
Deep Vascular Plexus	80	0	n/a	10
Deep Dermis	1890	0	n/a	4

The initial optical coefficients applied in this model were based upon an analysis of the literature (see page 45 and the published article [5]). Absorption coefficients from Meglinski and Matcher's work [153] were applied alongside reduced scattering coefficients from Zonios *et al* [164]. Published reduced scattering coefficients (μ_s' mm^{-1}) were converted to scattering coefficients (μ_s mm^{-1}) using the following relationship:

$$\mu_s = \frac{\mu_S'}{1-g} \qquad \text{Equation 17}$$

where g is the anisotropy factor. The anisotropy factors applied in this model were those introduced by van Gemert *et al* [188], and which have been used widely [22, 33, 77, 126, 153, 189]. Refractive indices from Ding *et al* [201] were applied separately to the stratum corneum, living epidermis and dermis.

The effect of melanosome diameter and number density upon the absorption and scattering coefficients of skin were considered in the mathematical model. The influence on absorption was simulated by adding a proportionate value of melanin absorption to a base epidermal absorption coefficient (Equation 18).

$$\mu_a = \mu_a^0 + C_{mel}\,\mu_a^{mel} \qquad \text{Equation 18}$$

where C_{mel} is the concentration (%) of melanin within the epidermal layer, μ_a^{mel} is the absorption coefficient of melanin and μ_a^0 is the absorption coefficient of the remaining epidermal layer. This is consistent with techniques applied elsewhere (for example, [153, 169, 246, 253]). The degree of scatter caused by melanosomes within the skin is primarily dependent upon their size. The relationship between mean melanosome size and scattering strength has been investigated previously (Equation 19) [144]:

$$\mu_s^{melanin} = \frac{32}{447} N_A \pi^4 C V_m \frac{a^3}{\lambda^4} \left(\frac{\varepsilon - \varepsilon_s}{\varepsilon + 2\varepsilon_s} \right)^2 \qquad \text{Equation 19}$$

where N_A is Avagadro's number (6.02×10^{23} mol^{-1}), C is the concentration of melanin (mol), V_m = 1.2×10^{-28} m^3 is described as the 'volume of a single monomer', a is the mean melanosome size (m), and ε and ε_s are the dielectric constants of melanin (2.72 Fm^{-1}) and water (1.81 Fm^{-1}) respectively. The model considers Equation 19 in a simulation of skin optics for the first time. Estimations of representative melanosome concentrations and sizes were based upon an analysis of the literature [7-10, 12, 13] (see also, page 14).

A single layer of the skin model, whose superficial and deep extents were freely moveable, was adopted to accommodate a simulated PWS lesion. Vessels, each consisting a wall and lumen, were created using the MATLAB *cylinder* command. This was used to produce a set of flat surfaces joined together to form a *n* sided open ended prism of 110 mm length (extending beyond the model boundaries), oriented horizontally in the model (parallel to the skin surface). A larger number of sides provides a truer approximation to a cylindrical vessel, but requires greater programming resources. A 10 sided prism was selected. The *rand* command was used to position and orientate the vessels with a uniform distribution throughout the layer. The maximum deviation in the x and y directions from the centre of the model was fixed at 3.5 mm, ensuring that each vessel remained within the region of interest defined by the circular aperture.

Optical properties of the vessel wall and lumen, as well as an appropriate range of vessel sizes and wall thicknesses, were derived from an analysis of the literature (see page 16). This conceptually simple introduction of horizontal, pseudo-cylindrical blood vessels into the skin model was applied to allow for easy interpretation of mean vessel parameers, including depths, diameters and numbers. The flexibility of the programme is desgined to allow for more complex vessel shapes, which may be used to provide more accurate replications of skin colour. Such an introduction would vastly increase the running time per beam of the programme, and would therefore only be possible at the present time if coupled with a convolution technique, for example.

Ray Tracing

Light transport through the skin model was simulated using a RTT ray-tracing technique, described previously (see page 51). Figure 21 shows the basic layout of the programme:

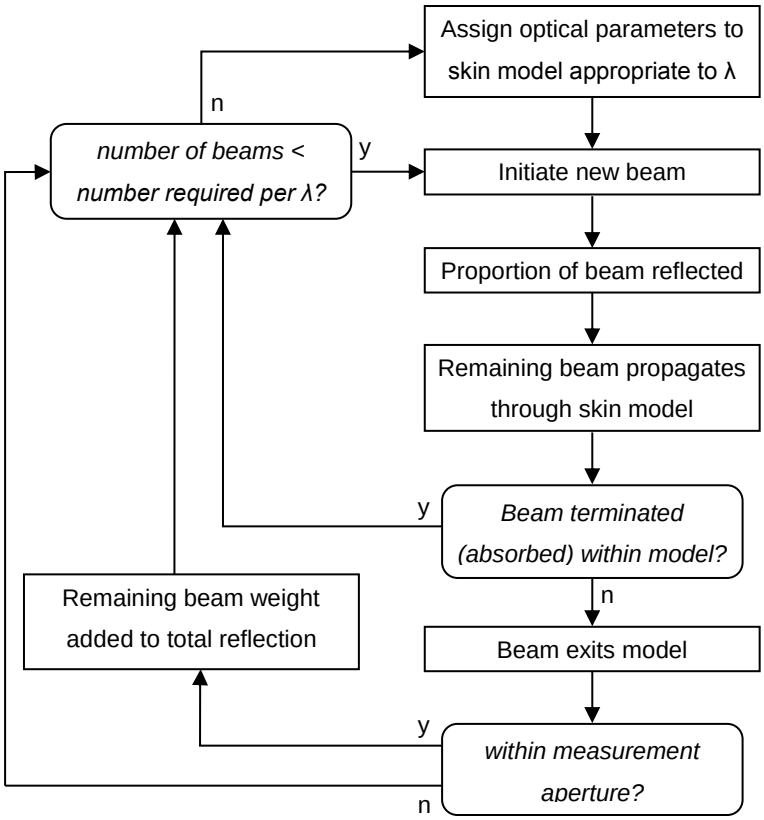

Figure 20: Flow chart showing basic structure of the programme.

Beam Initialisation

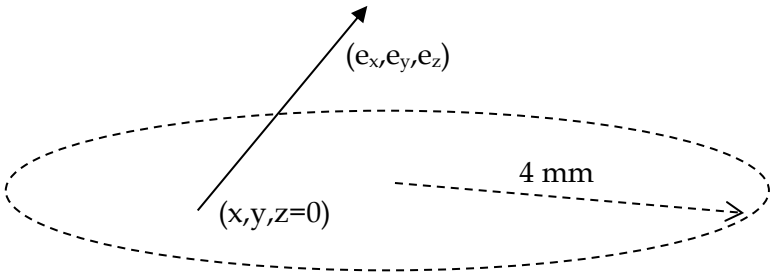

Figure 21: Illustration of a representative beam position and direction upon initiation.

Each ray, or beam, is initiated at the surface of the skin model within a circle of radius 4 mm. This represents the aperture of the Konica-Minolta CM2600-d spectrophotometer. Beam position is allocated using the MATLAB *rand* command,

which results in a uniform distribution across the aperture. This represents homogeneous illumination of the skin surface across the aperture.

Each beam is initiated with a direction in Cartesian space (Figure 22). The MATLAB *rand* command is again used to provide a uniform distribution of beam directions between -1 and 1 along the x and y direction vectors (e_x and e_y) and between 0 and 1 (into the skin) along the z direction vector (e_z). These values are subsequently normalised such that:

$$\sqrt{e_x^2 + e_y^2 + e_z^2} = 1 \qquad \text{Equation 20}$$

This uniform distribution of random beam directions represents a perfectly diffuse illuminant. Finally, each beam is attributed a *weight* of 1.0. The beam weight is used for comparison between the total quantity of incident light energy and the total quantity of reflected and backscattered light energy at each wavelength.

Interactions at the Skin Surface

The first interaction of the beam with the skin model is at the surface. The skin model assumes a perfectly smooth interface between the surface of skin and air. Reflection is thus approximated using the Fresnel equations for an unpolarised source (Equation 21).

$$R = \frac{R_s + R_p}{2} \qquad \text{Equation 21}$$

(Fresnel's Equations)

where: $R_s = \frac{\tan(\theta_i) - n_s(\lambda)\tan(\theta_t)}{\tan(\theta_i) + n_s(\lambda)\tan(\theta_t)}$ & $R_p = -\frac{\sin(\theta_i) - n_s(\lambda)\sin(\theta_t)}{\sin(\theta_i) + n_s(\lambda)\sin(\theta_t)}$

where R_s is the proportion of *s*-polarised (perpendicular, or *senkrecht* polarised) light reflected and R_p is the proportion of *p*-polarised (parrallel polarised) light reflected (thus R, being the mean of these, is the proportion of unpolarised light reflected[8]), θ_i and θ_t are respectively the incident and transmitted angles of the photon packet and $n_s(\lambda)$ is the refractive index of the skin. Surface reflection is simulated as a reduction in

[8] It is assumed that unpolarised light, as expected from a xenon flashlamp light source, does not have a greater amount of either *s*-polarised or *p*-polarised light.

the beam weight by the proportion *R* (Equation 21) and the total recorded reflectance is increased accordingly (Figure 23a). The remaining beam is refracted as it enters the skin model. The degree of refraction is calculated using Snell's law (Equation 22).

$$\theta_t = arcsin\left(\frac{1}{n_s(\lambda)}\sin(\theta_i)\right) \qquad \text{Equation 22}$$

After propagating through the skin model, the beam may return to the skin surface. A proportion of the beam is reflected back into the skin model as determined by the Fresnel equation (Equation 23) and the remaining (transmitted) beam is terminated (Figure 23b).

$$R = \frac{R_s + R_p}{2}, \qquad \text{Equation 23}$$

where: $R_s = \frac{n_s(\lambda)\tan(\theta_i) - \tan(\theta_t)}{n_s(\lambda)\tan(\theta_i) + \tan(\theta_t)}$ & $R_s = \frac{n_s(\lambda)\sin(\theta_i) - \sin(\theta_t)}{n_s(\lambda)\sin(\theta_i) + \sin(\theta_t)}$

and where $\theta_t = \arcsin\left(n_s(\lambda)\sin(\theta_i)\right)$

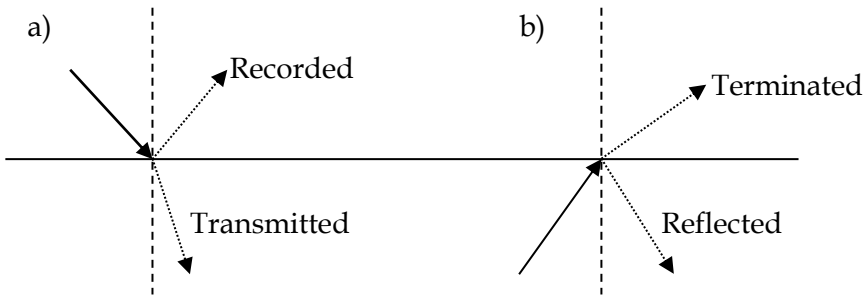

Figure 22: Illustration showing the concept of beam splitting simulated at the skin surface for a beam entering the skin (a) upon initiation, and for a beam exiting the skin (b).

If this occurs within the 8 mm diameter aperture of the simulated acceptance window, then the transmitted beam *weight* is recorded as part of the total reflectance. The direction of the transmitted (terminated) beam is of no consequence and so refraction is not simulated for a beam exiting the skin.

Calculating Path Length

Progression of the beam within the skin model occurs in stages or *steps*. At the end of each step a scattering event occurs during which the direction of the beam is altered. The mean distance between scattering events, i.e. the mean length of these steps, is determined using the RTT scattering coefficient (μ_s). The scattering coefficient may be defined as the proportion of energy lost from the direction of the beam per unit length.

Thus, the inverse of the scattering coefficient represents the mean distance between scattering events ($\hat{s}$):

$$\hat{s} = \frac{1}{\mu_s} \qquad \text{Equation 24}$$

The path length can assume any positive value, as described by the probability distribution function [153]:

$$p(s) = \mu_s e^{s\mu_s} e^{s\mu_a} + \mu_a e^{s\mu_s} e^{s\mu_a} \qquad \text{Equation 25}$$

Absorption is considered separately in this simulation. Thus, for the effects of scatter only (μ_a=0) the probability density function for the photon path length is:

$$p(s) = \mu_s e^{s\mu_s} \qquad \text{Equation 26}$$

Thus, the path length for a beam at any one step is simulated as:

$$s = \frac{-\log_e(rand)}{\mu_s} \qquad \text{Equation 27}$$

where *rand* is taken from a set uniformly distributed random numbers between 0 and 1, created using the MATLAB *rand* command. The mean of $-\log_e(rand)$ for a large dataset approaches unity. This is consistent with Equation 24 and is identical to the path length calculation described in [153].

Simulating Scatter

Scatter within the skin model is simulated as a change in the direction vectors (e_x,e_y,e_z). Apart from at boundaries, scattering occurs at the end of each *step*, alongside the calculation of a new step length (Equation 27). Non-boundary scattering is simulated in two stages:

1. The elevation angle (φ) is adjusted in accordance with the modified Henyey-Greenstein equation
2. The rotation angle (θ) is adjusted isotropically

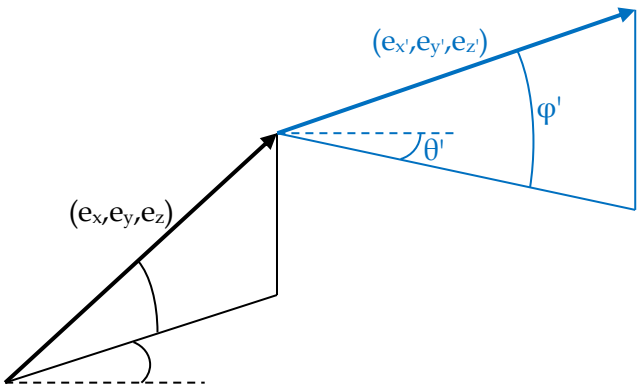

φ

θ

Figure 23: Illustration of the change in direction vector resulting from a scattering event in 3 dimensional Cartesian space.

The angle of rotation (θ) is defined as the angle between the x axis and a projection of the beam along the x-y plane. At each scattering event, isotropic scatter is simulated by the addition of an angle selected from a uniform distribution between 0 and 2π (created using the MATLAB *rand* function):

$$\theta' = \theta + 2\pi \cdot rand \qquad \text{Equation 28}$$

where θ is the incident angle of rotation of the incident beam and θ' is the altered angle of rotation.

The angle of elevation (φ) is defined as the angle between the beam and the x-y plane and may be positive (going deeper into the skin) or negative (going toward the surface). Scattering of φ is simulated through the modified Henyey-Greenstein equation [172]. This is executed programmatically as follows:

```
phi=asin(ez);  %elevation angle calculated from the direction vector
'ez'
if rand>b
    if rand>0.5, phi=phi+HG; %addition of HG angle in half of cases
    else         phi=phi-HG; %subtraction of HG angle in half of
cases
else
    phi=phi+2*pi*rand; %isotropic scatter
end
eznew=sin(phi);
```

where rand is the MATLAB *rand* function described previously and HG is a function which produces a value according to Equation 29.

$$HG = \frac{1-g^2}{\left[1+g^2-2g\cdot\cos(2\pi\cdot rand)\right]^{3/2}} \qquad \text{Equation 29}$$

where g is the anisotropy factor for the layer and wavelength in question. After the new values of θ and φ have been determined, the direction vector is subsequently recalculated from these two angles and normalised to correct for floating point errors.

Simulating Absorption

The RTT absorption coefficient defines the proportion of energy lost per unit path length through absorption effects. Absorption is simulated as a reduction in the beam *weight, W*:

$$W = We^{-\mu_a x} \qquad \text{Equation 30}$$

where x is the path length. Equation 30 is applied at the end of each step, as well as at each interaction with a boundary (either layer boundaries, including the skin surface, or boundaries associated with simulated blood vessels).

Layer Transitions

When a beam transfers between layers of the skin model, or to or from a vessel wall or lumen, the following calculations are performed. At first, the reduction in beam weight is calculated between the previous interaction or transition and the current transitional point. A proportion of beams will be terminated at this point, in accordance with the *roulette* procedure. For those beams which are not terminated, the remaining path length (s_{new}) is adjusted in accordance with the scattering coefficient of the new layer or structure ($\mu_s{}^{new}$), as follows:

$$s_{new} = \left(s_{old} - p\right)\frac{\mu_s^{old}}{\mu_s^{new}} \qquad \text{Equation 31}$$

where p is the distance along the beam path between the previous interaction or transition and the current transitional point.

Further to this, the direction of the beam may be adjusted where a change in refractive index occurs. The new direction is calculated using Snell's Law.

Terminating a Beam

A proportion of beams whose weight drop below a predetermined value (0.001) are terminated using the previously reported *roulette* technique [102, 126, 208, 236, 254-256]. This is a computational time saving stochastic function which terminates a proportion of the beams whilst amplifying the remaining beams to conserve beam weight on average. In this programme, 90% of roulette procedures result in the termination of a beam (selected using the *rand* function). The remaining 10% of beams

undergo a 10 fold increase in weight. The remaining properties of the beam, including direction and position, are not altered during the roulette procedure.

Termination may occur independently of the roulette procedure if a beam exits the skin model. This reduces the computational time of the simulation by ignoring those beam trajectories which are unlikely to return to the measurement aperture and therefore do not contribute appreciably to the simulated reflectance. Termination of a beam occurs at the skin surface as described previously, and at the remaining boundaries of the skin model. These extend to 100 mm in the x and y (horizontal) directions and 20 mm in the z (depth) direction.

Upon termination of a beam, the next beam is initiated until the desired number of iterations has been carried out.

Output

Spectral Reflectance

The simulated spectral reflection is the primary output from this simulation. It consists of 39 points over the visible spectrum from 360 nm to 740 nm (in 10 nm steps). Each point represents the sum of simulated beam weight reflected from the surface and returning from the model volume within the 8 mm diameter aperture. These data points are presented as a proportion of the total beam weight entering the model, and thus represent the measured reflectance as determined using the Konica-Minolta CM-2600d spectrophotometer.

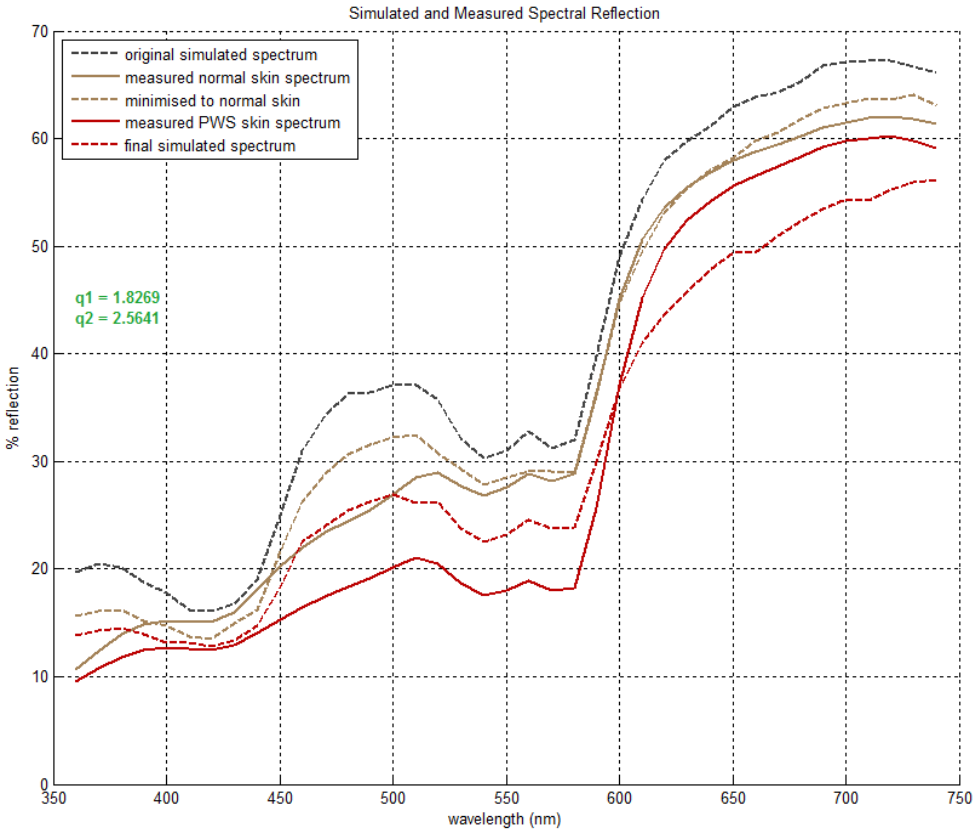

Figure 24: Example output of spectral reflectance produced by the programme.

In order to quantify the difference between measured and simulated data sets, an array comprising the difference values at each of the 39 wavelength steps (Q) is created. The absolute sum of these values (q) is presented alongside the spectral reflectance curves (Figure 25).

Beam Trajectories

The programme is capable of displaying an output of beam trajectories through the skin model for a single wavelength (Figure 26). These are depicted in 3 dimensional space and consist of straight lines between scattering events or boundary transitions. Each of these lines is assigned a colour according to the current beam weight, from light green (beam weight→1) to dark green (weight→0). The final image therefore consists of a single continuous path for every simulated beam which begins light green in colour and becomes darker as it is absorbed.

Vessel walls (depicted as yellow-grey in colour) and lumina (red) from the simulated lesion are also represented on the same axes (Figure 26). Each face of the wall or

lumina has transparent properties to ensure that beam trajectories remain visible through the layer.

This output was developed for easy visualisation of processes within the simulation and served primarily for verification and checking of the simulation during development.

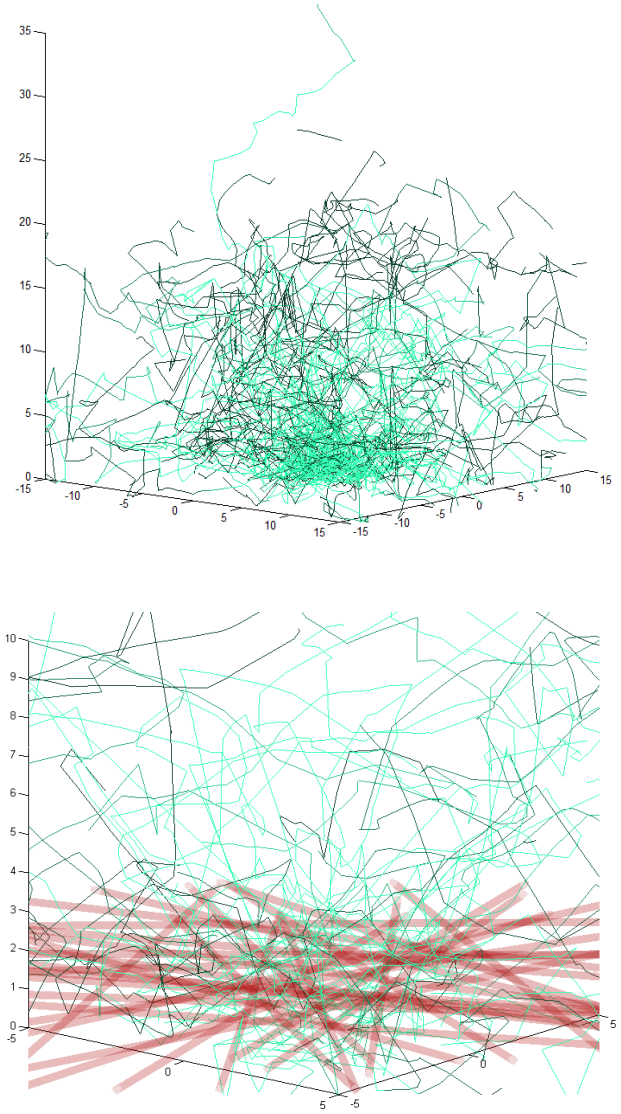

Figure 25: 3 dimensional plots of beam trajectories through the skin model with z-axis (depth) in the vertical direction. Upper figure demonstrates change in colour with reduction in beam weight. Lower plot shows positioning of simulated vessels. Dimensions in mm.

Minimisation

Two new minimisation procedures were developed for the interpretation of colour measurement data within the simulation. The first procedure adjusts the melanin properties within the skin model such that the measured spectral reflectance of non-PWS skin can be reproduced for an individual participant. The second procedure builds upon this, adding blood vessels and adjusting their properties in order that the simulated curve may be minimised to a colour measurement of PWS skin from the same individual (Figure 27).

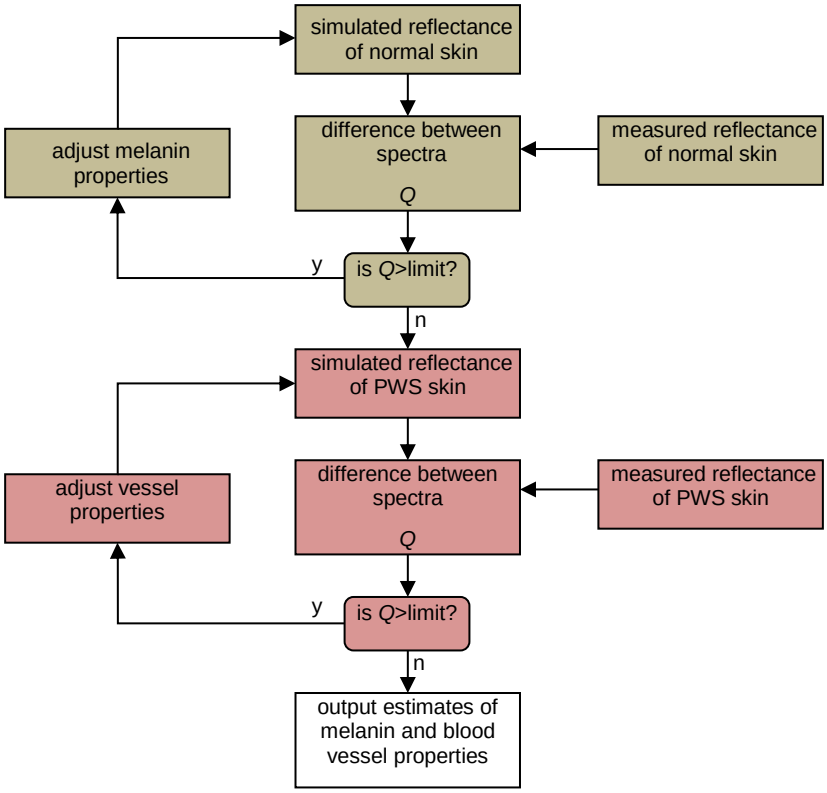

Figure 26: Outline of the minimisation procedure developed in the New Monte Carlo programme.

Melanin Adjustment

The range of quantities and diameters of melanosomes for each of the three epidermal layers was limited in accordance with the findings of a literature survey (see page 14). Stratum corneum granule diameter was limited to a minimum of 1 nm and a maximum of 20 nm [10, 13] whilst melanosome size in the living epidermis was allowed to vary from 30 nm to 400 nm [7, 8, 10, 12].

Due to the broadband absorption characteristics of melanin, it was expected that increasing the quantity of melanin in the epidermal layers of the skin model would reduce the simulated reflectance across the entire visible spectrum (and conversely, decreasing the quantity of melanin would increase the simulated reflectance). The characteristics of the melanin absorption spectrum also suggest that this effect would be greater towards the blue end of the light spectrum (Figure 28, repeated overleaf).

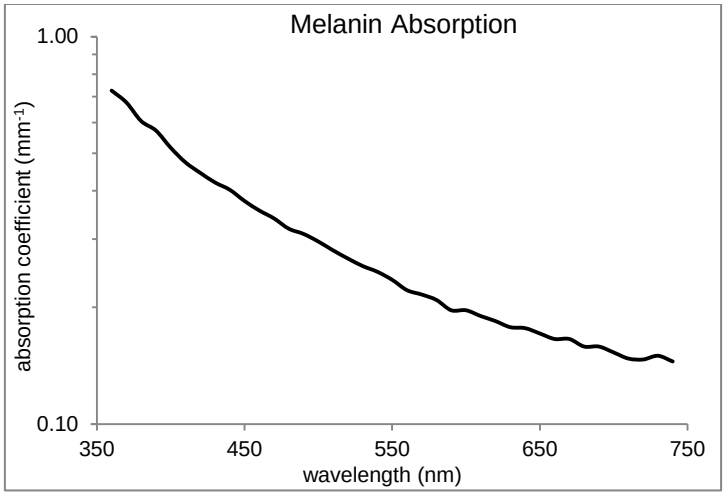

Figure 27: Variation of absorption coefficient with wavelength, from [7].

Epidermal scattering is also influenced by the quantity of melanin within the model, although the resultant effect of this on the simulated reflection spectra were expected to be minimal compared to the change in absorption coefficient. Changing the mean diameter of melanosomes within the skin model is performed independently of the total quantity of melanin. In this case, only the epidermal scattering coefficient of the skin model is adjusted, and the effects on absorption coefficient are ignored. An increase in mean melanosome diameter in each epidermal layer was expected to result in an increase in measured reflectance in the blue region of the visible spectrum but, due to the wavelength^{-4} dependence of scatter on melanosome diameter in the model, the effect on simulated reflection was expected to be negligible at the red end of the spectrum.

In order to achieve robust minimisation when adjusting melanin diameter and concentration parameters, the total difference between the measured and simulated spectra was divided into two sections. The parameter $qmel_1$ represents the total difference at the blue end of the spectrum and $qmel_2$, the total difference at the red end. If both parameters showed a simulated curve sufficiently greater than the measured curve, then the melanin concentration was increased. Similarly, if both parameters showed a simulated curve sufficiently less than the measured curve, then the melanin concentration was decreased. However, if $qmel_1$ showed that the simulated curve was sufficiently greater or less than the measured curve but $qmel_2$ was not, then the melanin diameter was decreased or increased respectively.

To improve the speed at which the procedure converged whilst maintaining precision, limits were set for these parameters whereby large deviations in melanin concentration or diameter were instigated if the difference between simulated and measured reflectance curves were great, and smaller deviations were carried out for small differences.

If the magnitude of $qmel_1$ or $qmel_2$ were not sufficiently large enough to require further adjustment to the melanin parameters (i.e. if there was adequate agreement between measured and simulated spectra) then the second minimisation procedure was instigated.

Blood Vessel Adjustment

The range of PWS vessel diameters was limited in accordance with the literature from a minimum of 20 µm to a maximum of 500 µm (page 16). Comparisons between dermal vessel characteristics and perceived skin colour from other work (see page 19) has suggested than an increase in PWS depth decreases the amount of light absorbed by the lesion at shorter wavelengths. Thus, it was expected that changing lesion depth would have its greatest effect in the blue-green regions of the visible spectrum, with deeper lesions resulting in greater values of reflectance in this region. Increasing vessel diameter with a fixed blood volume fraction has been shown to reduce the amount of red light absorbed (due to shadowing of erythrocytes within the vessel lumina [80]) and so was expected to have its greatest effect at the red end of the spectrum. Although the author was not able to find any direct commentary in the literature on the effect of increasing vessel number for a lesion of fixed depth and mean vessel diameter, it was expected that this would result in a broad decrease in the simulated reflectance over the majority of the spectrum. Variations in vessel wall thickness have not been shown to substantially affect PWS colour.

In accordance with the anticipated effects of adjusting PWS lesion depth, vessel diameter and vessel number, the spectrum was split into three regions ($qves_1$-$qves_3$) according to the aforementioned regions of greatest influence. Parameter adjustment was carried out as follows:

- If the simulated reflection differed greatly from the measured PWS skin sample over the majority of the spectrum ($qves_1$) then the number of vessels was adjusted.

- Otherwise, if the simulated reflectance was less than the measured reflectance over the majority of the spectrum ($qves_1$) then the depth of the simulated vessels was reduced, and *vice-versa*.
- Or if the simulated spectrum was very much greater than the measured spectrum at the red end of the spectrum ($qves_3$) relative to the blue/green end ($qves_2$), then vessel diameter was increased. Conversely, if $qves_2$ was much larger than $qves_3$, then vessel diameter was decreased.
- Otherwise, if $qves_1$ or $qves_2$ still showed enough of a discrepancy, the vessel number was adjusted accordingly.

This minimisation technique was designed to ensure fast convergence whilst maximising the probably of obtaining a realistic, unique and repeatable solution for any individual measurement of PWS skin.

Summary

A new Monte Carlo programme has been introduced for simulating light transport through PWS skin. A stochastic ray tracing technique is used to simulate the transport of light through an eight layer skin model.

The effects of varying melanin concentration and, for the first time, melanosome size were included in the model and a minimisation procedure developed with the aim of manipulating these parameters to reproduce clinically normal skin colour.

Horizontal, pseudo-cylindrical vessels, inclusive of vessel walls, may be added to the skin model with random positions and orientations to simulate PWS skin. The number, diameter and mean depth of vessels is manipulated within a second minimisation procedure with the aim of reproducing PWS skin colour.

The simulation was configured to output a plethora of data, including the optical properties of the skin model, the parameters used during minimisation and the accuracy of which measured skin colours were reproduced. Included within this output is a spectral reflectance graph equivalent to that available from the Konica-Minolta CM2600d. A further option exists to output a 3 dimensional representation of beam trajectories to aid with conceptualisation of the simulation.

6. Verification and Development of the Minimisation Procedures

6.1 Repeatability and Reproducibility of Spectrophotometry Measurements

The assessment of dark-current error found that over a sample of 50 consecutive measurements, the maximum measured value of reflectance (dark-current error) was 0.02% (to a precision of 0.01%). This value is minimal and is unlikely to have had a considerable effect upon the assessments made.

When performing assessments of repeatability through measurements of a fixed object, any concerns about saturation effects could be ignored as measured reflection was sufficiently below 100% across the spectrum (Figure 29).

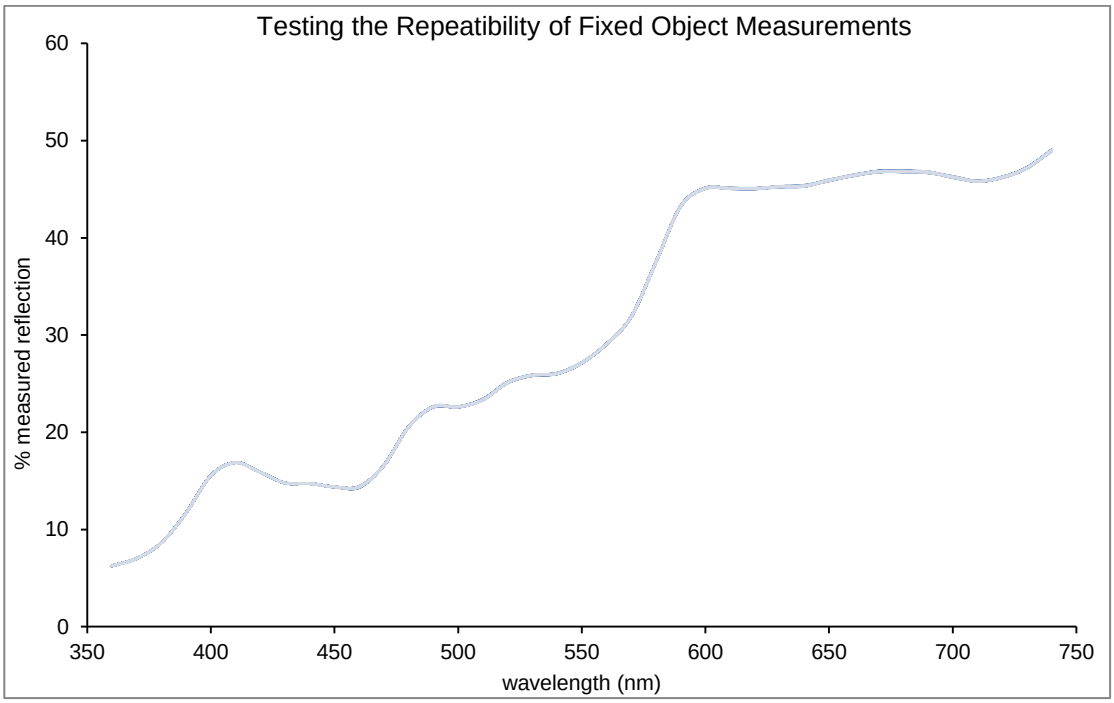

Figure 28: Graphical representation of 50 datasets taken consecutively from a fixed object of similar colour to skin.

The absolute maximum deviation from the mean across the measured spectrum for 50 consecutive measurements of a fixed object was 0.08% measured reflection. These results show that sources of error inherent to the device result in minimal deviation, and therefore the device has the potential to facilitate a high level of repeatability (Figure 29).

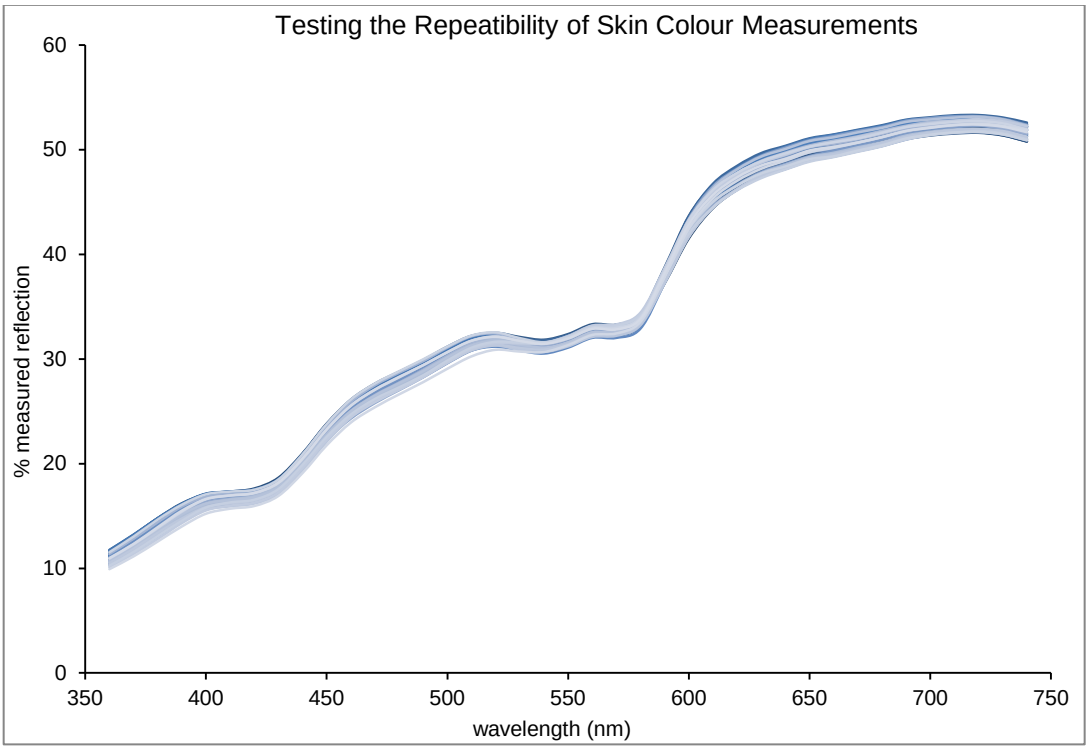

Figure 29: Graphical representation of 50 datasets taken consecutively from the inner forearm of the author.

It is clear from Figure 30 that measurements performed upon skin show greater variability than from a fixed source over the entire spectrum (Figure 29). The largest deviation from the mean across the measured spectrum was 1.4%. The coefficient of variation was also greater for the skin measurements compared to a fixed sample (0.020 compared to 0.0012). The broadband variations in measurements suggest that variation in the melanin content of the measured regions was the primary cause of this discrepancy, rather than changes in haemoglobin absorption (peaks at 400-450 nm and 530-600 nm regions) resulting from erythema or blanching. Thus, variation in the repositioning of the measurement aperture appears to be the primary cause of error in the context of repeatability, rather than blanching or erythema, or the inherent variations within the device.

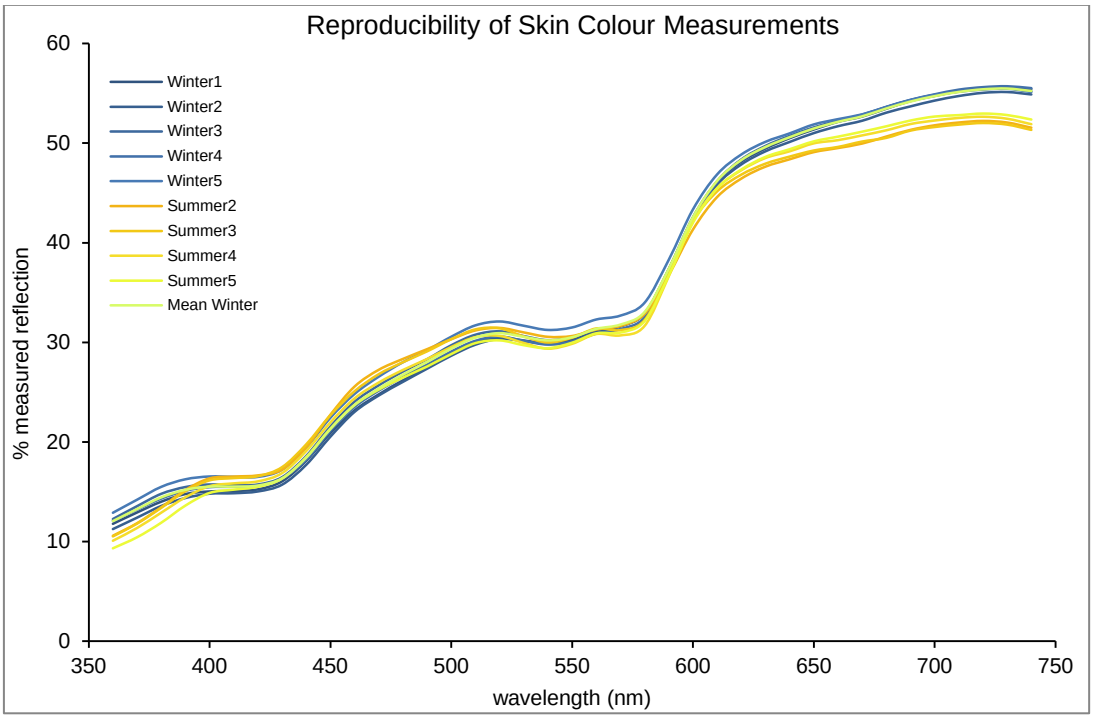

Figure 30: Graphical representation of 50 datasets taken from the inner forearm of the author.

Figure 31 shows a high value of reproducibility for measurements taken 1 week apart but a clear discrepancy between measurements taken in the winter compared to those taken in the summer. The maximum deviations for each of the winter and summer datasets were 1.2% and 1.3% measured reflectance respectively, which is comparable to the repeatability score. Their coefficients of variation were larger than those found whilst testing repeatability (0.43 and 0.41 respectively), although this is influenced by the smaller size of the dataset. When comparing the winter and summer data together, there is noticeably poorer reproducibility. The maximum overall deviation from the mean across the spectrum is greater, at 2.2% measured reflectance, although the overall coefficient of variation was similar, at 0.42. It is expected that the primary cause of variation between the datasets analysed here is a true change in skin colour resulting from sun exposure. This is despite choosing a region of skin which receives relatively little sun exposure (inner forearm, region overlying the flexor carpi).

6.2 Verifying Skin Optical Coefficients

An initial simulation of spectral reflectance was produced from the new Monte Carlo programme using the parameters derived from the literature (Table 4, page 94). Figure 32 shows the simulated spectral reflectance alongside the mean of measured values from 10 participants.

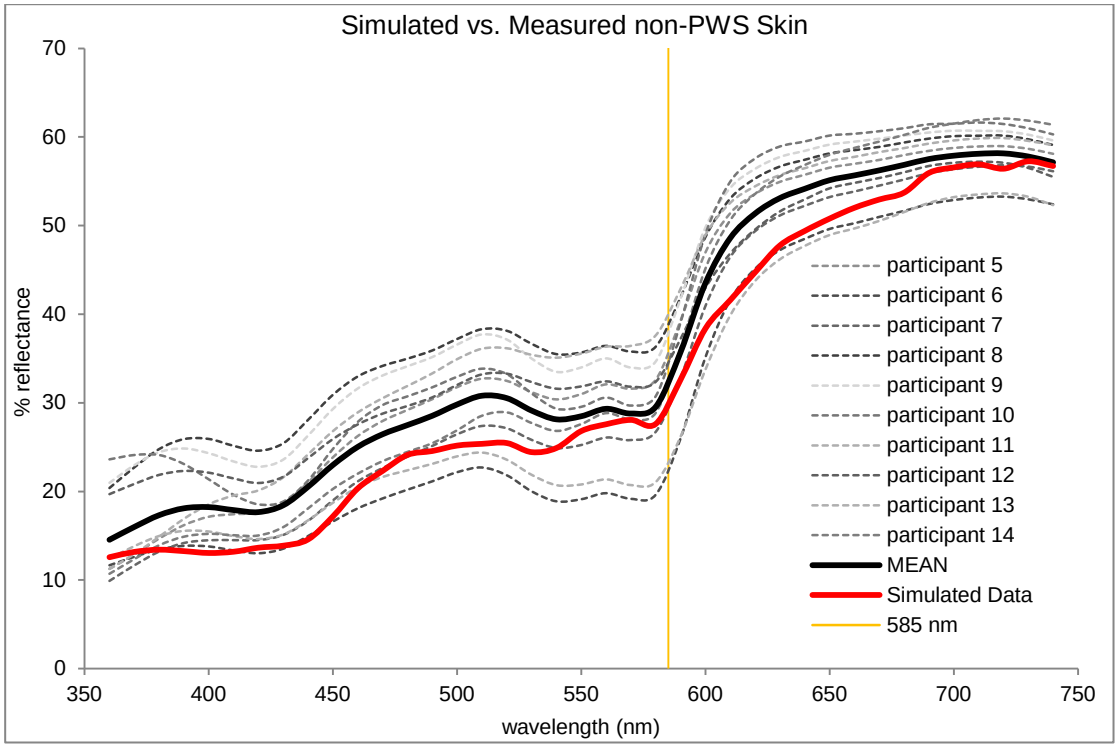

Figure 31: Comparison of simulated reflectance obtained from published data and measured skin reflectance from the participants of this study.

The general curve shape shown across the participant group appears to be derived primarily through the melanin absorption spectrum, causing a gradual decrease in absorption from 740 nm to 360 nm, onto which is superimposed the oxyhaemoglobin absorption spectrum, with peaks at around 440 nm, 540 nm and 570 nm (see Figure 7 on page 25). As scattering is greatest at the shorter wavelengths considered, the is likely to have reduced the relative difference in simulated reflectance between 360 nm and 740 nm.

Overall, the simulated spectrum shows similar characteristics to the average measured curve and all of the data points sit within the range of measured spectra. In comparison to the mean measured data, the simulated curve demonstrates less reflectance over the entire spectrum. This may be due to differences in skin type

between the participant group measured and those informing published data. The population demographic of the participant group in this study is typical of Salisbury and its surrounding areas and consists mainly of individuals with pale, Northern European skin types. The published data used to inform the simulation presented in Figure 32 is sourced from institutions based in the UK [153], Greece [164] and The Netherlands [188] and, although not explicitly stated, it is likely that these may include slightly darker skin types on average.

In detail, Figure 32 shows that the haemoglobin absorption peak at around 585 nm appears to be more prominent in affecting the measured reflectance for each of the participants than is shown on the simulated curve, reducing the difference between simulated and measured reflectance in this region and causing the curve to appear flatter. This may be a result of a more superficial effect from blood within the skin model than is seen in the participant population (perhaps caused by the assumed homogeneous spread of blood in the skin model). However, the blood absorption peak towards the blue end of the spectrum does not demonstrate this effect, suggesting that a smaller proportion of blue light returning to the surface is affected by dermal blood within the model compared to green light.

Adjusting Melanin Content

Increasing the quantity of epidermal melanin was expected to result in a universal decrease in simulated reflectance, with the greatest effect towards the blue and of the spectrum where the melanin absorption coefficient is greatest.

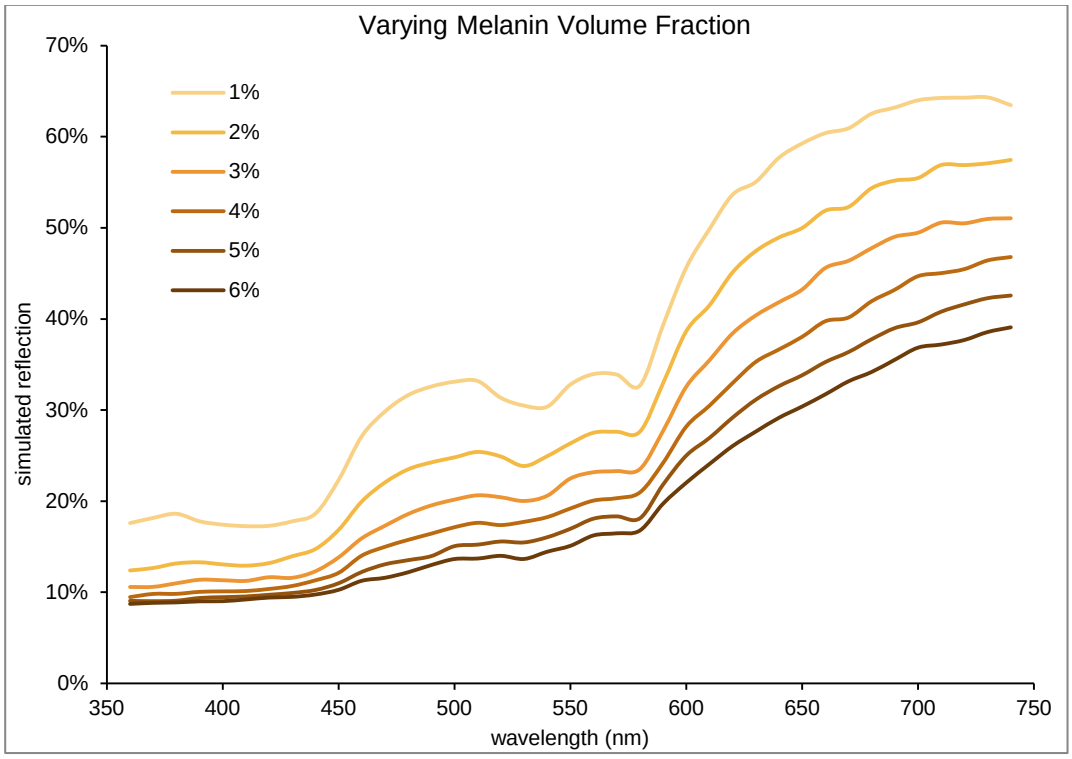

Figure 32: The effect of varying melanosome volume fractions upon the simulated reflectance spectrum.

The simulated effect of epidermal melanin within the skin model was assessed by increasing the mean epidermal content in 1% steps (weighted across the three layers according to volume, Figure 33). Increasing from a mean of 1% to 2% epidermal melanin volume resulted in a near uniform decrease in simulated reflection. Further increases in melanin content had a greater effect towards the red end of the spectrum and also resulted in a flatter simulated reflectance curve. Also, with each 1% increase in epidermal melanin volume, the overall decrease in simulated reflectance was less.

Approximately 5% of incident light is reflected from the surface of the model, as simulated using the Fresnel relations. Even at the shortest wavelengths and highest melanin concentrations considered here, simulated reflection is approximately 3-4% greater than this value (Figure 33). This is partly due to the distribution of melanin across the epidermis. For example, a skin model with a mean melanin volume fraction of 6% contains just 2.6% melanin volume fraction in the most superficial layer. This layer has an absorption coefficient of 5.76 mm^{-1} and an albedo (ratio of scattering coefficient to the sum of absorption and scattering coefficients) of 0.28 at 360 nm. Thus, although an albedo <0.5 shows that absorption is dominant in this case, a substantial amount of light scattering still occurs. The increase in flatness (decrease in

mean gradient) of the simulated spectra with increasing melanin content is likely to be a result of a reduction in the penetration of simulated light through the skin model and thus a decrease in the effect of blood absorption.

The literature survey (Chapter 4, page 49) suggests that increasing the mean diameter of melanosomes is expected to increase reflectance at the blue end of the spectrum but has negligible effect at the red end.

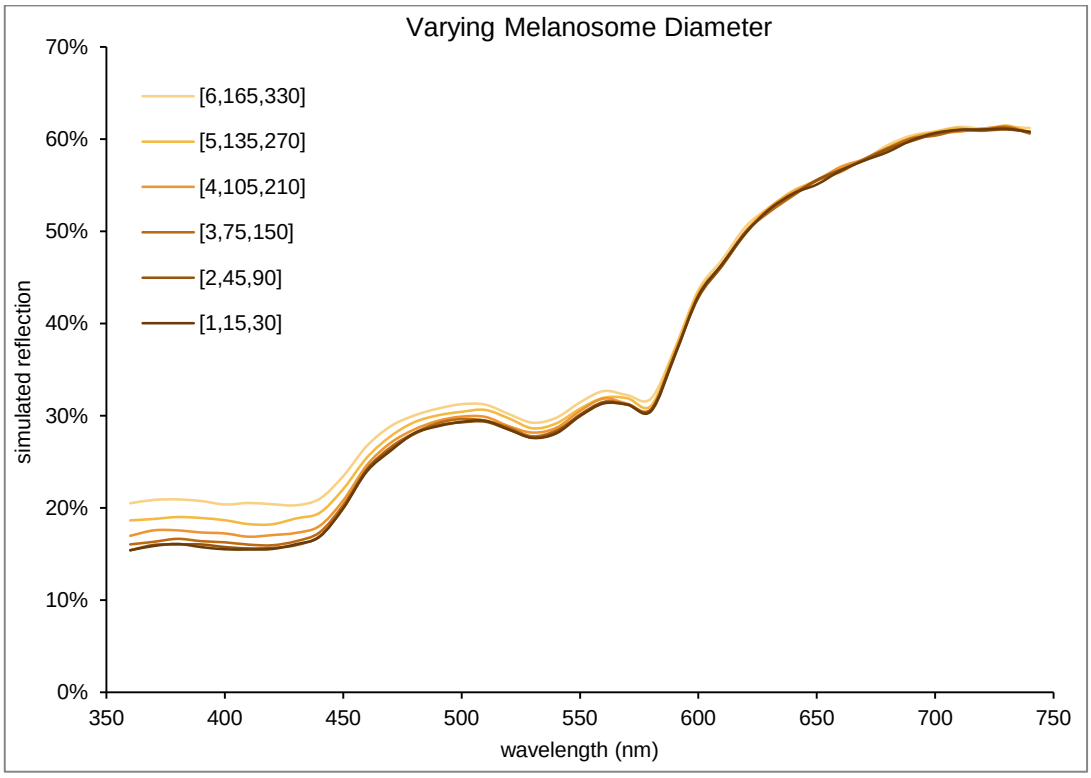

Figure 33: The effect of varying melanosome diameter upon the simulated reflectance spectrum. Lighter coloured lines represent larger simulated melanosome diameters (mean diameters given in nm for [stratum corneum, superficial living epidermis, deep living epidermis]).

As expected, increasing the diameter of melanosomes within the skin model had minimal effect in the region from 600 nm to 750 nm. The most noticeable increase in simulated reflectance occurred in the region from 360 nm to 450 nm. The overall effect of increasing melanin diameter was not as pronounced as changes in melanin volume fraction.

Minimisation Procedure - Melanin Adjustment

Section 5.2 describes two spectral regions used to inform melanin adjustment during minimisation. Based upon the preliminary results presented earlier in this chapter (see Figure 33 and Figure 34), the following regions were selected: 360-540 nm for

qmel1, used to inform melanosome diameter and 640-740 nm for *qmel2*, which is used to inform the quantity of epidermal melanin. 10 iterations of the melanin minimisation procedure were used for each participant assessment.

Verification of this minimisation procedure was carried out. The procedure began by producing a simulated spectrum from skin model optical coefficients derived from the literature, considered to be representative of type II Northern European skin (1.5 % epidermal melanin volume, melanosome diameters of 30 nm in the deep living epidermis, 15 nm in the superficial living epidermis and 1 nm in the stratum corneum). The melanin characteristics within the skin model were adjusted within the programme, and the output minimised to the mean spectrum from the first 10 participants enrolled into the study (Figure 35).

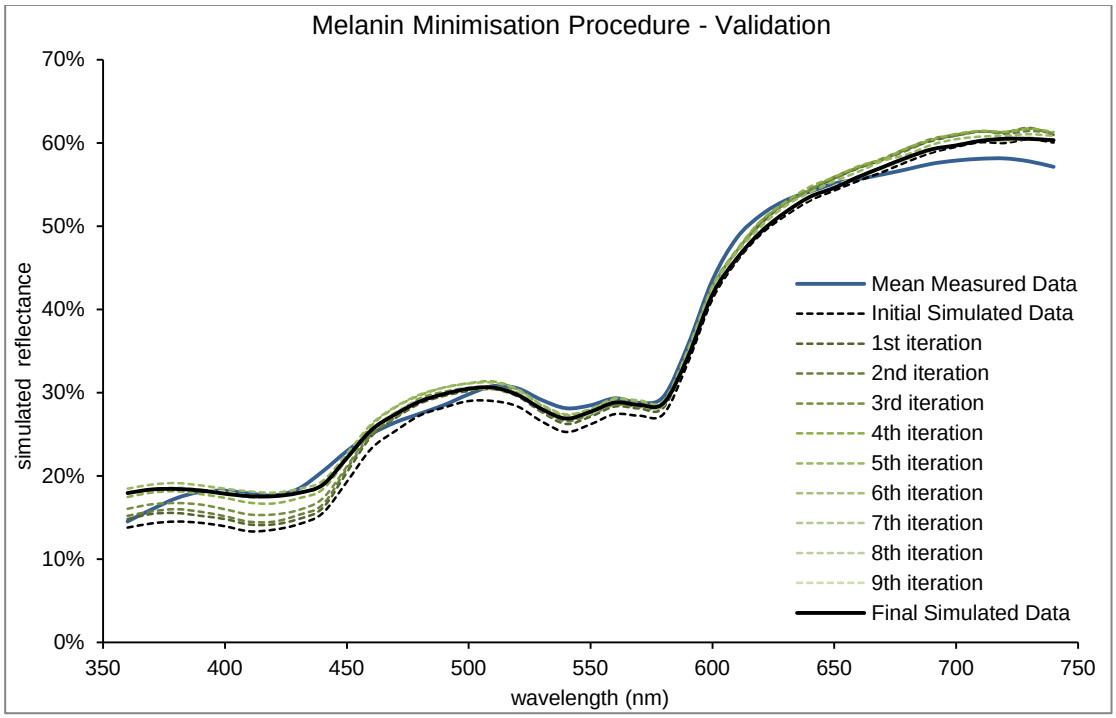

Figure 34: Simulated spectral reflection outputs obtained during verification of the melanin minimisation procedure.

The initial simulated data showed a close resemblance to the mean measured dataset. The minimisation procedure was successful in improving this fit over the majority of the spectrum, although the final fit was not improved at wavelengths greater than 600 nm (Figure 35). This is due to the smoothly varying spectral absorption and scattering properties of melanin, which do not allow for independent variation of simulated reflectance in this region using the current minimisation procedure.

To obtain a better understanding of the rate of convergence and the repeatability of the procedure, a further simulation was carried out using a different initial dataset. In this case, the procedure began with a skin model considered to be representative of dark Afro-Caribbean skin (5% epidermal melanin volume, melanosome diameters of 300 nm in the deep living epidermis, 150 nm in the superficial living epidermis and 10 nm in the stratum corneum, Figure 36).

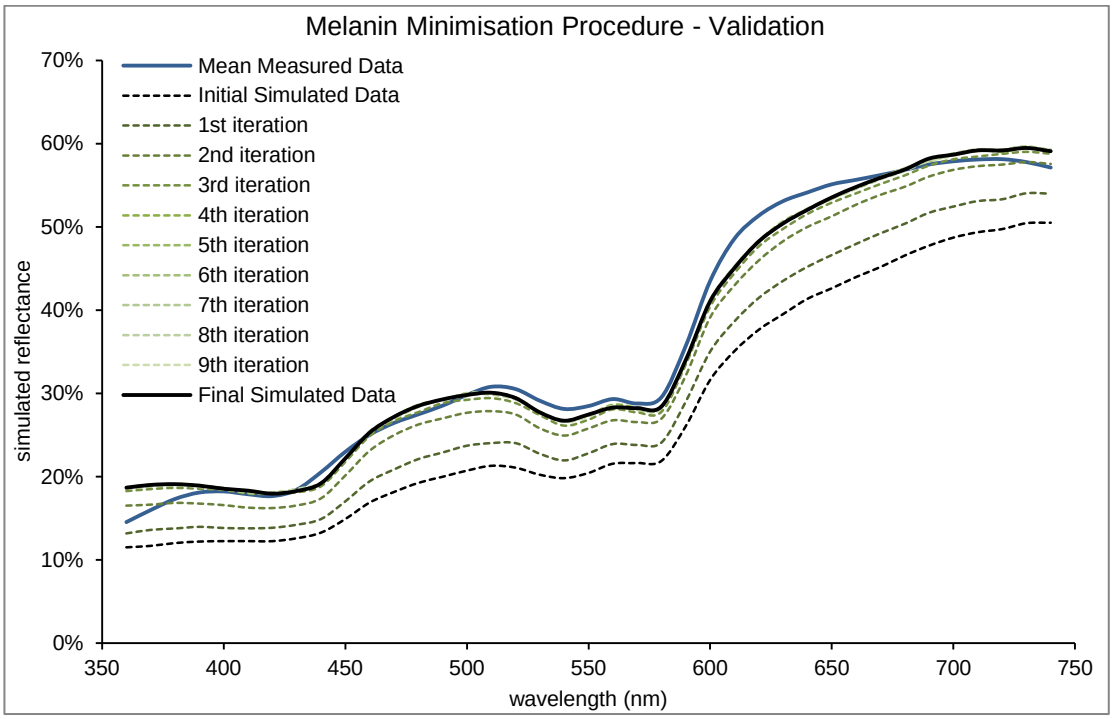

Figure 35: Simulated spectral reflection outputs obtained during further verification of the melanin minimisation procedure.

It can be seen from Figure 36 that the initial simulated reflectance differed substantially from the measured dataset. Convergence was fast, resulting in good agreement between simulated and measured spectra after only 3 iterations of the minimisation procedure (Figure 37). The procedure, involving 11 simulations in total, took an average of 28 hours to perform over the two validation experiments, using a quad-core processer with 16 Gb of RAM and a nominal clock rate of 2.66 GHz.

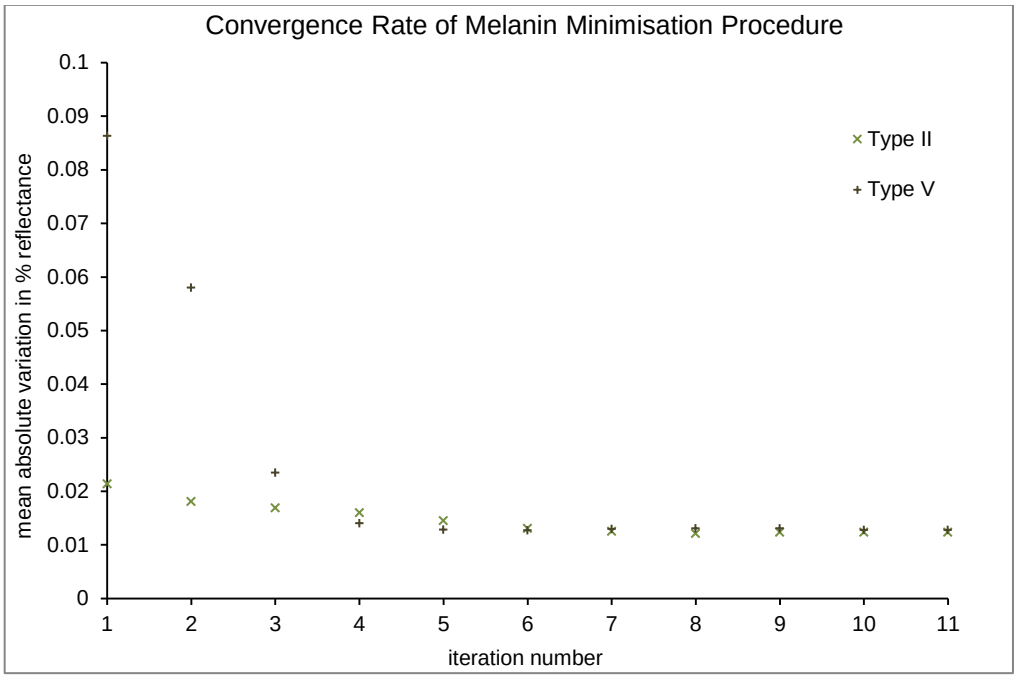

Figure 36: Convergence rates for two different initial skin models, where 1st data points correspond to initial simulated data.

The predicted melanin characteristics were relatively consistent from the two skin models (Table 5), although the technique of adjusting melanin content in all three layers of the skin model simultaneously does not allow for the exact same characteristics to be derived from any particular initial characteristics. For example, although the overall melanin content was very similar in the two predictions made here, the distribution mirrored that of the initial datasets in both cases. However, although the values of melanosome diameter varied across the two initial datasets, the distributions did not, allowing for the exact same predictions to be made.

Table 5: Final prediction of melanin characteristics for the mean participant dataset determined from two different initial skin models.

Estimated epidermal melanin characteristics		Type II	Type V
melanosome volume fraction	stratum corneum	0.5%	0.2%
	superficial living epidermis	1.0%	1.0%
	deep living epidermis	2.0%	2.4%
mean melanosome diameter	stratum corneum	11 nm	11 nm
	superficial living epidermis	165 nm	165 nm
	deep living epidermis	330 nm	330 nm

The predicted melanin volume fractions are consistent with values published elsewhere for Caucasian skin types [9]. The melanosome diameters, however, are

greater than those found in the literature for Caucasian skin types [7, 8, 10, 12, 13]. This suggests that either the relationships and parameters applied underestimate the degree of scattering caused by smaller diameter melanosomes, or the degree of scattering by the remaining epidermis is low at the blue end of the spectrum.

Adjusting PWS Vessel Properties

The anticipated effects of changing PWS vessel parameters upon the colour of PWS skin are discussed previously (Section 5.2, page 108). It was expected that changes in simulated lesion depth would have their greatest effect in the blue-green regions of the visible spectrum, with deeper lesions resulting in greater values of reflectance in this region. The effect of changing lesion depth was assessed in the simulation by introducing 10 vessels of 20 µm diameter and varying their mean depth within the model.

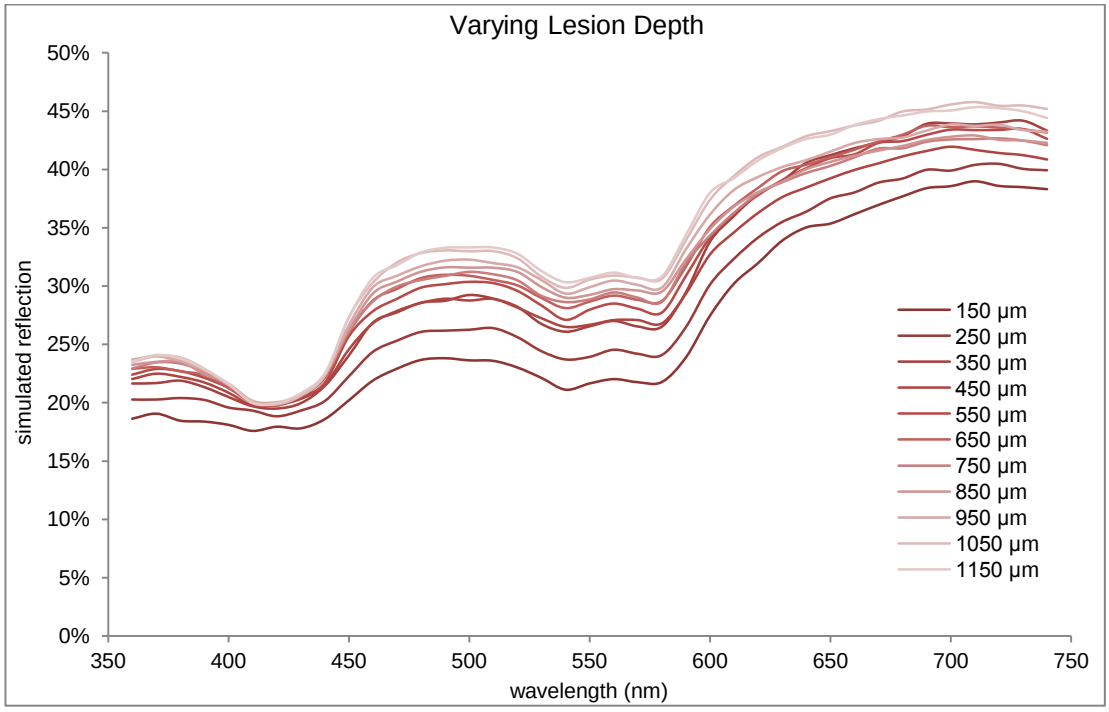

Figure 37: Simulated reflectance for vascular lesions of fixed vessel number, mean diameter and layer thickness, but mean depth varying from 150 µm to 1150 µm.

Increasing the depth of the lesion within the skin model was shown to cause a broadband increase in simulated reflectance. The increase in reflectance was less with each 100 µm step, as the proportion of light reaching the vessels decreased. This effect is particularly evident between 400 nm and 450 nm, where scattering is high (penetration depth is low) but absorption by blood is lower than neighboring

wavelength regions. It is also apparent from both Figure 38 and Figure 39 that the relationship between simulation reflection and depth is not consistent. This may be due to the stochastic nature of the programme, as the distribution of the vessels in the skin model both in terms of depth and lateral positioning may also have influenced the effect of the vessels upon simulated reflectance.

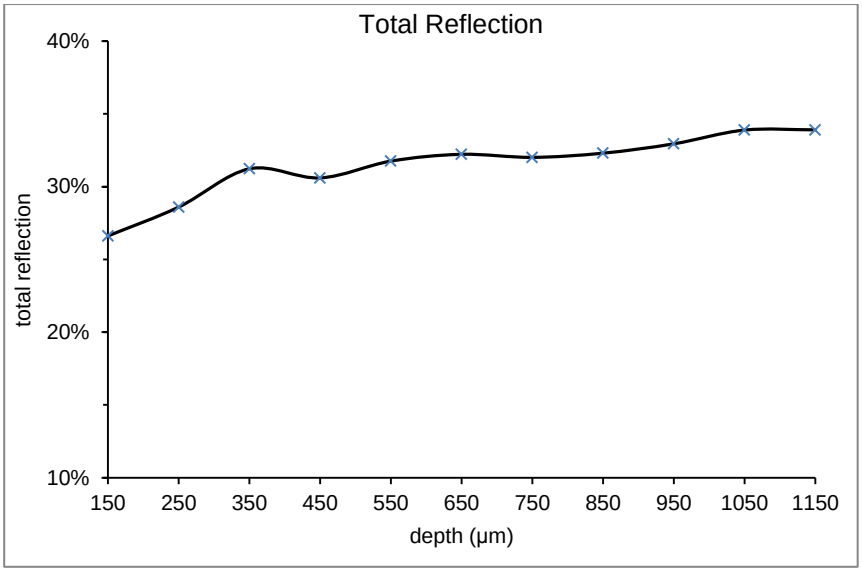

Figure 38: Total simulated reflectance for vascular lesions of fixed vessel number, mean diameter and layer thickness, but mean depth varying from 150 µm to 1150 µm.

Increasing vessel diameter within the skin model was expected to reduce the proportion of simulated reflection across the spectrum, with a greater effect at the red end.

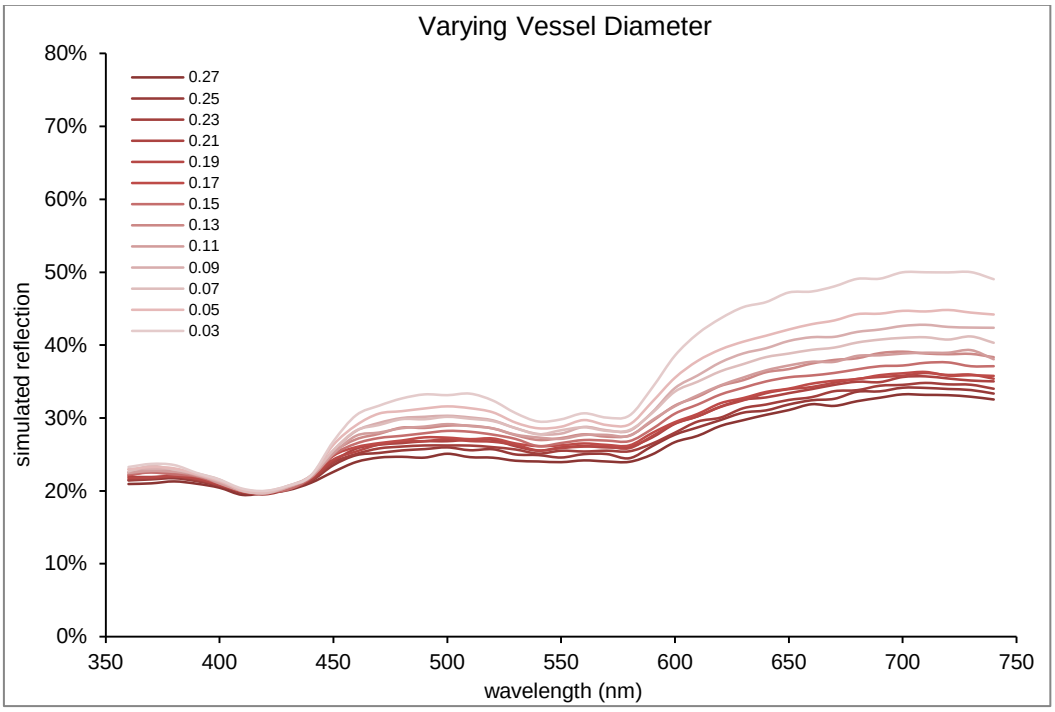

Figure 39: Simulated reflectance for vascular lesions consisting of 10 vessels at a mean depth of 500 µm, and vessel diameters varying from 0.03-0.27 µm.

Increasing the diameter of vessels was shown to increase simulated reflection across the spectrum. As expected, this effect is greatest at longer wavelengths, in particular at wavelengths longer than 630 nm (Figure 40). The effect is less pronounced at the haemoglobin absorption peaks (where the effective path length within the vessel is shortest and the albedo is smallest), in particular near 420 nm.

The effect of increasing vessel number upon skin colour is not well documented in the literature. The new Monte Carlo programme found that varying vessel number had a broad effect, but was most prominent in the regions from 450-530 nm and 630-740 nm (Figure 41).

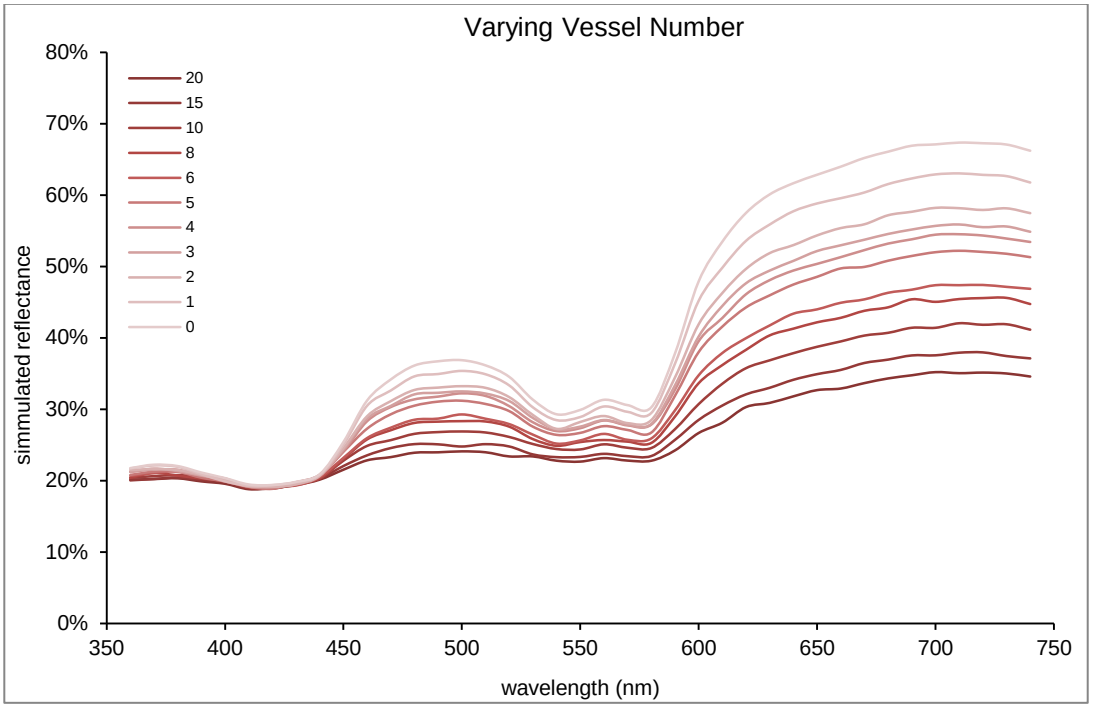

Figure 40: Simulated reflectance for vascular lesions of fixed mean vessel diameter (0.03 mm), lesion depth and layer thickness, but number of simulated PWS vessels varying from 0 to 12.

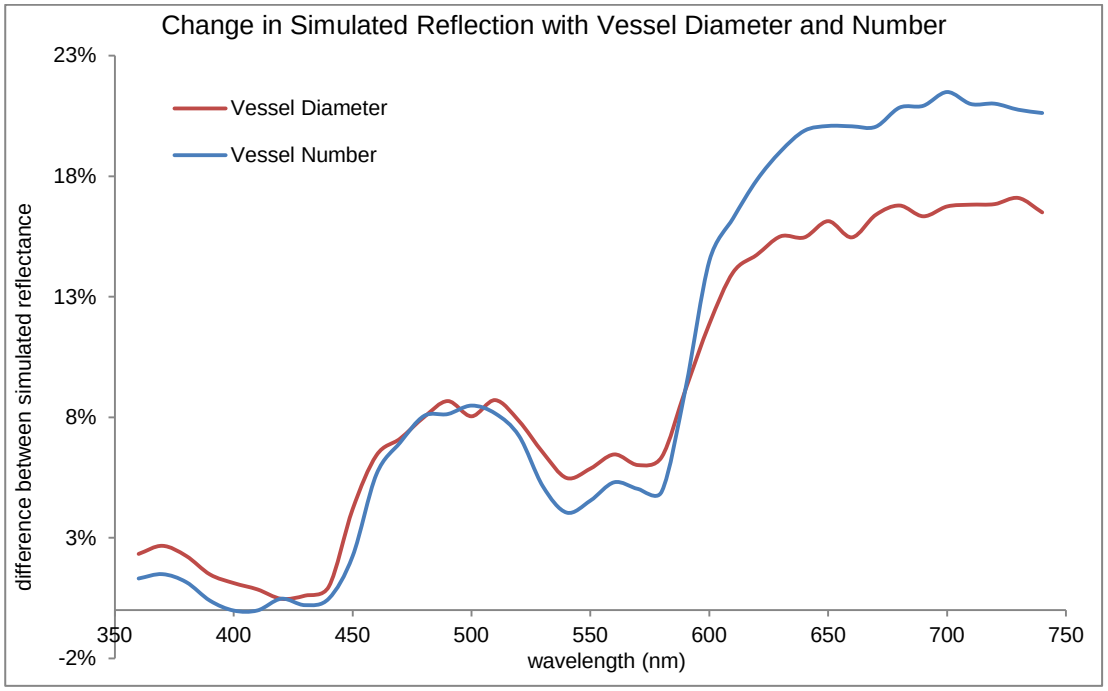

Figure 41: Absolute change in simulated reflectance resulting from a change in vessel number from 1-10 (blue), with a fixed diameter of 30 µm, and from a change in vessel diameter from 30 µm-270µm with a fixed number of 10 vessels.

On first inspection, the characteristics of varying vessel number appear to mirror those of vessel diameter. However, the effect of varying each parameter independently is shown in more detail in Figure 42 and Figure 43.

Figure 42 shows that a similar change in simulated reflectance can be achieved in the region 450-500 nm by adjusting either vessel number from 1-10 at a fixed diameter of 30 µm, or vessel diameter between 30 µm and 270 µm at a fixed number of 10. It also shows that the same adjustment results in a stronger response when adjusting vessel number at wavelengths greater than 590 nm, but a less strong response at wavelengths shorter than 460 nm and in the region from 510-580 nm.

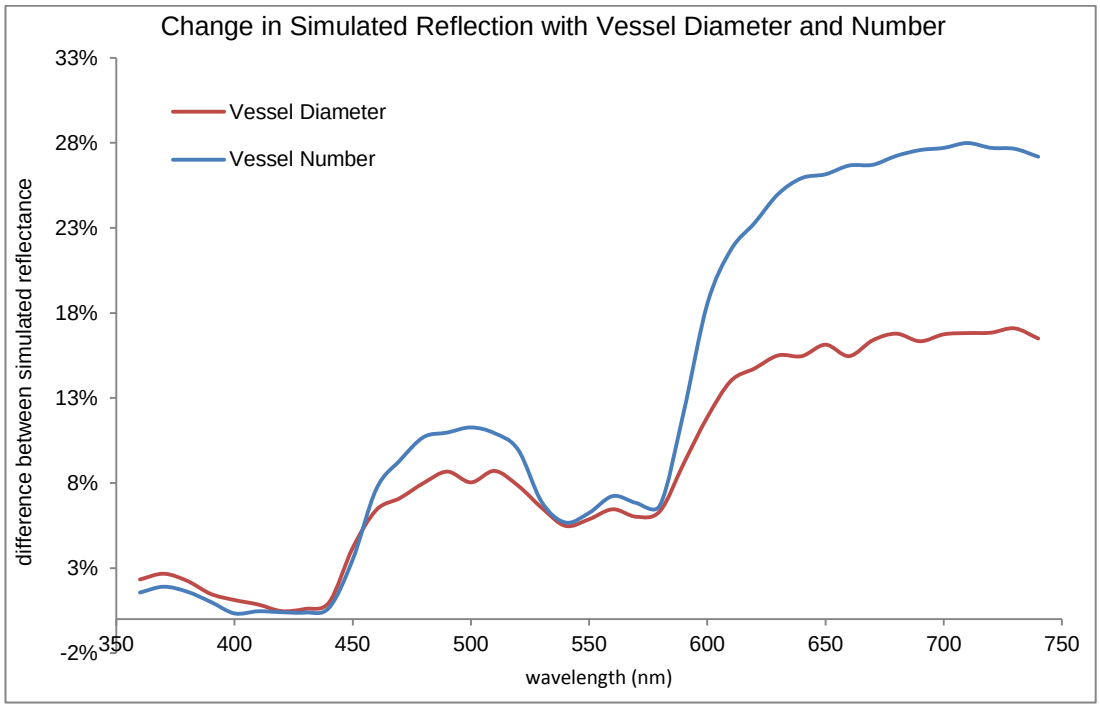

Figure 42: Absolute change in simulated reflectance resulting from a change in vessel number from 1-20 (blue), with a fixed diameter of 30 µm, and from a change in vessel diameter from 30 µm-270µm with a fixed number of 10 vessels.

Figure 43 shows that a similar change in simulated reflectance can be achieved in the regions 360-460 nm and 540-570 nm by adjusting either vessel number from 1-20 at a fixed diameter of 30 µm, or vessel diameter between 30 µm and 270 µm at a fixed number of 10. A much stronger response results from adjusting vessel number relative to vessel diameter in the remaining wavelength regions.

The work presented here has shown that, for a fixed epidermis, due to the difference in their contribution to spectral changes in simulated reflectance, any combination of vessel number, diameter and depths will result in a unique simulated output using the new Monte Carlo programme.

Minimisation Procedure - Vessel Adjustment

Section 5.2 (page 108) includes a description of the three spectral regions used to inform vessel parameter adjustment during minimisation. Based upon the preliminary results presented in this chapter (see Figure 38, Figure 40, Figure 41, Figure 42 and Figure 43), the following regions were selected:

- For the adjustment of vessel number, $qves_1$ covered the regions 450-530 nm and 630-740 nm.
- For the adjustment of vessel depth, $qves_2$ covered the entire wavelength region, from 340-740 nm.
- For the adjustment of vessel diameter, $qves_3$ covered the region 530-590 nm.

Due to overlap of the region $qves_2$ with $qves_1$ and $qves_3$, adjustment of lesion depth was performed independently of vessel number and diameter. This required an iterative technique, whereby vessel number and diameter were adjusted initially followed by lesion depth, before vessel number and diameter were again considered.

Verification of the PWS vessel minimisation procedure was carried out in a similar manner to the melanin minimisation procedure validation. The simulated spectrum was minimised to the mean measured spectral reflectance of PWS skin from the first 10 participants. The initial dataset was produced without introducing any PWS vessels to the model and with melanin properties obtained during verification of the melanin minimisation procedure (column 2, 'Type II' in Table 5). Twelve iterations of the vessel minimisation procedure were then carried out (Figure 44).

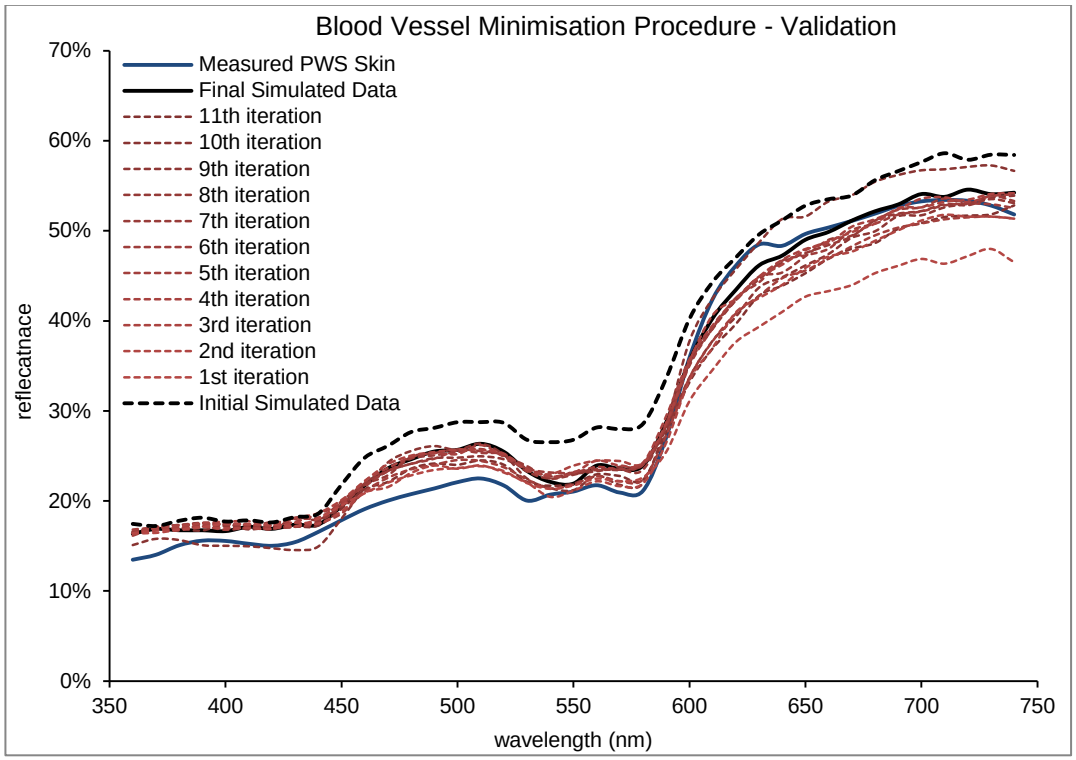

Figure 43: Simulated spectral reflection outputs obtained during verification of the blood vessel minimisation procedure.

Convergence was slower for the blood vessel minimisation procedure compared to the melanin minimisation procedure. This was expected due to the relative increase in complexity of the procedure.

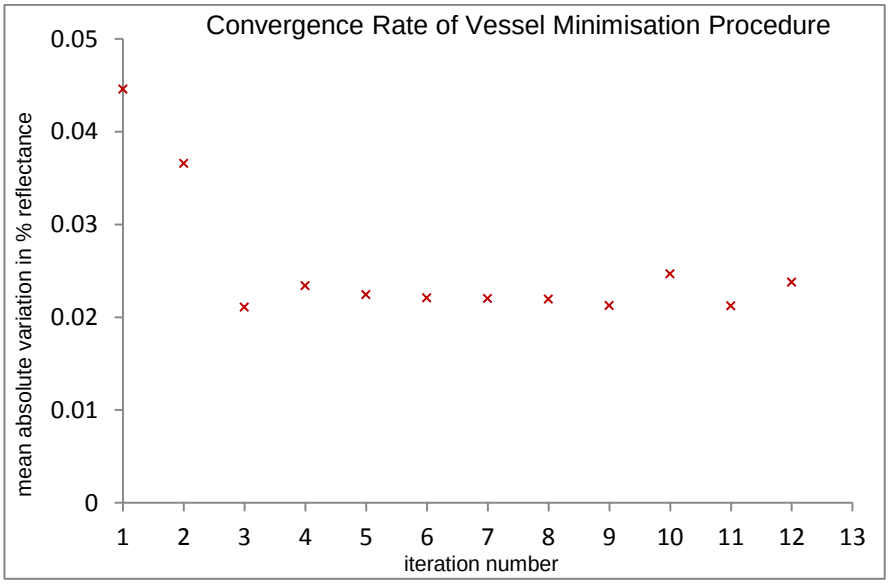

Figure 44: Convergence rate of vessel minimisation procedure, where 1st data point corresponds to initial simulated data.

Figure 45 shows that the blood vessel minimisation procedure provided fast convergence for the first two iterations, followed by steady (although not consistent)

improvement in closeness of fit for the remaining 10 iterations. Iteration numbers 4, 10 and 12 show an increase in the mean difference between measured and simulated datasets. These are as a result of changes in vessel number, which have substantial effect on the simulated spectrum. The results presented here suggest that greater than twelve iterations of the procedure may be necessary to confidently obtain close to the best fit possible using this minimisation technique. However, the procedure took a mean time of approximately 4.5 days using a quad-core processer with 16 GB of RAM and a nominal clock rate of 2.66 GHz. Participant 11 and the first session from participant 1 used 12 iterations of the PWS vessel minimisation procedure; the remaining assessments used 15 iterations.

The final simulated reflection shown in Figure 45 provided a close fit to the measured spectrum, with a mean deviation of less than 2% reflection. An excellent fit was produced in the region 540-740 nm (mean 1.3% deviation), although there was greater deviation from the measured dataset in the region from 460 nm-540 nm (mean 3.3% deviation). This was obtained using a skin model containing 7 vessels with an outside vessel diameter of 70 µm and a mean depth of 160 µm. The procedure was repeated on two occasions with the same input parameters and produced comparable results after 12 iterations (8 vessels of 70 µm diameter at a mean depth of 210 µm, and 7 vessels of 80 µm diameter at a mean depth of 180 µm, see Figure 45).

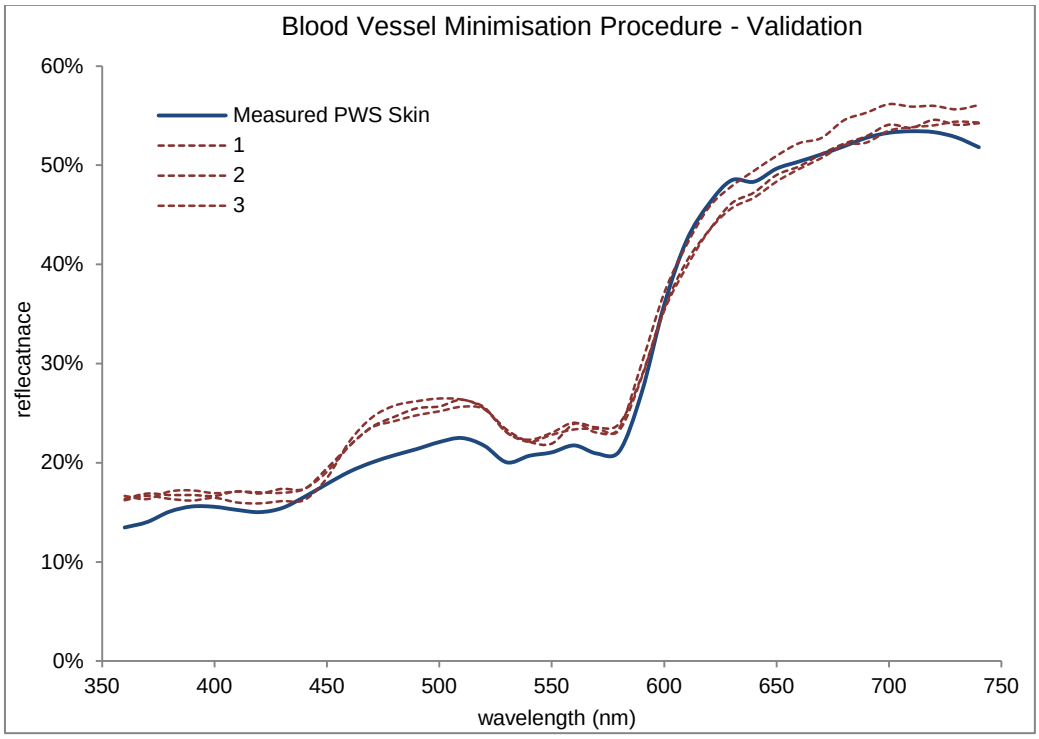

Figure 45: Repeated outputs from blood vessel minimisation procedure showing consistency of minimisation procedure after 12 iterations.

Inconsistencies in the final parameters, particularly the mean vessel depth, suggest that further iterations of the programme are necessary, and may result in a closer final fit. Comparing the final simulated data to the measured spectrum, the preliminary work presented in Figure 38, Figure 40, Figure 41, Figure 42 and Figure 43 suggest that a closer fit may have been produced using a skin model with slightly larger, more superficial (and therefore fewer) vessels.

Conclusions

These initial results show a good fit between measured and simulation spectral reflection and an acceptable total computation time (mean 12.5 days). The accuracy of the predicted vessel characteristics cannot be verified directly as the true vessel characteristics are not known, although they are in line with the range of parameters expected following a comprehensive survey of the literature. The primary standard for determining PWS vessel anatomy is through biopsy of the affected area. This method was considered unethical for the participants involved in this study. Instead, two alternative methods were used to estimate the characteristics of PWS vessels. The first method, OCT imaging, used an imaging technique to determine directly the depths, diameters and numbers of vessels in the skin. The second technique involved

inference of the vessel characteristics based upon their response to laser treatment. The results from these analyses are presented in the following chapter.

7. Results and Discussion

7.1 Participants Assessed by Spectrophotometry

Spectrophotometric data was acquired before and after a single session of laser treatment for a total of 10 participants. Room temperatures were recorded and found to have remained steady at 22.5°C (±1 °C) across the assessments made. This section comprises a case-by-case analysis of the accuracy of skin colour reproduction, the properties of epidermal melanin and PWS vessel properties predicted by the new Monte Carlo programme and how these properties relate to treatment effectiveness determined through color measurements.

Participant 1

The simulation reproduced adjacent skin colour with a mean difference from the measured spectrum of 2.3% reflection. The final skin model contained 1.5% epidermal melanin and a mean melanosome diameter of 250 nm. The simulated spectrum reproduced measured data well over the majority of the spectrum. Predicted reflection at wavelengths longer than 660 nm was greater than measured, but less between 500 nm and 620 nm (Figure 47). Due to the smoothly varying optical coefficients of melanin, it is not possible to improve the agreement between the simulated and measured spectra considerably in only these two regions using the current minimisation procedure. Simulated reflection was also greater in the region 360-380 nm, suggesting smaller melanosomes in the skin model would have resulted in a better reproduction of the measured colour of adjacent skin for this participant.

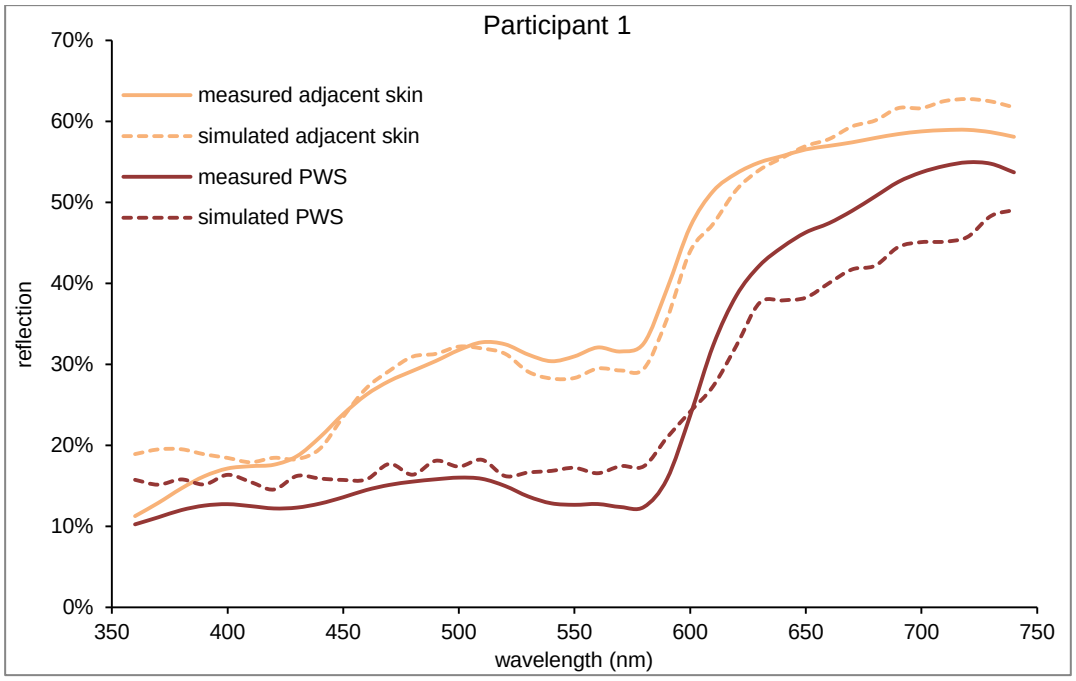

Figure 46: Pre-treatment measured spectra and simulation results for participant 1.

PWS skin colour was reproduced with a mean difference of 4.5% reflection after 12 iterations (16.5 days). The final PWS skin model contained 18 vessels of 180 µm diameter and a mean depth of 262 µm. Simulated reflection was greater than measured at wavelengths less than 600 nm, suggesting that a skin model containing more superficial vessels would have provided a closer fit between simulated and measured curves in this region (Figure 47, see also Figure 38 on page 121). However, decreasing the mean vessel depth would further contribute to the discrepancy between measured and simulated data points at wavelengths greater than 600 nm. Decreasing the vessel number or diameter would have reduced this latter discrepancy. Thus, it is likely that further iterations of the PWS minimisation procedure would have resulted in a closer fit between measured and simulated PWS spectra with fewer or thinner, more superficial vessels.

Post treatment adjacent skin was reproduced with a mean discrepancy of 2.3% reflection after 10 iterations of the melanin minimisation procedure. The simulated model contained a mean epidermal melanin volume of 1.7% and mean melanosome diameter of 252 nm. Again ,adjacent skin colour was reproduced well over the majority of the spectrum. Figure 48 shows that the predicted reflectance spectrum of post-treatment adjacent skin is greater than measured values in the region 660 nm to 740 nm but less in the region 500 nm to 640 nm. A change in the quantity of melanin used in the skin model may, using the current minimisation technique, improve the fit

in either one of these regions, but would result in a poorer fit in the remaining region. Predicted reflectance in the region 360 to 400 nm was substantially greater than measured reflectance, again suggesting that the use of smaller melanosome diameters in the skin model would have produced a closer fit overall.

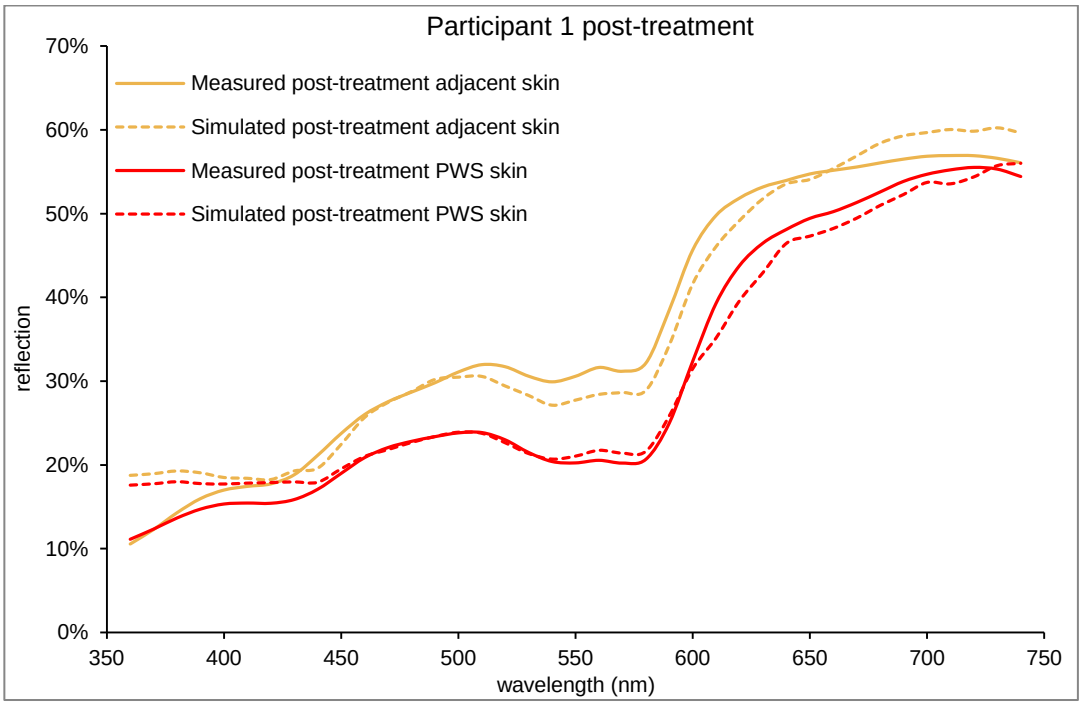

Figure 47: Simulation results for post-treatment skin of participant 1.

Post treatment PWS skin was reproduced well by the simulation at wavelengths greater than 450 nm, with a mean deviation between measured and simulated reflectance of 1.7% across the entire spectrum (12 iterations, 11 days). The skin model contained 8 vessels of 100 µm diameter with a mean depth of 215 µm. The primary area of discrepancy between simulated and measured data was in the region below 450 nm. It is expected that a decrease in the melanosome diameters used in the skin model would have improved the fit in this region.

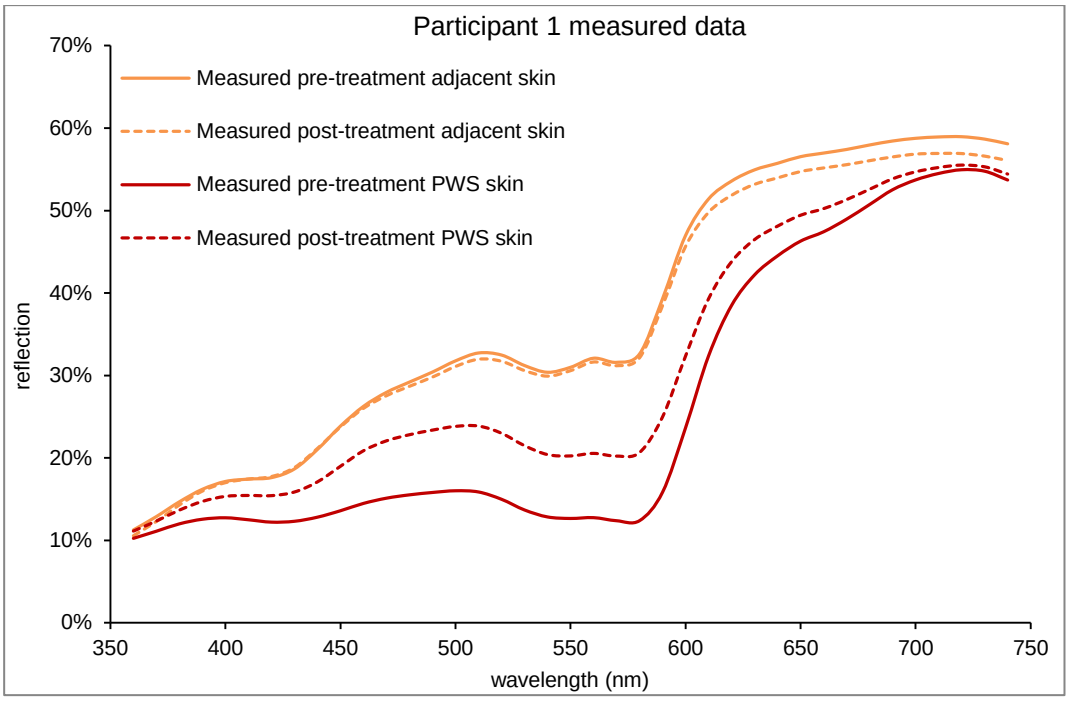

Figure 48: Colour measurement data for participant 1 taken before and after 1 session of laser treatment.

A treatment was performed using the Pulsed Dye Laser at a wavelength of 595 nm, radiant exposure of 14 Jcm^{-2} and pulse length of 6 ms. Figure 49 shows very little change in adjacent skin colour between treatment sessions. The slight reduction in reflectance towards the red end of the spectrum was attributed in the simulation to a small increase in epidermal melanin concentration.

Measurements of PWS skin colour show a substantial increase in reflectance over the majority of the spectrum, demonstrating a substantial reduction in PWS colour (difference in reflection between PWS and adjacent skin) after one treatment. The simulation results suggest that this was caused primarily by a reduction in vessel number. The predicted mean vessel diameter was also reduced following treatment, and the mean vessel depth increased, suggesting that the treatment was most effective at destroying larger, more superficial vessels.

Participant 2

Pre-treatment adjacent skin colour was reproduced with a mean discrepancy of 1.6% reflection from the measured spectrum after 10 iterations of the melanin minimisation procedure, using a skin model containing an epidermal melanin volume fraction of 3.3% and a mean melanosome diameter of 208 nm.

The greatest discrepancy between simulated and measured reflection of pre-treatment adjacent skin is evident in the region 520-600 nm. This suggests that absorption by blood had a greater influence in the measured skin sample than in the simulation. Due to the age of the participant (67 years at the time of the assessment), it is possible that the region assessed may have been influenced by age related ectasia of superficial vessels in the normal dermis, a prospect not considered in the simulation. The region below 450 nm wavelength was slightly underestimated by the simulation, suggesting the use of larger melanosomes in the skin model may have improved the fit between the measured and simulated datasets. Reflection between 600 nm and 700 nm was also underestimated by the simulation. Although the fit in this region may have been improved by reducing the epidermal melanin concentration, this would have resulted in a poorer fit outside of this region.

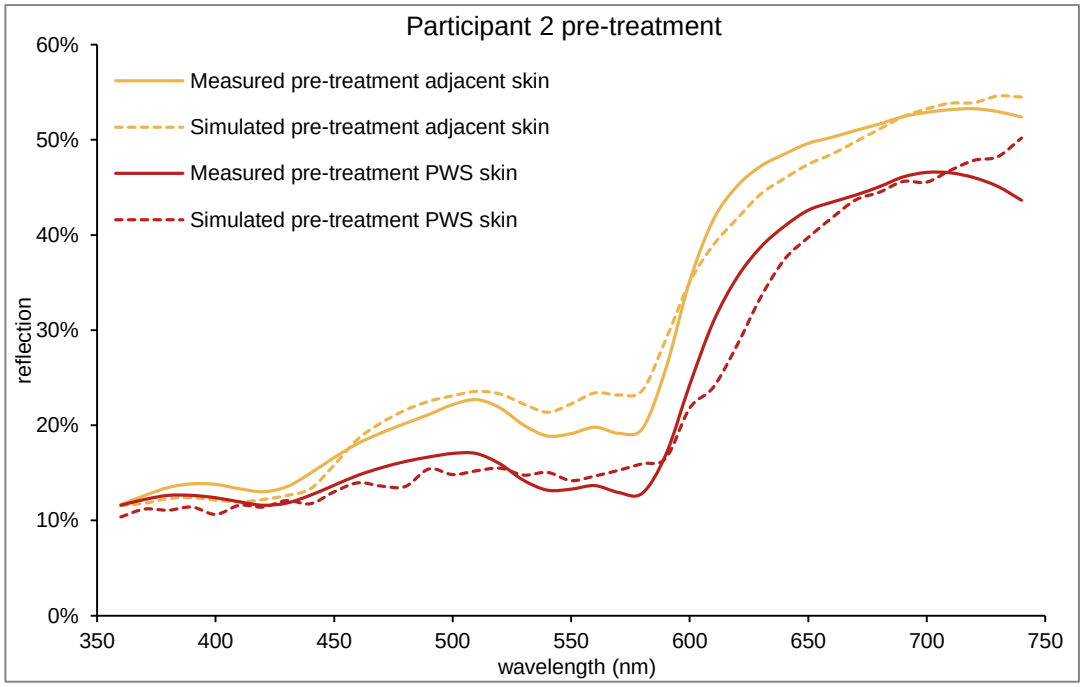

Figure 49: Pre-treatment measured and simulated spectral curves from participant 2.

Pre-treatment PWS skin was simulated with a mean difference from the measured dataset of 2.2% reflection after 15 iterations (8.5 days). The final pre-treatment PWS skin model contained 6 vessels of 160 µm diameter with a mean depth of 250 µm. The fit between measured and simulated curves in the region 360 nm to 600 nm was generally close. Between 600 and 700 nm, the simulation produced a lower proportion of simulated light than measured for this region. This discrepancy appears to

primarily have been inherited from the melanin characteristics derived in the adjacent skin minimisation procedure.

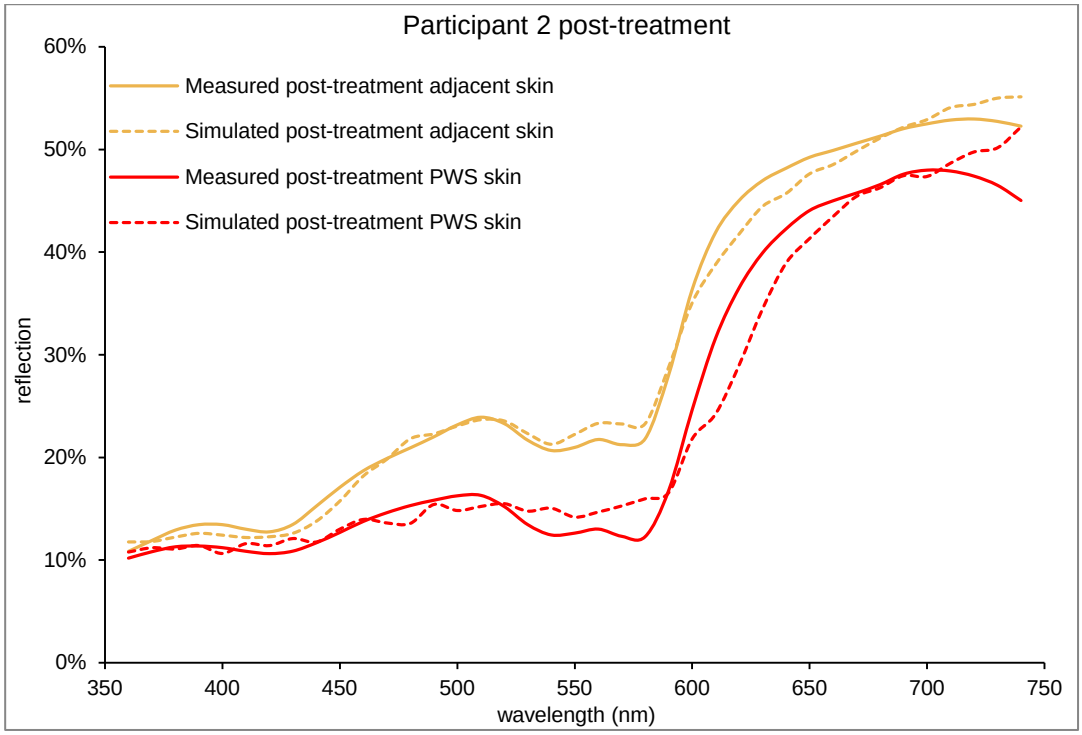

Figure 50: Post-treatment measured and simulated spectral curves from participant 2.

Post treatment adjacent skin was reproduced by the simulation with a mean deviation from the measured dataset of 1.1% reflection after 10 iterations of the melanin minimisation procedure. This was achieved with a skin model containing the same melanin parameters as pre-treatment adjacent skin. The overall fit between simulated and measured post-treatment adjacent skin was closer than for pre-treatment adjacent skin, although a slight overestimate in reflection was still present in the region 530 nm to 590 nm and a slight underestimate was still present in the region 610 nm to 690 nm.

Post treatment PWS skin was reproduced with a mean deviation of 1.6% reflectance (9 days) using a skin model containing 7 vessels of 170 µm diameter and a mean depth of 270 µm. The primary region of discrepancy between simulated and measured datasets was again an underestimate of the proportion of reflectance in the region 630 nm to 700 nm. Again, this appears to have been inherited from the melanin minimisation procedure.

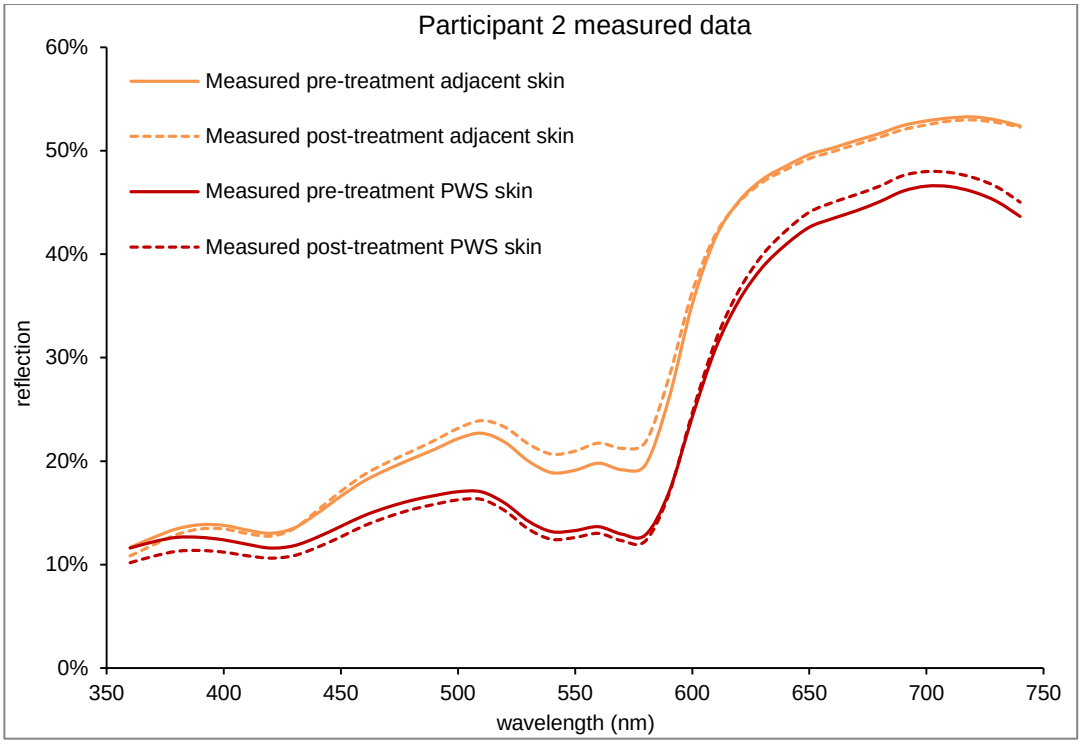

Figure 51: Colour measurement data of participant 2 taken before and after laser treatment.

Pulsed Dye Laser treatment was carried out using a radiant exposure of 14 Jcm^{-2} and a pulse length of 6 ms. Colour measurement data of adjacent skin shows that there was a slight increase in measured reflectance in the region 500 nm to 580 nm. This is most likely a result of a reduction in pigmentation, but may also be due to a reduction in the quantity of blood in the superficial epidermis of the adjacent skin sample. This subtle difference was not recognized by the melanin minimisation procedure, which predicted no change in the melanin properties between assessments. PWS skin showed very similar characteristics throughout, with a slight increase in measured reflection at wavelengths greater than 650 nm. It is therefore apparent that the laser treatment had little, if any, effect on the colour of the PWS lesion.

As a result of the small changes in measured reflection between sessions, the vessel minimisation procedure predicted similar vessel characteristics for both pre-treated and post-treated PWS datasets, with a slight increase in vessel number and depth, and a slight decrease in vessel diameter.

Participant 3

Pre-treatment adjacent skin was reproduced with a mean deviation from the measured dataset of 1.3% reflection. The skin model contained a melanin volume fraction of 0.7% and a mean melanosome diameter of 156 nm. The simulated spectral curve shape matched closely to the measured curve over the entire spectrum (Figure 53).

Pre-treatment PWS skin was reproduced with a mean deviation of 1.8% reflectance (4.5 days) using a skin model containing 4 vessels of 10 µm diameter and a mean depth of 218 µm. The simulated reflectance of PWS skin matched closely to that of simulated adjacent skin (much like their measured equivalents). Thus, discrepancies between simulated and measured pre-treatment PWS skin are likely to have been inherited primarily from the melanin minimisation procedure. It is of interest to note that measured reflection of PWS skin was greater that adjacent skin in the region 370-450 nm, although this was not reproduced by the simulation.

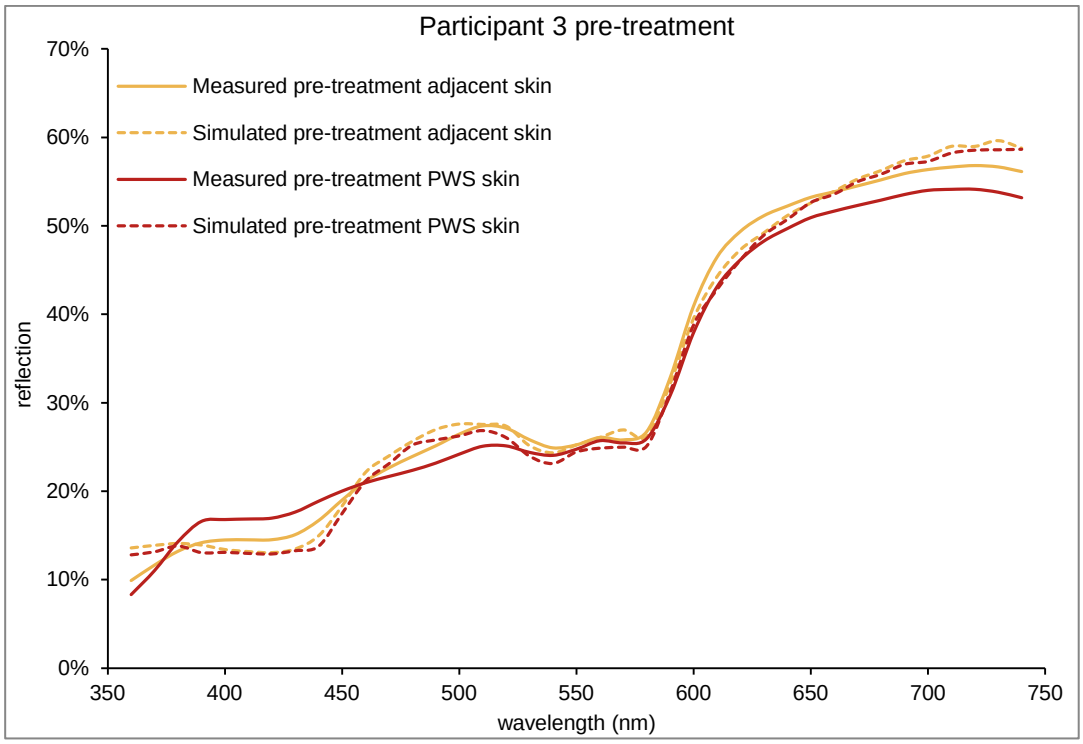

Figure 52: Pre-treatment measured and simulated spectral curves from participant 3.

Post-treatment adjacent skin colour was reproduced with a mean difference of 5.3% reflection from the measured spectrum. This employed a skin model containing an epidermal melanin volume of 2.2% and a mean melanosome diameter of 156 nm.

Unlike pre-treatment adjacent skin, the spectral curve shape was not matched closely by the simulation (Figure 52). This led to overestimates in reflection below 400 nm, in the region 460 nm to 510 nm and at wavelengths greater than 610 nm. A reduction in

the melanin volume applied to the skin model may have improved the fit in these regions (at the sacrifice of the remaining regions) and reduced the mean difference between measured and simulated reflection. A reduction in melanosome diameter is also likely to have improved the fit between measured and simulated spectra below 500 nm.

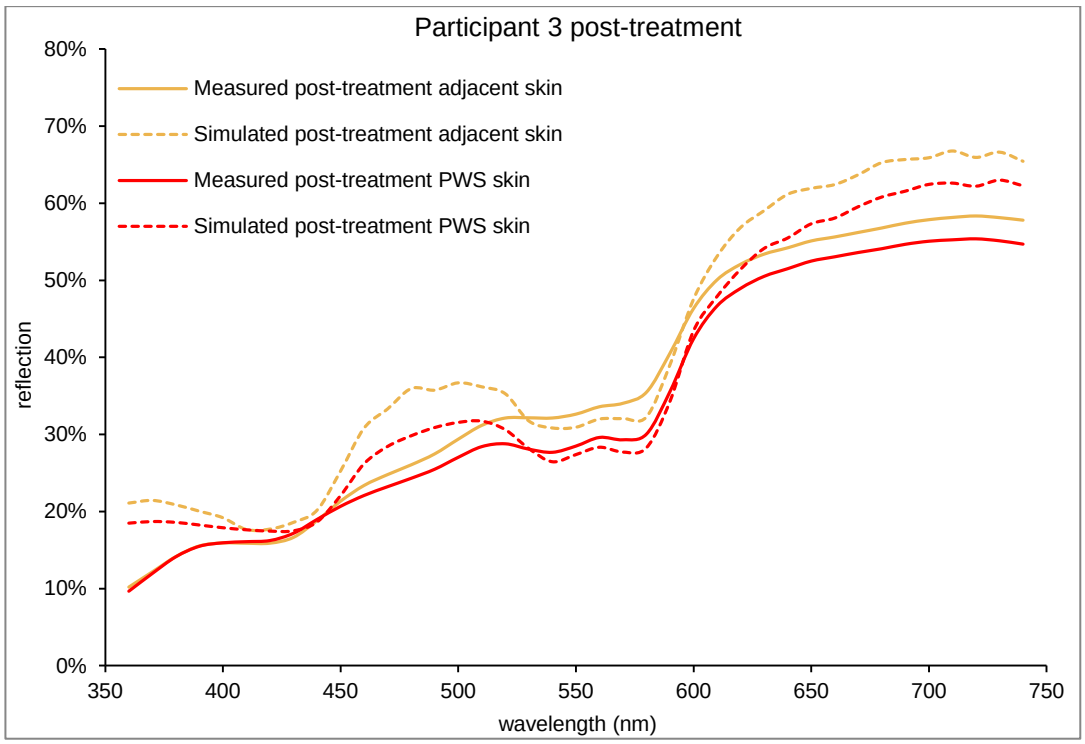

Figure 53: Post-treatment measured and simulated spectral curves from participant 3.

Post-treatment PWS skin was simulated with a mean difference from the measured dataset of 3.8% reflection after 15 iterations (4.5 days). The final post-treatment PWS skin model contained 4 vessels of 10 µm diameter with a mean depth of 265 µm. The difference in shape between measured and simulated curves appears to have been inherited from the melanin minimisation procedure. In particular, the simulation predicted greater reflectance than the measured data below 410 nm, between 460 nm and 520 nm and above 610 nm.

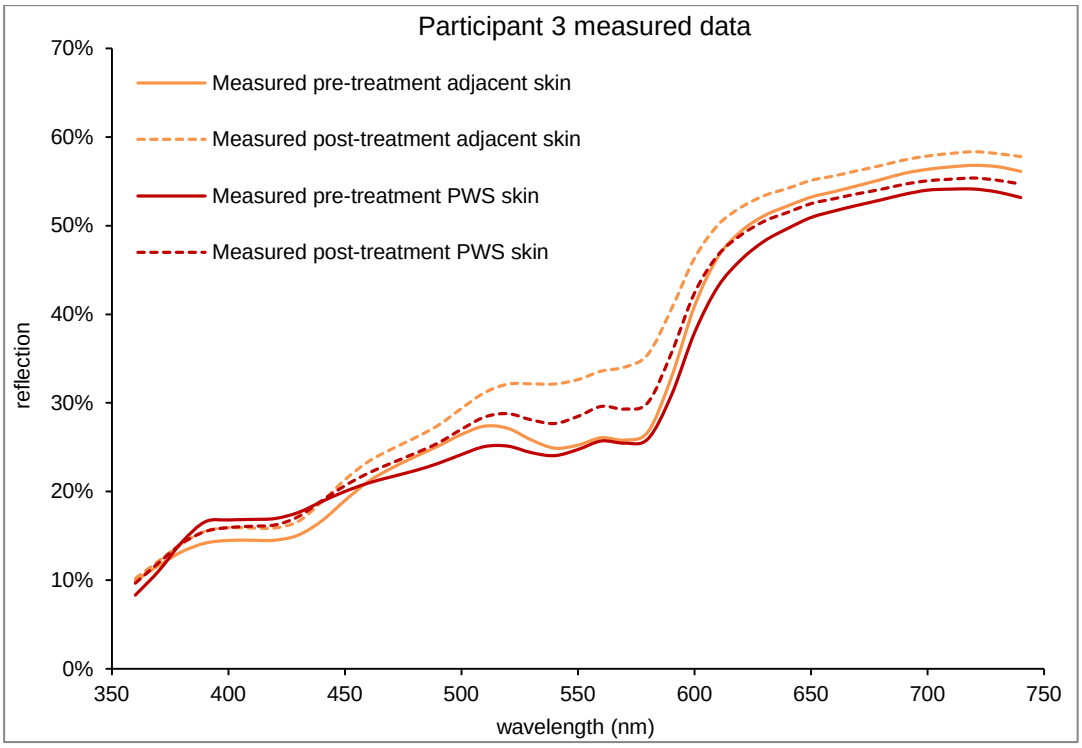

Figure 54: Colour measurement data of participant 3 taken before and after laser treatment.

Laser treatment was carried out using a radiant exposure of 14.5 Jcm^{-2} and a pulse length of 6 ms. Colour measurement data of adjacent skin shows a decrease in measured reflectance across the entire spectrum, in particular within the region 500 nm to 610 nm. This is likely to be as a result of increased pigmentation. As a result, the melanin minimisation procedure predicted that the epidermal melanin quantity increased from 0.7% to 2.2% between treatments, with no change in the mean melanosome diameter.

PWS skin measurements also showed a decrease in reflection with a greater emphasis in this region. Overall, the difference between PWS and adjacent skin was shown to be reduced between sessions, particularly in the region 500 nm to 600 nm. The PWS vessel minimisation procedure predicted the same number and diameter of vessels in the region measured, with a slight increase in the mean vessel depth. Thus, the simulation attributed the measured change in PWS colour between sessions primarily to a change in the melanin content of the overlying epidermis.

Participant 4

Pre-treatment adjacent skin colour was reproduced with a mean difference of 3.3% reflection from the measured spectrum. The final skin model contained an epidermal melanin volume fraction of 1.3% and a mean melanosome diameter of 291 nm.

Simulated reflection was greater than measured at wavelengths longer than 660 nm and shorter than 410 nm. The former region would have provided a closer fit if the epidermal melanin content had been lower, although this would have increased the difference between measured and simulated spectra in the region 500 nm to 610 nm, where simulated reflection was substantially lower than measured data. Reducing the mean melanosome diameter used in the skin model is likely to have improved the overall fit of the simulated spectrum by reducing the discrepancy below 410 nm.

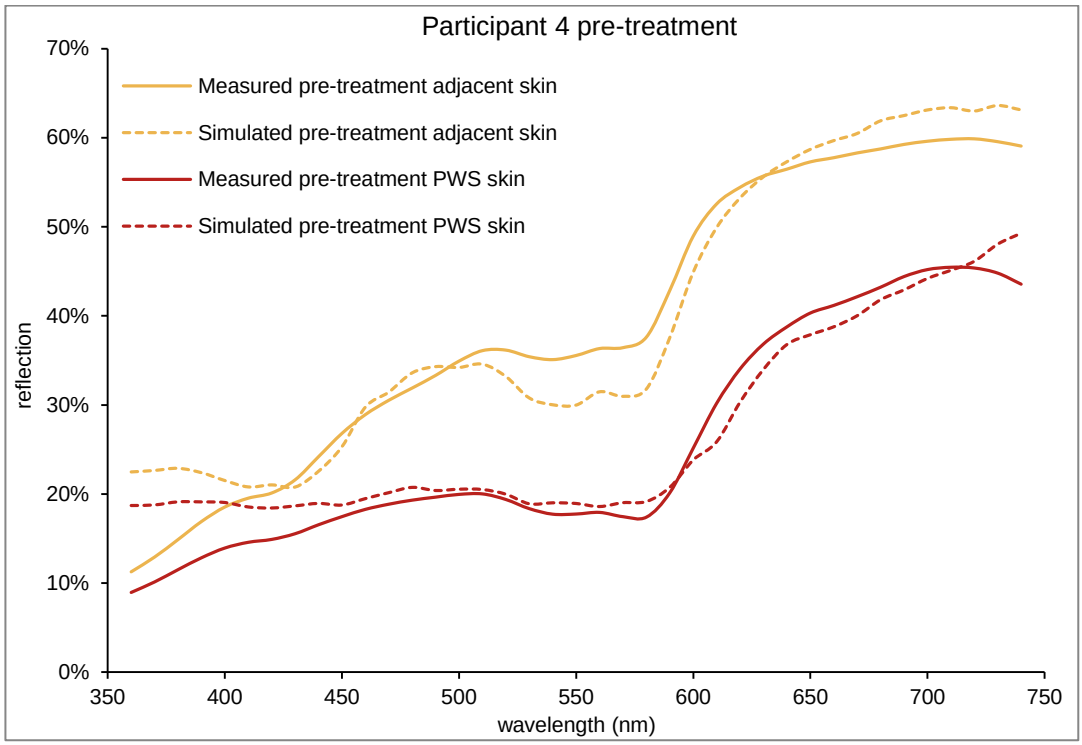

Figure 55: Pre-treatment measured and simulated spectral curves from participant 4.

Simulated pre-treatment PWS skin differed from the measured dataset by a mean value of 3.3% reflection after 15 iterations (13.5 days). The final pre-treatment PWS skin model contained 17 vessels of 100 µm diameter with a mean depth of 194 µm. The simulated spectrum demonstrated greater reflectance than the measured values below 450 nm, with the discrepancy between the two spectra increasing at smaller wavelengths. The discrepancy in this region, along with another at 740 nm, appears to have been inherited (in part, at least) from the melanin minimisation procedure.

Post treatment adjacent skin was reproduced with a mean deviation from the measured dataset of 3.0% reflection after 10 iterations of the melanin minimisation procedure. This was produced using a skin model containing 1.4 % melanin and a

mean melanosome diameter of 284 nm. As with pre-treatment adjacent skin, simulated reflection was less than the measured skin values in the region 500 nm to 610 nm (and further, up to 650 nm), suggesting that a slightly lower epidermal melanin volume fraction would have provided a closer fit between simulated and measured spectra overall. The discrepancy between measured and simulated data towards the blue end of the spectrum was smaller for post-treatment adjacent skin, but the use of smaller melanosomes may again have provided an improved fit in this region.

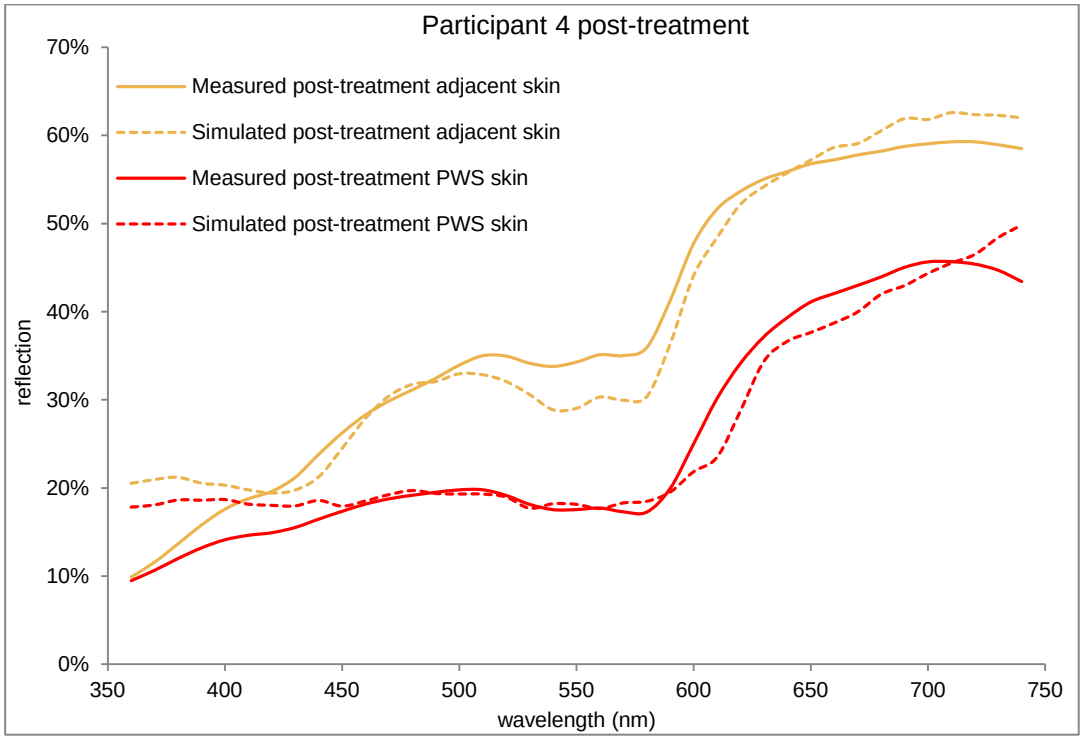

Figure 56: Post-treatment measured and simulated spectral curves from participant 4.

Post treatment PWS skin was reproduced closely over the majority of the spectrum, with a mean deviation of 2.5% reflectance (8.5 days). The final skin model contained 7 vessels of 180 µm diameter and a mean depth of 214 µm. As with the pre-treated PWS skin, the main region of discrepancy was below 450 nm, where simulated reflectance was increasingly higher than measured reflectance, mimicking the pattern from simulated adjacent skin.

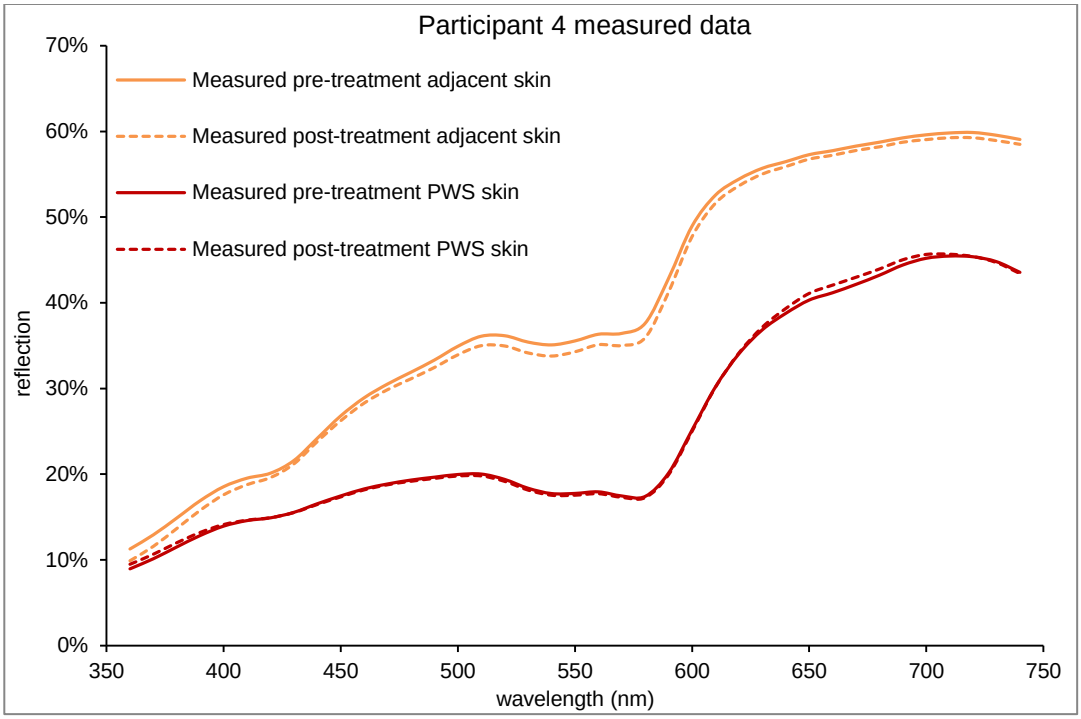

Figure 57: Colour measurement data of participant 4 taken before and after laser treatment.

Laser treatment was carried out using a radiant exposure of 16 Jcm^{-2} and a pulse length of 6 ms. Figure 58 shows that colour measurement data demonstrates very little change in either the assessed regions of adjacent or PWS skin between sessions. As a result, the simulation predicted very little change in the melanin and PWS vessel properties for this participant.

Participant 5

Pre-treatment adjacent skin colour was reproduced with a mean difference of 2.5% reflection from the measured spectrum. The final a skin model contained an epidermal melanin volume of 0.4% and a mean melanosome diameter of 194 nm.

Spectral reflection of adjacent skin was overestimated at 360 nm, in the region 460 nm to 510 nm and at wavelengths greater than 670 nm (Figure 59). A reduction in the (already low) melanin volume applied to the skin model may have improved the fit in these regions, but not in the remaining regions where reflectance was underestimated (400-450 nm and 540-630 nm). A reduction in melanosome diameter may also have improved the fit between measured and simulated spectra at 360 nm, but would have resulted in a larger discrepancy in the region 400 nm to 450 nm. Thus, although there are regions of noticeable discrepancy between the minimised and simulated spectra, it

is unlikely that further improvement could have been achieved using the current melanin minimisation procedure.

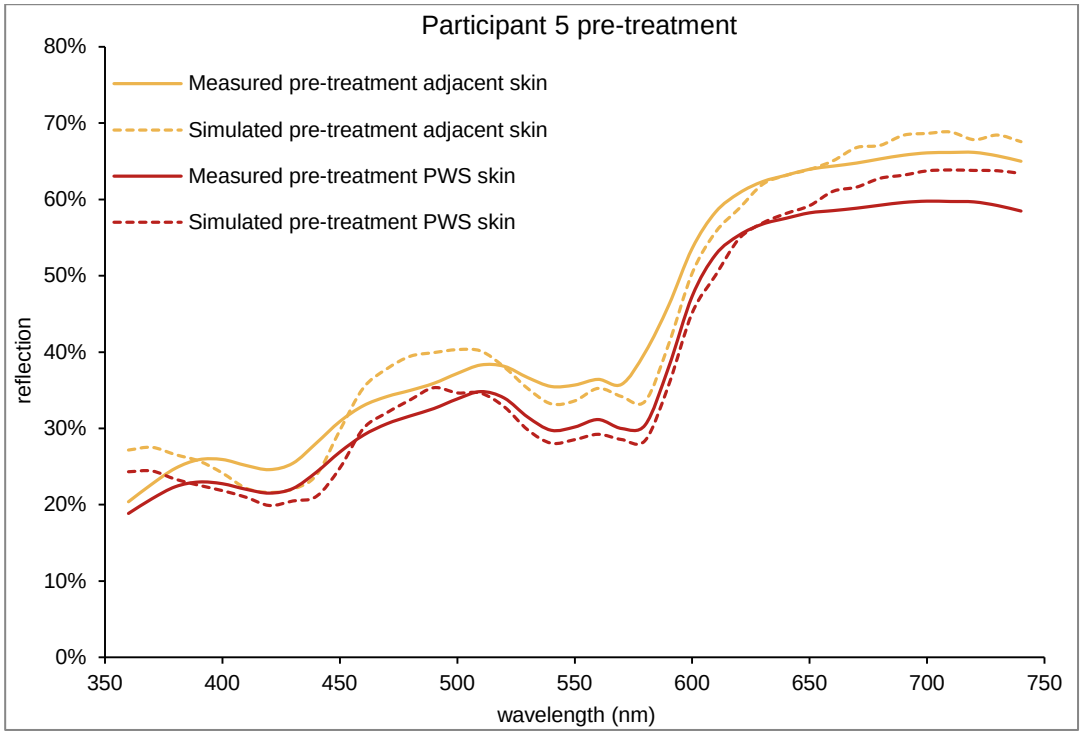

Figure 58: Pre-treatment measured and simulated spectral curves from participant 5.

Pre-treatment PWS skin was simulated with a mean difference from the measured dataset of 2.2% reflection after 15 iterations (9 days). The final pre-treatment PWS skin model contained 7 vessels of 40 µm diameter with a mean depth of 220 µm. The difference in shape between measured and simulated curves appears to have been inherited from the melanin minimisation procedure. The greatest discrepancy between measured and simulated data was at wavelengths greater than 650 nm, where the simulation overestimated the proportion of reflected light by a greater degree than the adjacent skin model. This suggests that a slight increase in vessel number or diameter could have improved the fit in this region, although it would have resulted in a poorer fit between 500 nm and 620 nm.

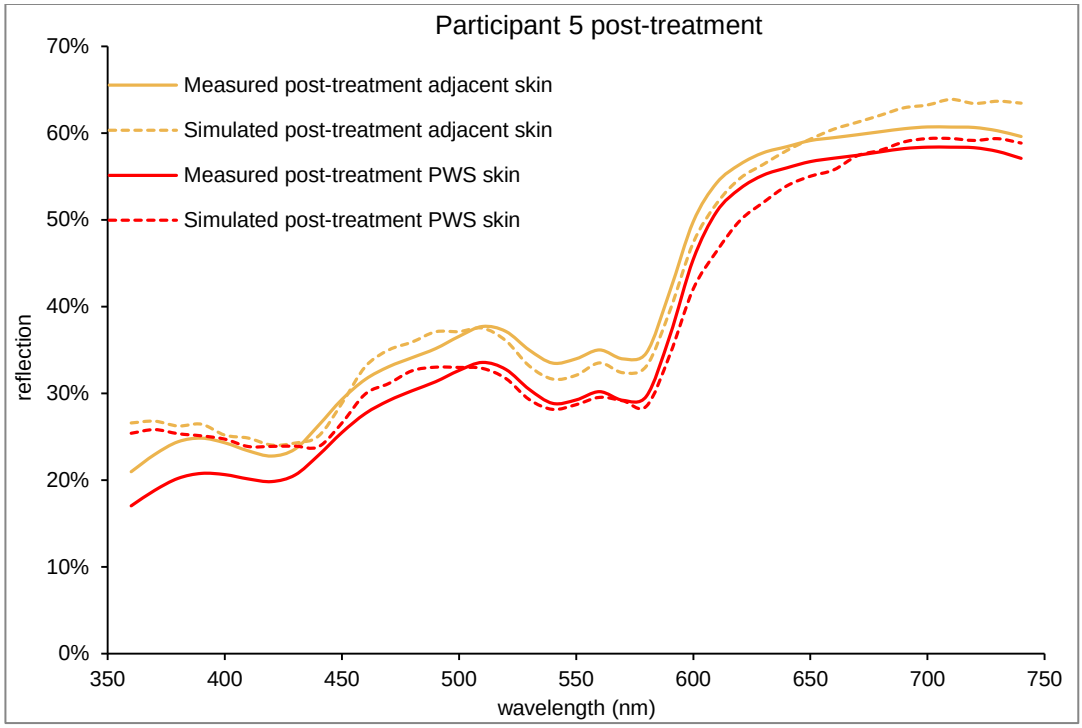

Figure 59: Post-treatment measured and simulated spectral curves from participant 5.

Post treatment adjacent skin was reproduced with a mean deviation from the measured dataset of 1.8% reflection after 10 iterations of the melanin minimisation procedure. This was produced using a skin model containing 0.8% melanin with a mean melanosome diameter of 318 nm. The simulated spectral curve shape matched more closely to the measured spectral curve than their pre-treatment equivalents, although there were similar discrepancies between the two curves throughout. It is notable that the simulated reflection was substantially overestimated at 360 nm, suggesting that the use of smaller melanosomes in the skin model would have improved the fit.

Post treatment PWS skin was reproduced with a mean deviation of 2.2% reflectance from the measured spectrum (12 days), using a skin model containing 13 vessels of 40 µm diameter and a mean depth of 360 µm. Spectral reflectance was overestimated by the simulation in the region 360 nm to 450 nm (Figure 60), further supporting the suggestion that the use of smaller melanosome diameters in the skin model would have been more suitable for this participant. The remaining simulated curve matched closely to the measured spectrum, with most regions of discrepancy apparently inherited from the melanin minimisation procedure.

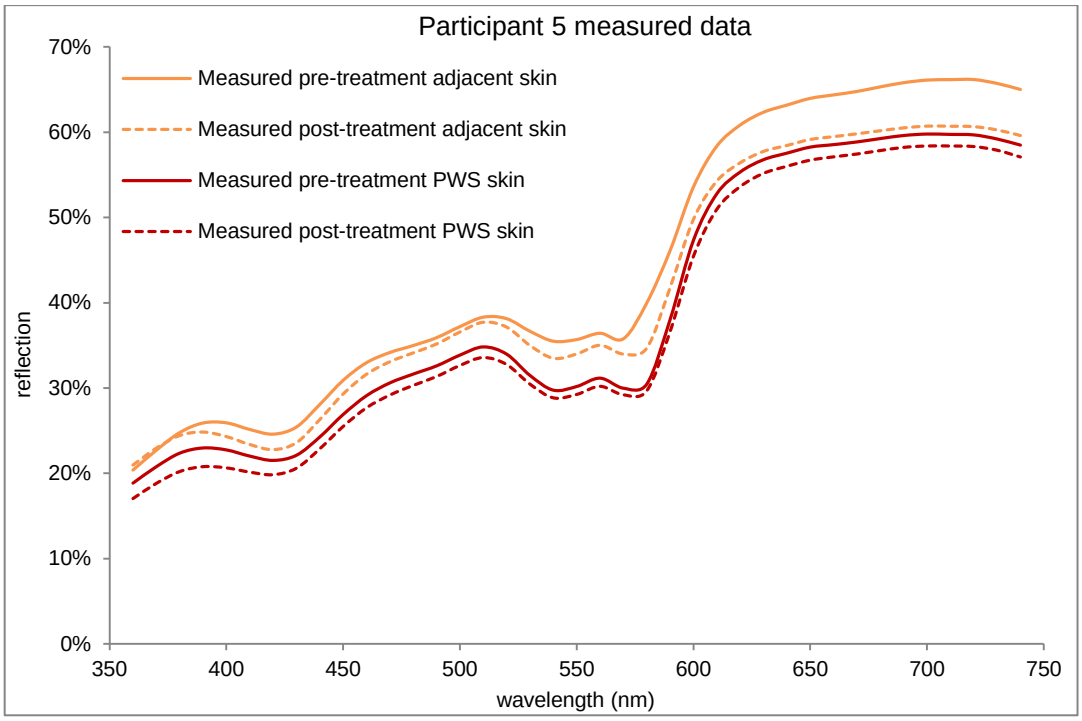

Figure 60: Colour measurement data of participant 5 taken before and after laser treatment.

Laser treatment was carried out using a radiant exposure of 14.5 Jcm^{-2} and a pulse length of 6 ms. Colour measurement data of adjacent skin shows a decrease in measured reflectance across the entire spectrum, in particular at wavelengths greater than 600 nm (Figure 59). This is likely to be as a result of increased pigmentation. The simulation predicts both an increase in melanin volume fraction from 0.4% to 0.8% and an increase in mean melanosome diameter, although the latter did not provide a good fit between measured and simulated spectra at shorter wavelengths.

PWS skin showed very similar characteristics throughout, with a slight reduction in measured reflection across the spectrum. The difference between PWS and adjacent skin colour was reduced overall, and in particular at wavelengths greater than 590 nm. This suggests that the laser treatment successfully reduced the colour of this participant's PWS lesion. The simulation attributed the small change in PWS skin colour to an increase in mean vessel depth and vessel number, suggesting that laser treatment successfully targeted superficial vessels.

Participant 6

Pre-treatment adjacent skin colour was reproduced with a mean difference of 1.5% reflection from the measured spectrum. The final skin model contained an epidermal melanin volume of 3.4% and a mean melanosome diameter of 269 nm.

The simulated spectrum demonstrated a greater degree of reflectance than the measured dataset in the region 520 nm to 580 nm, but less reflectance between 610 nm and 730 nm. It is unlikely that both of these discrepancies could be reduced with the current melanin minimisation procedure.

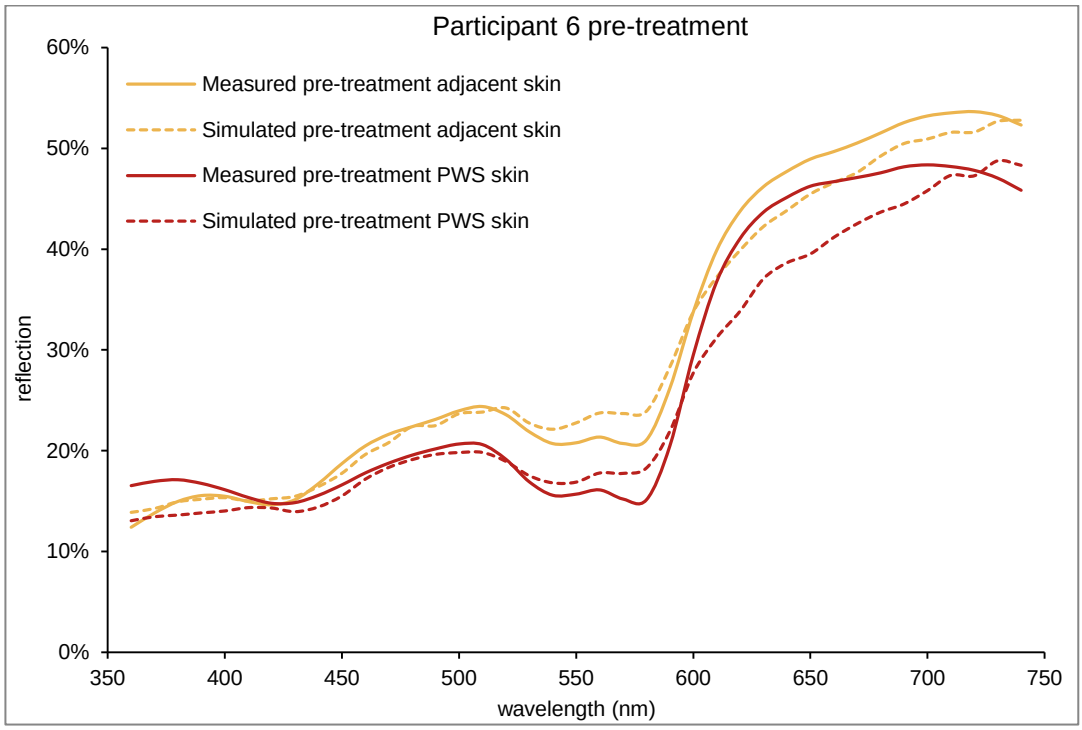

Figure 61: Pre-treatment measured and simulated spectral curves from participant 6.

Pre-treatment PWS skin was simulated with a mean difference from the measured dataset of 2.5% reflection after 15 iterations (8 days). The final pre-treatment PWS skin model contained 7 vessels of 60 µm diameter with a mean depth of 178 µm. The simulated spectrum demonstrated slightly greater reflectance than the measured data in the region 530 nm to 580 nm and less reflectance in the region 610 nm to 710 nm. In both regions, the discrepancies appear to have been inherited from the melanin minimisation procedure.

Post treatment adjacent skin was reproduced well over the majority of the spectrum with a mean deviation from the measured dataset of 2.5% reflection. This was produced using a skin model containing 2.0 % melanin and a mean melanosome diameter of 264 nm. Although there was a slight overestimate in the simulated reflection at wavelengths greater than 650 nm, the primary discrepancy between the two datasets was at the other end of the spectrum, below 400 nm. Although a

reduction in the mean melanosome diameter may have improved the fit at 360 nm, the difference between simulated and reflected curves between 400 nm and 450 nm would have increased. It is not likely that the current melanin minimisation procedure could have resulted in a close fit to the measured data below 400 nm. Again, it is of note that measured reflectance of this participant's PWS skin was greater than adjacent skin below 400 nm, although this was not reproduced by the simulation.

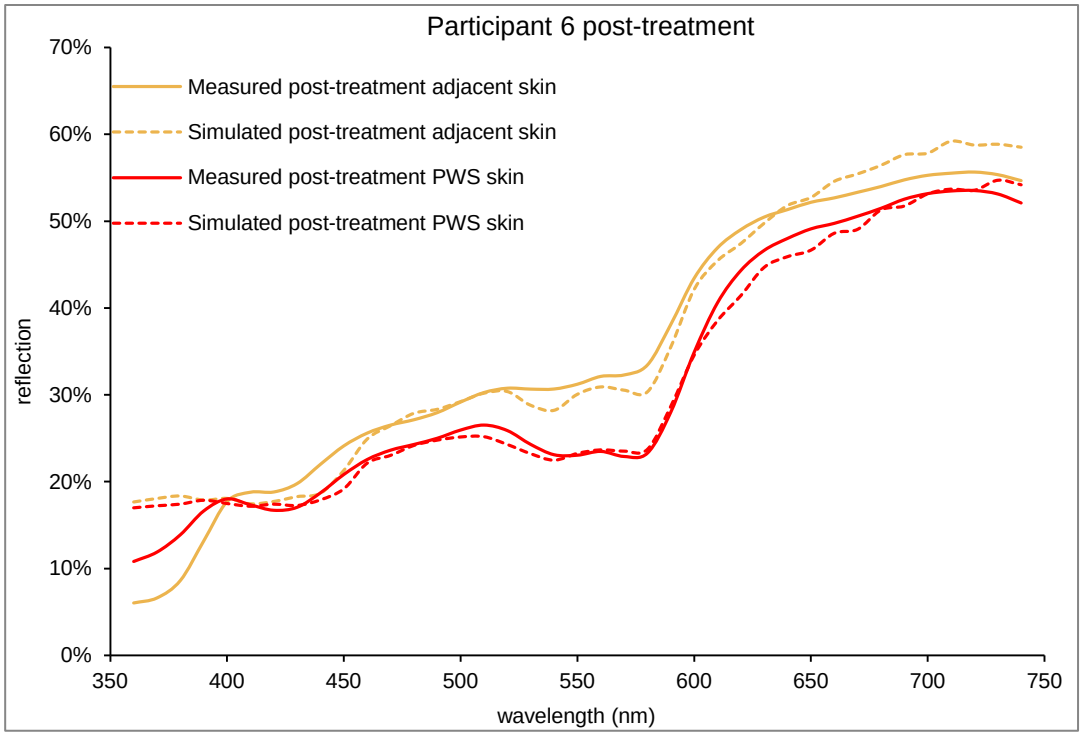

Figure 62: Post-treatment measured and simulated spectral curves from participant 6.

Post treatment PWS skin was reproduced with a mean deviation of 1.2% reflectance (6.5 days) using a skin model containing 5 vessels of 60 µm diameter and a mean depth of 224 µm. The simulated spectrum produced a close fit to the measured data over the majority of the spectrum, with the only region of notable discrepancy inherited from the melanin minimisation procedure below 400 nm.

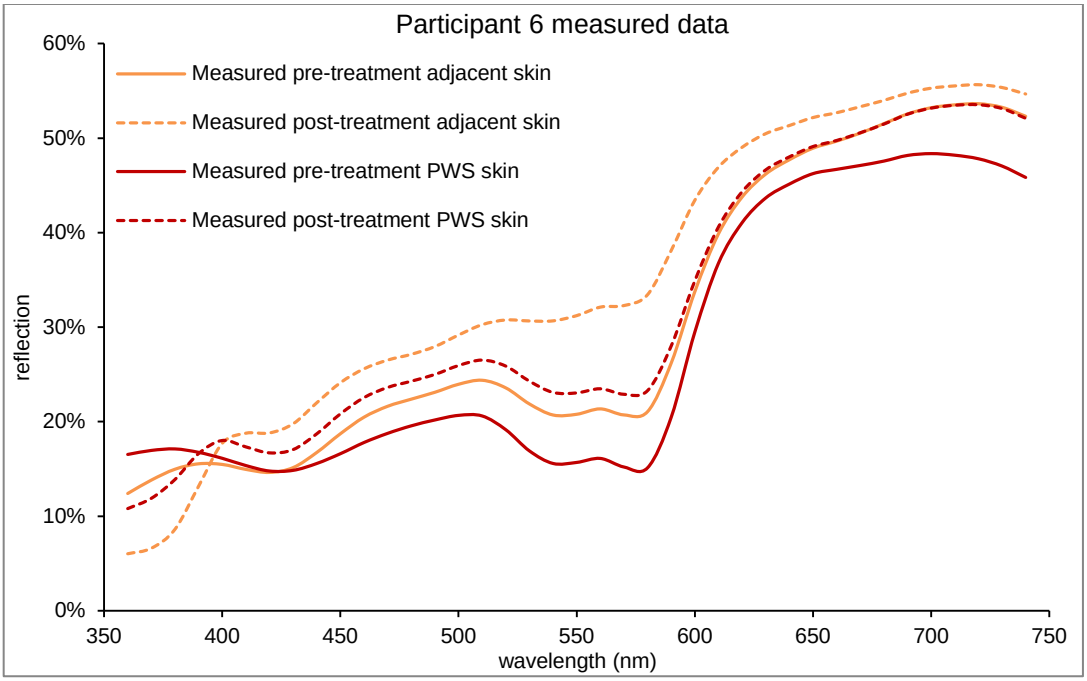

Figure 63: Colour measurement data of participant 6 taken before and after laser treatment.

Pulsed Dye Laser treatment was carried using 0.5 ms pulses with a radiant exposure of 10 Jcm^{-2}. Colour measurement data of adjacent skin shows a substantial reduction in the proportion of reflected light between sessions, the only exception to this being in the region below 400 nm. This was interpreted by the simulation as a decrease in melanin volume fraction from 3.4% to 2.0% with a negligible decrease in the mean melanosome diameter.

Measured PWS data shows a strong increase in reflection after treatment, except for in the region below 400 nm. The difference between adjacent and measured PWS skin was reduced at wavelengths greater than 620 nm but increased in the region 500-600 nm. The simulation predicted that these changes resulted from both a decrease in vessel number and an increase in the mean vessel depth, suggesting that laser treatment was successful at targeting the more superficial PWS vessels. Simulated vessel diameter remained unchanged. These combined results also suggest that the increase in measured contrast between adjacent and PWS skin in the region 500-600 nm was caused primarily by changes in epidermal melanin volume fraction.

Participant 7

Pre-treatment adjacent skin colour was reproduced with a mean difference of 1.8% reflection from the measured spectrum. The final skin model contained an epidermal

melanin volume of 1.9% and a mean melanosome diameter of 41 nm. The simulation produced a good overall match to the measured spectrum (Figure 65). There was a slight discrepancy in the region 450 nm to 600 nm, where simulated reflectance was greater than measured below 500 nm and less than measured above 500 nm. The match between measured and simulated datasets is not likely to be improved using the current melanin minimisation procedure.

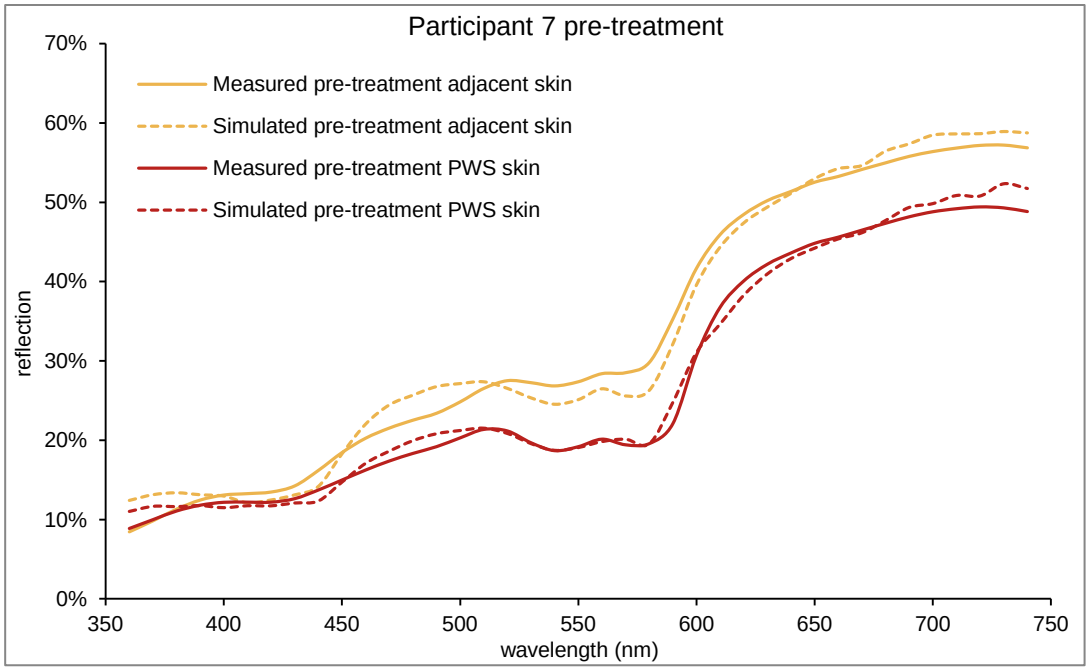

Figure 64: Pre-treatment measured and simulated spectral curves from participant 7.

Pre-treatment PWS skin was simulated with a mean difference from the measured dataset of 1.0% reflection (7 days) using a skin model containing 5 vessels of 90 µm diameter and with a mean depth of 225 µm. The fit between the measured and simulated spectra was close throughout, with the only noticeable discrepancies at the longest and shortest wavelengths considered, both of which appear to have been inherited from the melanin minimisation procedure.

Post-treatment adjacent skin colour was reproduced with a mean difference of 1.6% reflection from the measured spectrum from a skin model containing an epidermal melanin volume of 1.3% and a mean melanosome diameter of 41 nm. The simulation again produced a good overall match to the measured spectrum for post-treatment adjacent skin. The primary discrepancy was in the region 450 nm to 520 nm, where simulated reflectance was greater than measured. The match between measured and

simulated datasets cannot be improved for this single region without altering the fit in the remaining regions using the current melanin minimisation procedure.

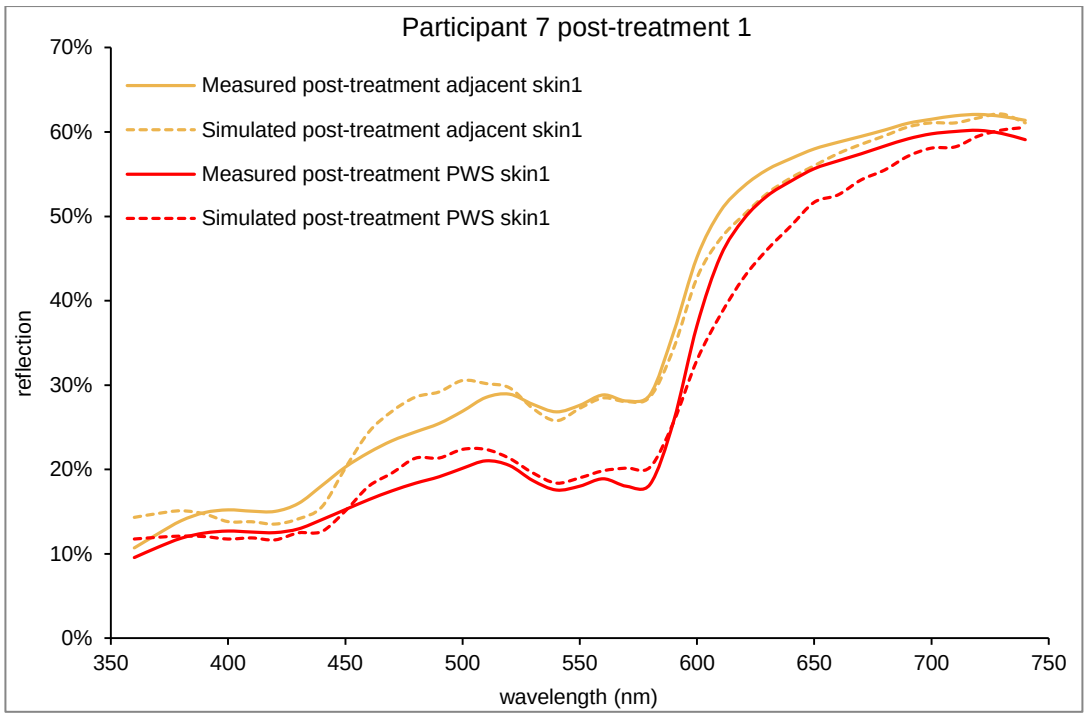

Figure 65: Post-treatment measured and simulated spectral curves from participant 7.

Post-treatment PWS skin was simulated with a mean difference from the measured dataset of 2.1% reflection after 15 iterations (5.5 days) using a skin model containing 4 vessels of 70 µm diameter and a mean depth of 245 µm. The simulated spectrum demonstrated slightly greater reflectance than the measured data in the region 460 nm to 510 nm, which appears to be inherited from the melanin minimisation procedure. The primary region of discrepancy was at wavelengths greater than 600 nm, where the simulation produced less reflection than measured. This appears to have been only partly inherited from the melanin minimisation procedure and, thus, it is likely that a skin model with slightly fewer or thinner vessels would have provided a closer fit in this region.

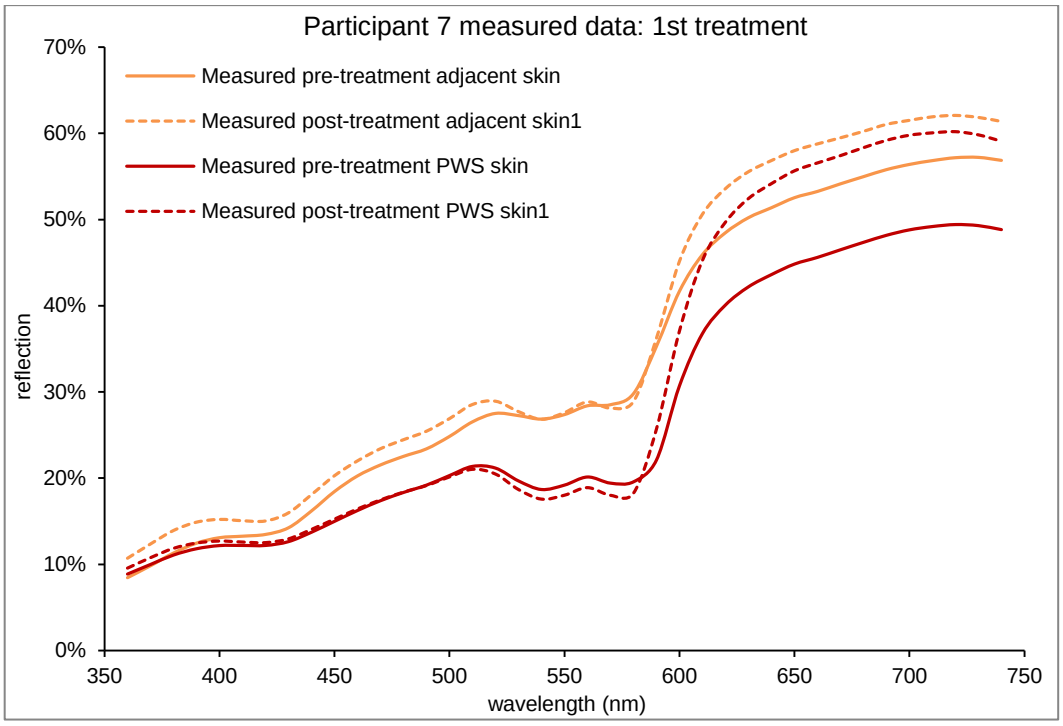

Figure 66: Colour measurement data of participant 1 taken before and after the first laser treatment for which assessments were carried out.

Laser treatment was carried using 0.5 ms pulses and a radiant exposure of 8.5 Jcm^{-2}. The measured adjacent skin data demonstrates an increase in reflectance between the first two measurement sessions in the region below 510 nm and at wavelengths greater than 590 nm (Figure 67). The simulation attributed this to a reduction in epidermal melanin concentration from 1.9% to 1.3%.

PWS skin colour showed very little change below 580 nm, but the proportion of reflected light increased considerably at wavelengths beyond 600 nm. The difference between measured reflectance in this region was reduced, indicating that the treatment was successful. The simulation attributed this to a reduction in both the number and diameter of PWS vessels.

A further session of laser treatment was carried using 0.5 ms pulses and a radiant exposure of 9.5 Jcm^{-2}.

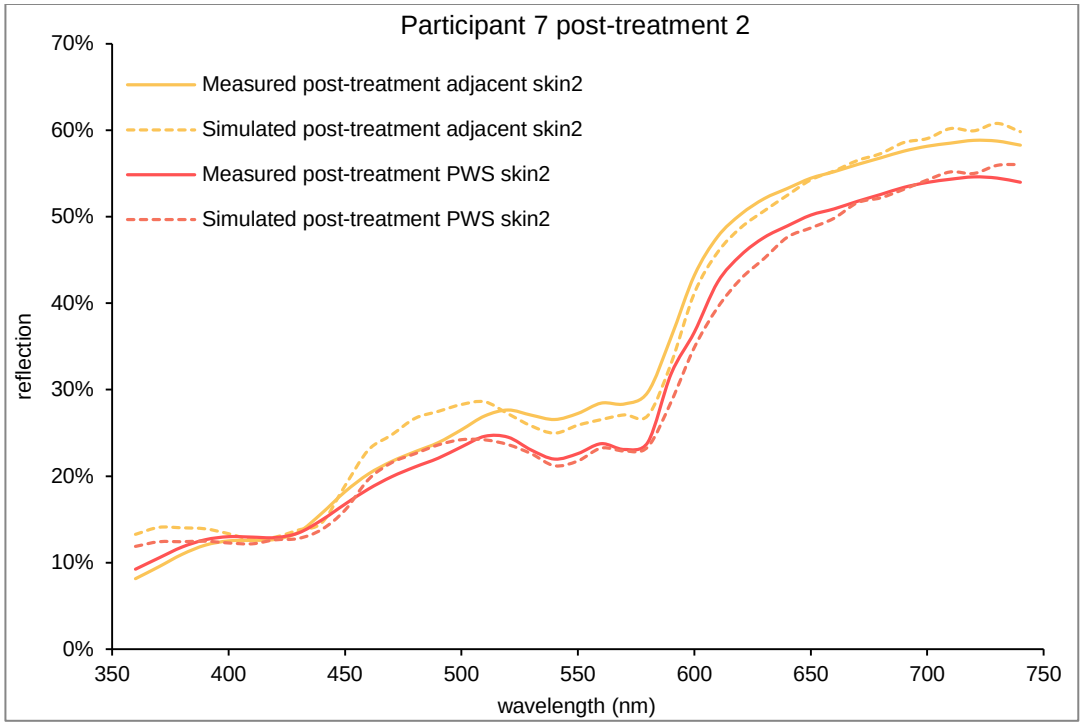

Figure 67: Measured and simulated spectral curves from participant 7 after the second treatment.

Adjacent skin colour after the second treatment was reproduced with a mean difference of 1.7% reflection from the measured spectrum. The final skin model contained an epidermal melanin volume of 1.7% and a mean melanosome diameter of 23 nm. The simulation produced a good overall match to the measured spectrum. The primary discrepancy was again in the region 450 nm to 520 nm, where simulated reflectance was greater than measured.

Simulated post-second-treatment PWS skin reproduced the measured data well, with a mean difference from the measured dataset of 1.1% reflection after 15 iterations (4.5 days) using a skin model containing 5 vessels of 70 µm diameter with a mean depth of 450 µm.

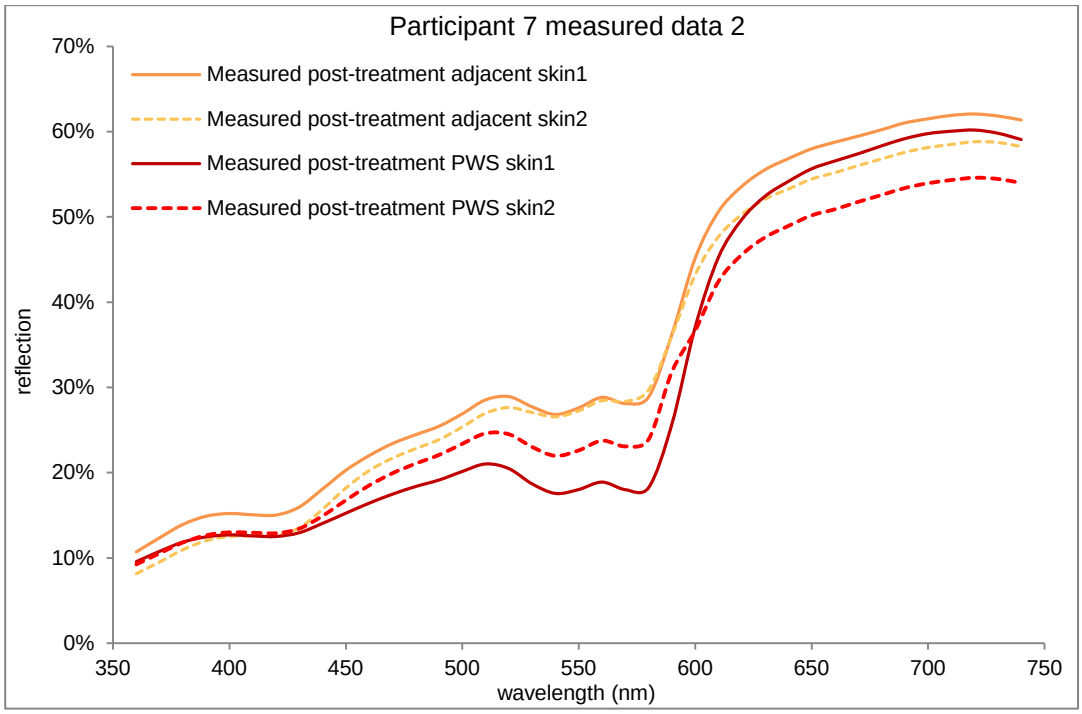

Figure 68: Colour measurement data of participant 7 taken before and after a second session of laser treatment.

The measured adjacent skin data (Figure 69) demonstrates a decrease in reflectance between measurement sessions in the region below 520 nm and at wavelengths greater than 590 nm. The simulation attributed this change to an increase in melanin content as well as a decrease in the mean melanosome diameter. PWS skin colour showed an increase in reflection below 600 nm and a decrease in reflectance at wavelengths greater than 600 nm. The difference between measured reflectance was reduced below 600 nm, but not at wavelengths greater than 600 nm. This indicates that the treatment was again successful. The simulation attributed this change to an increase in the mean vessel depth.

The results from this participant suggest different mechanisms for the reduction in apparent PWS colour for each treatment, despite employing similar laser settings on each occasion.

Participant 8

Pre-treatment adjacent skin colour was reproduced with a mean difference of 1.8% reflection from the measured spectrum. The final skin model contained an epidermal melanin volume of 1.4% and a mean melanosome diameter of 281 nm.

Agreement between simulated and measured reflectance was good throughout, with the primary region of discrepancy in the region 600 nm to 720 nm, where both

underestimation and overestimation of measured reflectance are present. A further region of underestimated reflection is noticeable at around 420 nm. These regions cannot be independently compensated for using the current minimisation procedure.

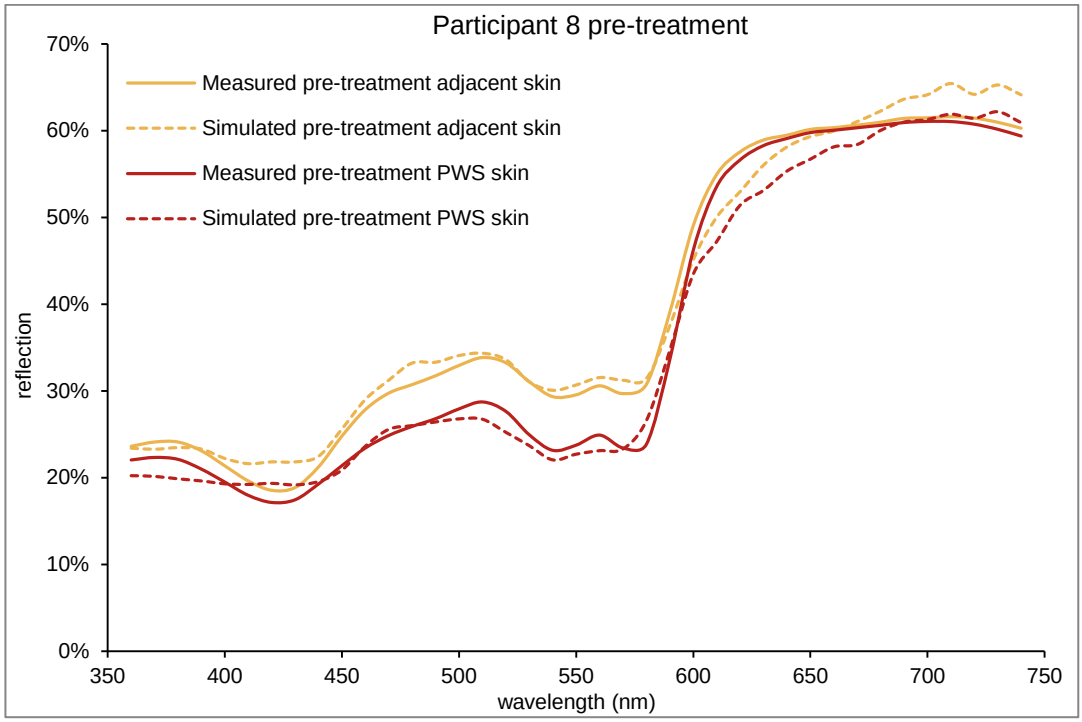

Figure 69: Pre-treatment measured and simulated spectral curves from participant 8.

Pre-treatment PWS skin was simulated with a mean difference from the measured dataset of 1.7% reflection after 15 iterations (8 days). The final pre-treatment PWS skin model contained 6 vessels of 20 µm diameter with a mean depth of 67 µm. The fit between simulated and measured reflectance was excellent in the region 450 to 600 nm. Between 600 nm and 700 nm, the simulated reflectance was less than the measured reflectance. This, as well as the overestimated reflectance at around 420 nm, appears to be inherited from the melanin minimisation procedure.

Post treatment adjacent skin was reproduced with a mean deviation from the measured spectrum of 2.1% reflection. This was produced using a skin model containing 1.2 % melanin and a mean melanosome diameter of 281 nm. The fit overall was poorer than that produced for pre-treatment skin, with a noticeable reduction in predicted reflectance, relative to measured data, in the region 500 nm to 650 nm.

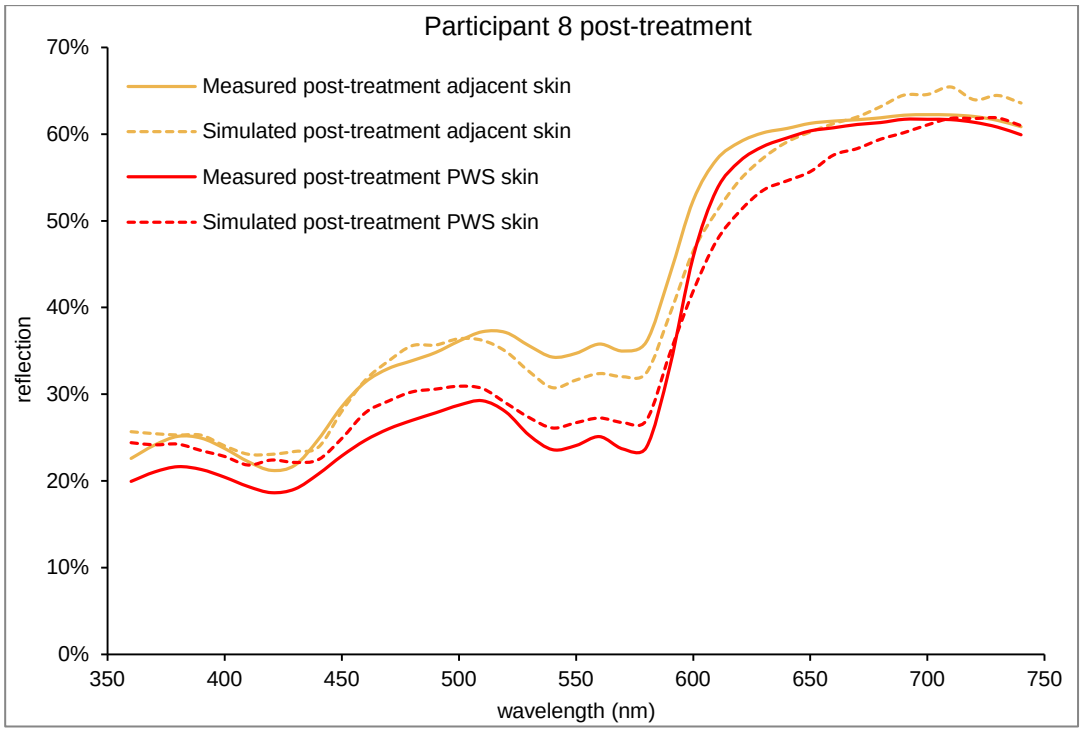

Figure 70: Post-treatment measured and simulated spectral curves from participant 8.

Post treatment PWS skin was reproduced with a mean deviation of 2.7% reflectance (6.5 days) using a skin model containing 4 vessels of 50 µm diameter and a mean depth of 215 µm. Simulated reflectance was greater than measured below 600 nm, suggesting that a reduction in the mean depth of vessels may have provided a better fit. The reduction in simulated reflection relative to measured values in the region 610 nm to 700 nm appears to be partly inherited from the melanin minimisation procedure but also suggest that the use of fewer or thinner vessels in the skin model could have improved the fit between measured and simulated data.

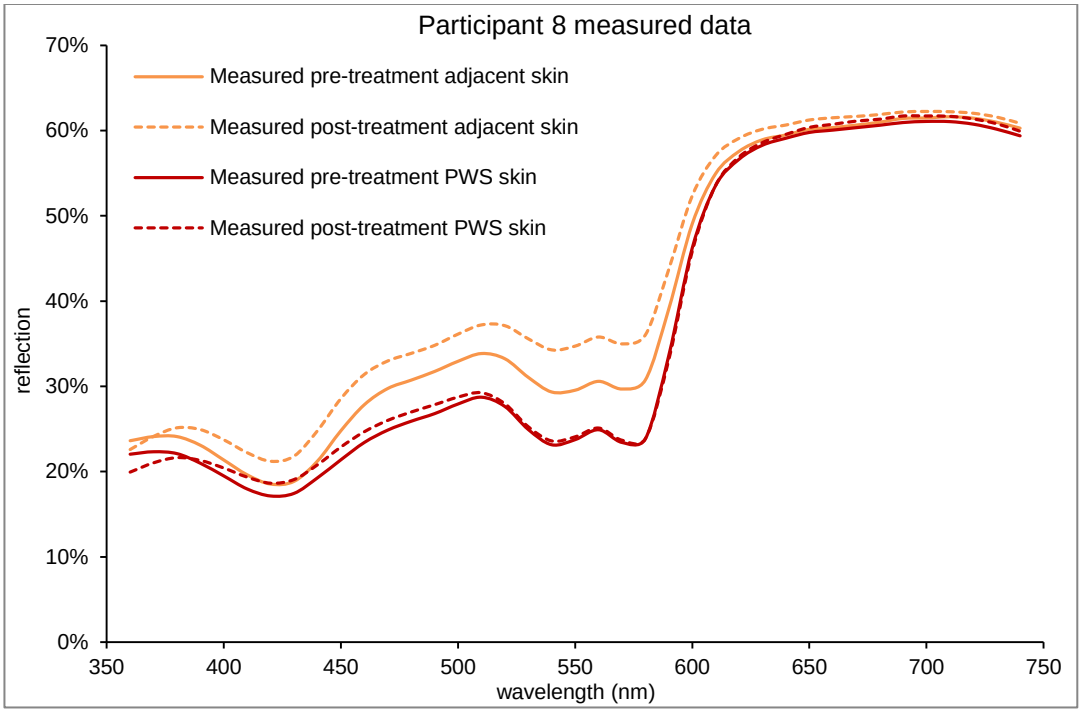

Figure 71: Colour measurement data of participant 8 taken before and after laser treatment.

Pulsed Dye Laser treatment was carried out using a radiant exposure of 14 Jcm^{-2} and a pulse length of 2 ms. The measured adjacent skin data (Figure 72) shows an increase in reflectance between measurement sessions over the majority of the spectrum, in particular across region 400 nm to 590 nm. PWS skin colour demonstrated very little change between sessions. The difference between PWS and adjacent skin was greater following treatment at wavelengths less than 690 nm.

The simulation predicted a decrease in melanin content, but no change in the mean melanosome diameter to account for the increase in reflection of adjacent skin between sessions. The simulation of post-treatment PWS skin used a model containing fewer vessels, although these were both wider and deeper, suggesting that laser treatment was successful in removing more superficial, thin vessels despite no apparent improvement in the contrast between PWS and adjacent skin colours.

Participant 9

Pre-treatment adjacent skin colour was reproduced with a mean difference of 2.2% reflection from the measured spectrum. The final model skin model contained an epidermal melanin volume fraction of 0.9% and a mean melanosome diameter of 331 nm.

Simulated reflection was greater than measured at wavelengths longer than 660 nm and at wavelengths shorter than 440 nm. The former region would have provided a closer fit if the epidermal melanin content had been lower, although this would have increased the difference between measured and simulated spectra in the middle wavelengths. Reducing the mean melanosome diameter would have improved the overall fit of the simulated spectrum and would have provided predicted melanosome diameters closer to what may be expected for a lighter skinned individual, such as this participant.

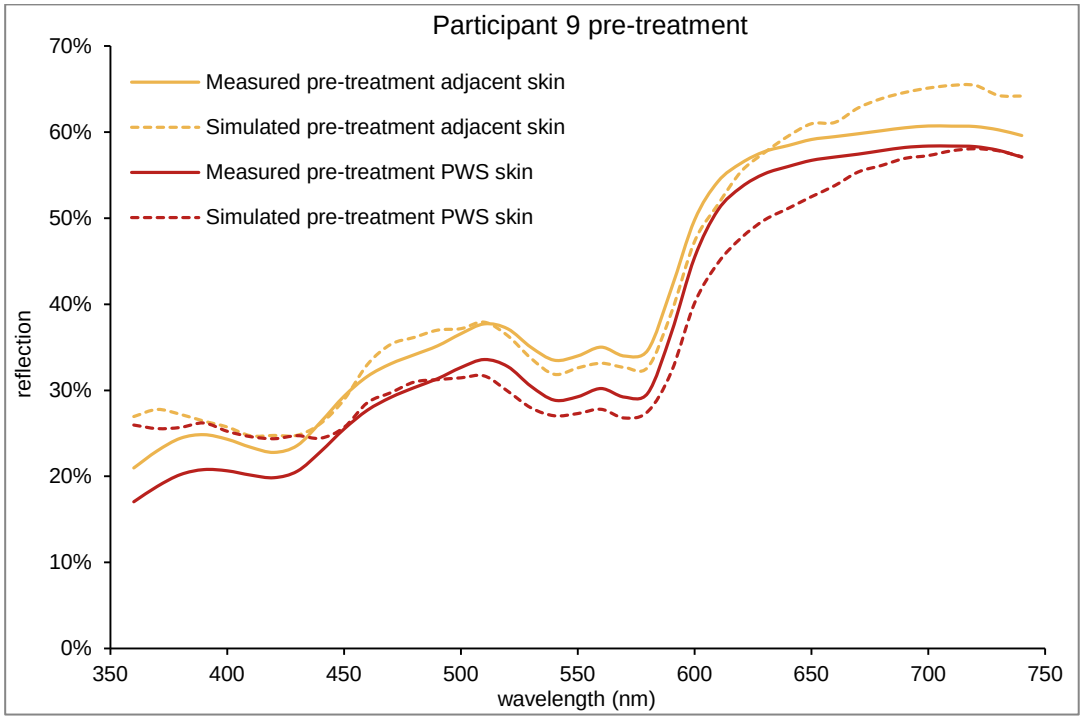

Figure 72: Pre-treatment measured and simulated spectral curves from participant 9.

Pre-treatment PWS skin was simulated with a mean difference from the measured dataset of 2.9% reflection after 15 iterations (7 days). The final pre-treatment PWS skin model contained 4 vessels of 60 µm diameter with a mean depth of 396 µm. The region of greatest discrepancy between measured and simulated curves was at wavelengths below 450 nm, where simulated PWS skin provided the same reflectance as simulated adjacent skin. Simulated reflection at wavelengths greater than 480 nm was consistently less than measured reflection, suggesting that a model containing deeper, fewer or thinner vessels would have provided a more accurate representation of the measured PWS region.

Post treatment adjacent skin was reproduced with a mean deviation from the measured dataset of 1.8% reflection. This was produced using a skin model

containing 1.2 % melanin and a mean melanosome diameter of 269 nm. These smaller melanosomes provided a closer fit than the pre-treatment spectrum below 450 nm. Again, simulated adjacent skin reflection was less than the measured skin values at wavelengths greater than 500 nm, suggesting that a slightly lower epidermal melanin volume fraction would have provided a closer fit.

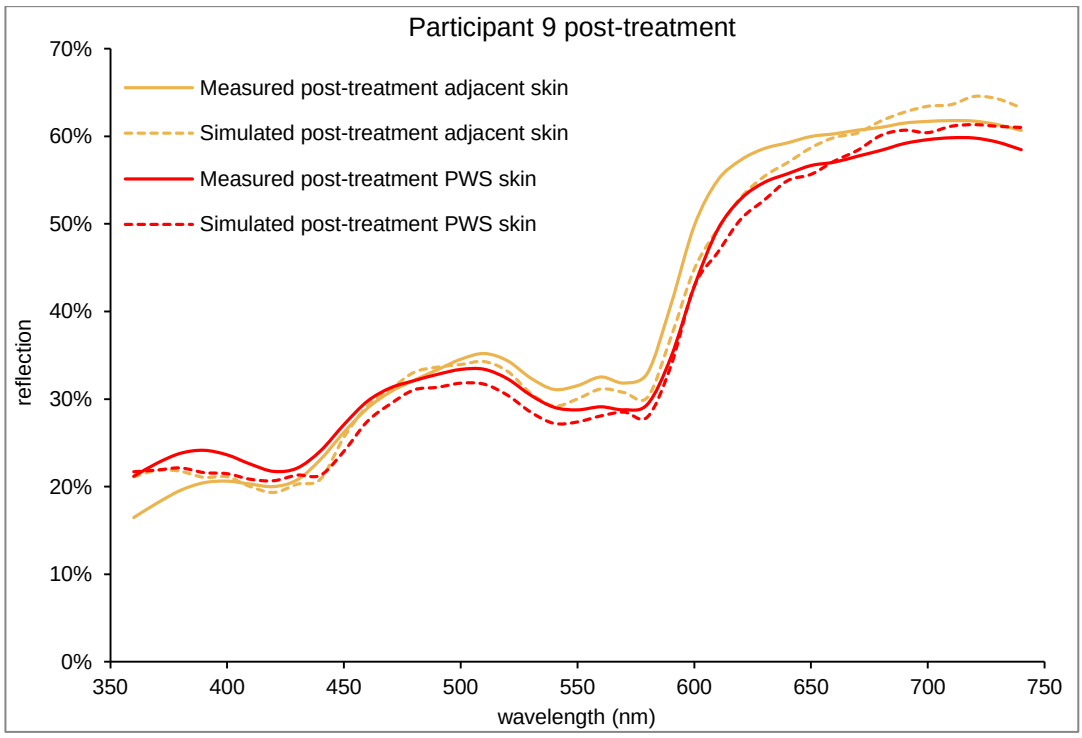

Figure 73: Post-treatment measured and simulated spectral curves from participant 9.

Post treatment PWS skin was reproduced closely over the entire spectrum, with a mean deviation of 1.5% reflectance (8 days) using a skin model containing 5 vessels of 50 µm diameter and a mean depth of 460 µm. Measured spectral reflectance was greater for the PWS region than for adjacent skin below 450 nm, and this was replicated in the simulation. Once again, measured PWS reflection was greater than adjacent skin below 450 nm.

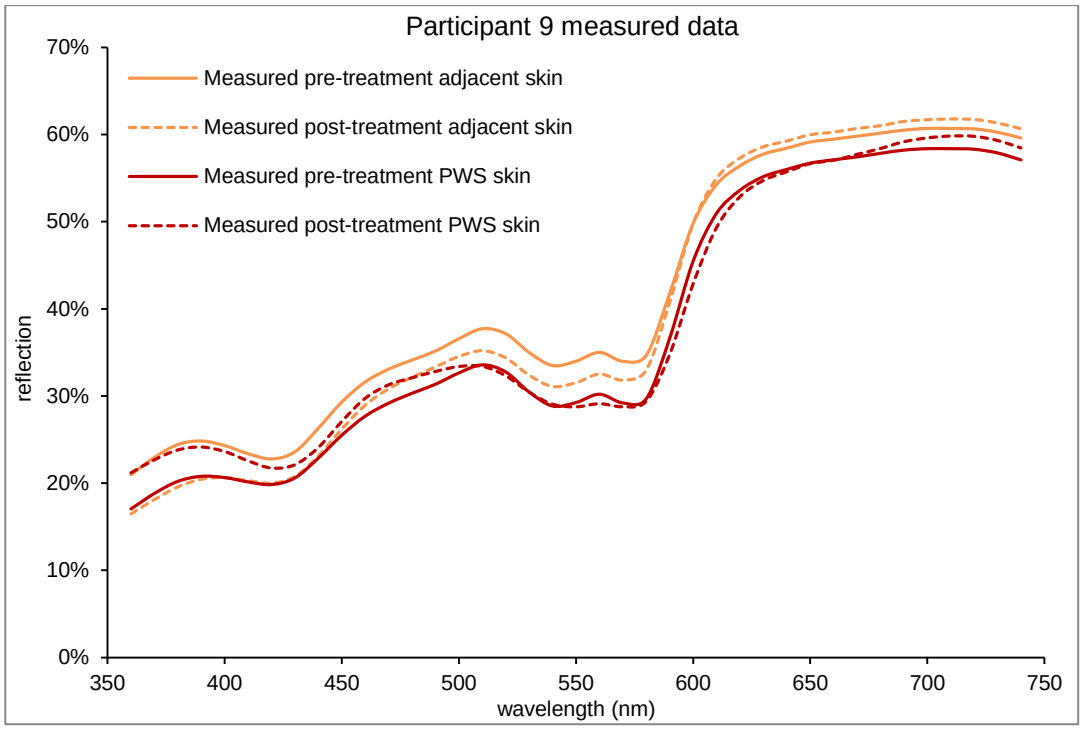

Figure 74: Colour measurement data of participant 9 taken before and after laser treatment.

Laser treatment was carried out using a radiant exposure of 17 Jcm^{-2} and a pulse length of 10 ms. Colour measurement data of adjacent skin shows a decrease in measured reflectance after treatment across the entire spectrum, in particular below 600 nm. The simulation predicted an increase in melanin from 0.9% to 1.2%, but a decrease in mean melanosome diameter. Due to the discrepancies between post-treatment adjacent simulated and measured spectra, the former result appears to be erroneous.

PWS skin showed similar characteristics before and after treatment at wavelengths greater than 600 nm, with an increase in relative reflection between PWS and adjacent skin at shorter wavelengths. The overall difference between PWS and adjacent skin was reduced following treatment. This was primarily attributed to an increase in the mean depth of PWS vessels by the simulation. The simulation also predicted a slight increase in vessel number and a reduction in mean PWS vessel diameter following laser treatment, suggesting that laser treatment successfully targeted larger, more superficial vessels.

Participant 10

Pre-treatment adjacent skin colour was reproduced well over the entire spectrum, with a mean difference of 1.5% reflection from the measured spectrum. This was produced from a skin model containing an epidermal melanin volume of 1.8% and a mean melanosome diameter of 384 nm.

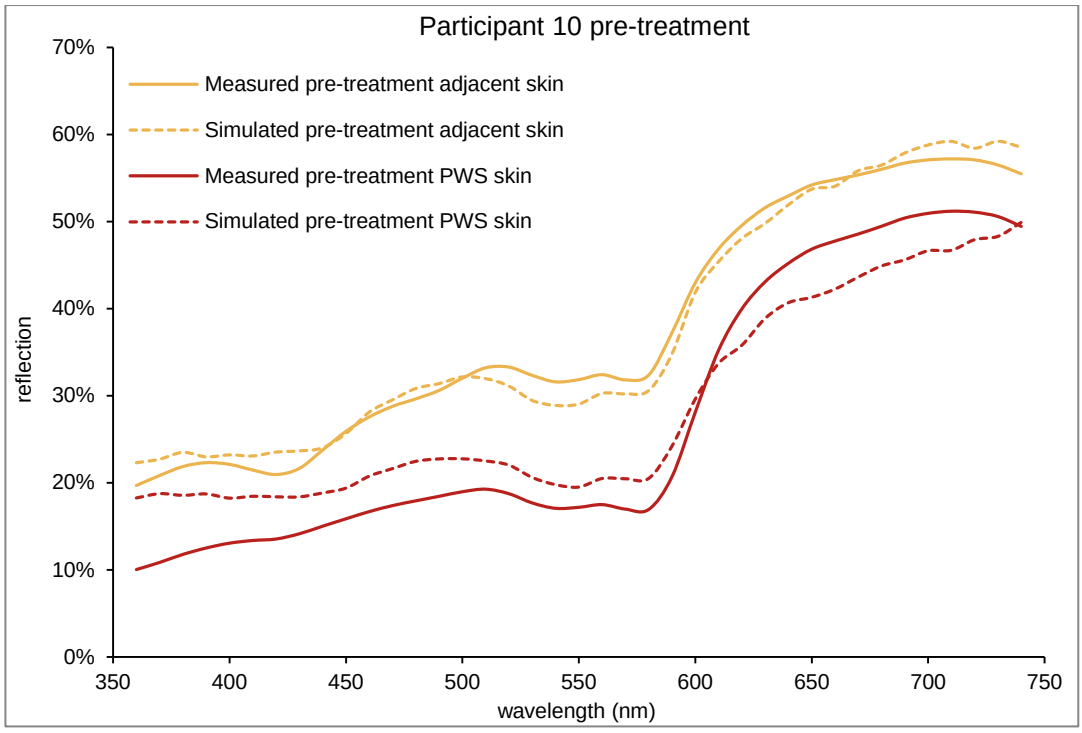

Figure 75: Pre-treatment measured and simulated spectral curves from participant 10.

Pre-treatment PWS skin was simulated with a mean difference from the measured dataset of 4.1% reflection (7.5 days). The final pre-treatment PWS skin model contained 6 vessels of 220 µm diameter with a mean depth of 246 µm. The simulated spectrum demonstrated greater reflectance than the measured values below 600 nm, with the discrepancy between the two spectra increasing at smaller wavelengths. It is likely than an increase in the mean depth of the vessels would have improved the fit in this region. At wavelengths greater than 600 nm, the simulated reflection was less than the measured data, suggesting that the use of fewer or smaller vessels in the skin model would have provided a better fit in this region. It is not certain, however, that these changes in the skin model's vessel architecture would have provided a close fit overall (particularly below 450 nm).

Post treatment adjacent skin was reproduced with a mean deviation from the measured dataset of 1.8% reflection. This was produced using a skin model containing 3.3 % melanin and a mean melanosome diameter of 244 nm. Again, adjacent skin colour was reproduced well by the simulation. The only notable discrepancies between the two curves were overestimates in the region 460 nm to 500 nm and near 360 nm. As a result, it is possible that the use of smaller melanosomes in the skin model would have marginally improved the fit overall. There was also an overestimate in the simulated reflection at 740 nm.

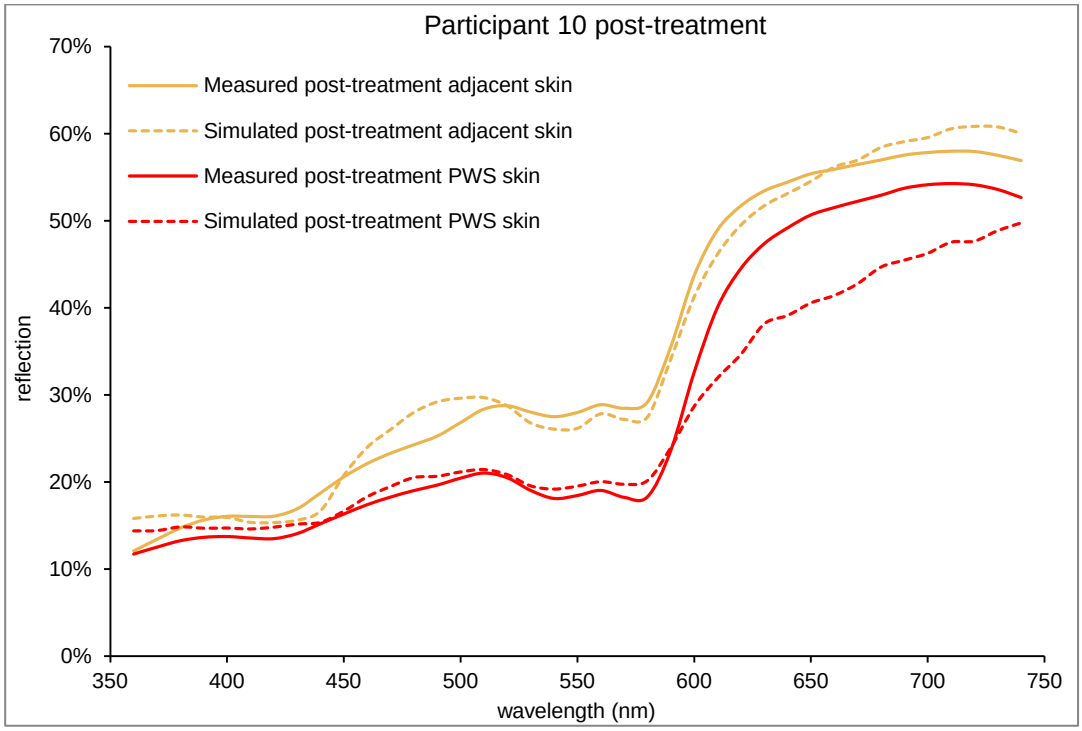

Figure 76: Post-treatment measured and simulated spectral curves from participant 10.

Post treatment PWS skin was reproduced with a mean deviation of 3.6% reflectance (11 days) using a skin model containing 9 vessels of 110 µm diameter and a mean depth of 294 µm. PWS skin was reproduced well below 600 nm. At wavelengths greater than 600 nm, where simulated reflectance was substantially lower than measured reflectance. This suggests that the use of fewer or smaller diameter vessels may have improved the fit between measured and simulated curves in this region, although such a change may have resulted in a poorer fit below 600 nm.

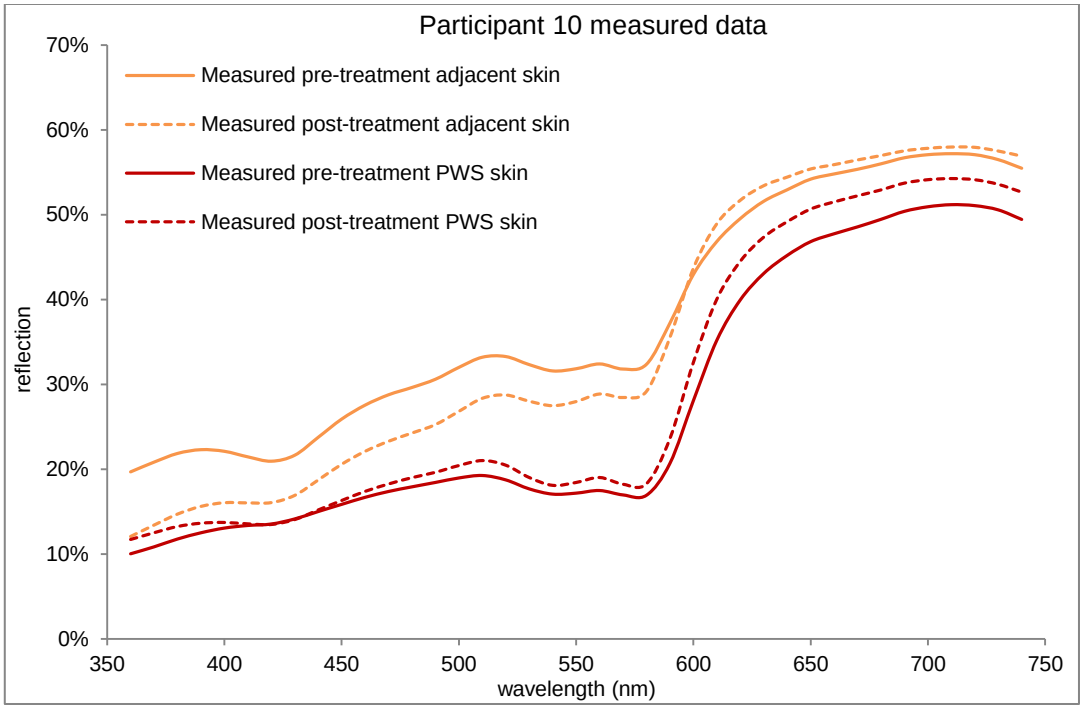

Figure 77: Colour measurement data of participant 10 taken before and after laser treatment.

A combined laser treatment was carried out for this participant, employing a 10 ms pulse of PDL (595 nm) at 10.5 Jcm^{-2} followed after a 0.5 s interval by a 15 ms pulse of Nd:YAG (1064 nm) at a radiant exposure of 70 Jcm^{-2}. Spectrophotometry measurements of adjacent skin show a reduction in the proportion of reflected light below 600 nm between sessions. The simulation attributed this change to an increase in melanin content from 1.8% to 3.3% although there was a reduction in the mean melanosome diameter, from 384 nm to 244 nm.

Although measured PWS skin colour did not change considerably between sessions, the difference between PWS and adjacent skin colour was reduced across the entire spectrum after treatment. The reduction in PWS skin colour was interpreted by the simulation as an increase in mean vessel depth and a reduction in the mean vessel diameter, suggesting that laser treatment targeted larger, more superficial vessels. Vessel number was predicted by the simulation to increase between sessions.

Summary

A total of 22 datasets were acquired across the 10 participants studied. The discrepancy between simulated and measured spectra was small throughout, only surpassing 5% reflection for one dataset (Table 6). The predicted melanin volume fractions are consistent with those expected for participants with pale, predominantly Northern European skin types, although for many of the participants, mean melanosome diameters were larger than expected for these skin types.

Table 6: Summary of the predicted melanin properties across the participant group.

p'pant no.	Age (years)	Pre-treatment			Post-treatment		
		% melanin volume fraction	mean melanosome diameter (nm)	Discrepancy (% reflection)	% melanin volume fraction	mean melanosome diameter (nm)	Discrepancy (% reflection)
1	37	1.5%	249	2.3%	1.7%	252	2.3%
2	68	3.3%	208	1.6%	3.3%	208	1.1%
3	13	2.2%	156	1.3%	0.7%	156	5.3%
4	38	1.3%	291	3.3%	1.4%	284	3.0%
5	3	0.4%	194	2.5%	0.8%	318	1.8%
6	29	2.4%	269	1.5%	2.0%	264	2.5%
7 (1)	7	1.9%	41	1.8%	1.3%	41	1.6%
7 (2)	7	1.3%	41	1.6%	1.7%	23	1.7%
8	7	1.4%	281	1.8%	1.2%	281	2.1%
9	19	0.9%	331	2.2%	1.2%	269	1.8%
10	69	1.8%	384	1.5%	3.3%	322	1.8%
mean	***29***	***1.7%***	***222***	***1.9%***	***1.7%***	***210***	***2.3%***

The primary region of discrepancy between simulated and measured adjacent skin colour was below 450 nm, where the majority of participants demonstrated a flatter curve than that produced by the simulation, therefore resulting in a simulated reflectance which was greater than the measured curve at 360 nm but less or equal in the region 400-450 nm. This is consistent with the apparent systematic overestimation of melanosome diameters. It is likely that the consideration of wavelengths below 400 nm only within the melanin minimisation procedure would have resulted in an improved fit between simulated and measured spectra and [predictions of smaller melanosome diameters for the majority of participants. It is also expected that the introduction of epidermal thickness or the proportionate distribution of melanin throughout the three epidermal layers of the skin model as parameters to be considered in the melanin minimisation procedure would increase the flexibility of the simulation, and improve the potential for matching simulated and measured spectra,

in particular towards the blue and of the visible spectrum where light scattering has greatest influence.

The discrepancy between measured and simulated PWS skin was marginally greater on average than for adjacent skin, in part due to the discrepancies inherited from the melanin minimisation procedure which could not be adequately compensated for within the PWS minimisation procedure. However, this discrepancy was decreased following the PWS minimisation procedure in some participants. Some compensation for discrepancies inherited from the melanin minimisation procedure was possible through the manipulation of PWS vessel parameters. These corrections are likely to have resulted in less accurate predictions of PWS vessel properties. Again, only one dataset showed a mean difference between measured and simulated spectra of greater than 5%.

The mean melanin properties predicted by the simulation did not vary considerably between first and second measurement sessions. This is consistent with the seasonal spread of data collection, for which there is no trend for more initial or follow up assessments carried out at any particular time of year for this participant group. There appeared to be a slight positive trend between particpant age and predicted epidermal melanin volume fraction (R^2=0.30) and mean melanosome diameter (R^2=0.23) which is consistent with studies published elsewhere [10, 257].

Overall, the predicted vessel number densities and diameters were within the range of expected values. Although mean vessel depths were largely within the expected range, the overall mean depth was less than would have been expected from previous biopsy studies (see page 19). This is likely to be a result of the low relative contribution of deeper PWS vessels to skin colour, as biopsy studies are likely to show PWS vessels which may not contribute to the measured colour of skin due to their depth within the skin or the presence of overlying vessels.

Table 7: Summary of the predicted PWS parameters.

p'pant no.	age (yrs.)	Pre-treatment				Post-treatment			
		no. of vessels	vessel diameter (μm)	vessel depth (μm)	Discrepancy (% reflection)	no. of vessels	vessel diameter (μm)	vessel depth (μm)	Discrepancy (% reflection)
1	37	18	180	262	5.2%	8	100	215	1.7%
2	68	6	160	250	1.9%	7	140	264	1.8%
3	13	4	10	218	2.3%	4	10	218	3.8%
4	38	17	100	194	2.6%	7	100	189	2.5%
5	3	7	40	222	2.2%	13	40	358	2.2%
6	29	7	60	178	2.5%	5	60	224	1.2%
7 (1)	7	5	90	225	1.0%	4	70	245	2.1%
7 (2)	7	4	70	245	2.1%	5	70	451	1.1%
8	7	6	20	67	1.7%	4	50	215	2.7%
9	19	4	60	396	2.9%	5	50	460	1.5%
10	69	6	220	246	4.1%	9	110	264	3.6%
mean	***29***	***8***	***92***	***228***	***2.6%***	***6***	***73***	***282***	***2.2%***

The predicted mean vessel number and diameter were reduced following treatment for this participant group, whilst the predicted mean vessel depth increased. These results suggest that laser treatment was more effective on superficial and larger PWS vessels for this participant group. This is consistent with experimental findings published elsewhere [258, 259].

7.2 Participants Assessed by OCT

Five participants were assessed by OCT. Room temperatures remained consistent at 22.5°C (±1 °C) across the assessments made.

Whilst analysing OCT data, it was found that determining the total vessel number was non-trivial, as some vessels may have been visible in each slice assessed (and therefore counted many times) whereas other may have been present in only one or two slices, depending on the orientation of the vessels relative to the imaging geometry. Furthermore, some vessels were found to divide and others weave in and out of the imaging 'slice'. Thus, the results presented represent an estimate of relative vessel number, rather than a measurement of the absolute number of vessels within the volume. Future study into this area may benefit from an automated system capable of identifying and tracing individual vessels within an OCT dataset as, to date, it appears that no such system has been completed [91].

Participant 1

As described in Section 7.1, a single region of PWS skin was analysed by both OCT and spectrophotometry for this participant prior to treatment. The simulation reproduced adjacent skin colour with a mean difference of 2.3% reflection after 10 iterations of the melanin minimisation procedure using a skin model containing 1.5% epidermal melanin and a mean melanosome diameter of 249 nm. PWS skin colour was reproduced with a mean difference of 4.5% reflection after 12 iterations, using a skin model containing 18 vessels of 180 µm diameter and a mean depth of 262 µm. It was suggested in the previous section that further iterations may have resulted in a closer agreement between measured and simulated reflectance providing that the simulated vessels were more superficial, fewer or with a smaller diameter.

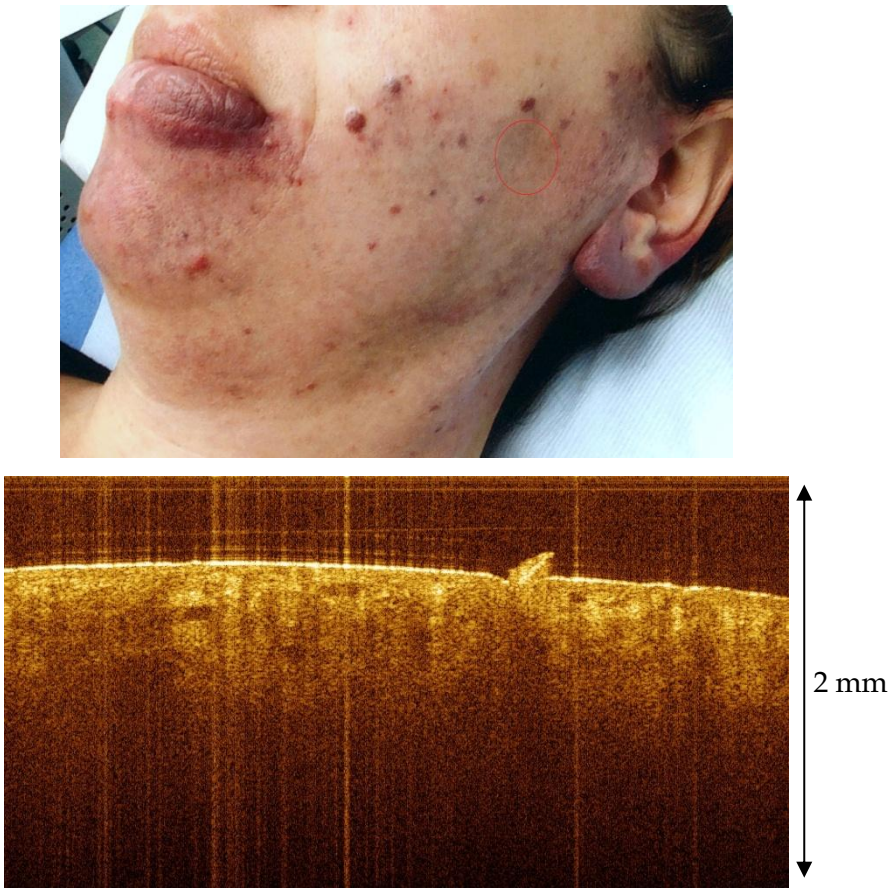

Figure 78: Photograph showing region analysed (top) and 4 mm wide OCT image of participant 1. Dimnesions are approximate.

A single 4 mm x 4 mm square region was imaged using the Thorlabs OCT system. A mean of 8.7 vessels was identified per slice. The mean diameter of these vessels was 70 µm and the mean depth was 300 µm. The contrast between PWS blood vessel lumina and adjacent skin tissue in the images was poor for this device (Figure 79), making it difficult to ensure that all vessels were identified and determine accurately the boundaries of each vessel (thus compromising the accuracy of vessel number estimates and diameter measurements). In general, very little tissue structure was visible below a depth of 500 µm from the skin surface using the Thorlabs device.

The PWS vessel number density predicted by the Monte Carlo programme was greater than that determined by OCT. This result, along with analysis of the simulated spectrum, suggests that the vessel number for participant 1 was overestimated by the Monte Carlo simulation. It is likely that further iterations of the blood vessel minimisation procedure would have resulted in either a reduction in vessel number, vessel diameter or both. This would have improved the agreement between OCT findings and, it appears, the accuracy of the prediction made by the

simulation. The mean vessel depth predicted by the simulation was less than that determined by OCT analysis. This difference would most likely have been greater if further iterations of the blood vessel minimisation procedure had been performed.

Participant 11

A single 4 mm x 4 mm square region of skin was imaged using the Thorlabs OCT system. A mean of 6.4 vessels was identified per slice, with a mean diameter of 97 µm and a mean depth of 240 µm.

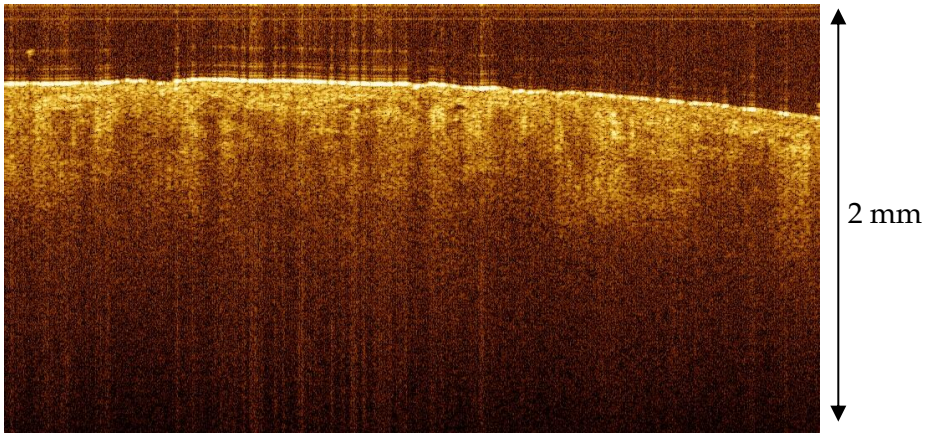

Figure 79: OCT image of participant 11 taken using the Thorlabs OCT system. Imaged region is 4 mm wide and 2 mm deep. Dimensions are approximate.

The simulation produced a close fit to the colour measurement of adjacent skin after 10 iterations of the melanin minimisation procedure, with a mean difference of 1.2% reflection per data point. The only noticeable region of discrepancy between the two curves was an underestimate in the regions 380-450 nm (Figure 81). The final skin model contained 1.9% epidermal melanin with a mean melanosome diameter of 150 nm. These values are within the expected range for this participant's skin type and the anatomical location of the measured area of skin.

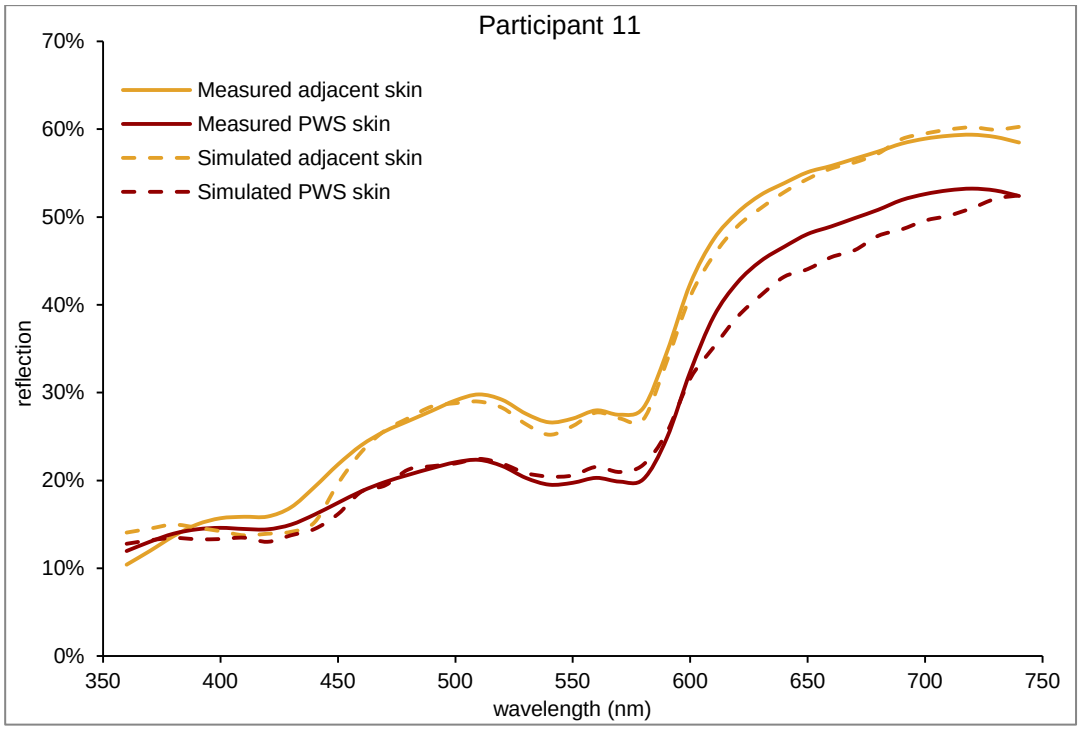

Figure 80: Simulation results for participant 11.

The simulation of PWS skin colour also demonstrated a close fit to the measured spectrum after 12 iterations of the blood vessel minimisation procedure (5.5 days), with a mean deviation per data point of 1.5% reflection. This spectrum was produced with a skin model containing 10 vessels of 80 µm diameter at a mean depth of 260 µm.

Analysing the spectrum in detail, it is likely that the suggested increase in melanosome diameter would have slightly improved the fit between the two curves below 450 nm, although again this would cause the difference between measured and simulated reflection to be greater below 380 nm. A decrease in vessel number or diameter would have improved the fit in the region of greatest discrepancy, at wavelengths greater than 620 nm, although either would have resulted in a poorer fit between 520 and 590 nm. Thus, it is possible that further iterations of the blood vessel minimisation procedure may have been able to reduce the mean difference in reflection per data point between the simulated and measured curves, although it is unlikely that the current minimisation procedure could have substantially improved the fit to the measured spectrum.

The number of vessels per 4 mm^2 region of skin predicted by the simulation was greater than that determined by OCT. However, the ratio of vessel number determined by OCT to that predicted by the simulation was higher for this participant

(0.64) than for participant 1 (0.48). These results suggest that the simulation overestimated the number of blood vessels (although by a smaller degree than for participant 1). Care must be taken in making this comparison due to the difference in volumes considered and the difficulties in accurately determining an absolute number of vessels by OCT analysis. It can, however, be concluded that both the diameters and the mean depth of PWS vessels predicted by the simulation for this participant are close to those determined by OCT analysis.

Participant 12

OCT data was acquired using the VivoSight system over two regions of the participant's PWS skin, each covering an area of 1x1 mm. The contrast between PWS vessels and surrounding skin tissue using the VivoSight was subjectively superior to the Thorlabs device, although the acquisition time was considerably longer, reducing the area of skin which could reasonably be imaged. In general, very little tissue structure was visible beyond a depth of 500 µm for this device (Figure 82).

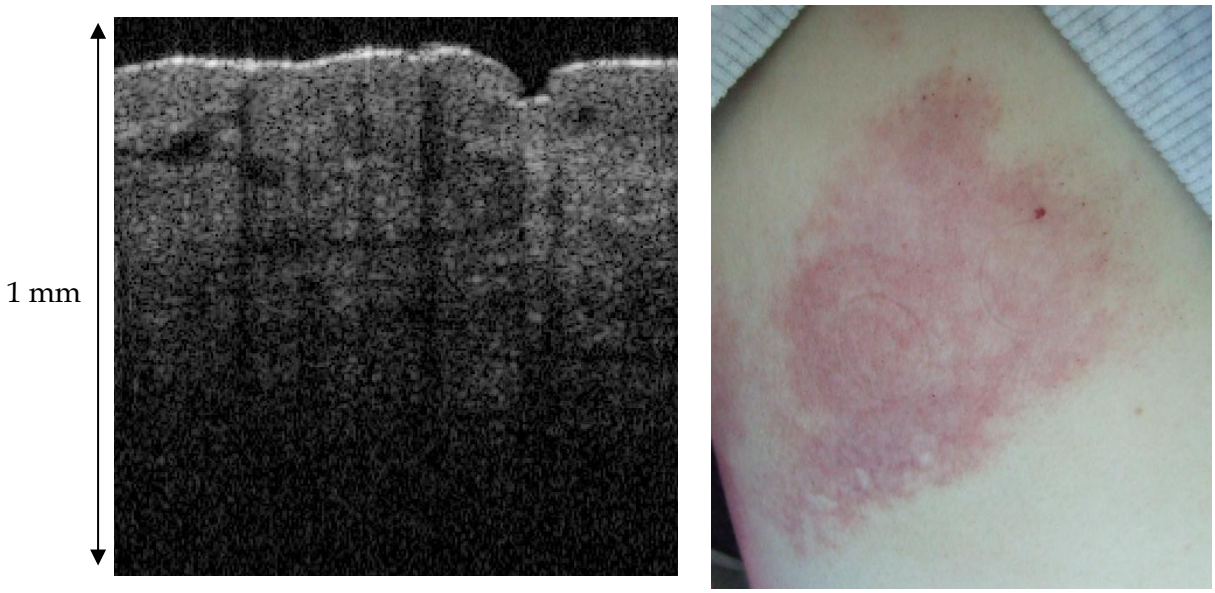

Figure 81: Left: OCT image of participant 12 showing vessels in both transverse and axial section. Image shows a 1mm x 1mm square volume of PWS skin. Right: Photograph of PWS skin showing temporary indentations in the two regions analysed. Dimensions are approximate.

Images were analysed every 50 µm through the volume. The mean depth of vessels identified was 240 µm in both regions imaged, whilst the mean diameters from each section were similar at 43 µm within the first volume and 41 µm in the second (total mean, 42 µm). The mean number of vessels per image was approximately 2.0 in the

first volume and 2.6 in the second (total mean, 2.3). It is assumed that 4 mm wide images, as obtained for the participants 1 and 11, would have resulted in a mean of four times as many (9.2) vessels identified per slice. This value is greater than either of the two previous participants, despite the apparently paler and less thick PWS skin determined by visual analysis (Figure 82, right).

Spectral measurements showed that the first volume of PWS skin assessed was paler than the second volume (Figure 83), which is consistent with the lower number of vessels identified by OCT. The Monte Carlo simulation of adjacent (clinically normal) skin reproduced the measured spectrum with a mean absolute deviation of 1.5% reflection. The final skin model contained an epidermal melanin volume fraction of 1.4%, with a mean melanosome diameter of 66 nm. The low epidermal melanin volume and small melanosome diameters predicted by the simulation is indicative of pale skin, which is apparent from the photograph of this participant (Figure 82). The region of largest discrepancy between simulated and measured adjacent skin reflectance was at wavelengths less than 500 nm, where simulated values were higher (450-500 nm) and lower (390-500 nm) than measured values. The remaining spectrum produced a very close fit to the measured spectrum, and it is not likely that further iterations of the current procedure would have resulted in an improvement overall.

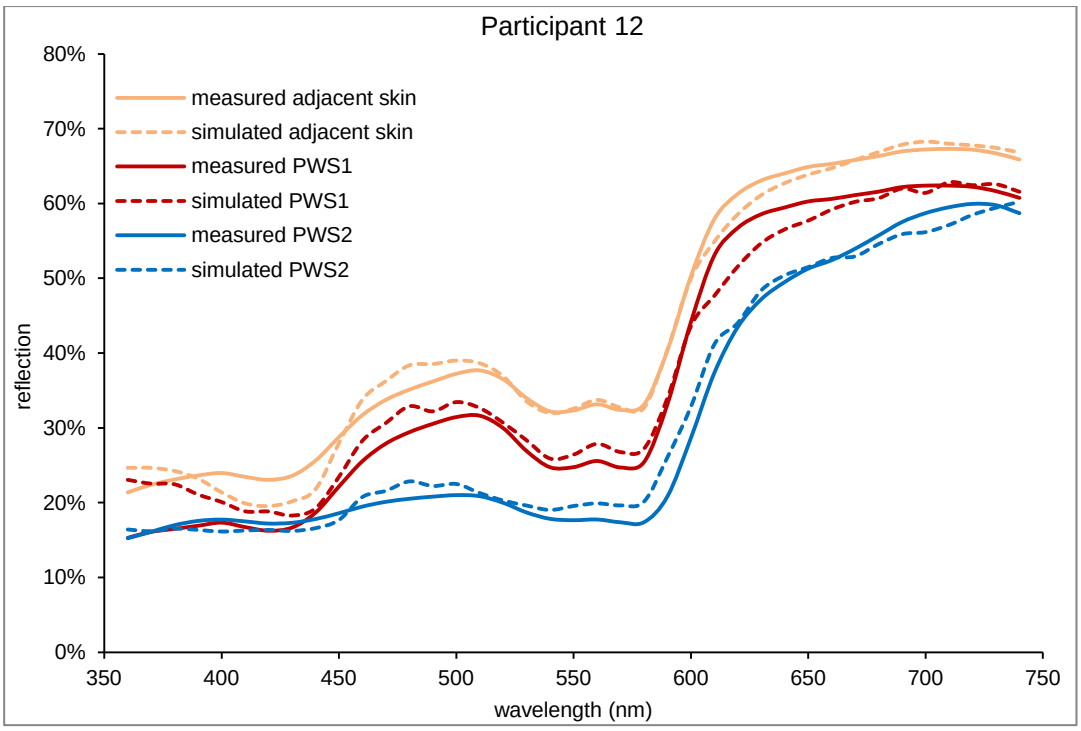

Figure 82: Simulation results for participant 12.

The first region of PWS skin was reproduced with a mean deviation of 2.3% reflectance between measured and simulated data points after 15 iterations of the blood vessel procedure (10.5 days). The final skin model contained 8 vessels of 40 µm diameter and a mean depth of 175 µm. The simulated spectrum at wavelengths less than 600 nm showed slightly greater reflectance than the measured spectrum, suggesting a more superficial mean vessel depth may have produced a closer fit. The remaining simulated spectrum, above 450 nm, was closely matched to the measured data, although a reduced amount of reflection in the region 610-670 nm was mirrored from the adjacent skin model.

The vessel number density and mean vessel diameter predicted by the simulation matched closely to those determined through OCT analysis. The predicted mean vessel depth was much less however.

Spectral reflectance from the second region of PWS skin was reproduced with a mean deviation of 1.5% reflectance between measured and simulated data points after another 15 iterations of the blood vessel procedure (19.5 days). This spectrum was produced from a skin model containing 10 vessels of 40 µm diameter and a mean depth of 155 µm. Overall, the simulated and measured spectra were closely matched, although a slight decrease in mean vessel depth may again have improved the fit in the region below 600 nm if accompanied by a slight reduction in vessel number or diameter to maintain the fit at wavelengths greater than 600 nm.

Relative to the first PWS region assessed for this participant, the simulation predicted that blood vessels in the second region were of the same diameter but were more numerous and closer to the surface on average. Although the OCT analysis also demonstrated a greater number of vessels, it did not show that these were closer to the surface on average. Compared to the OCT analysis of region 2, vessel diameter again showed very close agreement and mean vessel depth was much less. The ratio of vessel number density predicted by the simulation to that determined by OCT (0.96) was greater than either of the participants imaged using the Thorlabs device (0.64 and 0.48 respectively), but close to that for region 1 (1.0). Again, this discrepancy may be a result of the difference in sensitivity between the two OCT devices but suggests that the use of 3 more iterations of the PWS vessel minimisation procedure (compared to

participants 1 and 11) was successful in improving the accuracy of the predictions made.

Participant 13

One area of PWS skin was imaged twice using the VivoSight OCT system. The first image acquisition covered an area of 1x1 mm and the second acquisition covered 2x2 mm with the probe repositioned in the same place.

The first acquisition demonstrated a mean of 3.8 vessels per slice, with a mean depth of 280 µm and a mean diameter of 81 µm. The second acquisition contained images of the same resolution, but spanning double the area. Furthermore, the same number of images were taken for each acquisition, meaning that the distance between each slice doubled (to 100 µm) in the second acquisition. In the second acquisition, twice as many vessels were identified per slice (a mean of 7.7), with a mean depth of 280 µm and a slightly larger mean diameter of 91 µm.

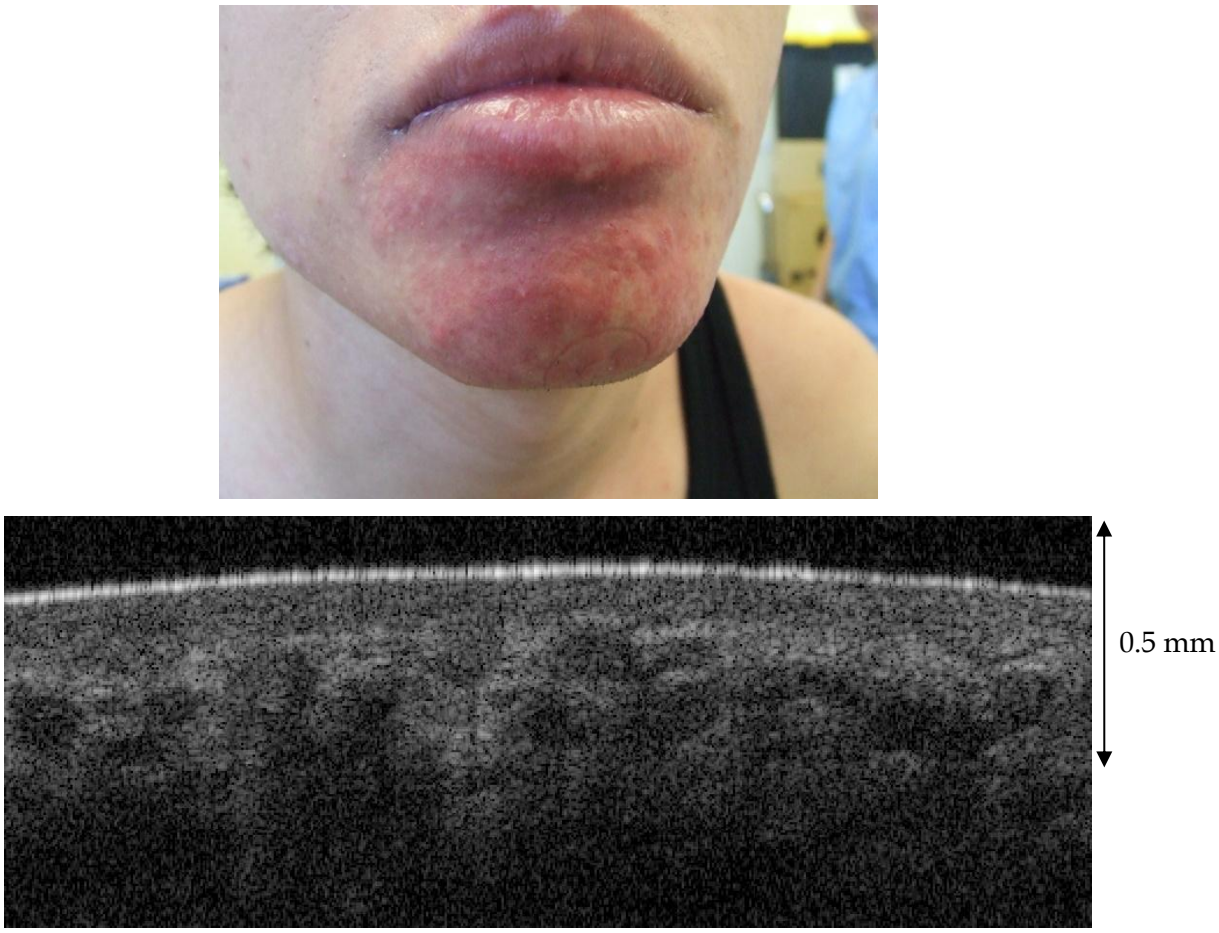

Figure 83: Photograph and 2 mm wide OCT image (bottom) of participant 13. Dimensions are approximate.

The Monte Carlo simulation produced a close reproduction of adjacent skin colour after 10 iterations, having a mean absolute difference of 1.1% reflection. The only notable region of discrepancy was in the region from 670 nm to 740 nm, where the simulated data points were consistently greater than the measured points (Figure 85). The final adjacent skin model contained 1.9% epidermal melanin, which is considered realistic for this participant's skin type and the anatomical location (Figure 84). The mean melanosome diameter of 274 nm is larger than expected for this participant's skin type.

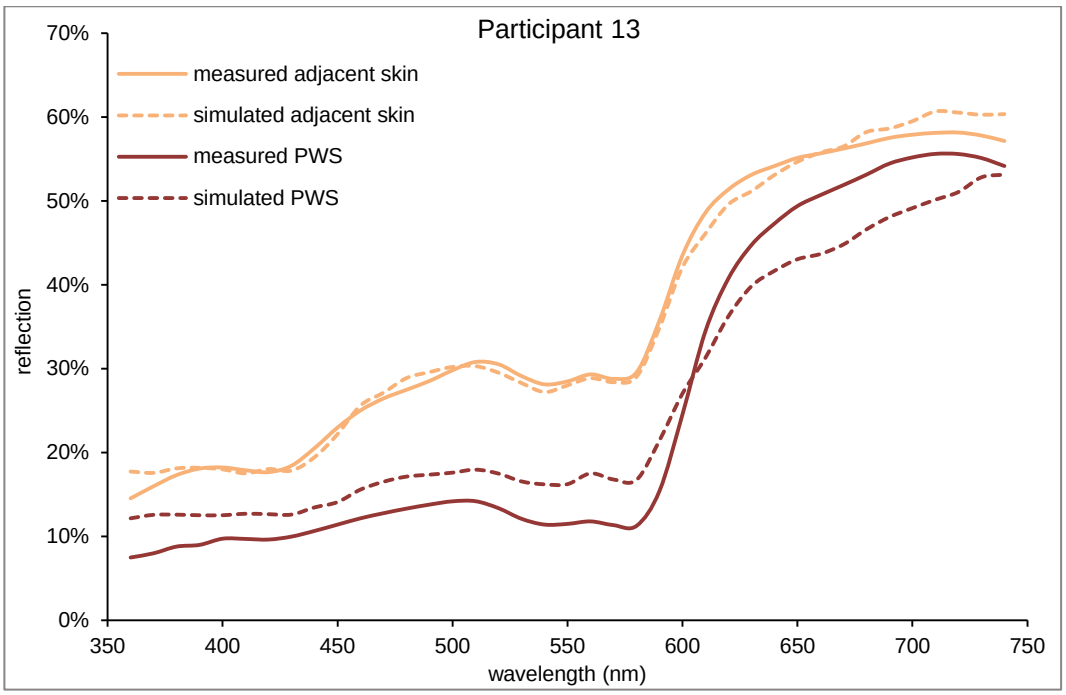

Figure 84: Simulation results for participant 13.

PWS skin colour was reproduced with a mean difference of 4.3% reflection after 15 iterations (10.5 days). The final PWS skin model contained 14 vessels of 80 µm diameter and a mean depth of 180 µm. The simulated reflection was greater at wavelengths less than 600 nm, suggesting that a skin model containing more superficial vessels would have provided a closer fit between simulated and measured curves. The simulated reflection was less at wavelengths greater than 600 nm which suggests that a decrease in the vessel number or diameter would also have improved the fit between simulated and measured reflection in this region. Much like participant 1, if the mean depth of the vessels was decreased, the need for a reduction in vessel number or diameter would be greater. Again, it is likely that further

iterations would have resulted in a closer fit between measured and simulated PWS spectra with more superficial but fewer or thinner vessels.

The ratio of vessel number density predicted by the simulation to that determined by OCT (1.10) was again much closer than participants 1 and 11 (0.64 and 0.48 respectively) and similar to that of participant 12 (1.00 and 0.96). Again, vessel diameter predicted by the simulation corresponded very closely to that determined by OCT analysis and the mean vessel depth was less. It is not likely that further iterations of the PWS minimisation procedure would have improved the agreement between PWS vessel parameters predicted by the simulation and those determined by OCT.

Participant 14

Two regions were imaged using the VivoSight system, each covering an area of 2 mm x 2 mm. In the first region, 5 vessels were identified per slice with a mean depth of 220 µm and mean diameter of 48 µm. The second region was identified as a haemangioma, or 'bleb' (a small raised, dark purple patch of PWS skin). In this region, there was also a mean of 5 vessels identified per slice, having a similar mean depth of 210 µm. However the mean vessel diameter determined by OCT was much larger, at 195 µm.

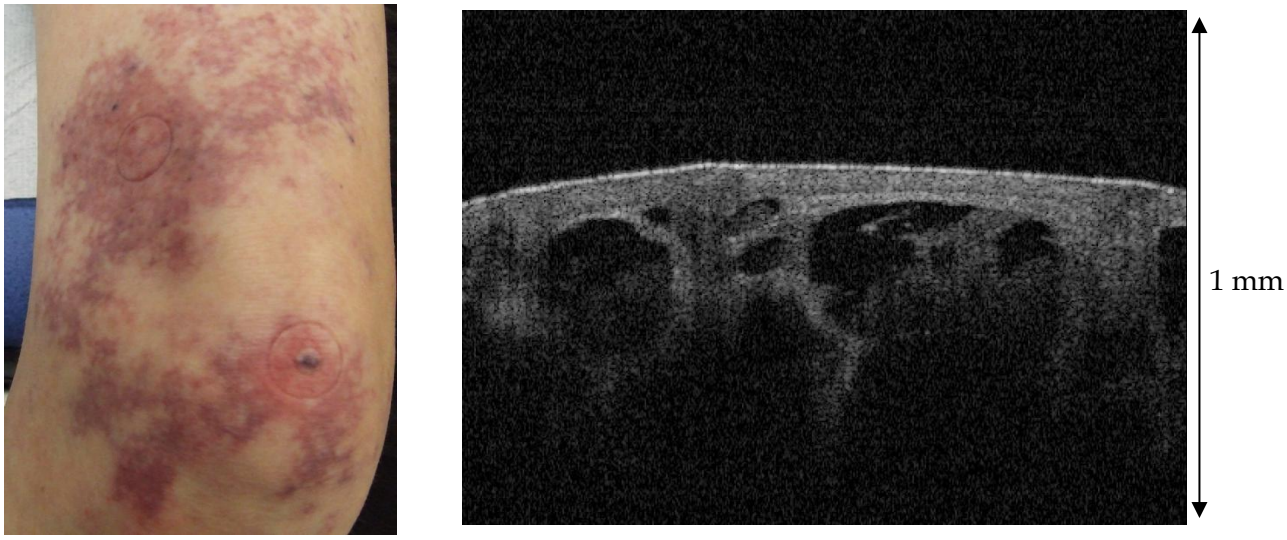

Figure 85: Left: photograph showing regions of OCT measurements on participant 14. Right: OCT image of 'bleb' area showing expansive vascular lakes.

After 10 iterations of the melanin minimisation procedure, the mean absolute difference between measured and simulated skin was 1.2% measured reflection. This was produced from a skin model containing 1.9% epidermal melanin volume, with a mean melanosome diameter of 273 nm. The simulated spectrum corresponded well with the measured spectrum for adjacent skin across almost the entire spectrum, differing most at the extreme ends (360 nm and 740 nm). The epidermal melanin concentration corresponds with that which might be expected for this participant's skin type and anatomical region (Figure 86). Predicted melanosome diameters were much larger than might be expected for this participant.

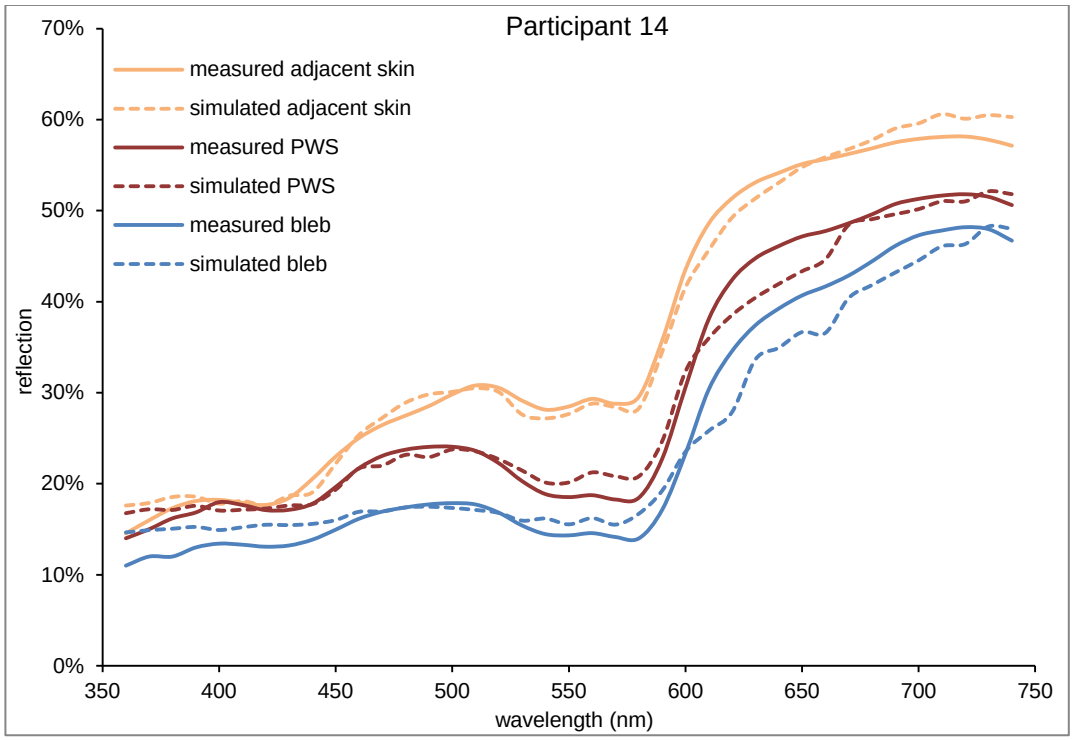

Figure 86: Simulation results for participant 14.

PWS skin colour in the first region was replicated with a mean of 1.8% deviation in reflection from the measured data after 15 iterations of the vessel minimisation procedure (12.5 days). This output was produced with a skin model containing 8 vessels of 50 µm diameter and a mean depth of 190 µm. The greatest deviation between measured and simulated PWS skin colour is apparent between 620 nm and 660 nm, suggesting that fewer or smaller diameter vessels may have resulted in a closer fit. There is also an increase in simulated reflection relative to measured data in the region 520 nm to 590 nm, suggesting that more superficial vessels would have

produced a closer fit in this region. In both cases however, the discrepancies between measured and simulated reflection are small.

The vessel parameters of PWS skin predicted by the simulation demonstrate close agreement with the values determined by OCT analysis for the first region. Vessel diameter was again very well matched between the two methods, as was mean vessel depth in this case. The PWS vessel number density predicted by the simulation relative to the number identified by OCT (1.25) was greater than the other participants included in this study.

The colour of the PWS 'bleb' was replicated by the Monte Carlo programme with a mean absolute difference between measured and simulated skin of 2.1% reflection. This output was achieved with a skin model containing 10 vessels of 220 μm diameter and a mean depth of 180 μm. The greatest deviation between the two datasets occurred at wavelengths greater than 620 nm, suggesting that a smaller diameter or number of vessels may have improved the fit between simulated and measured skin colour in this region.

The vessel diameter predicted by the simulation again matched well with that determined by OCT. Importantly, the simulation predicted an increase in the diameter of PWS vessels as the principal difference between the two regions assessed. This is consistent with the results of the OCT analysis. The mean depth predicted by the simulation also matched well to that determined by OCT analysis, although this was the only region analysed by the VivoSight system where the simulation did not underestimate the mean vessel depth relative to the OCT analysis. The ratio of simulated vessel number density to that determined by OCT (1.0) was consistent with the other participants imaged using the VivoSight and employing 15 iterations of the PWS minimisation procedure (1.00 and 0.96, and 1.10 respectively). It is not clear whether further iterations of the PWS minimisation procedure may have improved the agreement between PWS vessel parameters predicted by the simulation and those determined through OCT analysis.

Summary

Across the 5 participants analysed by OCT, the simulation reproduced adjacent skin colour well (mean 1.5% deviation between measured and simulated data points). Epidermal melanin volume fractions were again consistent with participants with

mainly pale, Northern European skin types. This shows agreement with visual observation. In consideration of these results, mean melanosome diameters were again larger than expected for this participant group.

Table 8: Summary of adjacent skin parameters predicted by the simulation.

Participant number	% melanin volume fraction	mean melanosome diameter (nm)	Discrepancy (% reflection)
1	1.5%	249	2.3%
11	1.9%	150	1.2%
12	1.4%	66	1.5%
13	1.9%	274	1.1%
14	1.9%	273	1.4%
mean	***1.7%***	***202***	***1.5%***

The primary region of discrepancy between simulated and measured adjacent skin colour was below 450 nm. This is consistent with the aforementioned larger than expected melanosome diameters as well as the results presented in Section 7.1, and supports the proposed use of shorter wavelength regions during the consideration of melanosome diameters within the melanin minimisation procedure.

Table 9: Summary of results from participants assessed using OCT.

Participant number	Simulated Values				OCT Measured Values		
	no. of vessels	mean vessel diameter (μm)	mean vessel depth (μm)	Discrepancy (% reflection)	number of vessels (4 mm²)	mean vessel diameter (μm)	mean vessel depth (μm)
1	18	180	262	5.2%	8.7	70	300
11	10	80	260	1.5%	6.4	97	240
12 (1)	8	40	175	2.3%	8.0	43	240
12 (2)	10	40	155	1.5%	10.4	41	240
13 (1)	14	80	180	4.3%	15.2	81	280
13 (2)	"	"	"	"	15.4	91	280
14 (1)	8	50	190	1.8%	10.0	48	220
14 (bleb)	10	220	180	2.1%	10.0	195	210
mean	***11.1***	***99***	***200***	***2.7%***	***10.5***	***83***	***251***

PWS skin colour was reproduced by the simulation with a mean deviation of 2.7% between measured and simulated data points over the 5 participants assessed. In general, the simulation showed good flexibility and was able to replicate measured reflectance spectra of varying shapes, although measured spectra involving large differences in reflection between the regions 360-550 nm and 630-740 nm were not reproduced well. The predicted PWS vessel parameters were consistent with those found elsewhere in the literature (Table 9).

The number and diameter of PWS vessels predicted by the simulation were similar to values determined through OCT analysis for the majority of participants. The greatest discrepancy in these parameters predicted by the simulation and determined through OCT is from participant 1, whose error in simulated reflection relative to measured skin colour is also largest. The mean vessel depth predicted by the simulation was less than that determined by OCT for all except participant 11. These results are consistent with those presented in Section 7.1.

Despite the similarities between the hardware employed by the two OCT devices used in this study (both devices employ a broadband swept source with a centre wavelength of 1300 nm, see also section 5.1), their performance appeared to differ substantially. The VivoSight was subjectively found to provide a clearer demarcation of vessel boundaries and this may be a factor contributing towards the trend of greater PWS vessel number densities identified for participants assessed by this device. Due to limited access to the two devices, a direct comparison was not carried out.

7.3 Participants Assessed by Expert Analysis of Photographs

Of the ten participants assessed by spectrophotometry before and after treatment, nine were assessed also by expert analysis of photographs. Photographs of PWS lesions were taken alongside each colour measurement for these participants. In this section, the results of the photographic analyses are compared to colour measurements.

As discussed in Section 2.1, previous work has shown that a reduced number of PWS vessels within a lesion causes a reduction in the apparent redness of a PWS lesion, whereas PWS lesions with larger diameter vessels appear less pink and more purple. Lesions whose vessels are deeper on average were found to appear less red, but with increased degrees of pink and purple hue. These conclusions are drawn upon when comparing the changes in skin colour determined through expert analysis of photographs following treatment to the predictions of melanin and PWS vessel properties made by the Monte Carlo simulation, previously discussed in Section 7.1.

The quality and reproducibility of photographic images was poor. This is mainly due to variations in geometry and ambient lighting conditions. This limits the strength of any conclusions drawn from this aspect of the study, in particular with regards to before and after comparisons. It is likley that the use of professional photography in a studio environment would have improved the reproducibility of photographs, although some variation will always be present [260, 261].

Participant 2

The darkness of pre-treatment adjacent skin was given a mean score of 2.75 by photographic analysis. This is the darkest of all the participants assessed through photography. The Monte Carlo programme predicted an epidermal melanin volume fraction of 3.3%, corresponding with the photographic analysis as the highest melanin content across the participant group. The predicted mean melanosome diameter of 208 nm is consistent with the expected value for this skin type.

Pre-treatment PWS severity had a mean score of 3.0 from the photographic analysis. The Monte Carlo programme predicted 6 vessels of 160 μm diameter with a mean depth of 250 μm.

Figure 87: Photographs of participant 2 before (left) and after (right) a single session of laser treatment.

The mean results of photographic analysis after treatment showed minimal change in adjacent skin darkness. This is in agreement with spectrophotometry, which showed minimal change in mean reflection of adjacent skin across the spectrum (from 29.8% to 30.2%).

Laser treatment was carried out using a radiant exposure of 14 Jcm^{-2} and a pulse length of 6 ms for this participant. The mean PWS severity score increased from 3.0 to 3.5. Furthermore, red, pink and purple hues were found to increase following treatment (by mean scores of 0.8, 0.8 and 0.4 respectively). These results suggest an increase in the mean depth and number of PWS vessels.

As discussed in Section 7.1, colour measurement data showed that the laser treatment had little, if any, effect on the colour of the PWS lesion. This suggests that the perceived difference determined through analysis of photographs may have been a result of differences in lighting, geometry or processing of the image. This, for example, may result in changes in shadowing, the proportion of red hue in both PWS skin and adjacent skin due to differences in illumination and post-processing performed by the camera, and differences in background colour. A noticeable increase in PWS severity is not likely to have taken place over this time frame (3 months). The

Monte Carlo programme predicted similar vessel characteristics for both pre-treated and post-treated PWS datasets, with a slight increase in vessel number and depth, and a slight decrease in vessel diameter. These changes are in support of the results from the analysis of photographs.

Participant 3

The darkness of pre-treatment adjacent skin was given a mean score of 1.5 by photographic analysis. This is one of the palest results from this patient group and close to the minimum score of 1.0 out of 7.0. This corresponds with the low epidermal melanin volume fraction (0.7%) and mean melanosome diameter of 156 nm predicted by the Monte Carlo programme.

Pre-treatment PWS severity had a mean score of 1.88 from the photographic analysis. The Monte Carlo programme predicted 6 vessels of 160 μm diameter with a mean depth of 250 μm.

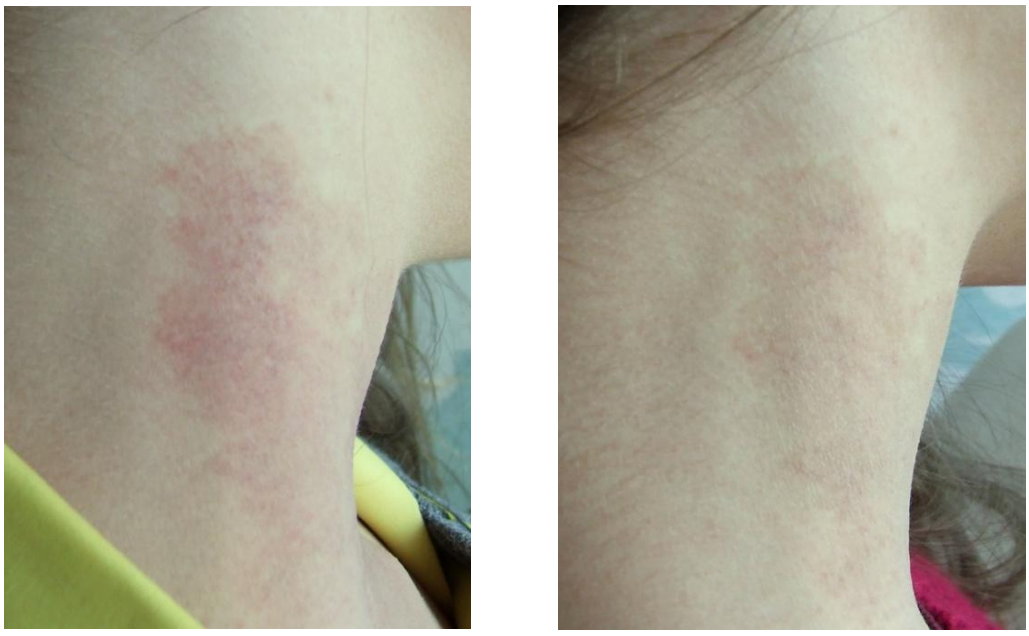

Figure 88: Photographs of participant 3 before (left) and after (right) a single session of laser treatment.

The mean results of photographic analysis showed no change in adjacent skin tone. However, colour measurement data of adjacent skin showed an increase in measured reflectance across the entire spectrum between sessions (from 33.3% to 36.4%).

Laser treatment was carried out using a radiant exposure of 14.5 Jcm^{-2} and a pulse length of 6 ms for this participant. Photographic analysis showed a decrease in the PWS severity score (0.5) as well scores of decreasing red (-1.25), pink (-1.19) and

purple (-0.56) hues. These results suggest a decrease in the depth and number of PWS vessels.

Spectrophotometry measurements showed a reduction in the difference between PWS and adjacent skin between sessions, particularly in the region 500 nm to 600 nm. The PWS vessel minimisation procedure predicted the same number and diameter of vessels in the region measured, with a slight increase in the mean vessel depth. Thus, the Monte Carlo programme attributed the measured change in PWS colour between sessions primarily to a change in the melanin content of the overlying epidermis, and do not support the results of the photographic analysis.

Participant 4

The darkness of pre-treatment adjacent skin was given a mean score of 2.25 by photographic analysis. This skin tone is thought to be in general agreement with the epidermal melanin volume fraction of 1.3% and a mean melanosome diameter of 291 nm predicted by the simulation.

Pre-treatment PWS severity had a mean score of 5.50 from the photographic analysis. This is the highest severity score from the participant group and corresponds well with the predictions of high vessel number density made by the Monte Carlo programme, (17 vessels of 100 μm diameter with a mean depth of 194 μm).

The mean results of photographic analysis showed no change in adjacent skin tone. This is in agreement with spectrophotometry measurements, which show minimal change in mean reflection across the spectrum (from 39.4% to 38.5%), and therefore with the melanin properties predicted by the simulation.

Laser treatment was carried out using a radiant exposure of 16 Jcm^{-2} and a pulse length of 6 ms for this participant. Photographic analysis showed a reduction in PWS severity of 0.8, as well as reduction in red and pink hues (scores of -0.6 and -0.5 respectively). There was no change in the mean degree of purple hue. These results suggest that the treatment was effective and resulted in an increase in the vessel depth and vessel number.

Figure 89: Photographs of participant 4 before (left) and after (right) a single session of laser treatment.

Colour measurement data demonstrated very little change in the assessed region of PWS skin between sessions and, as a result, the simulation predicted very little change in the PWS vessel properties. Changes in PWS characteristics determined by photographic assessment may have therefore been a result of changes in photographic conditions or presentation of photographs, or may have been outside of the region assessed by spectrophotometry.

Participant 5

The darkness of pre-treatment adjacent skin was given a mean score of 1.4 by photographic analysis. This is the palest of the participants assessed and corresponds with the lowest epidermal melanin volume fraction of 0.4% and the relatively small mean melanosome diameter of 194 nm predicted by the simulation.

Pre-treatment PWS severity had a mean score of 1.7 from the photographic analysis. The Monte Carlo programme predicted 7 vessels of 40 μm diameter with a mean depth of 220 μm. The prediction of thin vessels made by the programme is in agreement with the low PWS severity score.

Figure 90: Photographs of participant 5 before (left) and after (right) a single session of laser treatment.

The mean results of photographic analysis showed a negligible decrease (0.06) in adjacent skin tone. Colour measurement data gave a mean decrease in reflection of 2.8% across the spectrum (44.2% to 41.4%), and the Monte Carlo a modest increase in melanin volume fraction from 0.4% to 0.8%. These results support the findings of the photographic analysis, although an increase in the predicted mean melanosome diameter to 318 nm is not consistent with this participant's skin type.

Laser treatment was carried out using a radiant exposure of 14.5 Jcm^{-2} and a pulse length of 6 ms. Mean results from the photographic assessment showed a reduction in PWS severity from scores of 1.7 to 1.4. Scoring also showed a reduction in red (-0.3) and pink (-0.4) hues, as well as a small reduction in purple hue (-0.1). These results suggest that the treatment was successful, although the likely changes in PWS vessel parameters suggested by the analysis are not clear.

The spectral reflection of PWS skin was found to decrease for this participant following treatment, although the mean difference in spectral reflection between PWS and adjacent skin was reduced. Thus, it appears that the photographic assessment attributed the reduced contrast between PWS and adjacent skin colours to a reduction in severity, redness and pinkness whereas colour measurements showed instead a

darkening of adjacent skin. The Monte Carlo programme predicted an increase in the number density as well as the mean depth of PWS vessels. This does not support the reduction in pink and purple hues determined by photographic analysis.

Participant 6

The darkness of pre-treatment adjacent skin was given a mean score of 2.25 by photographic analysis. This relatively high score (with respect to the other participants assessed in this study) is supported by a high prediction of epidermal melanin volume fraction (3.4%) and mean melanosome diameter (269 nm).

Pre-treatment PWS severity had a mean score of 1.69 from the photographic analysis. The Monte Carlo programme predicted 7 vessels of 60 µm diameter with a mean depth of 178 µm. Again, the small predicted mean vessel diameter corresponds with the low severity score from the photographic analysis.

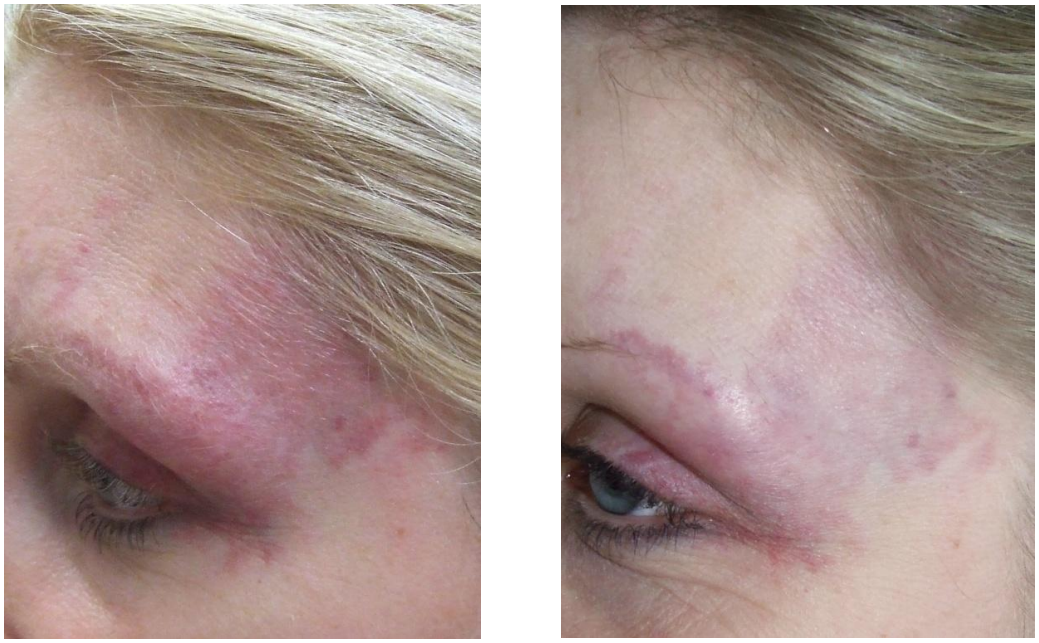

Figure 91: Photographs of participant 6 before (left) and after (right) a single session of laser treatment.

The mean results of photographic analysis showed an increase in the darkness of adjacent skin after treatment. However, spectrophotometry measurements showed a substantial lightening of adjacent skin from a mean of 30.6% reflection to 35.0% across the spectrum. As a result, the Monte Carlo programme predicted a decrease in melanin volume fraction from 3.4% to 2.0% and a negligible decrease in the mean melanosome diameter. This disagreement suggests that changes in the geometry,

lighting or post processing of the image were substantial sources of error in the photographic assessment.

Laser treatment was carried using 0.5 ms pulses with a radiant exposure of 10 Jcm^{-2}. Photographic assessments showed a reduction in PWS severity (by a score of 1.1), as well as pink (-0.9), red (-0.1) and purple (-1.1) hues. These results suggest a decrease in mean vessel depth and a reduction in the number of PWS vessels. Spectrophotometry also demonstrated a lightening of PWS skin from a mean 27.8% to 31.7% reflection across the spectrum. The Monte Carlo programme attributed this change to an increase in the mean vessel depth and a decrease in vessel number, thus supporting the results of the photographic analysis of PWS skin.

Participant 7

The darkness of adjacent skin prior to this participant's second treatment was given a mean score of 1.7 by photographic analysis. This relatively pale skin type is in agreement with the low prediction of epidermal melanin volume fraction (1.3%) and a small mean melanosome diameter (41 nm) made by the Monte Carlo programme.

Pre-treatment PWS severity had a mean score of 3.2 from the photographic analysis. The Monte Carlo programme predicted 5 vessels of 90 μm diameter and with a mean depth of 225 μm.

Figure 92: Photographs of participant 7 before (left) and after (right) a single session of

laser treatment.

The mean results of photographic analysis showed an increase in adjacent skin tone of 0.4. The darkness of adjacent skin was also found to increase by spectrophotometry (from a mean of 36.0% to 33.8% reflection across the spectrum) and the predicted melanin volume from (to 1.7%), although a reduction in the mean predicted melanosome diameter to 23 nm does not correspond with these results.

Laser treatment was carried out using a radiant exposure of 8.5 Jcm^{-2} and a pulse length of 0.5 ms. Photographic assessment showed a decrease in mean severity (by a score of 0.3) and pink hue (-0.3), but an increase in the degree of red (0.3) and purple (0.1) hues. These results suggest an increase in the mean vessel diameter and a reduction in mean vessel depth.

Colour measurements showed an increase in reflection below 600 nm and a decrease in reflectance at wavelengths greater than 600 nm, and the difference between measured reflectance was reduced below 600 nm, but not at wavelengths greater than 600 nm. This does not support an increase in the degree of redness as determined by photographic analysis but does support a decrease in the mean severity. In contrast to the changes suggested by photographic analysis following treatment, the Monte Carlo programme attributed this primarily to an increase in the mean vessel depth.

Participant 8

The darkness of pre-treatment adjacent skin was given a mean score of 1.8 by photographic analysis. This corresponds with the predictions of 1.4% epidermal melanin volume fraction and 281 nm mean melanosome diameter made by the Monte Carlo programme.

Pre-treatment PWS severity had a mean score of 1.8 from the photographic analysis. The Monte Carlo programme predicted 6 vessels of 20 µm diameter with a mean depth of 67 µm.

Figure 93: Photographs of participant 8 before (left) and after (right) a single session of laser treatment.

The mean results of photographic analysis showed no change in adjacent skin tone. In contrast, colour measurements found an increase in reflectance from a mean value of 39.7% to 42.2% across the spectrum and the simulation attributed this change to a reduction in melanin volume fraction.

Laser treatment was carried out using a radiant exposure of 14 Jcm^{-2} and a pulse length of 2 ms. Photographic analysis determined an increase in the severity of PWS skin following treatment, as well as an increase in red (0.9) and purple (0.2) hues. The mean change in pink hue was negligible. These results suggest an increase in the number and diameter of PWS vessels. However, measured PWS skin colour demonstrated very little change between sessions. The simulation of post-treatment PWS skin used a model containing fewer vessels, in contrast to the photographic results, although these vessels were wider, supporting the increase in purple hue determined by photographic analysis.

Participant 9

The darkness of pre-treatment adjacent skin was given a mean score of 2.6 by photographic analysis. This makes participant 9 one of the darker participants assessed by photography. This is supported by the predicted mean melanosome diameter of 331 nm but not by the low melanin volume fraction of 0.9%.

Pre-treatment PWS severity had a mean score of 3.2 from the photographic analysis. Although one of the higher severity scores from this participant group, the Monte Carlo programme predicted a low PWS vessel number density (4), small diameter vessels (60 µm) and a large mean depth of vessels (396 µm), all of which suggest a more subtle PWS.

Figure 94: Photographs of participant 9 before (left) and after (right) a single session of laser treatment.

The mean results of photographic analysis showed a slight decrease (0.25) in adjacent skin tone. This is in contrast to by colour measurements, which showed a slight increase in mean reflectance (from 41.4% to 40.0%) and, as a result, the Monte Carlo programme, which predicted an increase of 0.3% melanin volume fraction.

Laser treatment was carried out using a radiant exposure of 17 Jcm^{-2} and a pulse length of 10 ms. Photographic assessment showed an increase in PWS severity (0.75) but a reduction in pink hue (-0.4). The remaining parameters showed no change. Overall, these results suggest a decrease in the diameter of PWS vessels following treatment.

Colour measurement of PWS skin showed lightening of PWS skin at shorter wavelengths and therefore a slight reduction in PWS skin colour for this participant. This does not support the results of the photographic analysis, although the Monte Carlo programme did predict a reduction in diameter following laser treatment.

Participant 10

The darkness of pre-treatment adjacent skin was given a mean score of 2.7 by photographic analysis. This relatively dark skin type (with respect to this participant group) is supported by the predicted epidermal melanin volume fraction of 1.8% and a mean melanosome diameter of 384 nm.

Pre-treatment PWS severity had a mean score of 5.1 from the photographic analysis. This is one of the highest severity scores across the participant group and, like participant 4, the mean predicted vessel diameter was high, supporting this result.

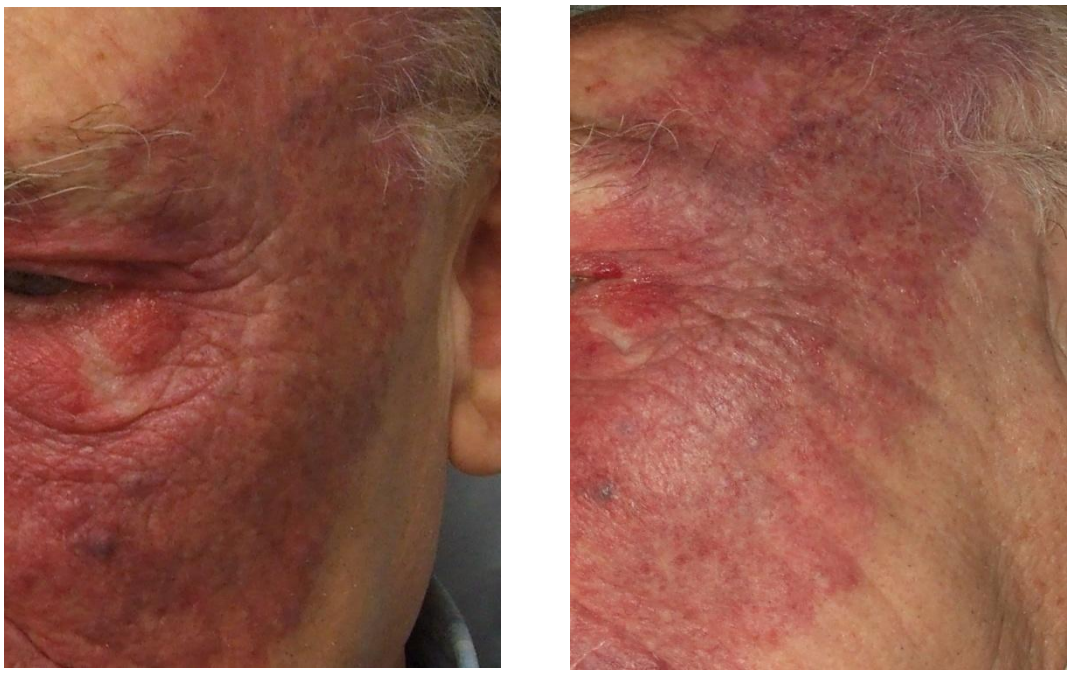

Figure 95: Photographs of participant 10 before (left) and after (right) a single session of laser treatment.

The mean results of photographic analysis showed no change in adjacent skin tone. In contrast, the mean measured reflection was reduced from 37.7% to 35.1% and the predicted melanin volume fraction increased by 1.5%. The predicted mean melanosome diameter decreased to 322 nm, a value still higher than expected for this participant's skin type.

A combined laser treatment was carried out for this participant, employing a 10 ms pulse of PDL (595 nm) at 10.5 Jcm^{-2} followed after a 0.5 s interval by a 15 ms pulse of Nd:YAG (1064 nm) at a radiant exposure of 70 Jcm^{-2}. Photographic assessments showed no change in the mean PWS severity following treatment, although the

degrees of red (-1.1), pink (-0.6) and purple (-0.4) hues were all reduced. These results suggest a reduction in the number and an increase in the depth of PWS vessels.

Colour measurement data of PWS skin shows an increase in reflection after treatment, in particular above 600 nm. The simulation attributed these changes to an increase in mean vessel depth, which is in agreement with the photographic assessment. Vessel number was also predicted by the simulation to increase between sessions, in contrast to the results suggested by photographic analysis.

Summary

Adjacent Skin

Skin tone, as determined by photographic analysis, varied from 1.4 to 2.8 out of a maximum possible 7.0 across the participant group, suggesting that the group consisted entirely of individuals with pale, primarily European skin types. A two-tailed Wilcoxon signed rank analysis showed that the participant skin type determined by photography varied significantly between each assessor, highlighting the subjectivity of the assessment, but did not vary significantly between treatment sessions for any individual assessor or for the mean skin types taken over all three assessors.

Table 10: Summary of pre-treatment parameters determined by photographic analysis, spectrophotometry and from the predictions made by the simulation. Where m_{vol} is the predicted epidermal melanin volume fraction and m_{diam} is the predicted mean melanosome diameter. R^2 refers to the coefficient of determination for skin darkness against each parameter.

participant number	skin darkness (photography)	Mean reflectance	m_{vol}	m_{diam}
2	2.8	30%	3.3%	208
3	1.5	33%	2.2%	156
4	2.3	39%	1.3%	291
5	1.4	44%	0.4%	194
6	2.3	31%	3.4%	269
7	1.7	36%	1.3%	41
8	1.8	40%	1.4%	281
9	2.6	41%	0.9%	331
10	2.7	38%	1.8%	384
	R^2	*0.09*	*0.17*	*0.4*

Adjacent skin darkness scores did not correspond with the mean measured reflectance across the spectrum (Table 10). However, this parameter did show some correlation with the melanin diameter predicted by the Monte Carlo programme, suggesting that changes in skin colour below 450 nm influenced the photographic assessment of skin colour (see Figure 34, page 117).

Melanin volume fractions predicted by the simulation varied from 0.4% to 3.4%. Two participants (2 and 6) were estimated to have melanin volume fractions which are suggestive of darker skin types than expected from the results of the photographic

analysis. The remaining participants are within the expected range. Mean melanosome diameters predicted by the programme are larger than expected for many of the participants.

Following treatment, the adjacent skin darkness score was found to decrease in the majority of participants. Coefficients of determination suggest some correlation between the change in adjacent skin darkness scores and the measured change in adjacent skin reflection, as well as melanin volume fraction and mean melanosome diameter predicted by the simulation (Table 11). However, a larger participant group would be necessary to consider whether photographic analysis could be a good predictor of the change in skin darkness.

Table 11: Summary of results from photographic assessment, simulated predictions and mean spectral reflectance obtained from colour measurement skin adjacent to PWS lesions. Where m_{vol} is the epidermal melanin volume fraction and m_{diam} is the mean melanosome diameter.

participant number	Change in skin darkness (photography)	Change in mean reflectance	Change in m_{vol}	Change in m_{diam}
2	-0.1	-0.4%	0.0%	0
3	-0.1	-3.1%	-1.4%	0
4	0.0	0.9%	0.1%	-7
5	-0.1	2.8%	0.4%	124
6	-0.4	-4.4%	-1.4%	-5
7	0.4	2.2%	0.3%	-125
8	0.0	-2.5%	-0.2%	0
9	-0.3	1.4%	0.3%	-62
10	0.0	2.6%	1.5%	-62
	R^2	*0.23*	*0.16*	*0.18*

PWS Skin

Photographic assessments of pre-treatment PWS skin demonstrated a wide range of mean severity scores, from 1.7 to 5.5 out of a maximum possible 7.0. The severity score corresponded well with the mean reflectance determined by spectrophotometry and, subsequently, the number and diameter of vessels predicted by the simulation (Table 12). Mean vessel depth predicted by the simulation was not found to correspond with PWS severity scores.

Table 12: Summary of pre-treatment PWS skin properties assessed by photographic analysis, colour measurement and Monte Carlo simulation. R^2 refers to the coefficient of determination for PWS severity against each parameter.

participant number	PWS severity (photography)	Mean reflectance	Contrast in mean reflectance	number of vessels	vessel diameter (mm)	mean vessel depth (μm)
2	3.0	24.4%	5.4%	6	0.16	250
3	1.9	32.2%	1.1%	4	0.01	218
4	5.5	25.6%	13.7%	17	0.1	194
5	1.7	39.3%	4.9%	7	0.04	222
6	3.8	27.7%	2.9%	7	0.06	178
7	3.2	31.2%	0.0%	4	0.07	245
8	1.8	37.0%	4.8%	6	0.02	67
9	3.2	37.9%	2.8%	4	0.06	396
10	5.1	27.4%	3.5%	6	0.22	246
	R^2=	*0.48*	*0.10*	*0.37*	*0.48*	*0.04*

The change in PWS colour following treatment was assessed in terms of the change in PWS severity, as well as the change in pink, red and purple hues (Table 13).

Table 13: Summary of change in PWS appearance assessed by photography, spectrophotometry and interpreted by the Monte Carlo Programme. R^2 refers to the coefficient of determination.

p'pant no.	Change in PWS severity	Change in Red hue	Change in Pink hue	Change in Purple hue	Change in mean reflectance	Change in contrast	Change in number of vessels	Change in vessel diameter (mm)	Change in mean vessel depth (μm)
2	0.5	0.81	0.81	0.44	-0.1%	-0.4%	1	-0.02	14
3	-0.5	-1.25	-1.19	-0.56	1.8%	-1.2%	0	0.00	-1
4	-0.8	-0.56	-0.50	0.00	0.1%	1.0%	-10	0.00	-5
5	-0.3	-0.31	-0.38	-0.13	-1.4%	1.4%	6	0.00	136
6	-1.1	-0.88	-0.13	-1.13	4.0%	-0.4%	-2	0.00	47
7	-0.3	0.31	-0.31	0.13	-0.4%	0.0%	1	0.00	206
8	0.8	0.88	-0.06	0.19	0.5%	2.2%	-2	0.03	148
9	0.8	0.06	-0.44	-0.06	0.8%	-2.0%	1	-0.01	64
10	0.0	-1.06	-0.56	-0.44	2.1%	2.3%	3	-0.11	18
				R^2 vs. severity=	*0.13*	*0.00*	*0.11*	*0.00*	*0.04*
				R^2 vs. Red=	*0.31*	*0.00*	*0.00*	*0.17*	*0.27*
				R^2 vs. Pink=	*0.04*	*0.04*	*0.00*	*0.01*	*0.01*
				R^2 vs. Purple=	*0.68*	*0.02*	*0.00*	*0.03*	*0.09*

The changes in PWS severity and pink hue assessed by analysis of photographs did not correspond with those determined by colour measurement, and therefore did not

correspond with any of the parameters predicted by the Monte Carlo simulation. The change in redness determined by photographic analysis showed some correspondence with the measured change in the mean spectral reflectance of PWS skin. This was reflected in the predicted change in mean vessel depth, which is in agreement with previous reports in the literature (see Section 2.1, page 19). The change in purple hue correlated strongly with the measured change in reflectance, but not with any of the parameters predicted by the Monte Carlo programme. Thus, the change in PWS severity and colour was not found to be a good predictor of changes in PWS vessel architecture as predicted by the new Monte Carlo programme.

8. Analysis

8.1 Simulating Clinically Normal Skin

Over the 14 participant (26 datasets) assessed, spectral reflectance of adjacent skin sites were reproduced by the simulation with a mean of 2.4% deviation from the measured data.

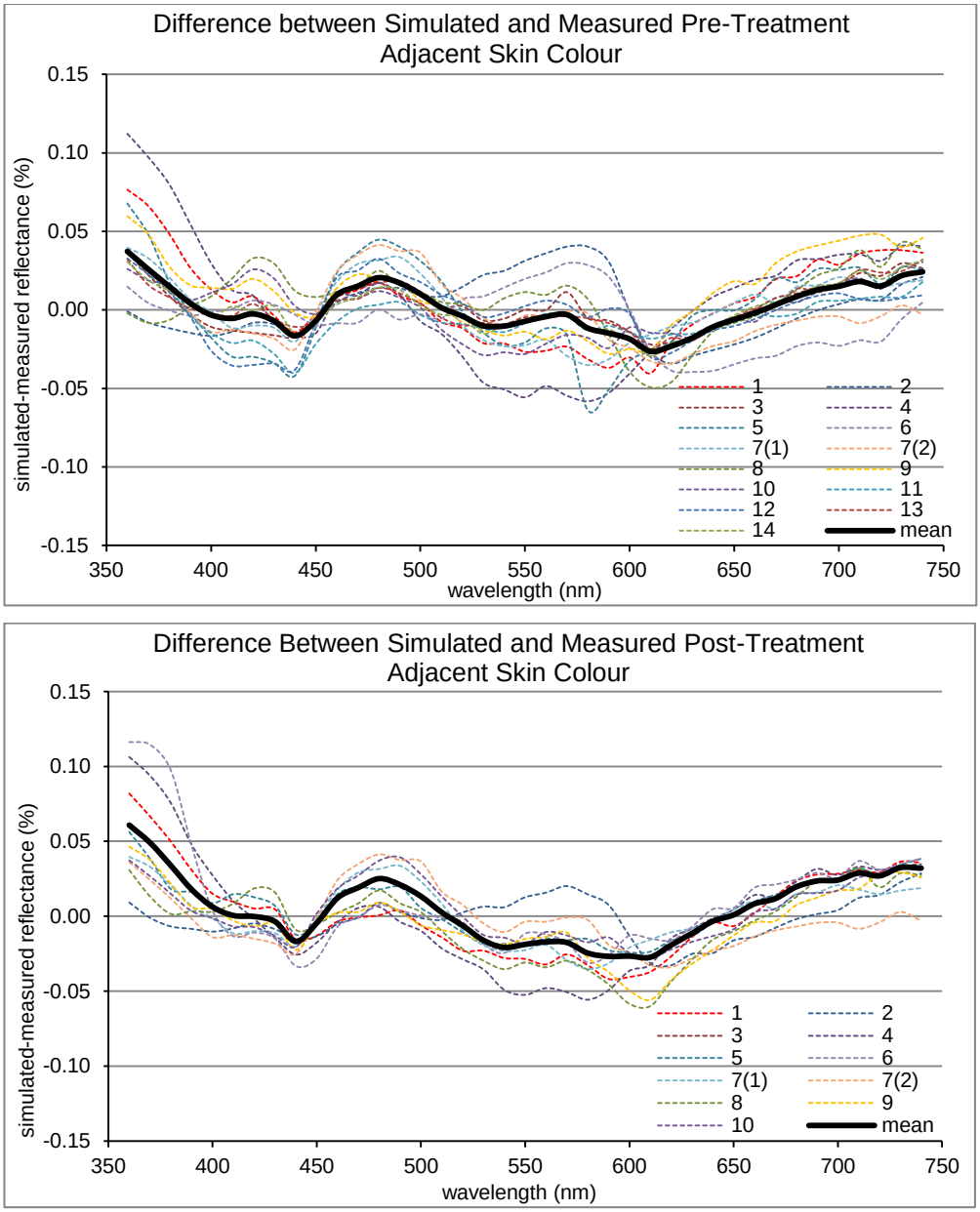

Figure 96: Difference between simulated and measured adjacent skin reflectance for the 10 participants assessed by multiple spectrophotometry sessions.

Figure 97 shows that the region below 400 nm was consistently overestimated by the simulation, whereas the mean difference between simulated and measured spectra was small between 400 nm and 450 nm. This suggests that greater consideration of

wavelengths below 400 nm within the melanin minimisation procedure would have resulted in a net improvement in the fit between measured and simulated spectra.

Mean simulated melanosome diameters across the epidermis predicted by the Monte Carlo programme ranged from 41 to 384 nm over the participants studied (mean 223 nm, Table 14). This range of diameters is broadly within that expected for these individuals, although some studies suggest that diameters of less than 160 nm may be most appropriate for this participant group [8, 10, 12]. The simulated outputs at wavelengths below 500 nm were manipulated within the programme by adjusting the diameters of melanosomes in the skin model. However, this process did not take into account wavelengths below 400 nm. It is likely that a closer fit between the simulated and measured spectra would have been obtained if the region 360-400 nm was considered during the manipulation of melanosome diameters. This would likely have resulted in smaller predicted melanosome diameters across the participant group, which would have fitted more closely with the results expected for participants of lighter, Northern European skin types. The predicted melanosome diameters did not show a correlation with skin darkness scores for the 9 participants assessed by photographic analysis (coefficient of determination for a linear fit, R^2=0.06).

Table 14: Summary of adjacent skin parameters predicted by the Monte Carlo simulation across all participants.

participant number	Pre-treatment		Post-treatment	
	m_{vol}	m_{diam}	m_{vol}	m_{diam}
1	1.5%	249	1.7%	252
2	3.3%	208	3.3%	208
3	2.2%	156	0.7%	156
4	1.3%	291	1.4%	284
5	0.4%	194	0.8%	318
6	3.4%	269	2.0%	264
7 (1)	1.3%	41	1.3%	41
7(2)	-	-	1.7%	23
8	1.4%	281	1.2%	281
9	0.9%	331	1.2%	269
10	1.8%	384	3.3%	322
11	1.9%	150	-	-
12	1.4%	66	-	-
13	1.9%	274	-	-
14	1.9%	273	-	-

Spectral reflectance of adjacent skin was consistently overestimated in the region 450-500 nm, where a peak in the simulated reflectance (between blood absorption peaks) was simulated but not replicated to the same degree in the majority of measured spectra. The simulation also overestimated spectral reflectance for most participants at wavelengths greater than 650 nm, but underestimated in the region 600-650 nm. This appears to be due to the inability of the model to replicate the steep gradient in measured reflectance found commonly within this participant group in the region 600-650 nm. Introducing the capacity to adjust the relative quantity of melanin throughout the three epidermal layers of the skin model may have resulted in an improved fit over this region, although further investigation would be necessary before an appropriate minimisation procedure could be developed.

The expert analysis of photographic images determined adjacent skin darkness scores ranging from 1.3 to 2.7 with a mean value of 2.0 and a standard deviation of 0.4 over the 10 participants assessed. Thus, the participants assessed by this method were likely to be primarily of pale Northern European skin types. Mean simulated epidermal melanin volumes varied from 0.4% to 3.3% over the entire participant group (mean 1.7%, Table 14). This is mainly within the ranges published for pale Northern European skin types, although the scientific literature suggests that epidermal melanin volumes less than 1% are not likely to have been observed for skin types identified in this participant group [6-11]. The melanin volume fractions predicted by the simulation were supported by the mean skin type determined by expert analysis of photographs (coefficient of determination for a linear fit, R^2=0.41 over 20 data points).

8.2 Simulating PWS Skin

PWS skin was reproduced by the simulation with a mean deviation of 2.4% reflectance from the measured data over 14 participants (27 datasets).

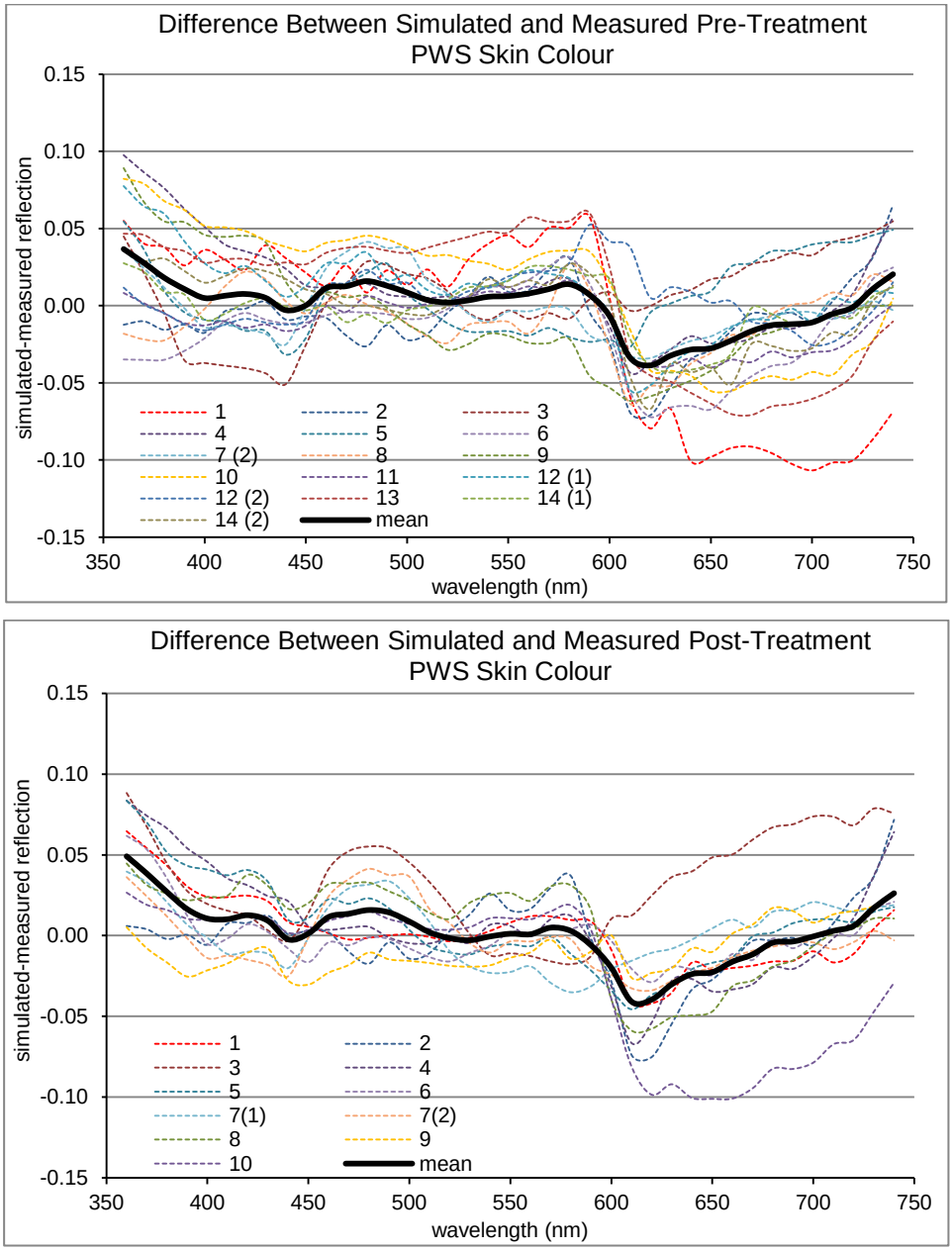

Figure 97: Difference between simulated and measured PWS skin reflectance for the 10 participants assessed by multiple spectrophotometry sessions.

The simulation replicated measured PWS skin data well for the majority of participants at wavelengths less than 600 nm, although an overestimation of reflectance below 400 nm appears to have been inherited from the melanin minimisation procedure as well as a slight overestimation between 450 nm and 500 nm. A noticeable discrepancy

between measured and simulated reflectance is apparent at 610 nm. This may have been partly inherited from the melanin minimisation procedure but again shows this simulation's inability to reproduce the steep gradient in reflectance measured for most of the participants in this wavelength region. The remaining discrepancies at wavelengths greater than 650 nm mimic those of the melanin minimisation procedure.

It is likley that a more accurate reproduction of PWS skin colour would result from the use of more realistic vessel architectures which account for vessel bends, splits and non-horizontal vessel directions as seen on OCT in this work and in biopsy studies elsewhere [231].

Vessel Number Density

The predicted vessel number densities varied from 4 to 18 over a 4 mm diameter circular area of skin. Of the two previous studies involving significant numbers of biopsies performed on PWS lesions, Barsky *et al* [32] reported vessel numbers over an equivalent area ranging from 36 to 194, whereas a figure for comparison could not be obtained from Fiskerstrand *et al*'s work [42]. Barsky *et al*'s vessel number densities are clearly much larger than those predicted by the Monte Carlo programme presented here. However, Barsky *et al* considered vessels down to a depth of 1800 μm, which is likely to be beyond the depth at which vessels contribute to the colour of PWS skin.

Table 15: Comparison of OCT analyses and prediction made by the Monte Carlo simulation for the five participants analysed by OCT.

	OCT			Simulation (ratio of OCT/Simulation)			
Participant Number	Number of Vessels/4mm	Diameter (μm)	Depth (μm)	Number of Vessels	Diameter (μm)	Depth (μm)	Optical Depth (μm)
1	8.7	70	300	18 (0.48)	110 (0.64)	220 (1.36)	117 (2.56)
11	6.4	97	240	10 (0.64)	80 (1.21)	260 (0.92)	112 (2.14)
12 (region 1)	8.0	43	240	8 (1.00)	40 (1.08)	175 (1.37)	57 (4.21)
12 (region 2)	9.6	41	240	10 (0.96)	40 (1.03)	155 (1.55)	51 (4.71)
13	11.4	86	280	14 (1.10)	80 (1.08)	180 (1.56)	98 (2.86)
14	10.0	48	220	8 (1.25)	50 (0.96)	190 (1.16)	117 (1.88)
14 (bleb)	10.0	195	210	10 (1.00)	180 (1.08)	220 (0.95)	125 (1.68)

The vessel number density predicted by the simulation corresponded with the mean value per image for a 4 mm volume imaged by OCT with a ratio of approximately 1.0 for the majority of regions imaged using the VivoSight (Table 15). This ratio was smaller for the Thorlabs device. The discrepancy between the two devices may have

been as a result of the apparent difference in image contrast. However, it is likely that further iterations of the blood vessel procedure would have resulted in fewer vessels predicted by the simulation for the two participants imaged using the Thorlabs device. Thus, the use of more iterations of this procedure for the participants imaged using the VivoSight appears to have improved the accuracy of the PWS blood vessel number density predicted by the simulation.

The pre-treatment vessel number predicted by the simulation showed agreement with the mean PWS severity determined by expert analysis of photographs (coefficient of determination for a linear fit, R^2=0.37 over 20 data points).

Vessel Diameters

Barsky *et al* [32] determined PWS vessel diameters raging in diameter from 10 μm to 106 μm with the majority below 25 μm from their biopsy study of 100 patients and Fiskerstrand *et al* [42] reported diameters up to 300 μm, with the majority below 120 μm across their biopsy study of 51 patients. The mean PWS vessel diameters predicted by the simulation ranged from 10 μm to 220 μm across the participants investigated, with the majority below 100 μm. It can be concluded that these predictions are well supported by the literature.

The vessel diameters predicted by the simulation correspond closely with those determined by OCT analysis (Table 15). In particular, those participants imaged using the VivoSight device differed by no more than 10% from the predicted values. For these participants, vessel diameters were determined with greater certainty due to the relative degrees of image contrast between the two imaging devices. However, the use of a greater number of iterations is again likely to be the primary reason for this apparent improvement in the predicted values.

The mean diameters predicted by the simulation correlated with the mean PWS severity determined by expert analysis of photographs (coefficient of determination for a linear fit, R^2= 0.44 over 20 data points).

Vessel Depths

Mean vessel depths predicted by the simulation study ranged from 67 μm to 460 μm. These appear to include mean PWS vessel depths which are more superficial than those reported in the aforementioned biopsy studies (which ranged from

approximately 200 μm to 400 μm [32, 42]). This is likely to be because the simulation only considered vessels which contributed to the colour of PWS skin, and not the deeper vessels which would also have been identified by biopsy.

The mean depth of blood vessels, as determined by OCT analysis, was greater than that predicted by the simulation in the majority of regions imaged, but was not consistent. This suggests that the simulation was not able to provide an accurate estimation of mean PWS vessel depth. Furthermore, it is likely that the true mean depth of PWS blood vessels is greater than that determined by the OCT analysis, due to the lack of information available below 500 μm, further separating the mean PWS vessel depth predicted by the programme and the likely true mean PWS vessel depth.

The mean optical depth (ρ) of the vessels in the skin model was also considered (Table 15). This is defined as:

$$\rho = \sum_{i}^{5} t_i(\mu'_{s,i} + \mu_{a,i}) + \left[d - \sum_{i}^{5} t_i\right](\mu'_{s,6} + \mu_{a,6}) \qquad \text{Equation 32}$$

where d is the mean depth of vessels and t is the thickness, μ_s' is the reduced scattering coefficient and μ_a is the absorption coefficient of the layer i. The mean optical depth (ρ) of simulated vessels at 740 nm (selected as the closest evaluated wavelength to the wavelength range used in OCT imaging) was between 1.6 and 4.7 times smaller than the mean vessel depth determined by OCT, and does not appear to serve as an adequate predictor of mean vessel depth.

The mean depths predicted by the simulation were not found to correlate with the mean PWS severity determined by expert analysis of photographs (coefficient of determination for a linear fit, R^2= 0.06 over 20 data points).

8.3 Predicting Treatment Effectiveness

Melanin Content

No direct trend was found between epidermal melanin volume fraction or melanosome diameter predicted by the programme and treatment effectiveness as determined through spectrophotometry (R^2 = 0.10 and 0.01 respectively) or through expert analysis of photographs (R^2 = 0.11 and 0.05 respectively). Adjacent skin darkness as determined by expert analysis of photographs was not found to be a strong indicator of treatment effectiveness as determined by change in measured PWS skin colour (R^2 = 0.10) or photographic PWS severity score (R^2 = 0.08). Thus, adjacent skin properties were not found to be directly indicative of treatment effectiveness for this participant group by any of the methods applied in this study.

Vessel Number

The Monte Carlo programme predicted pre-treatment vessel numbers ranging from 4 to 18 (mean 7.6) over the 3.5 mm diameter region allocated at the centre of the model. Post-treatment simulations involved fewer vessels on average (6.5). Although at first appearance this difference appears to be caused primarily by the influence of participants 1 and 4 (Figure 99), a two-tailed Wilcoxon signed-rank test concluded that there was a significant difference (reduction) in the number of vessels between the 'before treatment' and 'after treatment' groups at the α=0.05 (95% confidence) level. This suggests that laser treatment was effective in reducing the number of PWS vessels. This conclusion is supported by experimental work published elsewhere [42, 262].

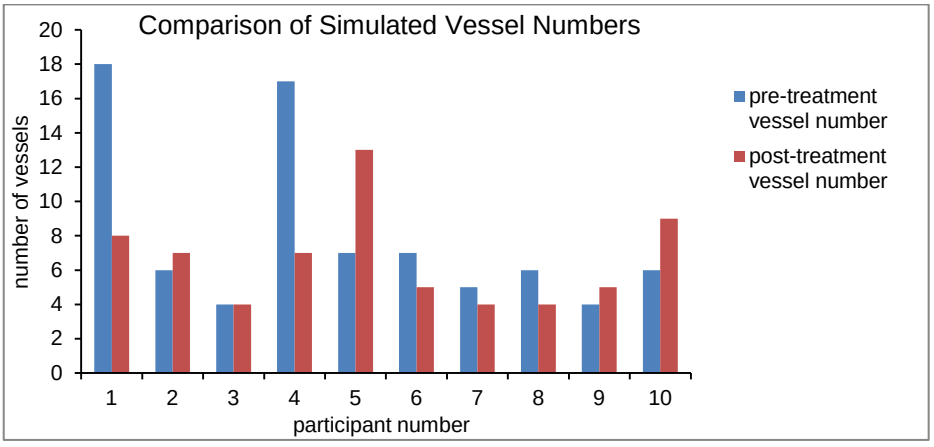

Figure 98: Histogram showing simulated PWS vessel numbers for participants analysed by skin colour measurements before and after treatment.

No correlation was found between the number of vessels predicted in pre-treatment PWS skin and the change in relative reflectance between PWS and adjacent skin as measured using spectrophotometry or the change in PWS properties assessed by photography. Thus, it appears that the predicted vessel number from this simulation is not a useful indicator of likely treatment response.

Vessel Diameter

The mean diameters of pre-treatment PWS vessels predicted by the simulation ranged from 10 μm to 220 μm for this participant group. A two-tailed Wilcoxon signed rank analysis showed a significant change in vessel diameter between treatment sessions over this group (at the α=0.05 level), with the mean diameter being reduced in 5 participants but increased in one. This suggests that laser treatment was generally more effective at treating larger PWS vessels. Again, this conclusion is supported by experimental work published elsewhere [42, 77, 262].

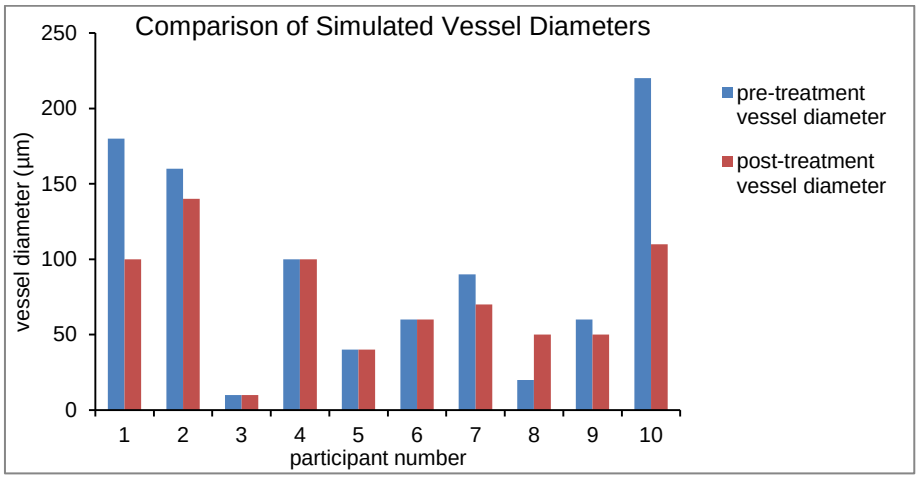

Figure 99: Histogram showing simulated PWS vessel diameters for participants analysed by skin colour measurements before and after treatment.

The effectiveness of laser treatment is determined partly by how well matched the pulse length is to the diameter of PWS vessels, which may be assessed using the thermal relaxation time. The pulse lengths of the laser used to deliver treatments to these participants was determined through measurements carried out using a photodiode (Appendix G). As discussed in Section 2.2 (page 26), the ratio of thermal relaxation time (τ) to the change in the difference in spectral reflection between PWS and adjacent skin over the wavelength range assessed was considered (Figure 101); where:

$$\tau \cong \frac{R^2}{4\chi}$$ Equation 33,

and R is the mean vessel radius predicted by the simulation.

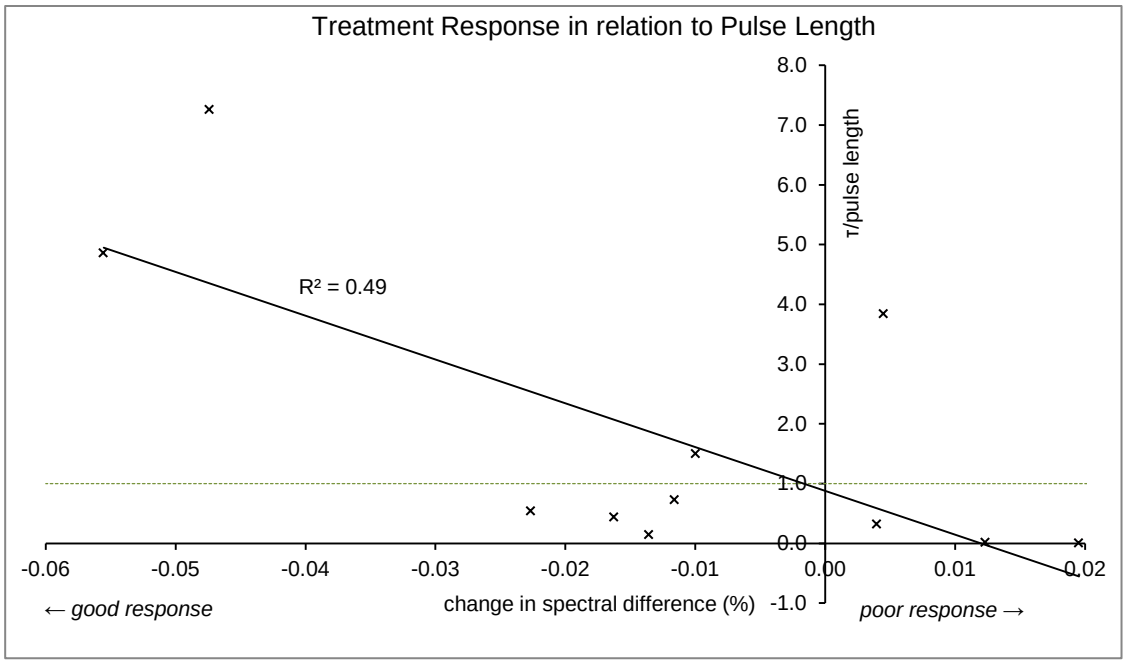

Figure 100: Comparison between predicted the difference in spectral reflection between normal and PWS skin following laser treatment and the ratio of predicted thermal relaxation times and estimates of the pulse lengths delivered.

Figure 101 suggests that treatments are more effective when pulse lengths delivered are less than the mean thermal relaxation time of the target vessels (τ, derived from the predicted vessel diameter). There is not, as expected, a stronger response at τ = pulse length. This limited dataset cannot provide an accurate relationship between treatment response, pulse length and predicted vessel diameters but suggests that further investigation would be of interest. This relationship is not supported by the treatment response determined by expert analysis of photographs (Figure 102).

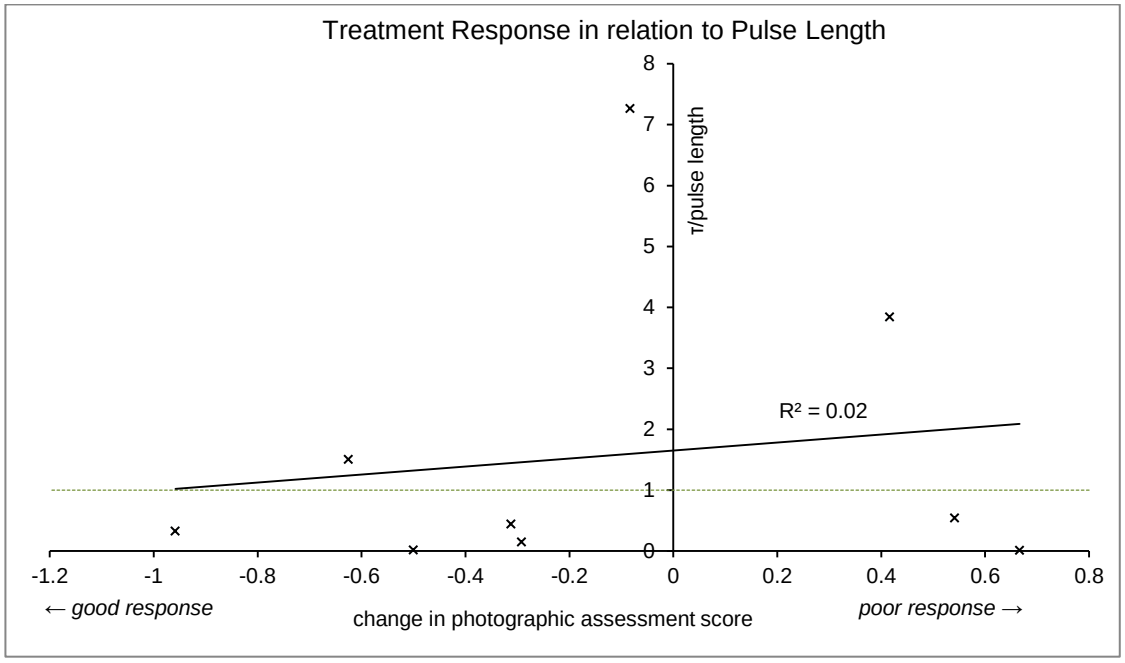

Figure 101: Comparison between ratio of predicted mean thermal relaxation time of PWS vessels to estimated pulse lengths delivered and the mean change in PWS severity following laser treatment assessed by photographic analysis.

Vessel Depth

The predicted individual mean PWS vessel depths of pre-treatment lesion ranged from 70 μm to 460 μm, varying substantially between participants. This is within the range expected from the literature survey (Section 2.1, page 17), with most participants having simulated vessel depths close to the 240 μm mean depth reported by Fiskerstrand *et al* [42]. Mean predicted vessel depths increased after treatment for the majority of participants, with a two-tailed Wilcoxon signed-rank analysis showing a significant difference between the two groups at the $\alpha=0.05$ (95% confidence) level. This suggests that laser treatment was generally most effective at treating the most superficial vessels from each PWS lesion. This again is supported by published experimental findings [42, 262].

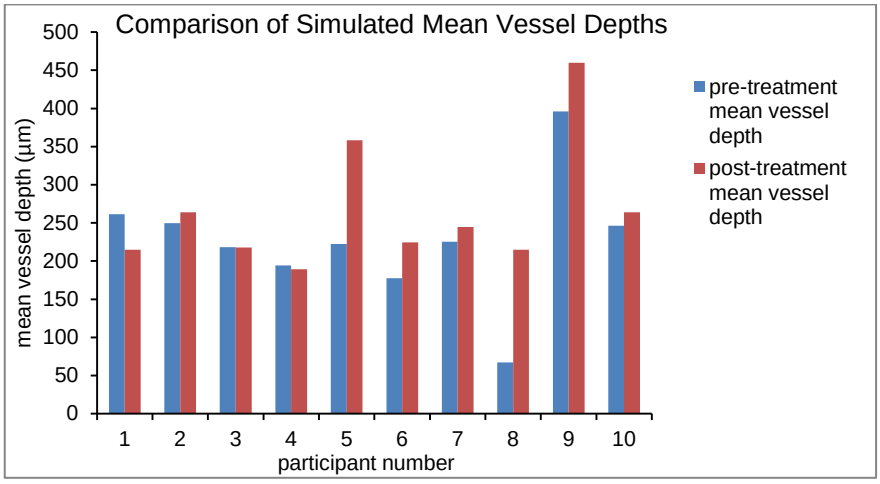

Figure 102: Histogram showing simulated PWS vessel depths for participants analysed by skin colour measurements before and after treatment.

It was expected that deeper vessels would receive a smaller proportion of the radiant exposure incident at the surface of the skin and therefore a PWS consisting of deeper vessels would respond less well to laser treatment. However, there appeared to be no direct relationship between the predicted mean PWS vessel depths and the change in the difference in measured reflection between PWS and adjacent skin (Figure 104).

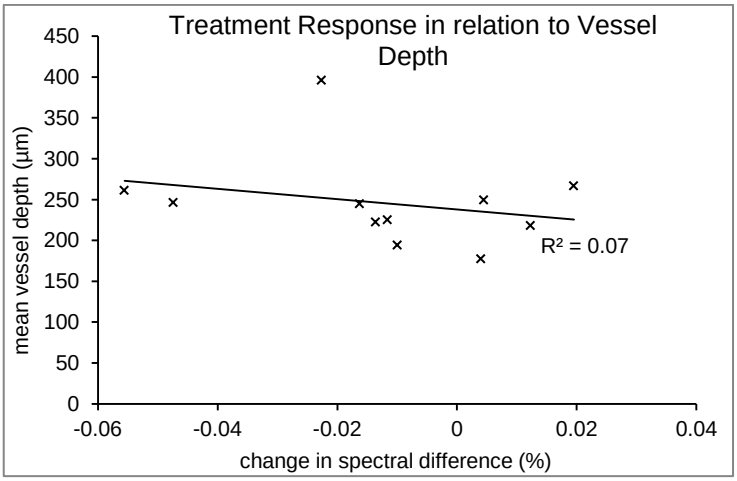

Figure 103: Comparison between predicted mean PWS vessel depths and the change in the difference in spectral reflection between normal and PWS skin following laser treatment.

The Monte Carlo programme provided estimates of absorption and scattering coefficients of the layers represented in the skin model. Thus, through a simple Beer-Lambert model, it is possible to estimate the proportion of laser light incident upon the surface which reaches the predicted mean depth of PWS vessels (L):

$$L = L_0 \exp\left[-\sum_{i=1}^{4} t_i \left(\mu_{a,i}^{600nm} + \mu_{s,i}^{600nm} \right) + \left(d - \sum_{i=1}^{4} t_i \right) \left(\mu_{a,5}^{600nm} + \mu_{s,5}^{600nm} \right) \right] \quad \text{Equation 34}$$

where L_0 is the beam energy incident at the surface of the skin; i represents the layer (layers 1-3 are of the epidermis, layer 4 is the region of dermis superficial to the PWS lesion and layer 5 contains the simulated lesion), t is the thickness of the layer and d is the mean depth of simulated PWS vessels. When compared to the change in the difference in measured reflection between PWS and adjacent skin, the estimated fluence at the predicted mean vessel depth shows a strong correlation with treatment response for this group of participants (exponential relationship, Figure 105).

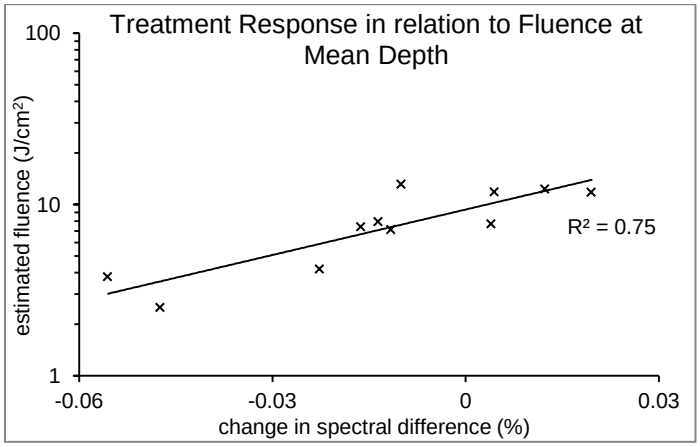

Figure 104: Comparison between predicted fluence at mean PWS vessel depths and the measured change in the difference in spectral reflection between normal and PWS skin following laser treatment.

When compared to assessments of treatment response determined by participant photographs, the predicted PWS vessel depth was not found to correlate with treatment effectiveness (R^2=0.01), or the estimated fluence at the mean depth of simulated PWS vessels (R^2=0.03).

Summary

Overall, the melanin and PWS vessel characteristics predicted by the new Monte Carlo programme appear to be realistic for the participant group considered. These results are supported by a thorough analysis of the literature coupled with expert analysis of participant photographs and, for PWS skin, measurements made through OCT. Furthermore, PWS vessel characteristics predicted by the simulated have been shown to correlate with the results of laser treatment, suggesting that they may serve as predictors for the effectiveness of laser therapy of an individual lesion.

9. Conclusions

9.1 Conclusions from the Work Presented

Literature Survey

The colour of PWS skin is determined primarily by the quantity and distribution of melanins and haemoglobins. The epidermis of pale skin types typically contains melanin volume fractions between 1% and 3%, with melanosomes ranging from 30 nm to 200 nm in diameter. Dermal blood volume fractions are typically between 0.2% and 0.6% in normal skin, but may be twenty times this in PWS skin. This increase is caused by a widening of the vessels from 6-30 μm diameter in normal skin to a typical range of 25-280 μm diameter in PWS skin, with larger vessels and 'vascular lakes' also forming in some cases, particularly in mature PWS. The principal result of this increase in dermal blood volume is a pink, red or purple lesion whose severity and hue varies with the number, depth and diameter of affected vessels.

Laser therapy is the treatment of choice for reducing the contrast in colour between PWS and adjacent, clinically normal skin. This is achieved by selective heating of haemoglobin. Current theoretical and case studies have established a wavelength of 595 nm to be most effective for treating a range of PWS lesions, although around half of participants are thought to respond poorly or not at all to treatment. Further selectivity of ectatic PWS vessels can be attained through selection of appropriate pulse lengths and energy per pulse. This can be achieved only with knowledge of the depth and diameter of vessels in an individual PWS. However, this information is not currently available for the vast majority of participants receiving laser treatment.

Development of the Simulation

An approach involving skin colour measurements and the inverse application of a skin model has been developed in this study, in an attempt to determine estimates of PWS vessel numbers, sizes and depths on an individual basis, such that these could be used to estimate the likely response of an individual lesion to laser treatment and subsequently inform appropriate laser treatment settings.

A Konica-Minolta CM2600d spectrophotometer was selected to perform colour measurements on 14 individuals immediately before treatment. On 10 participants, a second measurement was made at least 12 weeks after, ensuring that the healing process following treatment had been completed. In accordance with studies

published elsewhere in the literature, this device was found to provide excellent repeatability (mean SD per wavelength range of 0.5% reflection across 50 measured datasets) and reproducibility (SD of 0.9% across summer and winter datasets) of skin colour measurements under the protocol developed for this study. These colour measurement data were interpreted using a Monte Carlo simulation.

The Monte Carlo programme developed for this study employed a ray tracing algorithm to simulate light transport through an 8 layer skin model. A new minimisation procedure was developed with the aim of adjusting the quantity of melanin and the diameter of melanosomes in the skin model such that the simulation could reproduce adjacent skin colour. This reproduction was achieved with a mean discrepancy of 1.9% reflection from the measured data across the 14 participants (24 datasets). This is approximately double the expected variation between individual measurements of skin colour (SD=0.9%), demonstrating a consistently good fit across the participant group.

Resultant melanin parameters were considered realistic on the whole when compared to the literature. Melanin concentration (mean 1.7%, range 0.4% to 3.3%) corresponded well with participant skin types identified through expert analysis of photographs (types 1-3), although a review of the scientific literature suggests that epidermal melanin volumes less than 1% are not likely to have been observed for skin types identified in this participant group. The predicted mean melanosome diameters across the participant group (overall mean 223 nm, range 41 nm to 384 nm) was generally greater than expected for individuals of skin types 1-3. It is thought that a higher weighted consideration of shorter wavelengths within the melanin minimisation procedure is likely to have resulted in closer fits between simulated and measured spectra and smaller (more realistic) melanosome diameters within the skin models.

For those participants assessed before and after treatment, there was no significant difference in the melanin volume fraction determined by the simulation between measurement sessions. This is in agreement with the expert photographic analysis, which showed no significant change in skin type between sessions. The predicted melanosome diameters were found to vary significantly between the pre-treatment and post-treatment groups, further suggesting inaccuracies in this parameter.

A second minimisation procedure was developed with the aim of reproducing PWS skin colour. This involved the introduction of horizontal, pseudo-cylindrical vessels into the skin model whose number, diameters and range of depths could be manipulated in response to differences between measured and simulated spectra. PWS skin was reproduced with a mean deviation from the measured data of 2.4% reflection across the 14 participants (25 datasets). This is a value of 1.5% greater than the 0.9% expected variation between measured datasets, and 0.6% greater than the results from the melanin minimisation procedure. This again shows a close fit across the participant group, although particular wavelength regions were identified where the simulated reflectance consistently varied from the measured data. The use of three variables in the minimisation procedure rather than two limited the rate at which convergence could be obtained. This slower convergence along with the computational expense of the simulations (mean 8 days per procedure involving 14 iterations) was considered to be the primary cause for the increase in discrepancy of the PWS vessel minimisation procedure relative to the melanin minimisation procedure.

Predicting the Properties of Normal and PWS Skin

Photographic analysis suggested that the participants studied were primarily of pale Northern European skin types. Mean simulated epidermal melanin volumes were consistent with this, although two participants were predicted to have melanin concentration below the minimum of 1% expected from analysis of the literature.

When comparing the melanin volume fractions predicted by the simulation directly with the mean skin type determined by expert analysis of photographs, participants with assessments of darker skin types were generally found to have higher predictions of epidermal melanin volume fraction (coefficient of determination for a linear fit, R^2=0.41 over 20 data points).

Mean melanosome diameters predicted by the simulation were generally larger than expected for primarily Northern European skin types. It is likely that a higher weighted consideration of wavelengths less than 420 nm within the relevant phases of the melanin minimisation procedure would have both improved the fit between measured and simulated spectra in this region and reduced the predictions of mean melanosome diameters for the majority of participants. The predicted melanosome

diameters were found to correlate with skin darkness scores for the 9 participants assessed by photographic analysis (coefficient of determination for a linear fit, R^2=0.40).

When compared to the results of the literature analysis, the characteristics of PWS vessels predicted by the simulation were realistic on the whole, although the overall mean vessel number density is lower and the mean depth less than the results of skin biopsy studies suggest. This may be due to the increased influence of superficial vessels and the minimal contribution of the deepest PWS vessels upon skin colour. Further investigation would be necessary to determine whether changes in the PWS vessel minimisation procedure, such as a weighting towards the introduction of deeper vessels, could provide more realistic results.

Vessel number densities and mean diameters predicted by the simulation corresponded well with the results of OCT analyses from the 5 participants included in this part of the study, although predicted mean vessel depths were again generally less.

Vessel numbers and mean diameters predicted by the simulation showed agreement with the mean PWS severity determined by expert analysis of photographs. Once again, the predicted mean vessel depths were not supported by this assessment.

Predicting Treatment Effectiveness

Treatment response, as determined through spectrophotometry measurements, was not found to correlate directly with either the pre-treatment melanin volume fraction or mean melanosome diameter predicted by the simulation. This is supported by photographic analysis, which also showed no direct correlation between pre-treatment adjacent skin darkness scores and treatment effectiveness for this participant group.

The fluence of laser light reaching the depth of vessels was considered as a factor in determining the effectiveness of treatment. Using the predicted values of both mean vessel depth and the light absorption and scattering coefficients of overlying skin, estimates of the mean fluences reaching PWS vessels were made. These were found to correspond strongly (R^2>0.75) with treatment response assessed by spectrophotometry but did not correspond with treatment response determined by photographic assessment.

Laser treatment is widely believed to be more effective when pulse lengths match the thermal relaxation times of target vessels. The thermal relaxation time is a function of the vessel diameter. The pre-treatment vessel diameters (and therefore the ratio of thermal relaxation times to pulse lengths) predicted by the simulation were found to correlate with the treatment results determined both by spectrophotometry and photographic assessment (linear relationship, $R^2>0.25$).

Although comparison with OCT analysis and expert photographic analysis suggest that the simulation provided a reasonable approximation of PWS vessel number density, this parameter was not found to be a useful predictor of treatment response.

It can be concluded that the information contained within the colour of an individual PWS lesion may be extracted through the inverse application of a skin model. Furthermore, the results from this study suggest that the PWS parameters predicted by the new Monte Carlo model may be used to inform the likely efficacy of individual laser treatments and therefore to inform appropriate laser settings on an individual basis.

9.2 Future Work

The primary shortcoming within the current Monte Carlo programme is the accuracy with which adjacent skin is reproduced. Although the discrepancies between simulated and measured spectra are small on average, wavelength regions have been identified where consistent deviation are found. It has been considered within the analysis of this work that the adjustment of melanosome diameters should consider, with a greater weighting, the shortest wavelengths available. Furthermore, greater flexibility in the melanin minimisation procedure may be obtained from independent adjustment of melanin parameters from each epidermal layer within the skin model. As many of the discrepancies from the melanin minimisation procedure appear to have been translated to discrepancies following the PWS vessel minimisation procedure, such advances in the Monte Carlo programme are likely to result in better reproduction of skin colour measurements and greater confidence in the parameters derived.

This study was designed as a proof of principle, to determine whether the inverse application of a skin model could be used to determine PWS vessel parameters which may be used to inform laser treatment. As a result, the direct application of the technique within a clinical setting was not considered a priority. In order to improve the usability of this method within the clinic, processing times need to be improved. This may be achieved with greater consideration of expensive processes within the programme. Further to this, techniques involving programming onto computing graphic cards have been shown to vastly reduce processing times in Monte Carlo simulations of skin optics [263, 264]. An increase in processing speed may also allow for the use of more beams initiated per reflectance data point, further improving the accuracy of the colour reproduction by reducing stochastic 'noise'.

Further to this, greater confidence in the correlations between predicted parameters and the results of laser treatment would be obtained with a larger participant group. In particular, the inclusion of participants with darker skin types, as well as suitable skin lesions other than PWS, would serve to test the extent of the capabilities of the Monte Carlo programme developed in this study. With greater confidence in the relationship between the predicted parameters and the results of laser treatment, it may be possible for the programme to recommend treatment parameters and predict

likely degrees of fading from a session of laser treatment. From the results presented so far, the recommendation of appropriate pulse widths is likely to possible.

Further improvements to the current Monte Carlo programme may include the consideration of skin lipids and other constituents or chromophores within the skin model, with the ability to adjust these within the minimisation procedure. Such a technique would be of particular value for the adjacent skin minimisation procedure, but may also contribute to the PWS minimisation procedure when considering, for example, localised tissue oedema. The thickness of vessel walls as a proportion of the total vessel diameters is a further parameter that could be adjusted. This would provide a means of estimating the effect of this parameter upon PWS colour for the first time. Beyond these considerations, the consideration of more complex vessel architecture, involving bends, splits and directions other than horizontal for example, may be used to better represent PWS skin.

Greater coupling between the simulated and measured colour data may be achieved through consideration of the angular distribution of the illumination source. A direct measurement of this for a particular device could be translated directly into the illumination source within the Monte Carlo programme. This would provide a more accurate simulation than the uniform distribution applied at present. In addition, a skin surface scattering model beyond that of the Fresnel relations, such as those used in the computer graphics industry, may be considered [169].

Appendices

Appendix A

A summary of the work presented at the BMLA Annual Conference 2011[19]

Based upon a literature survey and backed up by theoretical modelling, this work considered the optimal laser treatment parameters for vascular lesions such as PWS. In particular, it focussed upon the choice of wavelength and pulsewidth.

Wavelength

A previous version of the Monte Carlo method presented in this thesis was used to simulate the transport of light through a 7 layered skin model. Initially, the simulation was used to determine the absorption and scattering coefficients of the author's left volar forearm. The model assumed a 1% volume fraction of melanin in the living epidermis (Caucasian skin) and assigned blood volume fractions to the dermal layers according to Meglinski and Matcher's work [153]. The simulation consisted 100,000 photon packets at each wavelength and 10 iterations of a minimisation procedure which considered the absorption and scattering coefficients of the dermis and epidermis were carried out.

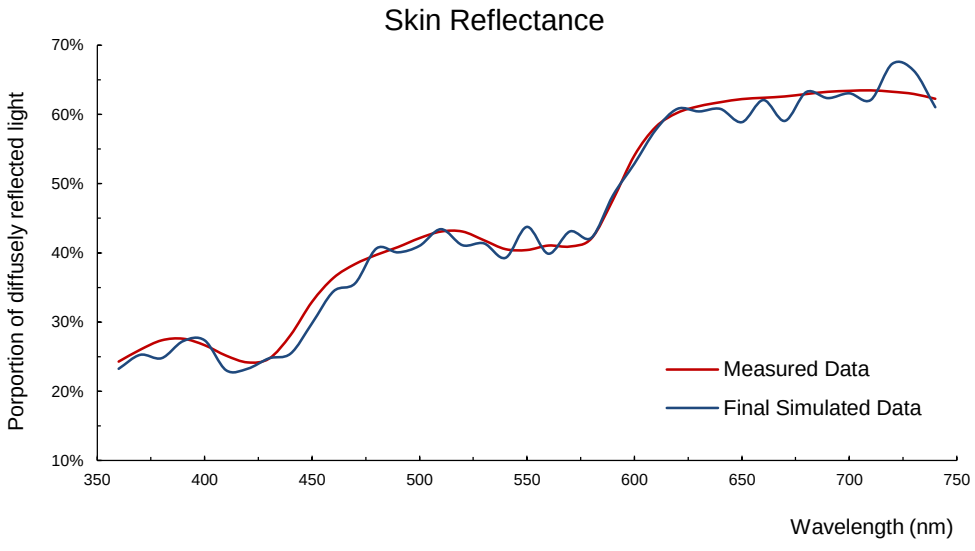

Figure 105: Comparison of mean reflectance data of the author's left volar forearm taken from 10 consecutive measurements using the Konica-Minolta CM2600d spectrophotometer.

Figure 106 shows good agreement between the skin model and the colour measurements performed on the author's left volar forearm.

Subsequently, a 500 µm thick homogeneous layer with a blood volume fraction of 20% was added to the skin model to simulate a vascular lesion. The layer was placed successively at depths of 100 µm, 600 µm and 1100 µm in the skin, to simulate a superficial, mid-dermal and deep dermal lesion respectively. The simulation was performed over 100,000 photon packets at each wavelength for each scenario (Figure 107).

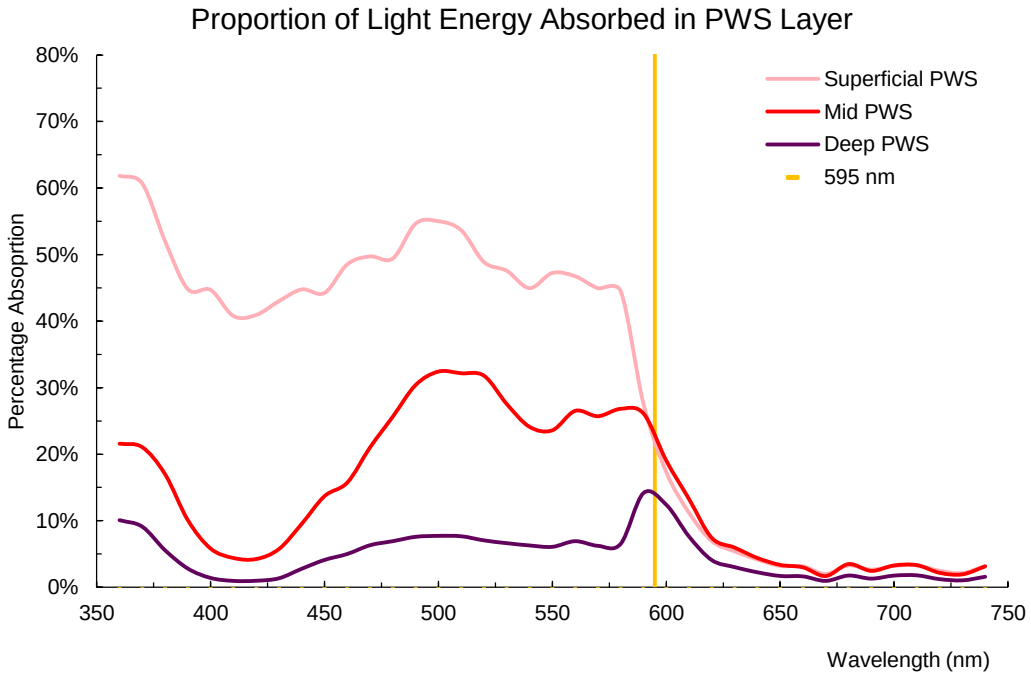

Figure 106: Proportion of laser light energy absorbed for blood layers at three depths (superficial dermis, mid dermis and deep dermis).

The simulation predicts green light (~500 nm) would be most suitable for superficial lesions but wavelengths similar to those in current routine practice (~595 nm) are best suited to deeper lesions. Infra-red wavelengths are considered to penetrate further and therefore may be more suitable for the deepest lesions [265-268], although a comparison could not be made during this study.

Pulse length

Equation 35, as described by Anderson and Parrish [56] was used to consider the optimal pulse length for targeting ectatic vessels:

$$\tau \cong \frac{R^2}{4\chi} \qquad \text{Equation 35}$$

where τ is the thermal relaxation time, the time required for significant cooling of a small target structure, R is the radius and χ is the thermal diffusivity. It has been

suggested that the optimal pulse length for a vascular laser treatment is equal to the thermal relaxation time of the target vessels [56].

The literature survey concluded that vessel diameters in normal skin varied from 6-30 μm [17, 20] whereas PWS skin contained vessels up to around 300 μm [20]. Table 16 summarises the thermal relaxation times for a range of vessel diameters found in PWS skin:

Vessel Diameter (2*R*)	**Optimal Pulse/Sequence Time** Anderson & Parrish [56]
30 μm	0.3 ms
50 μm	1.1 ms
100 μm	4.5 ms
200 μm	18 ms
300 μm	41 ms

Table 16: Summary of thermal relaxation times for various vessel sizes, calculated from Equation 35 [56] using a fixed value of $X = 1.39 \times 10^{-7}$ [72]

A review of the literature concluded that more contemporary works considering the optimal pulse lengths for vascular lesions [1, 231, 269] were in agreement with the above tabulated values.

Conclusions

The study concluded that information regarding the depth and size of affected vessels is required to choose optimal settings for the laser treatment of vascular lesions such as PWS.

Appendix B

A description of the Logarithm of the Inverse Reflectance (LIR)

In dermatological studies, it is most often the absorption of light that is of interest, rather than the reflection or backscatter. This has been approximated using the following relationship [101]:

$$\rho_a(\lambda) \propto log_{10}\frac{1}{\rho_r(\lambda)} \qquad \text{Equation 36}$$

where λ represents a wavelength within the visible spectrum, $\rho_a(\lambda)$ is the light absorption coefficient and $\rho_r(\lambda)$ is the light reflectance coefficient. This approximation, known as the LIR (Logarithm of the Inverse Reflectance), assumes that the skin can be described optically as consisting of layers, each of which homogeneously transmits and scatters light. The interface between these layers is assumed to have no effect.

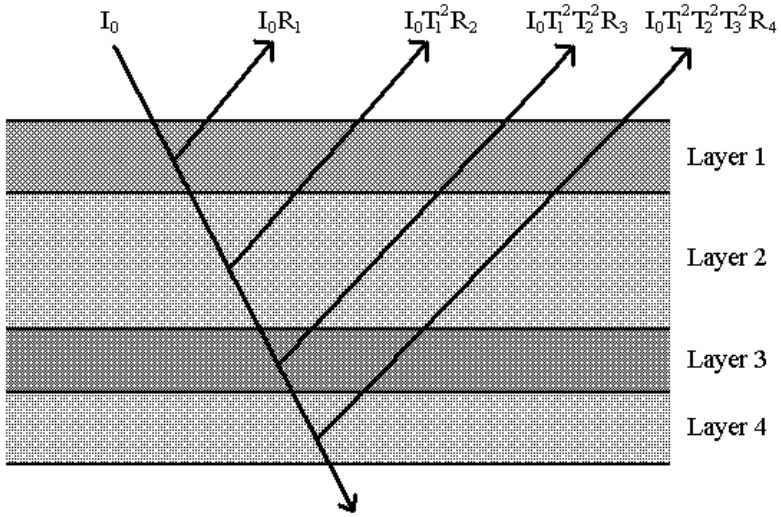

Figure 107: Demonstration of the LIR assumption, where I_0 is the intensity of incident light, R_N is the reflection from the Nth layer and T_N is the transmission through layer N.

From Figure 108, we can see that this model provides us with a reflected light intensity:

$$I_R = I_0(R_1 + T_1^2R_2 + T_1^2T_2^2R_3 + T_1^2T_2^2T_3^2R_4) \qquad \text{Equation 37}$$

this gives the total reflectance:

$$R_s = I_R/I_0 = R_1 + T_1^2R_2 + T_1^2T_2^2R_3 + T_1^2T_2^2T_3^2R_4 \qquad \text{Equation 38}$$

one further assumption of this model is that negligible reflection takes place from within the top layers of the skin and thus the vast majority of reflection occurs within the deepest layer, thus:

$$R_s \approx T_1^2 T_2^2 T_3^2 R_4 \qquad \text{Equation 39}$$

or

$$\log_{10}\left(\frac{1}{R_S}\right) = -2\log_{10}(T_1) - 2\log_{10}(T_2) - 2\log_{10}(T_3) - \log_{10}(R_4) \qquad \text{Equation 40}$$

If we define the absorption coefficient using the Beer-Lambert relationship: $T = e^{-\mu_t d}$, where μ_t is the attenuation coefficient and d is the optical path length, then substituting:

$$\log_{10}\left(\frac{1}{R_S}\right) = -2\log_{10}(e^{-\mu_{t1} d}) - 2\log_{10}(e^{-\mu_t 2d}) - 2\log_{10}(e^{-\mu_{t3} d}) - \log_{10}(R_4)$$

Equation 41

substituting $= -2\log_{10}(e^{-\mu_{ti} d})$ for ρ_{a_i}, the light absorption coefficient for layer *i:*

$$\log_{10}\left(\frac{1}{R_S}\right) = \rho_{a_1} + \rho_{a_2} + \rho_{a_3} + constant \qquad \text{Equation 42}$$

or

$$\rho_a \propto \log_{10}\frac{1}{R} \quad \text{where} \quad \rho_a = \rho_{a_1} + \rho_{a_2} + \rho_{a_3} \qquad \text{Equation 43}$$

Appendix C

*A description of CIEL*a*b* Colour Space*[9]

Colour space is a way of describing a given colour using a predetermined set of characteristics, or dimensions. Perhaps the most widely known colour space is the Commission Internationale de l'Eclairage (CIE) RGB colour space. This describes any perceptible colour using a mixture of three *primary* colours at 700 nm (red), 546.1 nm (green) and 435.8 nm (blue). In 1931, the CIE recognised that perceptible colours required negative values of these primary colours to describe them. To remedy this, they released the CIE*xyz* tristimulus values whose imaginary colour matching functions $\bar{x}(\lambda)$, $\bar{y}(\lambda)$ and $\bar{z}(\lambda)$ are capable of describing all perceptible colours without the need for negative values.

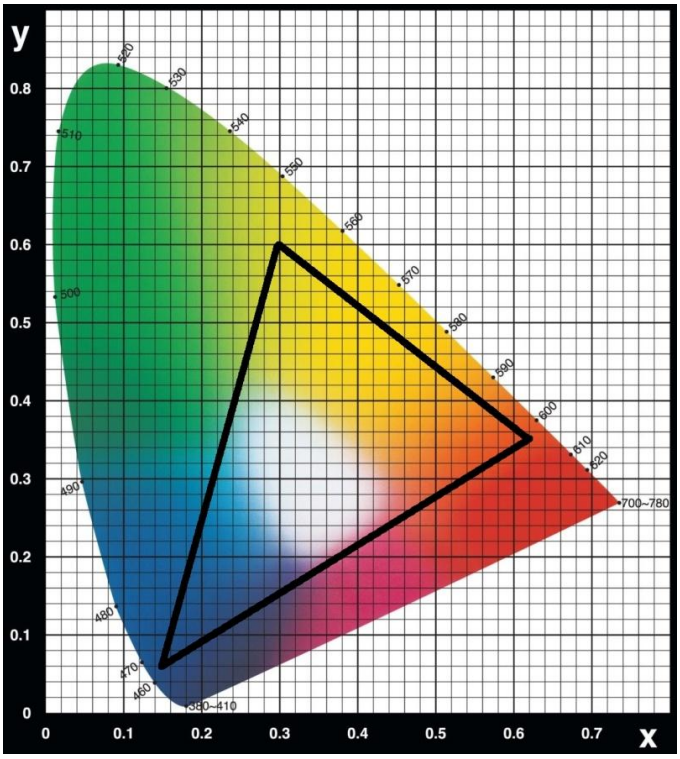

Figure 108*:* Chromaticity diagram in Yxy colour space comparing those colours described the xyz tristimulus values and those described by RGB values (black triangle). © Colour Graphs: Courtesy of Konica Minolta Sensing Europe B.V.

[9] from the publication: 27. Lister TS, Wright PA and Chappell PH. Spectrophotometers for the clinical assessment of port wine stain skin lesions: A review. *Lasers in Medical Science*, 2010, **25**(3): 449.

Although CIE*xyz* has found use in dermatological studies, its successor, the CIEL*a*b* (1976) model, has been given the most attention over the last two decades (66). Designed as a perceptually uniform colour space, it has the advantages of being conceptually simple and inherently meaningful in clinical assessment, in particular from a cosmetic perspective.

CIEL*a*b* defines colours in terms of three-dimensional co-ordinates in colour space. L* represents luminance, or lightness, where 0 corresponds to black and 100, a perfect white with intermediate values covering a greyscale which varies in a perceptually uniform manner. Similarly, a* represents colour in the red (+60) to green (-60) dimension and b* represents yellow (+60) to blue (-60). a* and b* co-ordinates may be conceptually related to Hering's opponent colour theory (67), based upon the proposition that the human retina contains opponent colour channels that distinguish colour according to their red vs. green and blue vs. yellow attributes.

Colour differences can be described in a number of ways, by evaluating the distance between two points in the defined three dimensional colour space. Koster *et al* (20) are amongst those who used ΔE as a colour difference descriptor when comparing normal and PWS skin:

$$\Delta E = [(\Delta L^*)^2 + (\Delta a^*)^2 + (\Delta b^*)^2]^{1/2} \qquad \text{Equation 44}$$

ΔE represents the Euclidean distance between two points in CIEL*a*b* colour space and describes the overall change in colour. This is both conceptually simple and meaningful, as it can be used to describe the overall perceived contrast between PWS and normal adjacent skin.

More recently, recognised deviations of CIEL*a*b* space from perceptual uniformity have resulted in new colour appearance models such as CIECAM02 (2002) used in Windows Vista's Windows Color System for example. However, the loss of conceptual simplicity from CIEL*a*b* has limited the popularity of these models to date in the field of dermatology.

Appendix D

Specifications of the Konica-Minolta CM2600d Spectrophotometer

The spectrophotometer used for this study is a commercially available device from Konica-Minolta (Tokyo, Japan). The device is designed to perform large numbers of measurements and is primarily used in the industrial sector, to determine the colour consistency of products in a manufacturing line for example. The fundamental setup of this device is much the same as other devices used for this purpose. However, rather than a single lamp, the CM2600d has three separate lamps for determining the UV and spectral contributions to the measured spectra and a further bulb to calculate specular contributions. The principal setup of the device is detailed in Figure 110. Unfortunately, for commercial reasons, Konica-Minolta are limited in the information they are willing to provide about the device and its components.

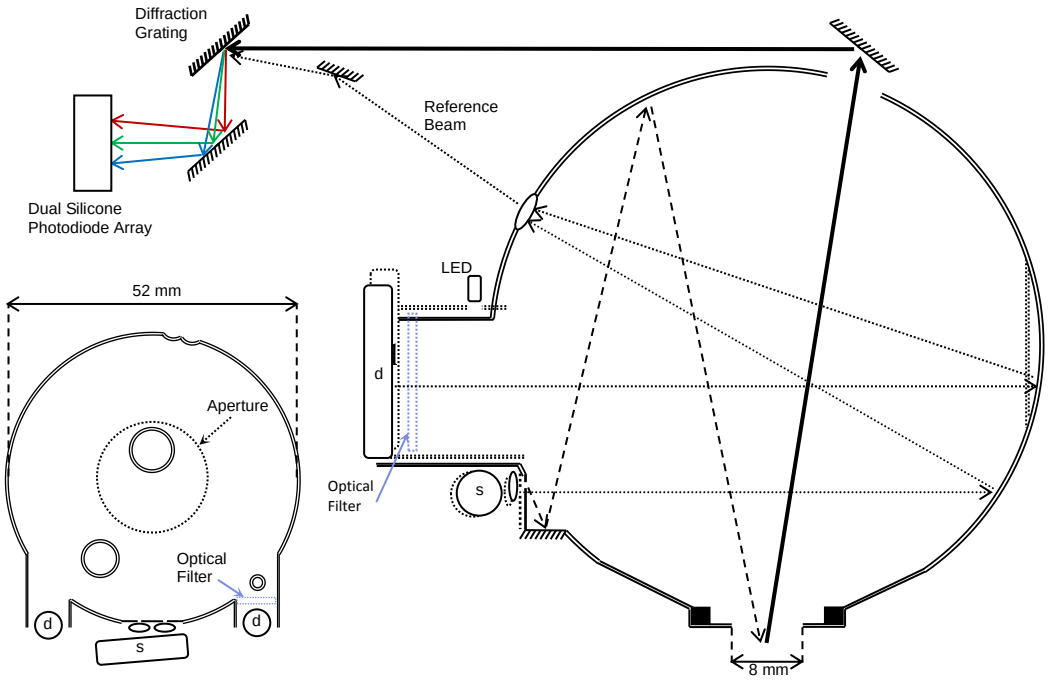

Figure 109: Schematic diagram showing the basic setup of the Konica-Minolta CM-2600d. Double lines represent the edges of the 52 mm diameter integrating sphere ($BaSO_4$ coated). The aperture at the bottom of the right diagram (dotted centre of left diagram) is placed at the skin surface. The letters 's' and 'd' refer to the xenon flashlamps used for spectral and diffuse measurements respectively. One of the 'd' illuminants has an optical filter to cut out UV components (below 400 nm).

Illumination

The device has three separate xenon flashlamps. Correction for the variation in intensity across the visible spectrum of each xenon lamp is achieved through calibration. Calibration is carried out by taking an average of three measurements from a standard white tile when starting the device, followed by an average of three 'black' measurements where the aperture is placed in free space. Corrections are made automatically to the subsequent measurements. During this study, calibration was performed before each set of measurements, *i.e.* between each participant.

Each of the three lamps has a specific function. The first (marked *d* but without a filter in Figure 110) is used to determine the diffuse reflectance (referred to as *specular excluded*). This is achieved by setting the lamp back from the integrating sphere and thus only illuminating the aperture indirectly, via the integrating sphere. Light returning from the aperture is deflected towards a diffraction grating and the intensity across the wavelength range is measured using a silicone photodiode array. A reference beam is also directed to the diffraction grating and to an adjacent silicone photodiode array to be measured simultaneously, such that an automated algorithm may be performed which accounts for variations between pulses for this lamp.

An equivalent process is used for the filtered lamp marked *d* in Figure 110. When a measurement of the spectral reflectance exclusive of contributions below 400 nm is required, both this lamp and the previously described *d* lamp are used successively. The data returned includes near zero values for wavelengths of 400 nm and below.

The third lamp, marked *s* in Figure 110, is used to determine the specular contribution to the measured spectrum. The light enters the integrating sphere through two lenses. The first focuses the beam onto the upper wall of the integrating sphere and illuminates the aperture directly from here. The second is focused on the laterally opposing wall and forms a reference beam as depicted in Figure 110. When taking a measurement, this lamp is triggered immediately after the *d* lamp(s). The specular component is internally calculated and added to the diffuse measurement. The *specular included* data is returned.

Up to two datasets can be returned during each measurement with the spectrophotometer. The choice was made for this study to return both the *specular*

included and *specular excluded* reflectance measurements including all light below 400 nm (unfiltered option). Specular included data were used as the primary input into the Monte Carlo programme.

There is a further LED which is used along with a viewing port (accessible by folding the mirror shown in Figure 110 down), but is not used for taking measurements.

Integrating Sphere

The integrating sphere is coated with $BaSO_4$ which is highly reflective at all wavelengths in the visible spectrum and forms a rough (diffusing) surface. It is not entirely spherical in shape but instead meets a conical surface near the aperture. It is also impregnated with various windows and indentations to accommodate the light sources and measurement optics. Furthermore, there is a thin horizontal ridge around the entire inner circumference of the integrating sphere approximately half way up. This appears to be where the two halves of the integrating sphere meet. Despite these imperfections, it was assumed that the light incident upon the aperture is perfectly diffuse.

Further Optics

Light is separated into its spectral components using a diffraction grating, the precise details of which are not available from the manufacturer. Measurements are made using a dual silicone photodiode array with a half bandwidth of 10 nm. According to the manufacturer's specifications, the half bandwidth for this array is equal to the measurement pitch (see Figure 111). This suggests that there will be some (minor) overlap in the measured contributions from neighbouring wavelength ranges.

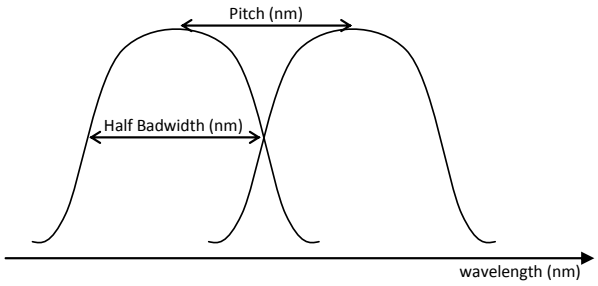

Figure 110: Demonstration of half bandwidth and wavelength pitch.

Appendix E

This appendix provides the values used for the analysis of absorption (Table A1) and reduced scattering coefficients (Table A2) reported in the literature. * denotes values obtained from graphical presentations. The remaining data was extracted directly from the text or tables of the publications unless otherwise stated below.

Absorption Coefficients

Meglinski and Matcher's calculated absorption coefficients were presented separately for the dermis and epidermis. Epidermal absorption coefficients were calculated using Meglinski and Matcher's equation 14 [153] with the following inputs: $C_{melanin}$ = 2.0%, C_{H20} = 20%, $\mu_a^{(0)} = (7.84 \times 10^6)\lambda^{-3.225}$ (equation 10 in their paper and from [107]) , $\mu_a^{melanin} = (5 \times 10^9)\lambda^{-3.33}$ and $\mu_a^{H_20}$ taken from [149]. The dermal absorption coefficients were calculated separately for the papillary layer, upper and lower blood net layers and the reticular dermis using the concentration and blood and water presented in their Table 2, value of $\mu_a^{H_20}$ taken from [149], and values of μ_a^{Hb} and $\mu_a^{Hb0_2}$ also taken from [149].

Svaasand *et al*'s epidermal and dermal absorption coefficients were calculated from their equation 6, with values of μ_{ab} calculated using their equation 2. Values of μ_{an} were calculated from [107], and a value of $\mu_{am,694}$ = 0.3 mm^{-1} corresponding to Caucasian skin (see their Figure 3). Epidermal and dermal blood volume fractions of 0.2% and 2% were applied to the epidermal and dermal layers respectively.

Zonios *et al*'s absorption coefficients were calculated from their equation 18 using parameters of melanin and absorption concentrations, as well as blood oxygen saturation, presented in their Table 2. The paper by Zonios *et al* did not describe the origin of the haemoglobin and oxyhaemoglobin extinction coefficients applied in their study, thus it was assumed that values taken from [270] were used, as was the case in a previous paper by Zonios *et al* [186].

The blood absorption coefficients used in these three studies are presented in Figure A1 for comparison.

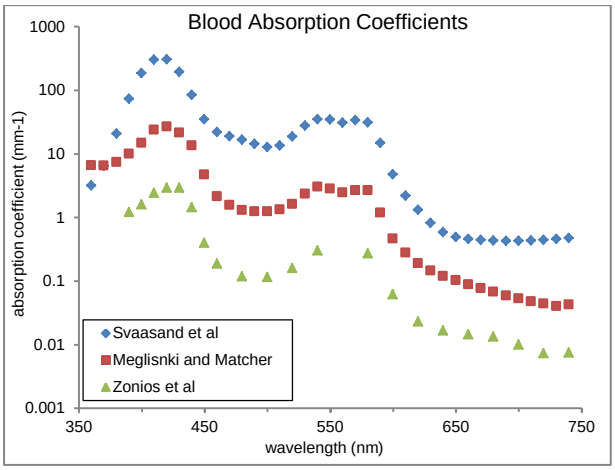

Figure 111: Blood absorption coefficients used in three of the studies analysed here.

Reduced Scattering Coefficients

Torricelli *et al*'s study presented separate datasets for the arm, head and abdomen from 3 participants. The mean of these 9 values for each wavelength, determined from graphical data, is presented here. Equation 3 from Svaasand *et al*'s work and Equation 19 from Zonios *et al*'s work were used to calculate the values presented in the Appendix. Zonios *et al*'s equation 19 required inputs of d_0, d_s and μ_s' which were selected as normal skin values from Zonois *et al*'s paper as 0.0625 µm, 0.49 µm and 2.1 mm^{-1} respectively.

Table 17: Absorption coefficients (mm^{-1}) available from the literature. Precision of recorded value is dependent upon the nature of the original values presented.

									in vivo absorption coefficients (mm^{-1})									
wavelength (nm)	Jacques 87	Prahl 1988*	Chan 1996*	Salomatina 2006 epidermis*	Salomatina 2006 dermis*	Graaf 1993	Simpson 1998*	Dognitz 1998*	Torricelli 2001* (mean)	Meglinski 2002 epidermis†	Meglinski 2002 dermis†*	Graaf 1993	Doornbos 1999† arm	Doornbos 1999† forehead	Svaasand 1995 epidermis	Svaasand 1995 dermis	Zonios 2006	Bosschaart 2011
360										0.60	0.79				1.50	0.41		
370										0.55	0.78				1.56	0.41		
380										0.50	0.89				1.84	0.52		
390										0.46	1.20				3.07	1.02	1.22	
400			1.4	1.5	0.9			0.6		0.42	1.78				5.83	2.13	1.61	
410										0.39	2.88				8.68	3.27	2.42	
420										0.36	3.23				8.68	3.28	2.92	
430										0.33	2.57				5.84	2.15	2.93	
440										0.31	1.62				3.05	1.04	1.44	
450		5.1	1	1	0.6					0.29	0.566				1.77	0.53	0.40	0.72
460		4.7								0.27	0.258				1.40	0.39	0.19	0.66
470		4.9								0.25	0.189				1.28	0.35		0.58
480		4.3								0.23	0.156				1.19	0.31	0.12	0.54
490		3.9								0.22	0.149				1.10	0.28		0.43
500		3.6	0.6	0.7	0.35			0.24		0.20	0.150				1.03	0.26	0.11	0.34
510		3.1								0.19	0.160				1.01	0.26		0.29
520		2.7								0.18	0.194				1.11	0.30	0.16	0.27
530		2.6								0.17	0.283				1.31	0.38		0.33
540		2.5								0.16	0.362				1.47	0.45	0.30	0.37
550		2.2	0.4	0.45	0.25					0.15	0.338				1.44	0.44		0.34
560		2.1								0.14	0.294				1.32	0.40		0.31
570		2.0								0.13	0.320				1.37	0.42		0.33
580		2.0								0.13	0.321				1.29	0.39	0.27	0.29
590		1.8								0.12	0.143				0.86	0.22		0.18
600		1.9	0.3	0.3	0.2					0.11	0.056				0.59	0.12	0.06	0.08
610		1.6							0.027	0.11	0.034				0.51	0.09		
620		1.5							0.023	0.10	0.023				0.47	0.08	0.02	
630	2.7	1.3	0.3	0.25	0.15	0.12	0.035	0.06	0.019	0.10	0.018	0.003	0.017	0.009	0.45	0.07		
640		1.3					0.032		0.017	0.09	0.015				0.42	0.06	0.02	
650		1.4	0.3	0.25	0.15		0.029		0.016	0.09	0.013				0.41	0.06		
660		1.4					0.026		0.015	0.08	0.011		0.013	0.005	0.40	0.06	0.01	
670		1.3					0.024		0.014	0.08	0.010				0.38	0.05		
680		1.3					0.022		0.013	0.08	0.008				0.37	0.05	0.01	
690		1.3					0.02		0.012	0.07	0.007				0.36	0.05		
700		1.1	0.2	0.25	0.15		0.01	0.04	0.012	0.07	0.007		0.009	0.002	0.35	0.05	0.01	
710		1.2					0.018		0.012	0.07	0.006				0.34	0.05		
720		1.1					0.017		0.012	0.06	0.006				0.33	0.04	0.01	
730		1.1					0.017		0.012	0.06	0.006				0.32	0.04		
740		1.1	0.2	0.2	0.15		0.017		0.013	0.06	0.006				0.31	0.04	0.01	

Table 18: Reduced scattering coefficients (mm^{-1}) available from the literature. Precision of recorded value is dependent upon the nature of the original values presented.

	in vivo reduced scattering coefficients (mm^{-1})														
Wavelength (nm)	Jacques 87	Prahl 1988*	Chan 1996*	Salomatina 2006 epidermis*	Salomatina 2006 dermis*	Graaf 1993	Simpson 1998*	Dognitz 1998*	Torricelli 2001* (mean)	Graaf 1993	Doornbos 1999 arm	Doornbos 1999 forehead	Svaasand 1995	Zonios 2006	Bosschaart 2011
360													80.6	2.25	
370													78.4	2.23	
380													76.3	2.22	
390													74.4	2.20	
400			3.4	10	7.5			4.2					72.5	2.18	
410													70.7	2.17	
420													69.0	2.15	
430													67.4	2.13	
440													65.9	2.12	
450		14.0	2.9	9	6								64.4	2.10	2.08
460		14.0											63.0	2.08	2.03
470		13.0											61.7	2.07	2.00
480		13.0											60.4	2.05	1.96
490		12.0											59.2	2.03	1.93
500		12.0	2.4	7	4.5			4.1					58.0	2.02	1.90
510		12.0											56.9	2.00	1.87
520		12.0											55.8	1.98	1.83
530		11.0											54.7	1.97	1.80
540		11.0											53.7	1.95	1.77
550		10.5	2.1	6	3.5								52.7	1.93	1.74
560		10.5											51.8	1.92	1.71
570		10.0											50.9	1.90	1.68
580		10.0											50.0	1.88	1.65
590		10.0											49.2	1.87	1.62
600		9.5	1.8	5	3								48.3	1.85	1.60
610		9.0							1.52				47.5	1.83	
620		9.0							1.48				46.8	1.82	
630/633	18.73	9.0	1.7	5	3	5.25	2.8	3.2	1.44	1.45	0.91	1.67	46.0	1.80	
640		9.0					2.7		1.39				45.3	1.78	
650		9.0	1.6	4.5	3		2.6		1.38				44.6	1.77	
660		8.5					2.5		1.35		0.87	1.62	43.9	1.75	
670		8.5					2.5		1.33				43.3	1.73	
680		8.0					2.4		1.31				42.6	1.72	
690		8.0					2.3		1.29				42.0	1.70	
700		8.0	1.4	1.3	2.5		2.3	2.9	1.29		0.81	1.54	41.4	1.68	
710		8.0					2.2		1.28				40.8	1.67	
720		7.5					2.2		1.27				40.3	1.65	
730		7.5					2.2		1.25				39.7	1.63	
740		7.5	1.3	1.3	2.5		2.1		1.21				39.2	1.62	

Appendix F

Included here is an example page from the document used to record the expert analyses of participant photographs.

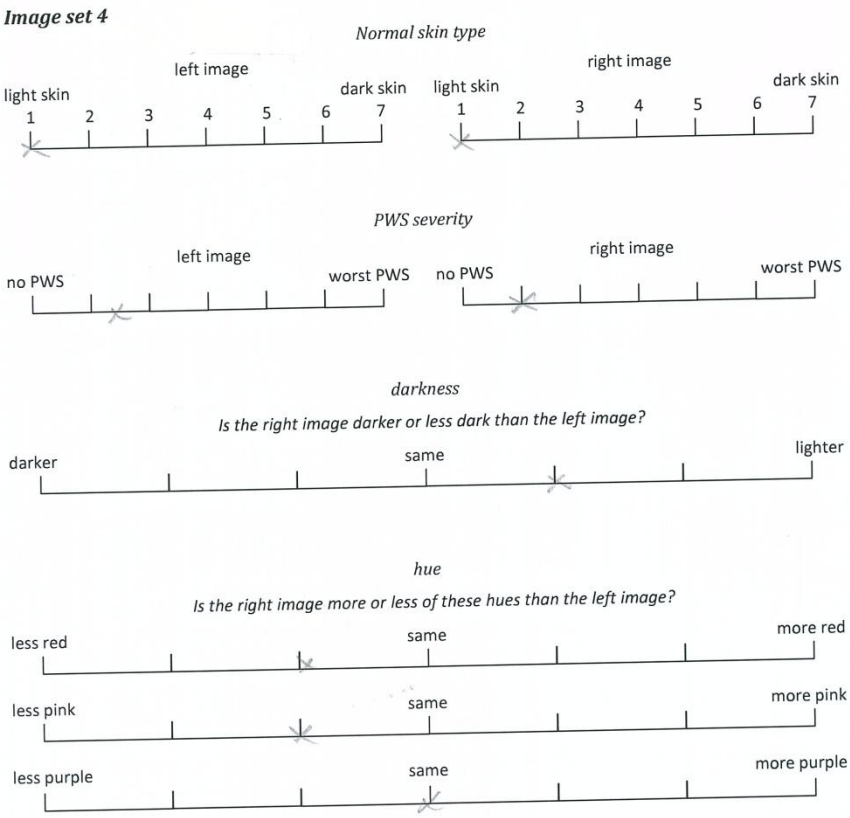

Appendix G

This Appendix provides a summary of the work carried out to determine appropriate temporal pulse lengths to be used in the analysis of results.

The temporal pulse profile of the Cynosure Cynergy Pulsed Dye Laser used for the treatment of participants enrolled into this study was determined using a simple photodiode and oscilloscope, setup as depicted in Figure 113.

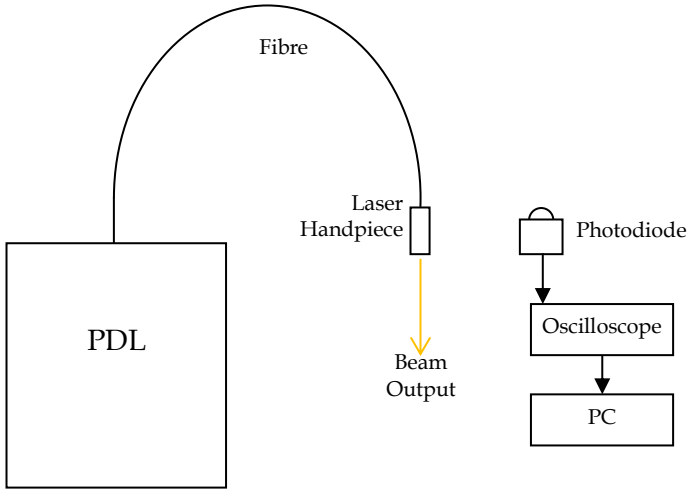

Figure 112: Experimental setup of temporal pulse profile recordings.

The photodiode was offset from the beam output to avoid damage from direct irradiation. Thus, recordings were made of the room illumination caused by diffuse reflection of the laser beam.

Data was recorded directly onto a PC and pulse lengths determined at the 10% level (Figure 114). Where a pulse consisted of more than one distinct peak, or 'pulselet', a weighted mean of the recorded pulsewidths (Ω) was used in the analysis as follows:

$$\Omega = \frac{1}{k}\left[\sum_{i=1}^{k} \frac{\left(\tau_i^F - \tau_i^S\right)\int_{\tau_i^S}^{\tau_i^F} E(t)\delta t}{\int_{\tau_1^S}^{\tau_k^F} E(t)\delta t}\right] \qquad \text{Equation 45}$$

where k is the number of pulselets, τ_i^S and τ_i^F are the start and finish times of pulselet i, and E is the relative energy density recorded by the photodiode.

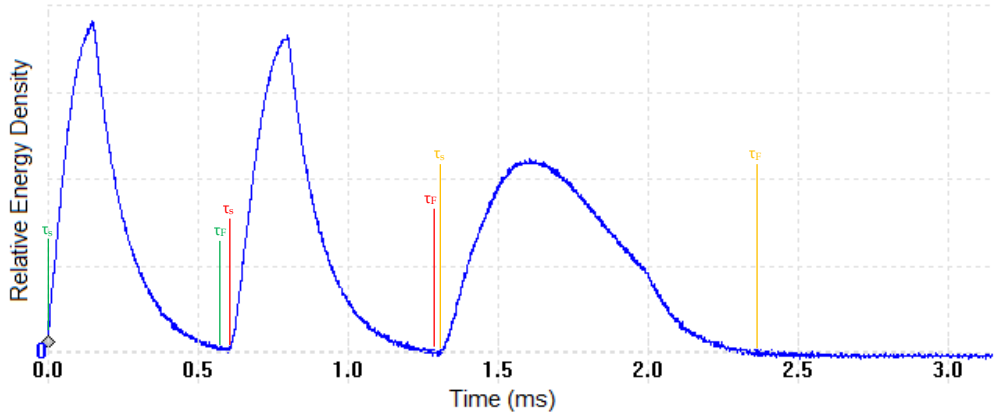

Figure 113: Example temporal pulse profile recording of a nominal 2 ms pulse.

References

1. Nelson JS, Milner TE, Tanenbaum BS*, et al.* Infra-red tomography of port-wine-stain blood vessels in human skin. *Lasers in Medical Science*, 1996, **11**(3): 199-204.

2. van Gemert MJC, Nelson JS, Milner TE*, et al.* Non-invasive determination of port wine stain anatomy and physiology for optimal laser treatment strategies. *Physics in Medicine and Biology*, 1997, **42**(5): 937-950.

3. McGrath JA and Uitto J. *Anatomy and organization of human skin*. In Rook's textbook of dermatology 7th ed. Wiley-Blackwell, 2004.

4. Standring ed. S. *Gray's anatomy: The anatomical basis of clinical practice: 39th edition*. 174. Churchill Livingstone, 2005.

5. Lister TS, Wright PA and Chappell PH. The optical properties of human skin. *Journal of Biomedical Optics*, 2012, **17**(9): 90901-90901.

6. Alaluf S, Atkins D, Barrett K*, et al.* Ethnic variation in melanin content and composition in photoexposed and photoprotected human skin. *Pigment Cell Research*, 2002, **15**(2): 112-118.

7. Bashkatov AN, Genina EA, Kochubey VI*, et al.* Optical properties of melanin in the skin and skin-like phantoms. *Proceedings of the SPIE - The International Society for Optical Engineering*, 2000, **4162**(219-226.

8. Minwalla L, Zhao Y, Le Poole IC*, et al.* Keratinocytes play a role in regulating distribution patterns of recipient melanosomes in vitro. *Journal of Investigative Dermatology*, 2001, **117**(2): 341-347.

9. Rawlings AV. Ethnic skin types: Are there differences in skin structure and function? *International Journal of Cosmetic Science*, 2006, **28**(2): 79-93.

10. Selby CC. An electron microscope study of the epidermis of mammalian skin in thin sections. I. Dermo-epidermal junction and basal cell layer. *The Journal of biophysical and biochemical cytology*, 1955, **1**(5): 429-444.

11. Tadokoro T, Kobayashi N, Zmudzka BZ*, et al.* Uv-induced DNA damage and melanin content in human skin differing in racial/ethnic origin. *Faseb J*, 2003, **17**(9): 1177-1179.

12. Thong HY, Jee SH, Sun CC*, et al.* The patterns of melanosome distribution in keratinocytes of human skin as one determining factor of skin colour. *British Journal of Dermatology*, 2003, **149**(3): 498-505.

13. Watt AAR, Bothma JP and Meredith P. The supramolecular structure of melanin. *Soft Matter*, 2009, **5**(19): 3754-3760.

14. Baden HP and Pathak MA. The metabolism and function of urocanic acid in skin. *The Journal of Investigative Dermatology*, 1967, **48**(1): 11-17.

15. Anderson RR and Parrish JA. The optics of human skin. *Journal of Investigative Dermatology*, 1981, **77**(1): 13-19.

16. Bashkatov AN, Genina EA, Tuchin VV*, et al.* Monte carlo study of skin optical clearing to enhance light penetration in the tissue: Implications for photodynamic therapy of acne vulgaris - art. No. 702209. *Conference on Advanced Laser Technologies*, *Levi, Finland*, 2007, 2209-2209.

17. Braverman IM. The cutaneous microcirculation: Ultrastructure and microanatomical organization. *Microcirculation-London*, 1997, **4**(3): 329-340.

18. Cotton S and Claridge E. Developing a predictive model of human skin coloring. *SPIE: Physics of Medical Imaging*, *Newport Beach, CA, USA*, 1996, 814-825.

19. Lister TS, Wright PA and Chappell PH. Light transport through skin. *Lasers in Medical Science*, 2011, **26**(6): 719-733.

20. Selim MM, Kelly KM, Nelson JS*, et al.* Confocal microscopy study of nerves and blood vessels in untreated and treated port wine stains: Preliminary observations. *Dermatologic Surgery*, 2004, **30**(6): 892-897.

21. Nishidate I, Aizu Y and Mishina H. Estimation of melanin and hemoglobin in skin tissue using multiple regression analysis aided by monte carlo simulation. *Journal of Biomedical Optics*, 2004, **9**(4): 700-710.

22. Jacques SL. Origins of tissue optical properties in the uva, visible, and nir regions. *OSA Trends in Optics and Photonics on Advances in Optical Imaging and Photon Migration. Vol.2. From the Topical Meeting*, *Orlando, USA*, 1996, 364-371.

23. Verkruysse W, Lucassen GW and van Gemert MJC. Simulation of color of port wine stain skin and its dependence on skin variables. *Lasers in Surgery and Medicine*, 1999, **25**(2): 131-139.

24. Poirier G. *Human skin modelling and rendering*. Masters Thesis, Waterloo University, 2003.

25. Lakmaker O, Pickering JW and van Gemert MJC. Modeling the color-perception of port wine stains and its relation to the depth of laser coagulated blood-vessels. *Lasers in Surgery and Medicine*, 1993, **13**(2): 219-226.

26. Yen A and Braverman IM. Ultrastructure of human dermal microcirculation - horizontal plexus of papillary dermis. *Journal of Investigative Dermatology*, 1976, **66**(3): 131-142.

27. Lister TS, Wright PA and Chappell PH. Spectrophotometers for the clinical assessment of port wine stain skin lesions: A review. *Lasers in Medical Science*, 2010, **25**(3): 449.

28. Jasim ZF and Handley JM. Treatment of pulsed dye laser-resistant port wine stain birthmarks. *Journal of the American Academy of Dermatology*, 2007, **57**(677-682.

29. Alper JC and Holmes LB. The incidence and significance of birthmarks in a cohort of 4,641 newborns. *Pediatric Dermatology*, 1983, **1**(1): 58-68.

30. Le KVT, Shahidullah H and Frieden IJ. Review of modern techniques in detecting port-wine stain response to laser therapy. *Dermatologic Surgery*, 1999, **25**(2): 127-132.

31. Chang CJ and Stuart Nelson J. Cryogen spray cooling and higher fluence pulsed dye laser treatment improve port-wine stain clearance while minimizing epidermal damage. *Dermatologic Surgery*, 1999, **25**(10): 767-772.

32. Barsky SH, Rosen S, Geer DE*, et al.* Nature and evolution of port wine stains - computer-assisted study. *Journal of Investigative Dermatology*, 1980, **74**(3): 154-157.

33. Svaasand LO, Norvang LT, Fiskerstrand EJ*, et al.* Tissue parameters determining the visual appearance of normal skin and port-wine stains. *Lasers in Medical Science*, 1995, **10**(1): 55-65.

34. Pickering JW and Van Gemert MJC. 585 nm for the laser treatment of port wine stains - a possible mechanism. *Lasers in Surgery and Medicine*, 1991, **11**(6): 616-618.

35. Ackermann G, Hartmann M, Scherer K*, et al.* Correlations between light penetration into skin and the therapeutic outcome following laser therapy of port-wine stains. *Lasers in Medical Science*, 2002, **17**(2): 70-78.

36. Chang CJ, Yu JS and Nelson JS. Confocal microscopy study of neurovascular distribution in facial port wine stains (capillary malformation). *Journal of the Formosan Medical Association*, 2008, **107**(7): 559-566.

37. Fiskerstrand EJ, Dalaker M and Norvang LT. Laser treatment of port-wine stains - a study comparing therapeutic outcome with morphologic characteristics of the lesions - preliminary-results. *Acta Dermato-Venereologica*, 1995, **75**(1): 92-93.

38. Schneider BV, Mitsuhashi Y and Schnyder UW. Ultrastructural observations in port wine stains
Archives of Dermatological Research, 1988, **280**(6): 338-345.

39. Braverman IM and Kehyen A. Ultrastructure and 3-dimensional reconstruction of several macular and papular telangiectases. *Journal of Investigative Dermatology*, 1983, **81**(6): 489-497.

40. Niechajev IA and Clodius L. Histology of port wine stain. *European Journal of Plastic Surgery*, 1990, **13**(2): 79-85.

41. Neumann R, Leonhartsberger H, Knobler R*, et al.* Immunohistochemistry of port-wine stains and normal skin with endothelium-specific antibodies pal-e, anti-icam-1, anti-elam-1, and anti-factor viii-rag. *Archives of Dermatology*, 1994, **130**(7): 879-883.

42. Fiskerstrand EJ, Svaasand LO, Kopstad G*, et al.* Laser treatment of port wine stains: Therapeutic outcome in relation to morphological parameters. *British Journal of Dermatology*, 1996, **134**(6): 1039-1043.

43. Lanigan SW and Cotterill JA. Reduced vasoactive responses in port wine stains. *British Journal of Dermatology*, 1990, **122**(5): 615-622.

44. Nagore E, Requena C, Sevila A*, et al.* Thickness of healthy and affected skin of children with port wine stains: Potential repercussions on response to pulsed dye laser treatment. *Dermatologic Surgery*, 2004, **30**(12): 1457-1461.

45. Childers MA, Franco W, Nelson JS*, et al.* Laser surgery of port wine stains using local vacuum pressure: Changes in skin morphology and optical properties (part i). *Lasers in Surgery and Medicine*, 2007, **39**(2): 108-117.

46. Kolkman RGM, Mulder MJ, Glade CP*, et al.* Photoacoustic imaging of port-wine stains. *Lasers in Surgery and Medicine*, 2008, **40**(3): 178-182.

47. Renfro L and Geronemus RG. Anatomical differences of port-wine stains in response to treatment with the pulsed dye-laser. *Archives of Dermatology*, 1993, **129**(2): 182-188.

48. Eubanks LE and McBurney EI. Videomicroscopy of port-wine stains: Correlation of location and depth of lesion. *Journal of the American Academy of Dermatology*, 2001, **44**(6): 948-951.

49. Nishidate I, Aizu Y and Mishina H. Estimation of bluish appearance of veins in skin tissue using spectrocolorimetry. *Optical Review*, 2002, **9**(6): 269-276.

50. Svaasand LO, Fiskerstrand EJ, Kopstad G*, et al.* Therapeutic response during pulsed laser treatment of port-wine stains: Dependence on vessel diameter and depth in dermis. *Lasers in Medical Science*, 1995, **10**(4): 235-243.

51. Findlay GH. Blue skin. *British Journal of Dermatology*, 1970, **83**(1): 127-&.

52. Noe JM, Barsky SH, Geer DE*, et al.* Port wine stains and the response to argon-laser therapy - successful treatment and the predictive role of color, age, and biopsy. *Plastic and Reconstructive Surgery*, 1980, **65**(2): 130-136.

53. Anderson RR and Parrish JA. Microvasculature can be selectively damaged using dye lasers: A basic theory and experimental evidence in human skin. *Lasers Surg Med*, 1981, **1**(3): 263-276.

54. Finley JL, Barsky SH, Geer DE*, et al.* Healing of port-wine stains after argon-laser therapy. *Archives of Dermatology*, 1981, **117**(8): 486-489.

55. Ohmori S and Huang CK. Recent progress in the treatment of portwine staining by argon-laser - some observations on the prognostic value of relative spectro-reflectance (rsr) and the histological classification of the lesions. *British Journal of Plastic Surgery*, 1981, **34**(3): 249-257.

56. Anderson RR and Parrish JA. Selective photothermolysis - precise microsurgery by selective absorption of pulsed radiation. *Science*, 1983, **220**(4596): 524-527.

57. Troilius A and Ljunggren B. Reflectance spectrophotometry in the objective assessment of dye laser-treated port-wine stains. *British Journal of Dermatology*, 1995, **132**(2): 245-250.

58. Troilius AM and Ljunggren B. Evaluation of port wine stains by laser doppler perfusion imaging and reflectance photometry before and after pulsed dye laser treatment. *Acta Dermato-Venereologica*, 1996, **76**(4): 291-294.

59. Haedersdal M, Efsen J, Gniadecka M*, et al.* Changes in skin redness, pigmentation, echostructure, thickness, and surface contour after 1 pulsed dye laser treatment of port-wine stains in children. *Archives of Dermatology*, 1998, **134**(2): 175-181.

60. Hansen K, Kreiter CD, Rosenbaum M*, et al.* Long-term psychological impact and perceived efficacy of pulsed-dye laser therapy for patients with port-wine stains. *Dermatologic Surgery*, 2003, **29**(1): 49-55.

61. Laube S, Taibjee S and Lanigan SW. Treatment of resistant port wine stains with the v beam (r) pulsed dye laser. *Lasers in Surgery and Medicine*, 2003, **33**(5): 282-287.

62. Lanigan SW and Taibjee SM. Recent advances in laser treatment of port-wine stains. *British Journal of Dermatology*, 2004, **151**(3): 527-533.

63. Kelly KM, Choi B, McFarlane S*, et al.* Description and analysis of treatments for port-wine stain birthmarks. *Archives of Facial Plastic Surgery*, 2005, **7**(5): 287-294.

64. Reynolds N, Exley J, Hills S*, et al.* The role of the lumina intense pulsed light system in the treatment of port wine stains - a case controlled study. *British Journal of Plastic Surgery*, 2005, **58**(7): 968-980.

65. Smit JM, Bauland CG, Wijnberg DS*, et al.* Pulsed dye laser treatment, a review of indications and outcome based on published trials. *British Journal of Plastic Surgery*, 2005, **58**(7): 981-987.

66. Yung A and Sheehan-Dare R. A comparative study of a 595-nm with a 585-nm pulsed dye laser in refractory port wine stains. *British Journal of Dermatology*, 2005, **153**(3): 601-606.

67. Tomson N, Lim SPR, Abdullah A*, et al.* The treatment of port-wine stains with the pulsed-dye laser at 2-week and 6-week intervals: A comparative study. *British Journal of Dermatology*, 2006, **154**(4): 676-679.

68. Lee JJ, Lee JC, Kim BS*, et al.* A comparison of acquired port-wine stain with congenital port-wine stain using an image analyzer. *Annals of Dermatology*, 2008, **20**(1): 1-5.

69. Anderson RR. *Laser tissue interactions*. In Goldman MP and Fitzpatrick RE, Cutaneous laser surgery. Mosby, 1994.

70. Garden JM, Polla LL and Tan OT. The treatment of port-wine stains by the pulsed dye-laser - analysis of pulse duration and long-term therapy. *Archives of Dermatology*, 1988, **124**(6): 889-896.

71. Dierickx CC, Casparian JM, Venugopalan V*, et al.* Thermal relaxation of port-wine stain vessels probed in-vivo - the need for 1-10 millisecond laser-pulse treatment. *Journal of Investigative Dermatology*, 1995, **105**(5): 709-714.

72. Shafirstein G, Baumler W, Lapidoth M*, et al.* A new mathematical approach to the diffusion approximation theory for selective photothermolysis modeling and its implication in laser treatment of port-wine stains. *Lasers in Surgery and Medicine*, 2004, **34**(4): 335-347.

73. Zonios G and Dimou A. Modeling diffuse reflectance from semi-infinite turbid media: Application to the study of skin optical properties. *Optics Express*, 2006, **14**(19): 8661-8674.

74. Lindberg LG and Oberg PA. Optical-properties of blood in motion. *Optical Engineering*, 1993, **32**(2): 253-257.

75. Friebel M, Roggan A, Muller G*, et al.* Determination of optical properties of human blood in the spectral range 250 to 1100 nm using monte carlo simulations with hematocrit-dependent effective scattering phase function. *Journal of Biomedical Optics*, 2006, **11**(3): Article Number: 034021.

76. Zijlstra WG, Buursma A and Meeuwsenvanderroest WP. Absorption-spectra of human fetal and adult oxyhemoglobin, de-oxyhemoglobin, carboxyhemoglobin, and methemoglobin. *Clinical Chemistry*, 1991, **37**(9): 1633-1638.

77. Verkruysse W, Pickering JW, Beek JF*, et al.* Modelling the effect of wavelength on the pulsed dye-laser treatment of port wine stains. *Applied Optics*, 1993, **32**(4): 393-398.

78. Milanic M, Jia WC, Nelson JS*, et al.* Numerical optimization of sequential cryogen spray cooling and laser irradiation for improved therapy of port wine stain. *Lasers in Surgery and Medicine*, 2011, **43**(2): 164-175.

79. Babilas P, Shafirstein G, Baumler W*, et al.* Selective photothermolysis of blood vessels following flashlamp-pumped pulsed dye laser irradiation: In vivo results and mathematical modelling are in agreement. *Journal of Investigative Dermatology*, 2005, **125**(2): 343-352.

80. Kimel S, Svaasand LO, Cao D*, et al.* Vascular response to laser photothermolysis as a function of pulse duration, vessel type, and diameter: Implications for port wine stain laser therapy. *Lasers in Surgery and Medicine*, 2002, **30**(2): 160-169.

81. Kienle A and Hibst R. A new optimal wavelength for treatment of port-wine stains. *Physics in Medicine and Biology*, 1995, **40**(10): 1559-1576.

82. Minkis K, Geronemus RG and Hale EK, *Port wine stain progression: A potential consequence of delayed and inadequate treatment?* 2009, Wiley Subscription Services, Inc., A Wiley Company. p. 423-426.

83. Bjerring P and Andersen PH. Skin reflectance spectrophotometry. *Photodermatology*, 1987, **4**(3): 167-171.

84. Widdowson DC, Shakespeare PG, Moore JC*, et al.* Construction of a novel port wine stain phantom and measurement of colour by digital imaging and reflectance spectrophotometry. *Lasers in Medical Science*, 2008, **23**(4): 369-374.

85. Lanigan SW and Cotterill JA. Objective assessments of port wine stains - response to temperature-change. *British Journal of Dermatology*, 1988, **118**(6): 803-809.

86. Sevila A, Nagore E, Botella-Estrada R*, et al.* Videomicroscopy of venular malformations (port-wine stain type): Prediction of response to pulsed dye laser. *Pediatric Dermatology*, 2004, **21**(5): 589-596.

87. Jung B, Kim CS, Choi B*, et al.* Use of erythema index imaging for systematic analysis of port wine stain skin response to laser therapy. *Lasers in Surgery and Medicine*, 2005, **37**(3): 186-191.

88. Koster PHL, van der Horst C, Bossuyt PMM*, et al.* Prediction of portwine stain clearance and required number of flashlamp pumped pulsed dye laser treatments. *Lasers in Surgery and Medicine*, 2001, **29**(2): 151-155.

89. Tang SV, Gilchrest BA, Noe JM*, et al.* In vivo spectrophotometric evaluation of normal, lesional, and laser-treated skin in patients with port-wine stains. *Journal of Investigative Dermatology*, 1983, **80**(5): 420-423.

90. Yong-Gee SA, Kurwa HA and Barlow RJ. Objective assessment of port-wine stains following treatment with the 585 nm pulsed dye laser. *Australas J Dermatol*, 2001, **42**(4): 243-246.

91. Bazant-Hegemark F, Meglinski I, Kandamany N*, et al.* Optical coherence tomography: A potential tool for unsupervised prediction of treatment response for port-wine stains. *Photodiagnosis and Photodynamic Therapy*, 2008, **5**(3): 191-197.

92. Salvini C, Massi D, Cappetti A*, et al.* Application of optical coherence tomography in non-invasive characterization of skin vascular lesions. *Skin Research and Technology*, 2008, **14**(1): 89-92.

93. Gabay S, Lucassen GW, Verkruysse W*, et al.* Modelling the assessment of port wine stain parameters from skin surface temperature following a diagnostic laser pulse. *Lasers in Surgery and Medicine*, 1997, **20**(2): 179-187.

94. Li BC, Majaron B, Viator JA*, et al.* Accurate measurement of blood vessel depth in port wine stained human skin in vivo using pulsed photothermal radiometry. *Journal of Biomedical Optics*, 2004, **9**(5): 961-966.

95. Lao YQ, Zhou FF and Wang HY. In vivo photoacoustic imaging of subcutaneous vasculature and vascular anomalies in small animals. *European Physical Journal-Applied Physics*, 2008, **41**(2): 151-155.

96. Viator JA, Au G, Paltauf G*, et al.* Clinical testing of a photoacoustic probe for port wine stain depth determination. *Lasers in Surgery and Medicine*, 2002, **30**(2): 141-148.

97. Zhang EZ, Laufer JG, Pedley RB*, et al.* In vivo high-resolution 3d photoacoustic imaging of superficial vascular anatomy. *Physics in Medicine and Biology*, 2009, **54**(4): 1035-1046.

98. Zhang HF, Maslov K, Li M-L*, et al.* In vivo volumetric imaging of subcutaneous microvasculature by photoacoustic microscopy. *Opt. Express*, 2006, **14**(20): 9317-9323.

99. Pickering JW, Mordon SR and Brunetaud JM. The objective reporting of laser treatment of port wine stains. *Lasers in Medical Science*, 1992, **7**(4): 415-421.

100. Sheard C and Brown GE. The spectrophotometric analysis of the color of the skin: And the observations by this method in normal and in pathologic subjects
Arch Intern Med, 1926, **38**(6): 816-831.

101. Dawson JB, Barker DJ, Ellis DJ*, et al.* A theoretical and experimental-study of light-absorption and scattering by in-vivo skin. *Physics in Medicine and Biology*, 1980, **25**(4): 695-709.

102. Wang L, Jacques SL and Zheng L. Mcml - monte carlo modeling of light transport in multi-layered tissues. *Computer Methods and Programs in Biomedicine*, 1995, **47**(2): 131-146.

103. Sheehan-Dare RA and Cotterill JA. Copper-vapor laser treatment of port-wine stains - clinical-evaluation and comparison with conventional argon-laser therapy. *British Journal of Dermatology*, 1993, **128**(5): 546-549.

104. Farrell TJ, Patterson MS and Wilson B. A diffusion-theory model of spatially resolved, steady-state diffuse reflectance for the noninvasive determination of tissue optical-properties in-vivo. *Medical Physics*, 1992, **19**(4): 879-888.

105. (ISI) AIfSI. *Web of knowledge (wok)*. [cited: 27 January]; Available from: http://isiknowledge.com/.

106. Verkruysse W, Zhang R, Choi B*, et al.* A library based fitting method for visual reflectance spectroscopy of human skin. *Physics in Medicine and Biology*, 2005, **50**(1): 57-70.

107. Zhang R, Verkruysse W, Choi B*, et al.* Determination of human skin optical properties from spectrophotometric measurements based on optimization by genetic algorithms. *Journal of Biomedical Optics*, 2005, **10**(2):

108. Diffey BL, Oliver RJ and Farr PM. A portable instrument for quantifying erythema induced by ultraviolet-radiation. *British Journal of Dermatology*, 1984, **111**(6): 663-672.

109. Clarys P, Alewaeters K, Lambrecht R*, et al.* Skin color measurements: Comparison between three instruments: The chromameter (r), the dermaspectrometer (r) and the mexameter (r). *Skin Research and Technology*, 2000, **6**(4): 230-238.

110. Moncrieff M, Cotton S, Claridge E*, et al.* Spectrophotometric intracutaneous analysis: A new technique for imaging pigmented skin lesions. *British Journal of Dermatology*, 2002, **146**(3): 448-457.

111. Takiwaki H, Overgaard L and Serup J. Comparison of narrow-band reflectance spectrophotometric and tristimulus colorimetric measurements of skin color - 23 anatomical sites evaluated by the dermaspectrometer(r) and the chroma-meter-cr-200(r) *Skin Pharmacology*, 1994, **7**(4): 217-225.

112. Fullerton AL, K.-P. Wilhelm, D. Perrenoud, J. Serup,. Interlaboratory comparison and validity study of the minolta chromameters cr-200 and cr-300. *Skin Research and Technology*, 1996, **2**(3): 126-135.

113. Van den Kerckhove E, Staes F, Flour M*, et al.* Reproducibility of repeated measurements on healthy skin with minolta chromameter cr-300. *Skin Research and Technology*, 2001, **7**(1): 56-59.

114. Neumann RA, Knobler RM and Lindmaier AP. Photoelectric quantitative-evaluation of argon-laser treatment of port wine stains. *British Journal of Dermatology*, 1991, **124**(2): 181-186.

115. Serup J and Agner T. Colorimetric quantification of erythema - a comparison of 2 colorimeters (lange micro color and minolta chroma meter cr-200) with a clinical scoring scheme and laser-doppler flowmetry. *Clinical and Experimental Dermatology*, 1990, **15**(4): 267-272.

116. Kim CS, Jung BJ, Choi B*, et al.* Clinical feasibility of various optical instruments for quantitative evaluation of pulsed dye laser treatment of port wine stain skin. *Photonic Therapeutics and Diagnostics*, 2005, **5686**(73-79.

117. Takiwaki H. Measurement of skin color: Practical application and theoretical considerations. *The journal of medical investigation*, 1998, **44**(3-4): 103-108.

118. Takiwaki H, Miyaoka Y, Skrebova N*, et al.* Skin reflectance-spectra and colour-value dependency on measuring-head aperture area in ordinary reflectance spectrophotometry and tristimulus colourimetry. *Skin Research and Technology*, 2002, **8**(2): 94-97.

119. Shriver MD and Parra EJ. Comparison of narrow-band reflectance spectroscopy and tristimulus colorimetry for measurements of skin and hair color in persons of different biological ancestry. *American Journal of Physical Anthropology*, 2000, **112**(1): 17-27.

120. Yohn JJ, Huff JC, Aeling JL*, et al.* Lesion size is a factor for determining the rate of port-wine stain clearing following pulsed dye laser treatment in adults. *Cutis*, 1997, **59**(5): 267-270.

121. Shimada M, Yamada Y, Itoh M*, et al.* Melanin and blood concentration in a human skin model studied by multiple regression analysis: Assessment by monte carlo simulation. *Physics in Medicine and Biology*, 2001, **46**(9): 2397-2406.

122. Yudovsky D and Pilon L. Rapid and accurate estimation of blood saturation, melanin content, and epidermis thickness from spectral diffuse reflectance. *Applied Optics*, 2010, **49**(10): 1707-1719.

123. Zonios G and Dimou A. Melanin optical properties provide evidence for chemical and structural disorder in vivo. *Optics Express*, 2008, **16**(11): 8263-8268.

124. Aizu Y, Isokawa M, Yuasa T*, et al. Spectrophotometric investigation of skin blood vessels on the basis of color perception*. In 18th congress of the international commission for optics: Optics for the next millennium, technical digest. SPIE - Int Soc Optical Engineering, 1999.

125. Nishidate I, Aizu Y, Yokoi N*, et al. Color appearance of skin tissues and blood vessels: In vitro and in vivo experiments*. In Iwata K, Optical engineering for sensing and nanotechnology. SPIE - Int Soc Optical Engineering, 2001.

126. Nishidate I, Maeda T, Aizu Y*, et al.* Visualizing depth and thickness of a local blood region in skin tissue using diffuse reflectance images. *Journal of Biomedical Optics*, 2007, **12**(5):

127. Hamzavi I, Shiff N, Martinka M*, et al.* Spectroscopic assessment of dermal melanin using blue vitiligo as an in vivo model. *Photodermatology Photoimmunology & Photomedicine*, 2006, **22**(1): 46-51.

128. Mazzoli A, Munaretto R and Scalise L. Preliminary results on the use of a noninvasive instrument for the evaluation of the depth of pigmented skin lesions: Numerical simulations and experimental measurements. *Lasers in Medical Science*, 2010, **25**(3): 403-410.

129. Randeberg LL, Larsen EL and Svaasand LO. Characterization of vascular structures and skin bruises using hyperspectral imaging, image analysis and diffusion theory. *Journal of Biophotonics*, 2010, **3**(1-2): 53-65.

130. Stam B, van Gemert M, van Leeuwen T*, et al.* 3d finite compartment modeling of formation and healing of bruises may identify methods for age determination of bruises. *Medical and Biological Engineering and Computing*, 2010, **48**(9): 911-921.

131. Nickell S, Hermann M, Essenpreis M*, et al.* Anisotropy of light propagation in human skin. *Physics in Medicine and Biology*, 2000, **45**(10): 2873-2886.

132. Sandell JL and Zhu TC. A review of in-vivo optical properties of human tissues and its impact on pdt. *Journal of Biophotonics*, 2011, **4**(11-12): 773-787.

133. Stratonnikov AA, Meerovich GA, Ryabova AV*, et al.* Application of backward diffuse reflection spectroscopy for monitoring the state of tissues in photodynamic therapy. *Quantum Electronics*, 2006, **36**(12): 1103-1110.

134. Wang Y, Liao XH, Gu Y*, et al.* The change of reflection spectra and fluorescence spectra of port wine stains during pdt. *Spectroscopy and Spectral Analysis*, 2011, **31**(11): 2969-2972.

135. Mehrubeoglu M, Kehtarnavaz N, Marquez G*, et al.* Skin lesion classification using oblique-incidence diffuse reflectance spectroscopic imaging. *Applied Optics*, 2002, **41**(1): 182-192.

136. Salomatina E, Jiang B, Novak J*, et al.* Optical properties of normal and cancerous human skin in the visible and near-infrared spectral range. *Journal of Biomedical Optics*, 2006, **11**(6): 9.

137. Wallace VP, Crawford DC, Mortimer PS*, et al.* Spectrophotometric assessment of pigmented skin lesions: Methods and feature selection for evaluation of diagnostic performance. *Physics in Medicine and Biology*, 2000, **45**(3): 735-751.

138. Berg J, Tymoczko J and Stryer L. *Biochemistry: 6th ed*. W. H. Freeman, 2006.

139. Kosmachevskaya OV and Topunov AF. Hemoglobins: Diversity of structures and functions. *Applied Biochemistry and Microbiology*, 2009, **45**(6): 563-587.

140. Lukin JA, Kontaxis G, Simplaceanu V*, et al.* Quaternary structure of hemoglobin in solution. *Proceedings of the National Academy of Sciences*, 2003, **100**(2): 517-520.

141. Platt JR. *Electronic structure and excitation of polyenes and porphyrins*. In A H, Radiation biology volume iii: Visible and near-visible light. McGraw Hill, 1956.

142. Hsu M-C and Woody RW. Origin of the heme cotton effects in myoglobin and hemoglobin. *Journal of the American Chemical Society*, 1971, **93**(14): 3515-3525.

143. Meredith P, Powell BJ, Riesz J*, et al.* Towards structure-property-function relationships for eumelanin. *Soft Matter*, 2006, **2**(1): 37-44.

144. Riesz J. *The spectroscopic properties of melanin*. PhD Thesis, University of Queensland, 2007.

145. Zonios G, Dimou A, Bassukas I*, et al.* Melanin absorption spectroscopy: New method for noninvasive skin investigation and melanoma detection. *Journal of Biomedical Optics*, 2008, **13**(1):

146. Kaxiras E, Tsolakidis A, Zonios G*, et al.* Structural model of eumelanin. *Physical Review Letters*, 2006, **97**(21): 218102.

147. Stepien K, Dzierzega-Lecznar A, Kurkiewicz S*, et al.* Melanin from epidermal human melanocytes: Study by pyrolytic gc/ms. *Journal of the American Society for Mass Spectrometry*, 2009, **20**(3): 464-468.

148. Doi M and Tominaga S. *Spectral estimation of human skin color using the kubelka-munk theory*. In Eschbach R and Marcu GG, Color imaging viii: Processing, hardcopy, and applications. SPIE - Int Soc Optical Engineering, 2003.

149. Prahl SA and Jacques SL. *Optical properties spectra*. [cited: 18th June]; Available from: http://omlc.ogi.edu/spectra/.

150. Bohnert M, Walther R, Roths T*, et al.* A monte carlo-based model for steady-state diffuse reflectance spectrometry in human skin: Estimation of carbon monoxide concentration in livor mortis. *International Journal of Legal Medicine*, 2005, **119**(6): 355-362.

151. Andree S, Helfmann J and Gersonde I. *Determination of chromophore concentrations from spatially resolved skin measurements*. In Ramanujam N and Popp J, Clinical and biomedical spectroscopy and imaging. SPIE - Int Soc Optical Engineering, 2003.

152. Randeberg LL, Haugen OA, Haaverstad R*, et al.* A novel approach to age determination of traumatic injuries by reflectance spectroscopy. *Lasers in Surgery and Medicine*, 2006, **38**(4): 277-289.

153. Meglinski IV and Matcher SJ. Quantitative assessment of skin layers absorption and skin reflectance spectra simulation in the visible and near-infrared spectral regions. *Physiological Measurement*, 2002, **23**(4): 741-753.

154. Mourant JR, Freyer JP, Hielscher AH*, et al.* Mechanisms of light scattering from biological cells relevant to noninvasive optical-tissue diagnostics. *Applied Optics*, 1998, **37**(16): 3586-3593.

155. Graaff R, Aarnoudse JG, Zijp JR*, et al.* Reduced light-scattering properties for mixtures of spherical particles: A simple approximation derived from mie calculations. *Appl. Opt.*, 1992, **31**(10): 1370-1376.

156. Saidi IS, Jacques SL and Tittel FK. Mie and rayleigh modeling of visible-light scattering in neonatal skin. *Appl. Opt.*, 1995, **34**(31): 7410-7418.

157. Anderson RR and Parrish JA. *Optical properties of human skin*. In Regan JD and Parrish JA, The science of photomedicine. Plenum, 1982.

158. Kienle A, Lilge L, Vitkin IA*, et al.* Why do veins appear blue? A new look at an old question. *Applied Optics*, 1996, **35**(7): 1151-1160.

159. Prahl SA. *Light transport in tissue*. PhD Thesis, The University of Texas at Austin, 1988.

160. Thomsen S. Anatomic and physiologic factors influencing transcutaneous optical diagnosis of deep-seated lesions. *Optical Biopsy II, Proceedings Of*, *San Jose, USA*, 1998, 130-139.

161. Rajadhyaksha M, Grossman M, Esterowitz D*, et al.* In vivo confocal scanning laser microscopy of human skin: Melanin provides strong contrast. *J Investig Dermatol*, 1995, **104**(6): 946-952.

162. Bhandari A, Hamre B, Frette O*, et al.* Modeling optical properties of human skin using mie theory for particles with different size distributions and refractive indices. *Optics Express*, 2011, **19**(15): 14549-14567.

163. Magnain C, Elias M and Frigerio JM. Skin color modeling using the radiative transfer equation solved by the auxiliary function method: Inverse problem. *Journal of the Optical Society of America a-Optics Image Science and Vision*, 2008, **25**(7): 1737-1743.

164. Zonios G and Dimou A. Light scattering spectroscopy of human skin in vivo. *Optics Express*, 2009, **17**(3): 1256-1267.

165. Baranoski GVG, Krishnaswamy A and Kimmel B. Increasing the predictability of tissue subsurface scattering simulations. *Visual Computer*, 2005, **21**(4): 265-278.

166. Faber DJ, Aalders MCG, Mik EG*, et al.* Oxygen saturation-dependent absorption and scattering of blood. *Physical Review Letters*, 2004, **93**(2):

167. Igarashi M, *The appearance of human skin*, in *Technical Report*. 2005, Columbia University: New York.

168. Bashkatov AN, Genina EA, Kochubey VI*, et al.* Optical properties of human skin, subcutaneous and mucous tissues in the wavelength range from 400 to 2000 nm. *Journal of Physics D-Applied Physics*, 2005, **38**(15): 2543-2555.

169. Donner C, Weyrich T, d'Eon E*, et al.* A layered, heterogeneous reflectance model for acquiring and rendering human skin. *Acm Transactions on Graphics*, 2008, **27**(5):

170. Welch AJ and van Gemert MJC, *Optical-thermal response of laser-irradiated tissue*. 1995, Plenum Publishing Corporation: New York.

171. Cheong WF, Prahl SA and Welch AJ. A review of the optical-properties of biological tissues. *Ieee Journal of Quantum Electronics*, 1990, **26**(12): 2166-2185.

172. Jacques SL, Alter CA and Prahl SA. Angular dependence of hene laser light scattering by human dermis. *Lasers in the Life Sciences*, 1987, **1**(4): 309-333.

173. Chan EK, Sorg B, Protsenko D*, et al.* Effects of compression on soft tissue optical properties. *Ieee Journal of Selected Topics in Quantum Electronics*, 1996, **2**(4): 943-950.

174. Simpson CR, Kohl M, Essenpreis M*, et al.* Near-infrared optical properties of ex vivo human skin and subcutaneous tissues measured using the monte carlo inversion technique. *Physics in Medicine and Biology*, 1998, **43**(9): 2465-2478.

175. Graaff R, Dassel ACM, Koelink MH*, et al.* Optical properties of human dermis in vitro and in vivo. *Applied Optics*, 1993, **32**(4): 435-447.

176. Pierard GE. E.M.C.O. Guidance for the assessment of skin colour. *British Journal of Dermatology*, 2002, **10**(1.

177. Svaasand LO, Aguilar G, Viator JA*, et al.* Increase of dermal blood volume fraction reduces the threshold for laser-induced purpura: Implications for port wine stain laser treatment. *Lasers in Surgery and Medicine*, 2004, **34**(2): 182-188.

178. Bosschaart N, Mentink R, Kok JH*, et al.* Optical properties of neonatal skin measured in vivo as a function of age and skin pigmentation. *Journal of Biomedical Optics*, 2011, **16**(9):

179. Torricelli A, Pifferi A, Taroni P*, et al.* In vivo optical characterization of human tissues from 610 to 1010 nm by time-resolved reflectance spectroscopy. *Physics in Medicine and Biology*, 2001, **46**(8): 2227-2237.

180. Mourant JR, Fuselier T, Boyer J*, et al.* Predictions and measurements of scattering and absorption over broad wavelength ranges in tissue phantoms. *Applied Optics*, 1997, **36**(4): 949-957.

181. Doornbos RMP, Lang R, Aalders MC*, et al.* The determination of in vivo human tissue optical properties and absolute chromophore concentrations using spatially resolved steady-state diffuse reflectance spectroscopy. *Physics in Medicine and Biology*, 1999, 4): 967.

182. Pickering JW, Bosman S, Posthumus P*, et al.* Changes in the optical properties (at 632.8 nm) of slowly heated myocardium. *Appl. Opt.*, 1993, **32**(4): 367-371.

183. Wan S, Anderson RR and Parrish JA. Analytical modeling for the optical-properties of the skin with in vitro and in vivo applications. *Photochemistry and Photobiology*, 1981, **34**(4): 493-499.

184. Dognitz N, Wagnieres G, Kienle A*, et al.* Determination of the absorption and reduced scattering coefficients of human skin and bladder by spatial frequency domain reflectometry. *Laser-Tissue Interaction, Tissue Optics, and Laser Welding Iii, Proceedings Of*, 1998, **3195**(102-109.

185. Ma X, Lu JQ and Hu X-H. Effect of surface roughness on determination of bulk tissue optical parameters. *Optics Letters*, 2003, **28**(22): 2204-2206.

186. Zonios G, Bykowski J and Kollias N. Skin melanin, hemoglobin, and light scattering properties can be quantitatively assessed in vivo using diffuse reflectance spectroscopy. *Journal of Investigative Dermatology*, 2001, **117**(6): 1452-1457.

187. Prahl SA. *Optical property measurements using the inverse adding-doubling program*. In Welch AJ and Gemert MJCv, Optical-thermal response of laser irradiated tissue. Plenum Publishing Corporation, 1995.

188. van Gemert MJC, Jacques SL, Sterenborg HJCM*, et al.* Skin optics. *Biomedical Engineering, IEEE Transactions on*, 1989, **36**(12): 1146-1154.

189. Bruls WAG and Vanderleun JC. Forward scattering properties of human epidermal layers. *Photochemistry and Photobiology*, 1984, **40**(2): 231-242.

190. Henyey LG and Greenstein JL. Diffuse radiation in the galaxy. *The Astrophysical Journal*, 1941, **93**(70-83.

191. Dunn A and Richards-Kortum R. Three-dimensional computation of light scattering from cells. *Ieee Journal of Selected Topics in Quantum Electronics*, 1996, **2**(4): 898-905.

192. Canpolat M and Mourant JR. High-angle scattering events strongly affect light collection in clinically relevant measurement geometries for light transport through tissue. *Physics in Medicine and Biology*, 2000, 5): 1127.

193. Reynolds LO and McCormick NJ. Approximate 2-parameter phase function for light-scattering. *Journal of the Optical Society of America*, 1980, **70**(10): 1206-1212.

194. Sharma SK, Roy AK and Somerford DJ. New approximate phase functions for scattering of unpolarized light by dielectric particles. *Journal of Quantitative Spectroscopy and Radiative Transfer*, 1998, **60**(6): 1001-1010.

195. Toublanc D. Henyey-greenstein and mie phase functions in monte carlo radiative transfer computations. *Appl. Opt.*, 1996, **35**(18): 3270-3274.

196. Sharma SK and Banerjee S. Role of approximate phase functions in monte carlo simulation of light propagation in tissues. *Journal of Optics a-Pure and Applied Optics*, 2003, **5**(3): 294-302.

197. Lu Q and Luo QM. On phase function of monte carlo simulation of light transport in turbid media. *3rd International Conference on Photonics and Imaging in Biology and Medicine*, *Wuhan, Peoples R China*, 2003, 122-130.

198. Yongji F and Jacques SL. Monte carlo simulation study on phase function. *Proceedings of the SPIE - The International Society for Optical Engineering*, 2006, **6084**(1): 39-45.

199. Schneiderheinze DHP, Hillman TR and Sampson DD. Modified discrete particle model of optical scattering in skin tissue accounting for multiparticle scattering. *Optics Express*, 2007, **15**(23): 15002-15010.

200. Liu PY. A new phase function approximating to mie scattering for radiative transport-equations. *Physics in Medicine and Biology*, 1994, **39**(6): 1025-1036.

201. Ding H, Lu JQ, Wooden WA*, et al.* Refractive indices of human skin tissues at eight wavelengths and estimated dispersion relations between 300 and 1600 nm. *Physics in Medicine and Biology*, 2006, **51**(6): 1479.

202. Lai J-C, Zhang Y-Y, Li Z-H*, et al.* Complex refractive index measurement of biological tissues by attenuated total reflection ellipsometry. *Appl. Opt.*, 2010, **49**(16): 3235-3238.

203. Tuchin VV, Utz SR and Yaroslavsky IV. Tissue optics, light-distribution, and spectroscopy. *Optical Engineering*, 1994, **33**(10): 3178-3188.

204. Tearney GJ, Brezinski ME, Southern JF*, et al.* Determination of the refractive-index of highly scattering human tissue by optical coherence tomography. *Optics Letters*, 1995, **20**(21): 2258-2260.

205. Enejder AMK, Swartling J, Aruna P*, et al.* Influence of cell shape and aggregate formation on the optical properties of flowing whole blood. *Applied Optics*, 2003, **42**(7): 1384-1394.

206. Nilsson AMK, Alsholm P, Karlsson A*, et al.* T-matrix computations of light scattering by red blood cells. *Applied Optics*, 1998, **37**(13): 2735-2748.

207. Li H, Lin L and Xie S. Refractive index of human whole blood with different types in the visible and near-infrared ranges. *Proceedings of the SPIE - The International Society for Optical Engineering*, 2000, **3914**(517-521.

208. Keijzer M, Jacques SL, Prahl SA*, et al.* Light distributions in artery tissue - monte-carlo simulations for finite-diameter laser-beams. *Lasers in Surgery and Medicine*, 1989, **9**(2): 148-154.

209. Müller G and Roggan A. *Laser-induced interstitial thermotherapy*. 39. SPIE, 1995.

210. Vuylsteke ME and Mordon SR. Endovenous laser ablation: A review of mechanisms of action. *Ann Vasc Surg*, 2012, **26**(3): 424-433.

211. Hammer M, Yaroslavsky AN and Schweitzer D. A scattering phase function for blood with physiological haematocrit. *Physics in Medicine and Biology*, 2001, **46**(3): N65-N69.

212. Turcu I. Effective phase function for light scattered by blood. *Applied Optics*, 2006, **45**(4): 639-647.

213. Yaroslavsky AN, Yaroslavsky IV, Goldbach T*, et al. Different phase function approximations to determine optical properties of blood: A comparison*. SPIE - Int Soc Optical Engineering, 1997.

214. Lister TS, Wright PA and Chappell PH. Simulating light transport through skin for color prediction of port wine stain lesions: A review. *Journal of Biomedical Optics*, 2012, **17**(11): 110901.

215. Geronemus RG and Ashinoff R. The medical necessity of evaluation and treatment of port-wine stains. *Journal of Dermatologic Surgery and Oncology*, 1991, **17**(1): 76-79.

216. Klein A, Baumler W, Landthaler M*, et al.* Laser and ipl treatment of port-wine stains: Ttherapy options, limitations, and practical aspects. *Lasers in Medical Science*, 2011, **26**(6): 845-859.

217. Troilius A, Wrangsjo B and Ljunggren B. Patients with port-wine stains and their psychosocial reactions after photothermolytic treatment. *Dermatologic Surgery*, 2000, **26**(3): 190-196.

218. Huang YC, Ringold TL, Nelson JS*, et al.* Noninvasive blood flow imaging for real-time feedback during laser therapy of port wine stain birthmarks. *Lasers in Surgery and Medicine*, 2008, **40**(3): 167-173.

219. van der Horst C, Koster PHL, de Borgie C*, et al.* Effect of the timing of treatment of port-wine stains with the flash-lamp-pumped pulsed dye-laser. *New England Journal of Medicine*, 1998, **338**(15): 1028-1033.

220. Huikeshoven M, Koster PHL, de Borgie C*, et al.* Redarkening of port-wine stains 10 years after pulsed-dye-laser treatment. *New England Journal of Medicine*, 2007, **356**(12): 1235-1240.

221. Yoshida K, Miyaki M, Ojima N*, et al.* Relationship between microstructure of the skin surface and surface reflection based on geometric optics. *Journal of Dermatological Science*, 2012, **66**(3): 225-232.

222. Cula OG, Dana KJ, Murphy FP*, et al.* Skin texture modeling. *International Journal of Computer Vision*, 2005, **62**(1): 97-119.

223. Godfain E. Optical simulations of skin diagnosis with account of multiple surface scattering events. *18th Congress of the International Commission for Optics - Optics for the Next Millennium*, *San Francisco, Ca*, 1999, 627-628.

224. Bouguer P. *Essai d'optique sur la gradation de la lumiere*. Claude Jombert, 1729.

225. Andersen PH and Bjerring P. Noninvasive computerized analysis of skin chromophores invivo by reflectance spectroscopy. *Photodermatology Photoimmunology & Photomedicine*, 1990, **7**(6): 249-257.

226. Amelink A, van den Heuvel AP, de Wolf WJ*, et al.* Monitoring pdt by means of superficial reflectance spectroscopy. *Journal of Photochemistry and Photobiology B-Biology*, 2005, **79**(3): 243-251.

227. Glennie DL, Farrell TJ, Hayward JE*, et al.* Integrating spheres for improved skin photodynamic therapy. *Journal of Biomedical Optics*, 2010, **15**(5): 8.

228. Gioux S, Mazhar A, Lee BT*, et al. Preclinical and clinical validation of a novel oxygenation imaging system*. In Tromberg BJ, Yodh AG, Tamura M*, et al.*, Optical tomography and spectroscopy of tissue ix. Spie-Int Soc Optical Engineering,

229. Venugopalan V, You JS and Tromberg BJ. Radiative transport in the diffusion approximation: An extension for highly absorbing media and small source-detector separations. *Physical Review E*, 1998, **58**(2): 2395-2407.

230. Meglinski IV and Matcher SJ. Computer simulation of the skin reflectance spectra. *Computer Methods and Programs in Biomedicine*, 2003, **70**(2): 179-186.

231. Pfefer TJ, Barton JK, Smithies DJ*, et al.* Modeling laser treatment of port wine stains with a computer-reconstructed biopsy. *Lasers in Surgery and Medicine*, 1999, **24**(2): 151-166.

232. Shimada M, Yamada Y, Itoh M*, et al.* Melanin and blood concentration in human skin studied by multiple regression analysis: Experiments. *Physics in Medicine and Biology*, 2001, **46**(9): 2385-2395.

233. Wilson BC and Adam G. A monte-carlo model for the absorption and flux distributions of light in tissue. *Medical Physics*, 1983, **10**(6): 824-830.

234. Flock ST, Patterson MS, Wilson BC*, et al.* Monte-carlo modeling of light-propagation in highly scattering tissues 1. Model predictions and comparison with diffusion-theory. *Ieee Transactions on Biomedical Engineering*, 1989, **36**(12): 1162-1168.

235. Flock ST, Wilson BC and Patterson MS. Monte-carlo modeling of light-propagation in highly scattering tissues 2. Comparison with measurements in phantoms. *Ieee Transactions on Biomedical Engineering*, 1989, **36**(12): 1169-1173.

236. Prahl SA, Keijzer M, Jacques SL*, et al.* A monte carlo model of light propagation in tissue. *Proceedings of the SPIE - The International Society for Optical Engineering|Proceedings of the SPIE - The International Society for Optical Engineering*, 1989, **5**(102-111.

237. Wang L and Jacques SL. *Monte carlo modeling of light transport in multi-layered tissues in standard c*. University of Texas, 1992.

238. Keijzer M. *Light transport for medical laser treatments*. PhD, Technische University, 1993.

239. Lucassen GW, Verkruysse W, Keijzer M*, et al.* Light distributions in a port wine stain model containing multiple cylindrical and curved blood vessels. *Lasers in Surgery and Medicine*, 1996, **18**(4): 345-357.

240. Mantis G and Zonios G. Simple two-layer reflectance model for biological tissue applications. *Appl. Opt.*, 2009, **48**(18): 3490-3496.

241. Krackowizer P and Brenner E. Thickness of the human skin: 24 points of measurement. *Phlebologie*, 2008, **37**(2): 83-92.

242. Graaff R, Koelink MH, de Mul FFM*, et al.* Condensed monte carlo simulations for the description of light transport. *Appl. Opt.*, 1993, **32**(4): 426-434.

243. Wang Q, Agrawal A, Wang NS*, et al.* Condensed monte carlo modeling of reflectance from biological tissue with a single illumination detection fiber. *Selected Topics in Quantum Electronics, IEEE Journal of*, 2010, **16**(3): 627-634.

244. Doronin A and Meglinski I. Online object oriented monte carlo computational tool for the needs of biomedical optics. *Biomed. Opt. Express*, 2012, **2**(9): 2461-2469.

245. Meglinski I and Doronin A. *Mc online*. [cited: 5 Oct 2012]; Available from: http://biophotonics.otago.ac.nz/MCOnline.aspx.

246. Maeda T, Arakawa N, Takahashi M*, et al.* Monte carlo simulation of spectral reflectance using a multilayered skin tissue model. *Optical Review*, 2010, **17**(3): 223-229.

247. van Drooge AM, Beek JF, van der Veen JPW*, et al.* Hypertrophy in port-wine stains: Prevalence and patient characteristics in a large patient cohort. *Journal of the American Academy of Dermatology*, **67**(6): 1214-1219.

248. Alster TS and Wilson F. Treatment of port-wine stains with the flashlamp-pumped pulsed dye laser: Extended clinical experience in children and adults. *Ann Plast Surg*, 1994, **32**(5): 478-484.

249. Podoleanu AG, Rogers JA and Jackson DA. Three dimensional oct images from retina and skin. *Optics Express*, 2000, **7**(9): 292-298.

250. Yingtian P and Farkas DL. Noninvasive imaging of living human skin with dual-wavelength optical coherence tomography in two and three dimensions. *Journal of Biomedical Optics*, 1998, **3**(4):

251. Gambichler T, Jaedicke V and Terras S. Optical coherence tomography in dermatology: Technical and clinical aspects. *Archives of Dermatological Research*, 2011, **303**(7): 457-473.

252. Moretti G, Ellis R and Mescon H. Vascular patterns in the skin of the face. *Jour Invest Dermatol*, 1959, **33**(3): 103-112.

253. Zonios G, Bassukas I and Dimou A. Comparative evaluation of two simple diffuse reflectance models for biological tissue applications. *Applied Optics*, 2008, **47**(27): 4965-4973.

254. Yaroslavsky AN, Yaroslavsky LV, Goldbach T*, et al.* Influence of the scattering phase function approximation on the optical properties of blood determined from the integrating sphere measurements. *Journal of Biomedical Optics*, 1999, **4**(1): 47-53.

255. Eze R and Kumar S. Laser transport through thin scattering layers. *Appl. Opt.*, 2010, **49**(3): 358-368.

256. Shen H and Wang G. A tetrahedron-based inhomogeneous monte carlo optical simulator. *Physics in Medicine and Biology*, 2010, **55**(4): 947-962.

257. Matts PJ, Dykes PJ and Marks R. The distribution of melanin in skin determined in vivo. *British Journal of Dermatology*, 2007, **156**(4): 620-628.

258. Kono T, Sakurai H, Takeuchi M*, et al.* Treatment of resistant port-wine stains with a variable-pulse pulsed dye laser. *Dermatologic Surgery*, 2007, **33**(8): 951-956.

259. Edstrom DW, Hedblad MA and Ros AM. Flashlamp pulsed dye laser and argon-pumped dye laser in the treatment of port-wine stains: A clinical and histological comparison. *British Journal of Dermatology*, 2002, **146**(2): 285-289.

260. Currie CLA and Monk BE. Can the response of port-wine stains to laser treatment be reliably assessed using subjective methods? *British Journal of Dermatology*, 2000, **143**(2): 360-364.

261. Widdowson DC, Moore JC, Wright PA*, et al.* Determination of the effects of blood depth in the dermis on skin colour in a novel skin phantom using digital imaging. *Lasers in Medical Science*, 2010, **25**(1): 55-59.

262. Koster PHL, van der Horst C, van Gemert MJC*, et al.* Histologic evaluation of skin damage after overlapping and nonoverlapping flashlamp pumped pulsed dye laser pulses: A study on normal human skin as a model for port wine stains. *Lasers in Surgery and Medicine*, 2001, **28**(2): 176-181.

263. Alerstam E, Lo WC, Han TD*, et al.* Next-generation acceleration and code optimization for light transport in turbid media using gpus. *Biomed Opt Express*, 2010, **1**(2): 658-675.

264. Alerstam E, Svensson T and Andersson-Engels S. Parallel computing with graphics processing units for high-speed monte carlo simulation of photon migration. *J Biomed Opt*, 2008, **13**(6): 3041496.

265. Yang MU, Yaroslavsky AN, Farinelli WA*, et al.* Long-pulsed neodymium:Yttrium-aluminum-garnet laser treatment for port-wine stains. *Journal of the American Academy of Dermatology*, 2005, **52**(3): 480-490.

266. Alster TS and Tanzi EL. Combined 595-nm and 1,064-nm laser irradiation of recalcitrant and hypertrophic port-wine stains in children and adults. *Dermatologic Surgery*, 2009, **35**(6): 914-919.

267. Kono T, Groff WF, Chan HH*, et al.* Long-pulsed neodymium:Yttrium-aluminum-garnet laser treatment for hypertrophic port-wine stains on the lips. *Journal of Cosmetic and Laser Therapy*, 2009, **11**(1): 11-13.

268. Jasim ZF and Handley JM. Treatment of pulsed dye laser-resistant port wine stain birthmarks. *Journal of the American Academy of Dermatology*, 2007, **57**(4): 677-682.

269. van Gemert MJC, Smithies DJ, Verkruysse W*, et al.* Wavelengths for port wine stain laser treatment: Influence of vessel radius and skin anatomy. *Physics in Medicine and Biology*, 1997, **42**(1): 41-50.

270. van Assendelft OW. *Spectrophotometry of haemoglobin derivatives*. 55-57. Royal Vangorcum Ltd., 1970.